nagra.

Arbeitsbericht NAB 21-21

TBO Bözberg-1-1: Data Report

Dossier VIII
Rock Properties, Porewater Characterisation and Natural Tracer Profiles

February 2022

P. Wersin, L. Aschwanden, L. Camesi,
E.C. Gaucher, T. Gimmi, A. Jenni, M. Kiczka,
U. Mäder, M. Mazurek, D. Rufer,
H.N. Waber, C. Zwahlen & D. Traber

National Cooperative
for the Disposal of
Radioactive Waste

Hardstrasse 73
P.O. Box 280
5430 Wettingen
Switzerland
Tel. +41 56 437 11 11

www.nagra.ch

nagra.

Arbeitsbericht NAB 21-21

TBO Bözberg-1-1: Data Report

Dossier VIII Rock Properties, Porewater Characterisation and Natural Tracer Profiles

February 2022

P. Wersin[1], L. Aschwanden[1], L. Camesi[1], E.C. Gaucher[1], T. Gimmi[1], A. Jenni[1], M. Kiczka[1], U. Mäder[1,2], M. Mazurek[1], D. Rufer[1], H.N. Waber[1], C. Zwahlen[1] & D. Traber[3]

[1] Rock-Water Interaction, University of Bern

[2] Rock-Water Consulting, Boll

[3] Nagra

Keywords:
BOZ1-1, Jura Ost, TBO, deep drilling campaign, rock properties, petrophysical parameters, water content, porosity, mineralogy, clay content, clay mineral composition, porewater chemistry, natural tracer profiles

National Cooperative for the Disposal of Radioactive Waste

Hardstrasse 73
P.O. Box 280
5430 Wettingen
Switzerland
Tel. +41 56 437 11 11

www.nagra.ch

Nagra Arbeitsberichte ("Working Reports") present the results of work in progress that have not necessarily been subject to a comprehensive review. They are intended to provide rapid dissemination of current information.

This NAB aims at reporting drilling results at an early stage. Additional borehole-specific data will be published elsewhere.

In the event of inconsistencies between dossiers of this NAB, the dossier addressing the specific topic takes priority. In the event of discrepancies between Nagra reports, the chronologically later report is generally considered to be correct. Data sets and interpretations laid out in this NAB may be revised in subsequent reports. The reasoning leading to these revisions will be detailed there.

This Dossier was prepared by the Rock-Water Interaction Group of the University of Bern (authors are listed in the individual chapters). D. Traber was the responsible Nagra project manager.

The authors warmly acknowledge the laboratory work of:
P. Bähler and C. Pichler efficiently produced a substantial part of the data presented in this report.
U. Eggenberger, J. Krbanjevic, M. Wolffers J.W. Zucha and F. Gfeller provided data for mineralogical and BET analyses as well as evaluation tools.
D. Roos, J. Richards and L. de Doliwa Zielinski performed sampling and processing of the cores.
T. Oyama (CRIEPI, Japan) kindly collaborated in the context of porewater squeezing.

We also acknowledge the experimental and analytical work performed at Hydroisotop GmbH.

We are also grateful for the excellent work of the drill-site team who successfully provided sealed core samples according to our specifications.

N. Schwendener from IRM (University of Bern) provided X-ray CT scans of a substantial number of core samples, with support by L. Keller (ZHAW) for some of the CT sessions.

We thank P. Blaser and M. Unger for editorial work.

The comments and suggestions of Andreas Gautschi on an earlier version of the manuscript are gratefully acknowledged.

Table of Contents

List of Tables

List of Figures

Electronic Appendices

App. A Comprehensive data base with results of laboratory analyses (xls format)

App. B Detailed documentation of advective displacement experiments (xls format)

Note: The Appendices are available upon request.

1 Introduction

1.1 Context

To provide input for site selection and the safety case for deep geological repositories for radioactive waste, Nagra has drilled a series of deep boreholes ("Tiefbohrungen", TBO) in Northern Switzerland. The aim of the drilling campaign is to characterise the deep underground of the three remaining siting regions located at the edge of the Northern Alpine Molasse Basin (Fig. 1-1).

In this report, we present the results from the Bözberg-1-1 borehole.

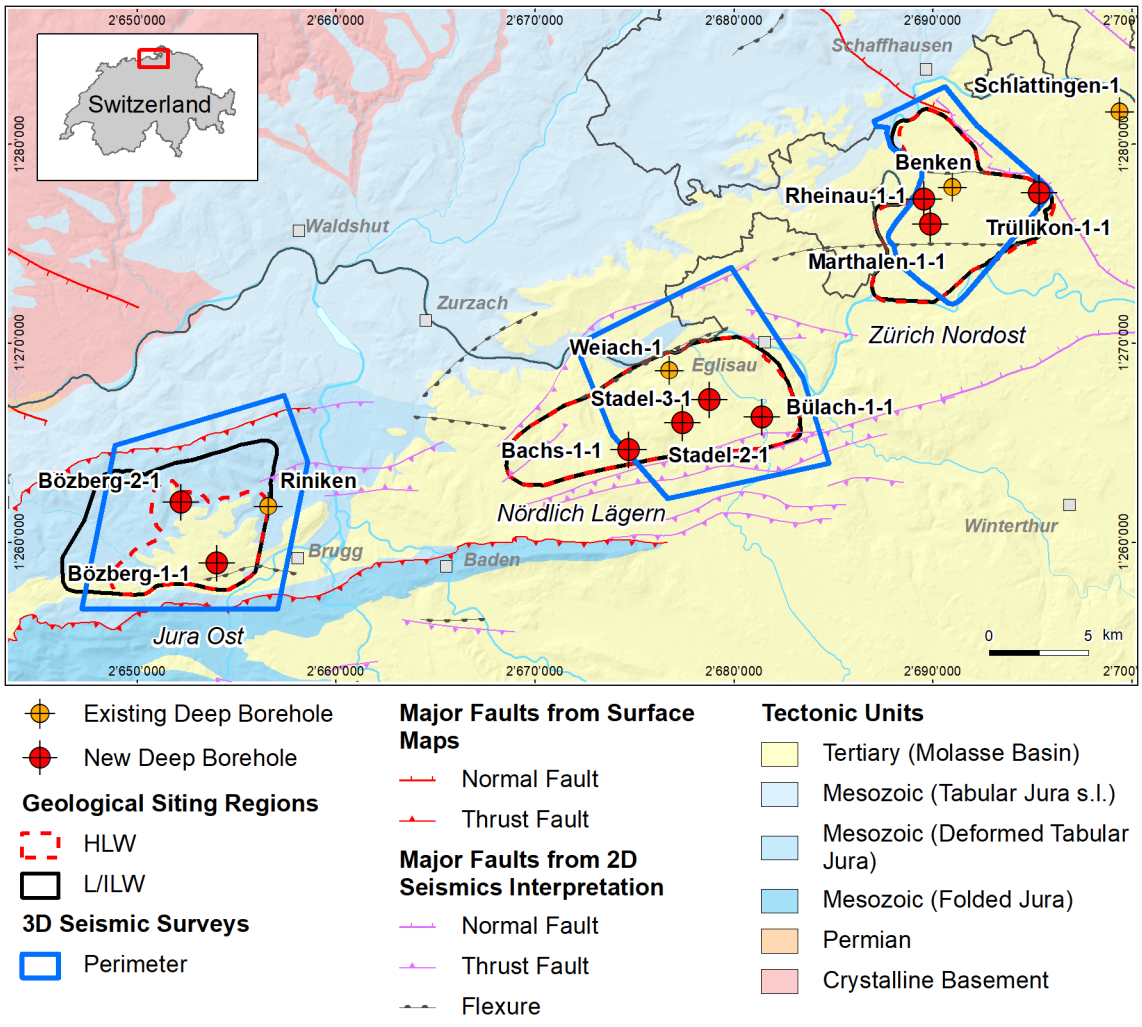

Fig. 1-1: Tectonic overview map with the three siting regions under investigation

1.2 Location and specifications of the borehole

The Bözberg-1-1 (BOZ1-1) exploratory borehole is the fourth borehole drilled within the framework of the TBO project. The drill site is located in the southern part of the Jura Ost siting region (Fig. 1-2). The borehole specifications are provided in Tab. 1-1.

Due to a lost packer system, the borehole was cemented up to 682 m MD[1] (*cf.* Dossier I). Resuming coring operations, a sidetrack was initiated with a kickoff point (KOP) at 709 m MD. This sidetrack was labelled Bözberg-1-1B (BOZ1-1B). BOZ1-1B reached a final depth of 1'037.39 m MD. For easier communication and labelling, the name BOZ1-1 is generally used for this borehole, including the sidetrack, unless stated otherwise.

Tab. 1-1: General information about the BOZ1-1 borehole

Siting region	Jura Ost
Municipality	Bözberg (Canton Aargau / AG), Switzerland
Drill site	Bözberg-1 (BOZ1)
Borehole	Bözberg-1-1 (BOZ1-1) including sidetrack Bözberg-1-1B (BOZ1-1B)
Coordinates	LV95: 2'653'995.815 / 1'258'925.446
Elevation	Ground level = top of rig cellar: 513.29 m above sea level (asl)
Borehole depth	1'037.39 m measured depth (MD) below ground level (bgl) for BOZ1-1B
Drilling period	27th April 2020 – 2nd December 2020 (spud date to end of rig release)
Drilling company	PR Marriott Drilling Ltd
Drilling rig	Rig-16 Drillmec HH102
Drilling fluid	Water-based mud with various amounts of different components such as[2]: 0 – 250 m: Polymers 250 – 882 m: Potassium silicate & polymers 882 – 1'037.39 m: Sodium chloride & polymers

The lithostratigraphic profile and the casing scheme are shown in Fig. 1-3. The comparison of the core versus log depth[3] of the main lithostratigraphic boundaries in the BOZ1-1 borehole is shown in Tab. 1-2.

[1] Measured depth (MD) refers to the position along the borehole trajectory, starting at ground level, which for this borehole is the top of the rig cellar. For a perfectly vertical borehole, MD below ground level (bgl) and true vertical depth (TVD) are the same. In all Dossiers depth refers to MD unless stated otherwise.

[2] For detailed information see Dossier I.

[3] Core depth refers to the depth marked on the drill cores. Log depth results from the depth observed during geophysical wireline logging. Note that the petrophysical logs have not been shifted to core depth, hence log depth differs from core depth.

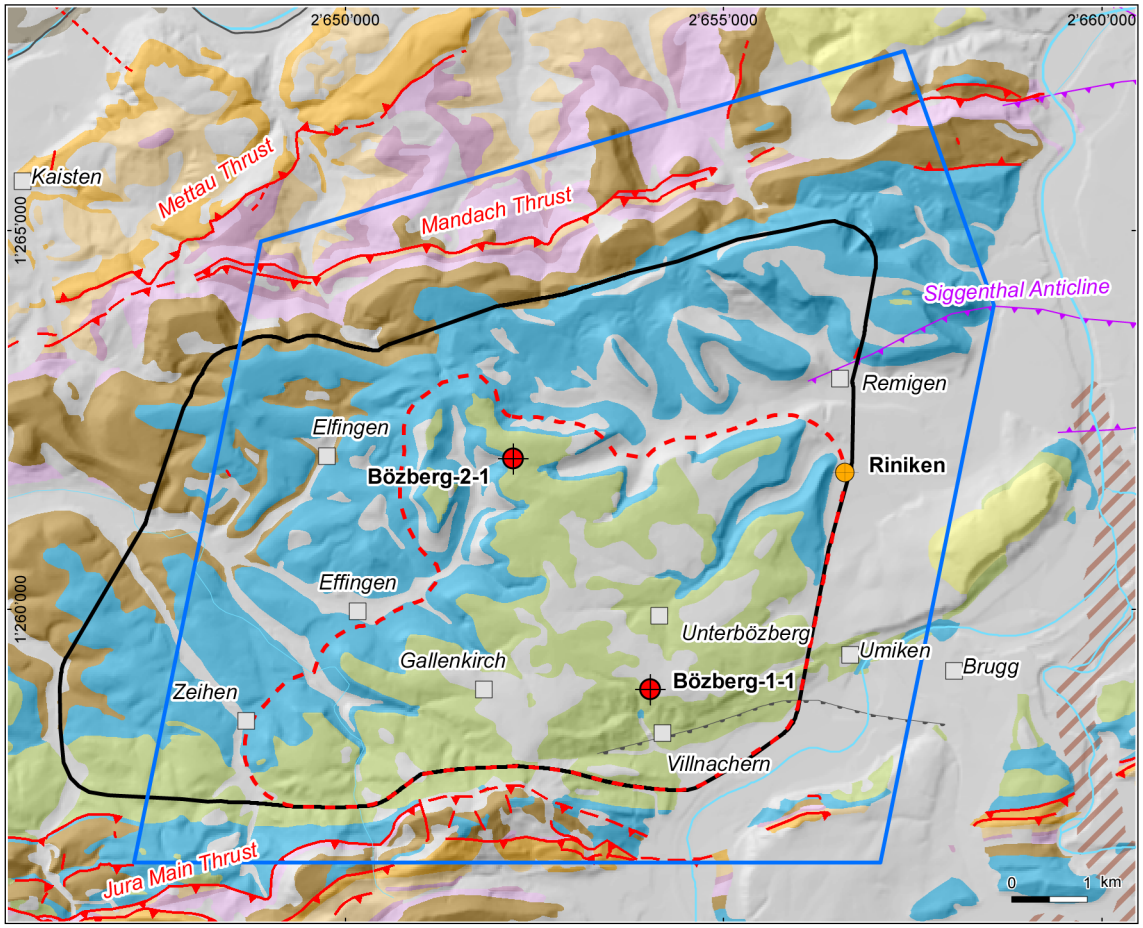

Fig. 1-2: Overview map of the investigation area in the Jura Ost siting region with the location of the BOZ1-1 borehole in relation to the boreholes Riniken and BOZ2-1

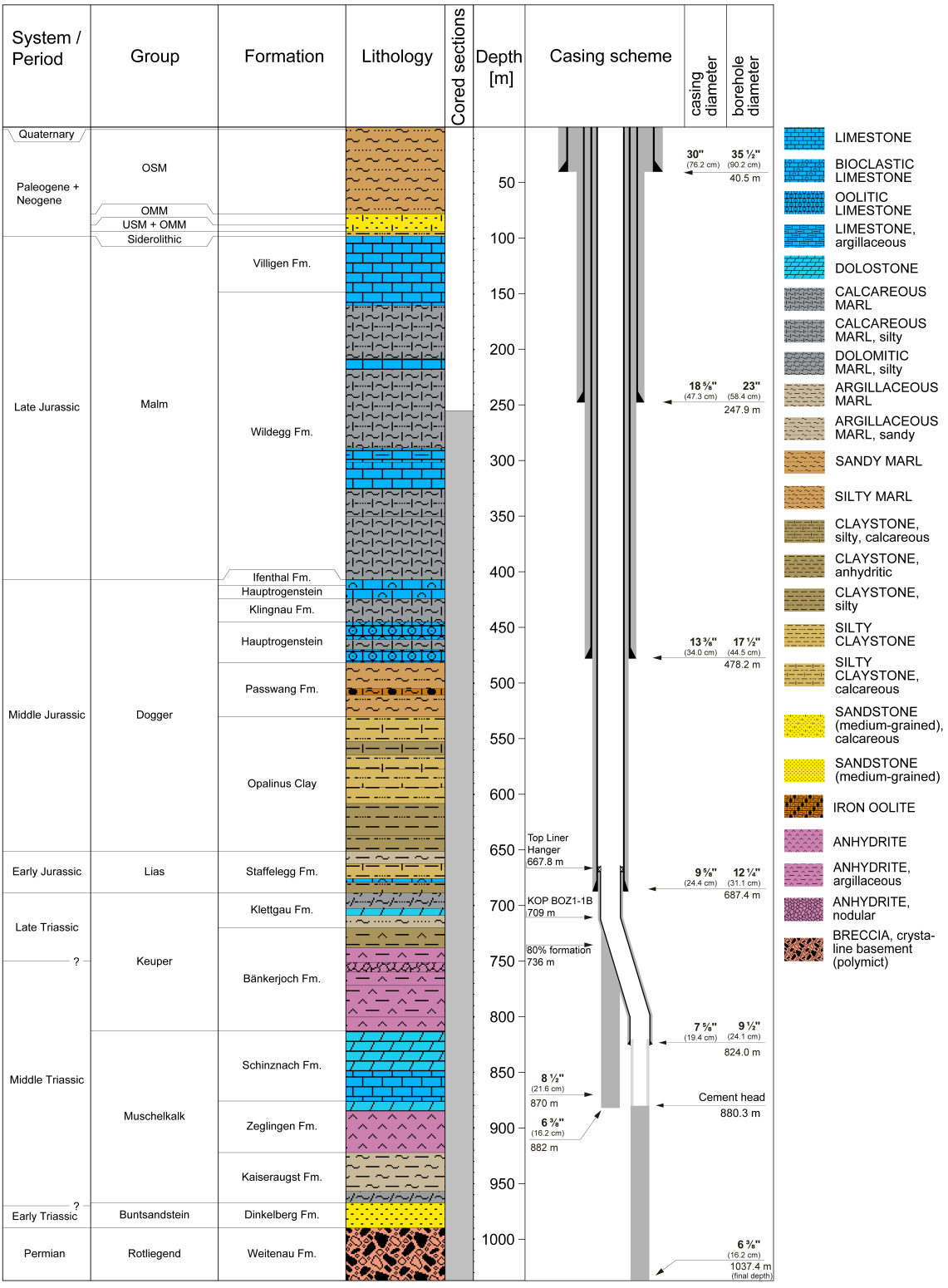

Fig. 1-3: Lithostratigraphic profile and casing scheme for the BOZ1-1 borehole[4]

[4] For detailed information see Dossier I and III.

Tab. 1-2: Core and log depth for the main lithostratigraphic boundaries in the BOZ1-1 borehole[5]

System / Period	Group	Formation	Core depth in m	Log depth in m (MD)	
Quaternary			**2**		—
Paleogene + Neogene	OSM		78		—
	OMM		88		—
	USM / OMM		94		—
	Siderolithic		**98**		—
Jurassic	Malm	Villigen Formation	148		—
		Wildegg Formation	406.67	406.72	—
	Dogger	Ifenthal Formation	411.91	411.94	—
		Hauptrogenstein	424.11	424.13	—
		Klingnau Formation	444.85	444.93	—
		Hauptrogenstein	481.50	481.55	—
		Passwang Formation	530.28	530.32	—
		Opalinus Clay	651.39	651.46	—
	Lias	Staffelegg Formation	**688.72**	**688.76**	—
Triassic	Keuper	Klettgau Formation	720.03	720.21	—
		Bänkerjoch Formation	812.62	812.45	—
	Muschelkalk	Schinznach Formation	875.89	876.05	—
		Zeglingen Formation	922.22	922.30	—
		Kaiseraugst Formation	967.38	967.70	—
	Buntsandstein	Dinkelberg Formation	**989.89**	**989.83**	—
Permian	Rotliegend	Weitenau Formation	1037.39 final depth		

[5] For details regarding lithostratigraphic boundaries see Dossier III and IV; for details about depth shifts (core goniometry) see Dossier V.

1.3 Documentation structure for the BOZ1-1 borehole

NAB 21-21 documents the majority of the investigations carried out in the BOZ1-1 borehole, including laboratory investigations on core material. The NAB comprises a series of stand-alone dossiers addressing individual topics and a final dossier with a summary composite plot (Tab. 1-3).

This documentation aims at early publication of the data collected in the BOZ1-1 borehole. It includes most of the data available approximately one year after completion of the borehole. Some analyses are still ongoing (e.g. diffusion experiments, analysis of veins, hydrochemical interpretation of water samples) and results will be published in separate reports.

The current borehole report will provide an important basis for the integration of datasets from different boreholes. The integration and interpretation of the results in the wider geological context will be documented later in separate geoscientific reports.

Tab. 1-3: List of dossiers included in NAB 21-21

Black indicates the dossier at hand.

Dossier	Title	Authors
I	TBO Bözberg-1-1: Drilling	M. Ammen, P.-J. Palten, J. Vliek, K. Gollob & K. Hilgendorf
II	TBO Bözberg-1-1: Core Photography	D. Kaehr & M. Gysi
III	TBO Bözberg-1-1: Lithostratigraphy	M. Schwarz, P. Schürch, H. Naef, P. Jordan, R. Felber, T. Ibele & M. Gysi
IV	TBO Bözberg-1-1: Microfacies, Bio- and Chemostratigraphic Analyses	S. Wohlwend, H.R. Bläsi, S. Feist-Burkhardt, B. Hostettler, U. Menkveld-Gfeller, V. Dietze & G. Deplazes
V	TBO Bözberg-1-1: Structural Geology	A. Ebert, L. Gregorczyk, S. Cioldi, E. Hägerstedt, & M. Gysi
VI	TBO Bözberg-1-1: Wireline Logging, Micro-hydraulic Fracturing and Pressure-meter Testing	J. Gonus, E. Bailey, J. Desroches & R. Garrard
VII	TBO Bözberg-1-1: Hydraulic Packer Testing	R. Schwarz, R. Beauheim, S.M.L. Hardie, M. Voß & A. Pechstein
VIII	TBO Bözberg-1-1: Rock Properties, Porewater Characterisation and Natural Tracer Profiles	P. Wersin, L. Aschwanden, L. Camesi, E.C. Gaucher, T. Gimmi, A. Jenni, M. Kiczka, U. Mäder, M. Mazurek, D. Rufer, H.N. Waber, C. Zwahlen & D. Traber
IX	TBO Bözberg-1-1: Rock-mechanical and Geomechanical Laboratory Testing	E. Crisci, L. Laloui & S. Giger
X	TBO Bözberg-1-1: Petrophysical Log Analysis	S. Marnat & J.K. Becker
	TBO Bözberg-1-1: Summary Plot	Nagra

1.4 Scope and objectives of this dossier

The dossier at hand summarises the laboratory work of the Rock-Water Interaction Group (RWI) of the University of Bern, Institute of Geological Sciences, dedicated to rock and porewater characterisation of core materials obtained from the BOZ1-1 borehole. The level of ambition is to document observations and measurements and to provide a quality-assured dataset. Closely related data obtained by other laboratories (e.g. CEC data by PSI) are integrated with our data.

Data are evaluated and discussed to some degree, including consistency and plausibility checks. An in-depth discussion, sophisticated modelling efforts and regional comparisons with data from other sites are beyond the scope of this report. Additional data obtained by other groups (e.g. hydraulic tests, groundwater sampling, geophysical borehole and core logging, structural logging) are considered in several cases but not in a comprehensive way. An integrated interpretation of all available data is deferred to a later stage of the TBO programme, when results from several boreholes can be synthesised for a siting region.

Throughout this report, rock samples used for analysis are identified by their mid-sample depth in m.

2 Geoscientific data available for the BOZ1-1 borehole

Paul Wersin, Martin Mazurek, Lukas Aschwanden, Eric C. Gaucher

2.1 Geological information

The BOZ1-1 borehole is located in the southern part of the siting region Jura Ost close to the village of Villnachern (Fig. 1-1). Jura Ost lies in the Deformed Tabular Jura between the autochthonous Tabular Jura in the NW and the Folded Jura in the south. The Deformed Tabular Jura is delineated by the E-W running Jura Main Thrust about 2 km south of BOZ1-1 and the Mandach Thrust (WSW-ENE) to the north. It borders the Wölflinswil Graben to the west and the Siggenthal Anticline to the east. Tectonically, the Deformed Tabular Jura is compressively overprinted by the Alpine forefront.

According to seismic interpretations, no relevant faults have been revealed in the Mesozoic layers at the borehole location. However, field and seismic data indicate the occurrence of NNE-SSW striking subvertical strike-slip faults (Madritsch & Hammer 2012). The regional dip of the Mesozoic layers is subhorizontal towards the SE.

2.2 Hydrogeological conditions

Tab. 2-1 gives a summary of the hydraulic tests performed. The results of the hydraulic packer tests in the BOZ-1 borehole and of the fluid logging in the Malm aquifer are documented in Dossier VII.

Fluid logging in the Malm was conducted from 252 to 480 m depth. The main inflow zone in this interval was at about 310 m depth, a second inflow zone was identified at about 410 m depth. The main inflow zone was subsequently investigated with a double packer test. The transmissivity was too low to sample groundwater.

Tab. 2-1: Results of hydraulic packer tests in borehole BOZ1-1

The best estimates for transmissivity T, hydraulic conductivity K and hydraulic head are indicated. Hydraulic heads in the clay-rich formations are believed to be affected by transient hydromechanical processes. See Dossier VII for further details.

Top [m MD]	**Bottom** [m MD]	**Length** [m]	**Geological units**	**T** [m^2/s]	**K** [m/s]	**(Apparent) Head** [m asl]
300.92	328.24	27.32	Wildegg Fm.	3E-08	1E-09	364
492.05	511.05	19.00	Passwang Fm.	1E-12	6E-14	556
511.15	530.14	18.99	Passwang Fm.	3E-12	1E-13	505
538.00	557.00	19.00	Opalinus Clay	1E-12	6E-14	626
538.00	557.00	19.00	Opalinus Clay	1E-12	6E-14	626
602.35	608.10	5.75	Opalinus Clay	2E-13	4E-14	660
651.00	674.14	23.14	Staffelegg Fm.	8E-13	3E-14	831
674.00	690.00	16.00	Staffelegg Fm.	3E-11	2E-12	643
702.10	720.59	18.49	Klettgau Fm. – Bänkerjoch Fm. (Keuper aquifer)	6E-11	3E-12	463
845.69	867.00	21.31	Schinznach Fm. (Muschelkalk aquifer)	5E-05	2E-06	393
845.78	882.00	36.22	Schinznach Fm. – Zeglingen Fm. (Muschelkalk aquifer)	9E-06	3E-07	397

2.3 Groundwater samples

Groundwater samples with variable degrees of drilling-fluid contamination were obtained from the Muschelkalk aquifer. Note that in this unit two important fault zones occur (Section 2.4) and large mud losses were experienced (Section 2.5). The sequence of groundwater sampling was done in the two fault zones, with a first packer interval named MUK1 (845.69 – 867.00 m) and a second packer interval named MUK2 (845.78 – 882.00 m). The sample from MUK2 was selected for further analysis and interpretation. The groundwater is highly contaminated by the drilling mud with a remaining tracer (uranine) representing a contamination of 19.6% (Lorenz et al., *in prep.*) in the last GW samples. The very high value of pH (11.2), the abnomalous concentrations of K (8 g/L) and Si (1 g/l) confirm this contamination by the alkaline drilling mud (pH 12.3; K 60 g/L, Si 37 g/L). This high contribution of the drilling mud makes the decontamination process relatively uncertain.

For the present report, values for the chemically conservative parameters Cl and Br and the water-isotope ratios $\delta^{18}O$ and $\delta^{2}H$ are of interest, as these serve as boundary conditions for the porewater data. These values are reproduced in Tab. 2-2 along with information on the chemical water type and mineralisation of the groundwater.

Tab. 2-2: Conservative parameters for groundwater from the Muschelkalk aquifer corrected for drilling-fluid contamination (extrapolated values), test interval MUK2

Parameter	**Unit**	**Muschelkalk aquifer**
Test interval		845.78 – 882.00 m
Chemical type		**Na-Cl (Ca-SO_4)**
Mineralisation (TDS)	[g/L]	21
Chloride (Cl^-)	[mg/L]	9'731 to 10'046
Bromide (Br^-)	[mg/L]	0.81 to 0.82
$\delta^{18}O$ of water	[‰$_{VSMOW}$]	-10.17 to -10.02
$\delta^{2}H$ of water	[‰$_{VSMOW}$]	-74.1 to -72.9

2.4 Structural logging

The results of structural core logging are documented in Dossier V, where the following types of structural features are distinguished:

- Fault planes and fault zones (shear structures); these are mainly oriented parallel or sub-parallel to bedding
- Brittle extensional fractures (structures without shear or slip indication, e.g. joints, veins, tension gashes), these exhibit large variation in orientation and dip (1 – 90°).
- Stylolites, two classes with two different orientation and dipping trends
- Larger open pores.

High numbers of natural structures were encountered in the Wildegg Formation, the Keuper (Klettgau Formation, Bänkerjoch Formation) and the Muschelkalk (Schinznach Formation, Zeglingen Formation, Kaiseraugst Formation). Particularly, in the carbonates of the lowermost Schinznach Formation and the uppermost Zeglingen Formation from 859.80 m to 882.00 m MD (core depth) high abundancies of subvertical, NNW-SSE striking fractures and open tension gashes are observed – some constitute prominent fracture zones. Furthermore, a 41.25 m thick fault zone was identified in the Zeglingen Formation from 883.75 m to 915.54 m depth. A compilation of all individual fault zones and mirror-like fault zones encountered at BOZ1-1 is provided in Tab. 2-3.

Tab. 2-3: Fault zones and mirror-like fault planes (MirFP) zones in the cored section of the BOZ1-1 borehole (Dossier V)

Top [m MD]	**Bottom** [m MD]	**Thickness** [m]	**Formation**	**Type**
269.9	271.23	1.33	Wildegg Formation	Fault zone
318.31	318.56	0.25	Wildegg Formation	Fault zone
334.64	334.7	0.06	Wildegg Formation	Fault zone
411.66	411.69	0.03	Iffenthal Formation	MirFP zone
437.78	437.9	0.12	Klingnau Formation	Fault zone
445.41	445.49	0.08	Hauptrogenstein	Fault zone
515.01	515.07	0.06	Passwang Formation	MirFP zone
611.71	611.8	0.09	Opalinus Clay	Fault zone
679.14	679.15	0.01	Staffelegg Formation	MirFP zone
679.27	679.35	0.08	Staffelegg Formation	Fault zone
685.65	685.97	0.32	Staffelegg Formation	Fault zone
688.54	688.76	0.22	Staffelegg Formation / Klettgau Formation	Fault zone
699.23	699.45	0.22	Klettgau Formation	MirFP zone
709.22	709.69	0.47	Klettgau Formation	MirFP zone
716.73	716.75	0.02	Klettgau Formation	Fault zone
720.31	720.7	0.39	Bänkerjoch Formation	MirFP zone
725.35	725.5	0.15	Bänkerjoch Formation	MirFP zone
727.75	727.93	0.18	Bänkerjoch Formation	MirFP zone
742.77	742.83	0.06	Bänkerjoch Formation	Fault zone
786.11	786.52	0.41	Bänkerjoch Formation	MirFP zone
787.97	788.03	0.06	Bänkerjoch Formation	MirFP zone
792.16	794.66	2.5	Bänkerjoch Formation	MirFP zone
798.6	802	3.4	Bänkerjoch Formation	Fault zone
804.39	804.8	0.41	Bänkerjoch Formation	MirFP zone
850.27	851.52	1.25	Schinznach Formation	Fault zone
856.51	857.19	0.68	Schinznach Formation	Fault zone
883.75	915.54	31.79	Zeglingen Formation	Fault zone
955.47	961.21	5.74	Kaiseraugst Formation	MirFP zone
961.83	961.89	0.06	Kaiseraugst Formation	MirFP zone
965.58	965.71	0.13	Kaiseraugst Formation	MirFP zone

2.5 Drilling conditions and drilling muds

Paul Wersin

After destructive drilling down to 250 m depth a wireline coring technique with a triple core barrel was used for BOZ1-1 (Dossier I). The drilling mud for the cored section of BOZ1-1 was a K-silicate polymer from 250 to 882 m (Tab. 2-4). Considerable mud losses started to occur in the fractures of the Muschelkalk, continuing further down and resulting in a total mud loss of ~ 119 m^3. At 882 m, the borehole was cemented back, and a sidetrack (BOZ1-1B) was drilled, using NaCl polymer as drilling mud, starting coring from 825 m depth and reaching the final depth at 1'037 m. Further considerable mud losses occurred in the Dinkelberg Formation (~ 278 m^3).

The composition of the K silicate polymer is listed in Tab. 2-5. Besides K silicate, the mud contains Xanthan gum (Flowzan, a biopolymer), soda ash and other conditioners for achieving the desired density and viscosity/rheology.

Tab. 2-4: Drilling muds and depth intervals and main mud loss events

Depth interval [m]	**Geological unit**	**Drilling mud**	**Comments**
0 – 250	Quaternary – Malm	Pure Bore	Destructive drilling
250 – 882	Malm – Schinznach Fm.	Potassium silicate	Large mud loss (65.3 m^3) at 859.80 – 882.24 m in fracture zone in the Schinznach Fm. (total mud loss in Muschelkalk (119 m^3)
825 – 1'037	Schinznach Fm. – Weitenau Fm.	NaCl polymer	Side track BOZ1-1B, dynamic mud loss (273 m^3) from 996 – 1'037 m depth, probably mainly caused by fracture zone at 996 m

Tab. 2-5: Composition of K polymer drilling mud (Lorenz et al. *in prep.*)

Parameter	**Units**	**K-silicate**
Depth	[m]	845.69 – 867.00
pH		12.3
EC	[µS/cm]	85'900
uranine	[ppb]	1'307
Alk (pH 8.2)	[meq/l]	1'163
DOC	[mg/L]	2'780
Na	[mg/L]	1'762
K	[mg/L]	59'921
NH_4	[mg/L]	< 1
Ca	[mg/L]	57
Mg	[mg/L]	10.1
Si	[mg/L]	37'327
Cl	[mg/L]	442
SO_4	[mg/L]	7'024
NO_3	[mg/L]	12.8
Br	[mg/L]	< 1
F	[mg/L]	< 1
Sr	[mg/L]	1.16
Ba	[mg/L]	0.9

The values are the mean of 5 analyses of samples taken in the suction pit and in the shaker for the mud monitoring. First sample 18/09/2020 22:30, last sample 25/09/2020 23:30.

3 Sampling and applied methods

3.1 Sampling strategy

Paul Wersin

A suite of 8 different sample types were investigated (Tab. 3-1). Sample types and the general procedures of core sampling, sample conditioning and storage are described by Rufer (2019).

Tab. 3-1: Sample types and sampling strategy

Sample type	**Main study targets**	**Sampling (by on-site team)**
RP (various rock properties), PW (porewater chemistry)	Characterisation of rock and porewater chemistry	Sample lithology representative of the current lithofacies and the sampled core section (usually 3 m). Sampling with a regular spacing in order to obtain a representative data set
SQ (squeezing)	Characterisation of porewater chemistry	Focussed on clay-rich lithologies due to methodological constraints
AD (advective displacement)	Characterisation of porewater chemistry	Focussed on clay-rich lithologies due to methodological constraints
DI (diffusion experiments)	Diffusion coefficients, cation exchange & sorption parameters at PSI	Coverage of a wide range of lithologies (in particular clay-mineral contents)
OD (out-diffusion)	Characterisation of porewater chemistry	Focussed on clay-poor lithologies due to methodological constraints
NG (noble gas analysis)	Concentrations and isotopic compositions of dissolved noble and reactive gases	Sampling with a regular spacing, with situational tightening of the sampling interval close to potentially water-conducting features
GM (geomechanics)	Mineralogy and grain density of samples studied for their geomecha-nical properties by other laboratories	Representative sampling of the most relevant lithologies within the Opalinus Clay
V	Petrography, structure, and geochemistry of veins	Opportunistic sampling at later stages

3.2 Laboratory programme

Paul Wersin

In total, 245 samples were investigated, and Tab. 3-2 provides an overview. Samples of types RP, PW, SQ, AD, DI, NG and GM were all investigated by RWI (main studies of DI and GM samples were performed by other laboratories; see Tab. 3-1). In Tab. 3-3, the analytical programme for the various sample types and the different laboratories is shown in more detail.

Tab. 3-2: Numbers of samples analysed for the different geological units
In the case of the NG samples, the number refers to the total number of samples collected.

Unit	**RP, PW**	**SQ**	**AD**	**DI**	**OD**	**NG**	**GM**	**V**	**Total**
Wildegg Fm.	14			9		6		9	23
Ifenthal Fm.						1			0
Hauptrogenstein	9		1	2	1	2		2	13
Klingnau Fm.	4			3	1	1		2	8
Passwang Fm.	17	2	2	7	1	4			29
Opalinus Clay	20	5	1	11		7	4	9	37
Staffelegg Fm.	13	1	1	5		2		3	20
Klettgau Fm.	6		1	2		3			9
Bänkerjoch Fm.	10			3		5			13
Schinznach Fm.	5					5			5
Zeglingen Fm.	4					3			4
Kaiseraugst Fm.	4					2			4
Dinkelberg Fm.	2					2			2
Weitenau Fm.	3					2			3
All	111	8	6	42	3	45	4	25	245

Tab. 3-3: Analytical programme performed for the different sample types
××: standard programme, ×: selected samples only, calc.: calculated.

Method	**PW, RP**	**SQ**	**AD**	**DI**	**OD**	**NG**	**GM**
Bulk mineralogical composition incl. CNS analysis	××	××	××	××	×		××
Clay mineralogy			××	××			
Bulk wet density	××		calc.		×	calc.	
Grain density	××		calc.	××	×		××
Water content	××	××	××	××	×	××	
BET surface area				××			
Cation-exchange properties			××	×*			
Aqueous extraction	××	××	××				
Porewater squeezing		××					
Advective displacement of porewater			××				
Out-diffusion experiments					××		
Water isotopes	××	××	××				
Chlorine-37	×						
Dissolved noble gases						×	
Dissolved reactive gases						×**	

* Subsamples collected during sample preparation, re-packed and sent to PSI for analysis

** planned

3.3 Analytical methods and methods of raw-data processing

Paul Wersin

Experimental procedures of RWI and associated analytical methods, formalisms to process measured data and quantification of propagated errors are documented in Waber (ed.) (2020) and are not repeated here. Moreover, Mazurek et al. (2021) provide additional information for situations where the current practice is not documented or deviates from that described in Waber (ed.) (2020).

For aqueous extraction, an alternative approach with a modified procedure regarding sample preparation was applied for selected samples. This consisted in extracting the same subsample that had been heated for water content determination. The reasoning behind was to reduce the uncertainty related to the water content in the standard procedure which can be considerable, in particular for samples with low water contents. Aliqouts of ~ 30 g of dry rock sample (after water content determination) were contacted with ~ 30 g of degassed O_2- and CO_2-free ultrapure water, extracted by the standard procedure (Waber (ed.) 2020) and anaylsed for Cl, Br, and SO_4 with ion chromatography. Note that due to the previous heating under air, oxidation of sulfide had modified the SO_4 contents in the rock sample. Also, this may have altered the organic carbon fraction, which may have affected some of the Br data (Section 5.2).

4 Results

4.1 Documentation of measured and calculated data

Paul Wersin

Raw data collected in the frame of the analytical programme are organised in a FileMaker data base, including raw-data files, graphics and photographs. The main purpose of this data base is to ensure the full documentation and traceability of original and derived data presented in this report. From this data base, the relevant data were exported into a comprehensive Excel sheet, which is attached in Appendix A. The objective of this sheet is not to fully document all analyses made but, per parameter and sample, to indicate the "best" or most representative value in case multiple measurements were made, and to list parameters calculated from the original measurements. For example, only one composition is given for squeezed and advectively displaced porewaters in a sample, even though multiple aliquots were collected and analysed. Explanatory notes to this sheet follow here.

Bulk mineralogy (X-ray diffraction and CNS analysis)

- Contents of minerals not detected by X-ray diffraction are set to 0, as the actual detection limits are difficult to quantify. "tr" = present in trace amounts.
- Clay-mineral content is not measured directly but is calculated by difference to 100%.
- Pyrite content is calculated from the measured S content, assuming that pyrite is the main S reservoir in the rock. This is not the case in anhydrite-bearing rocks, which are typically free of pyrite. Here, the S is used to calculate the content of anhydrite.
- Column "Füchtbauer name" refers to the nomenclature of clastic rocks as defined in Naef et al. (2019). Names are listed only for rock compositions that have < 10 wt.-% minerals not represented in the Füchtbauer triangle (i.e. minerals other than clays, calcite, dolomite/ ankerite, siderite, quartz, K-feldspar, plagioclase). In particular, this means that evaporitic rocks are not given a Füchtbauer name. If a rock contains ≥ 90 wt.-% minerals represented in the Füchtbauer triangle but also contains anhydrite, this is stated in brackets.
- The Füchtbauer triangle does not distinguish between limestones and dolostones. In cases when the contents of calcite exceed those of dolomite/ankerite, the terms "limestone" or "calcareous" are used in this report, and "dolostone" or "dolomitic" are used if the opposite applies.

Clay mineral groups

- All data refer to wt.-% of the total rock.
- Illite/smectite ML (85-90) refers to a mixed-layer phase with 85 – 90% illite layers, Chl/Sm ML (85-95) designates a chlorite-smectite mixed-layer phase with 85 – 95 % chlorite (analogous for the other listed mixed-layer phases).

End-member clays

- All data refer to wt.-% of the total rock.
- Illite, smectite and chlorite partially occur in mixed-layer phases. Here, the respective total contents of the end members are calculated. For example, if a sample contains 10 wt.-% illite and 8 wt.-% illite/smectite mixed layers containing 75% illite, the end-member illite content would be 16 wt.-%.

Petrophysical parameters

- Bulk wet density was measured, and bulk dry density was calculated using equation 5-14 in Waber (ed.) (2020).
- Pycnometer porosity was calculated from densities using equation 5-16 in Waber (ed.) (2020).
- Water content (dry) was calculated from water content (wet) using $w_d = w_w/(1-w_w)$.
- Water-loss porosity was calculated using bulk wet density (equation 5-9 in Waber ed. 2020) or grain density (equation 5-7 in Waber ed. 2020).
- The formalisms to calculate water content from isotope diffusive exchange experiments are detailed in Mazurek et al. (2021).

Cl^- and Br^- from aqueous extracts recalculated to pore-water concentrations using water content

- Concentrations are given relative to bulk porewater as well as relative to various assumptions regarding anion accessibility in the pore space. The calculation is made using equation 6-1 in in Waber (ed.) (2020). The variants pertaining to the dependence of anion accessibility on clay-mineral content are discussed in Chapter 5.
- In case of aqueous extracts obtained from the subsamples on which water contents had been determined, the corresponding Cl^- and Br^- are used for recalculation to pore-water concentrations.

Errors

- The error columns refer to analytical uncertainty or instrument precision for measured parameters and to propagated errors for calculated parameters, following the formalisms documented in Waber (ed.) (2020) and Appendices A and B.

4.2 Mineralogical composition

Martin Mazurek

4.2.1 Whole rock

A total of 172 mineralogical analyses were performed in the section Malm – Permian. The full dataset is documented in Appendix A, and Tab. 4.2-1 provides formation-specific summaries. The depth trends for the most relevant minerals are shown graphically in Fig. 4.2-1, and a representation in the Füchtbauer triangle is given in Fig. 4.2-3. The Dinkelberg Formation ('Buntsandstein') and the Permian Weitenau Formation are dominated by clastic minerals, i.e. quartz, feldspars and clay minerals, and thus correspond to siltstones/sandstones in the Füchtbauer nomenclature. A sharp upwards decrease in clay-mineral content is observed in the interval Kaiseraugst Formation – Zeglingen Formation. A minimum in clay-mineral content can be seen at the base of the Schinznach Formation, from where the values increase towards the top of the Bänkerjoch Formation (but some outliers do occur). Much of the lithological heterogeneity in the Triassic is due to the highly variable contents of anhydrite and dolomite. Less heterogeneity but systematic depth trends are found in the overlying Dogger – Lias section, and these are discussed in detail further below. In the Wildegg Formation, a zigzag depth pattern composed of 3 trend lines is observed for the major constituents: quartz and clay-mineral contents increase upwards until reaching a maximum at about 340 m. Then the values decrease until a minimum at about 310 m, from where they increase again. Calcite contents show reversed trend lines.

The depth profiles of the contents of S and N (based on CNS analysis) are shown in Fig. 4.2-2. S contents are ≤ 0.5 wt.-% in the Wildegg Formation and in the Triassic (excluding anhydrite-bearing samples), with the exception of the Kaiseraugst Formation. Higher contents are only found in the Dogger–Lias section (particularly in the Passwang Formation and the Staffelegg Formation), consistent with the generally reducing depositional environment in this period (S is attributed mainly to diagenetic pyrite). The contents of N are < 0.05 wt.-% in the Wildegg Formation and below detection in the Hauptrogenstein and the entire Triassic and Permian (with exceptions in the upper part of the Klettgau Formation). A steady upwards decrease is observed in the interval Opalinus Clay – Passwang Formation, starting with a maximum at the top of the clay-rich sub-unit, i.e. in the lowermost part of the Opalinus Clay. The highest values are found in the Rietheim Member of the Staffelegg Formation. A general positive correlation exists with the content of C(org).

Tab. 4.2-1: Bulk-rock mineralogy: formation-specific means, medians, standard devations and ranges [wt.-%]

In addition to the listed phases, one sample from the Dinkelberg Formation contains 1 wt.-% barite, and one sample from the Bänkerjoch Formation contains 1 wt.-% celestite. For the calculation of statistical parameters, values below detection were set to 0. In several cases, systematic depth trends of mineral contents were observed (see below). This means that in these cases the data do not follow a Gaussian distribution, which is a pre-requisite for the calculation of meaningful standard deviations. In such cases, the ranges (also listed) are more meaningful.

Formation (number of analyses)	**Member**		**S** [wt.-%]	**N** [wt.-%]	**C(inorg)** [wt.-%]	**C(org)** [wt.-%]	**Quartz** [wt.-%]	**K-feldspar** [wt.-%]	**Plagioclase** [wt.-%]	**Calcite** [wt.-%]	**Dolomite/Ank.** [wt.-%]e	**Siderite** [wt.-%]	**Magnesite** [wt.-%]	**Anhydrite** [wt.-%]	**Goethite** [wt.-%]	**Haematite** [wt.-%]	**Pyrite** [wt.-%]	**Clay minerals** [wt.-%]
Wildegg Fm. (23)		Mean	0.15	0.01	8.22	0.42	7.3	2.4	0.3	66.7	1.6	0.0	0.0	0.0	0.0	0.0	0.3	21.0
		Median	0.11	0.00	8.04	0.42	7.3	2.5	0.0	63.6	1.5	0.0	0.0	0.0	0.0	0.0	0.2	21.7
		Stdev	0.14	0.02	1.69	0.07	3.4	1.6	0.5	14.6	1.7	0.0	0.0	0.0	0.0	0.0	0.3	9.7
		Min	0.00	0.00	5.64	0.28	1.3	0.0	0.0	46.2	0.0	0.0	0.0	0.0	0.0	0.0	0.0	4.7
		Max	0.50	0.04	11.2	0.61	11.9	4.6	1.5	93.6	5.9	0.0	0.0	0.0	0.0	0.0	0.9	40.3
Hauptrogenstein (all) (13)		Mean	0.27	0.00	8.72	0.35	5.1	0.9	0.2	68.7	3.7	0.0	0.0	0.0	1.3	0.0	0.5	19.2
		Median	0.25	0.00	9.52	0.31	4.0	0.7	0.0	74.4	3.7	0.0	0.0	0.0	0.0	0.0	0.5	15.0
		Stdev	0.29	0.01	1.63	0.15	3.1	1.1	0.5	11.9	3.1	0.0	0.0	0.0	3.4	0.0	0.5	9.2
		Min	0.00	0.00	4.79	0.11	2.1	0.0	0.0	39.9	0.0	0.0	0.0	0.0	0.0	0.0	0.0	11.8
		Max	0.96	0.04	10.1	0.57	13.0	3.0	1.3	80.6	9.1	0.0	0.0	0.0	11.0	0.0	1.8	41.8
Hauptrogenstein (3)	Upper ('Spatkalk')	Mean	0.00	0.00	9.09	0.19	2.9	0.7	0.0	70.4	4.9	0.0	0.0	0.0	5.7	0.0	0.0	15.2
		Median	0.00	0.00	9.12	0.17	2.1	0.7	0.0	69.9	5.6	0.0	0.0	0.0	6.0	0.0	0.0	15.0
		Stdev	0.00	0.00	0.44	0.08	1.3	0.8	0.0	8.6	4.6	0.0	0.0	0.0	5.5	0.0	0.0	0.8
		Min	0.00	0.00	8.65	0.11	2.1	0.0	0.0	62.1	0.0	0.0	0.0	0.0	0.0	0.0	0.0	14.5
		Max	0.00	0.00	9.52	0.28	4.4	1.5	0.0	79.3	9.1	0.0	0.0	0.0	11.0	0.0	0.0	16.0
Klingnau Fm. (8)		Mean	0.61	0.00	7.49	0.43	6.6	1.5	0.3	58.7	3.3	0.1	0.0	0.0	1.1	0.0	1.1	26.7
		Median	0.30	0.00	7.47	0.40	5.4	1.6	0.0	56.0	4.1	0.0	0.0	0.0	0.5	0.0	0.6	27.6
		Stdev	0.77	0.00	1.60	0.14	3.3	1.6	0.5	13.3	2.9	0.4	0.0	0.0	1.7	0.0	1.4	8.4
		Min	0.00	0.00	4.47	0.33	4.1	0.0	0.0	37.3	0.0	0.0	0.0	0.0	0.0	0.0	0.0	14.3
		Max	2.26	0.00	9.64	0.76	14.0	4.7	1.2	80.3	6.9	1.2	0.0	0.0	5.0	0.0	4.2	39.0
Hauptrogenstein (10)	Lower	Mean	0.35	0.00	8.61	0.40	5.8	1.0	0.3	68.2	3.3	0.0	0.0	0.0	0.0	0.0	0.7	20.4
		Median	0.28	0.00	9.61	0.32	4.5	0.4	0.0	74.9	3.4	0.0	0.0	0.0	0.0	0.0	0.5	15.2
		Stdev	0.28	0.01	1.85	0.13	3.2	1.2	0.5	13.1	2.8	0.0	0.0	0.0	0.0	0.0	0.5	10.3
		Min	0.00	0.00	4.79	0.24	3.4	0.0	0.0	39.9	0.0	0.0	0.0	0.0	0.0	0.0	0.0	11.8
		Max	0.96	0.04	10.1	0.57	13.0	3.0	1.3	80.6	7.8	0.0	0.0	0.0	0.0	0.0	1.8	41.8
Passwang Fm. (29)		Mean	0.86	0.03	3.46	0.63	23.5	4.3	2.4	28.6	0.3	0.0	0.0	0.0	0.0	0.0	1.6	38.8
		Median	0.70	0.04	3.48	0.64	21.5	5.1	2.7	29.0	0.0	0.0	0.0	0.0	0.0	0.0	1.3	39.6
		Stdev	0.43	0.02	1.93	0.18	8.6	1.8	1.3	15.9	0.9	0.0	0.0	0.0	0.0	0.0	0.8	10.5
		Min	0.19	0.00	0.37	0.20	10.9	0.0	0.0	3.1	0.0	0.0	0.0	0.0	0.0	0.0	0.4	10.2
		Max	2.02	0.06	7.81	0.96	45.2	6.4	4.4	65.1	4.5	0.0	0.0	0.0	0.0	0.0	3.8	56.0
Opalinus Clay (37)	All	Mean	0.40	0.06	1.34	0.89	21.0	4.8	2.8	8.6	0.2	2.7	0.0	0.0	0.0	0.0	0.7	58.2
		Median	0.32	0.07	1.19	0.88	20.8	4.9	2.9	7.6	0.0	3.1	0.0	0.0	0.0	0.0	0.6	61.0
		Stdev	0.33	0.01	0.44	0.17	5.5	1.2	0.6	4.2	0.8	2.1	0.0	0.0	0.0	0.0	0.6	9.0
		Min	0.04	0.00	0.69	0.58	14.4	0.0	0.0	3.1	0.0	0.0	0.0	0.0	0.0	0.0	0.1	35.5
		Max	1.49	0.08	2.79	1.50	32.4	6.5	4.0	18.8	4.1	7.4	0.0	0.0	0.0	0.0	2.8	69.0

Tab. 4.2-1: (continued)

Formation (number of analyses)	**Member**		**S** [wt.-%]	**N** [wt.-%]	**C(inorg)** [wt.-%]	**C(org)** [wt.-%]	**Quartz** [wt.-%]	**K-feldspar** [wt.-%]	**Plagioclase** [wt.-%]	**Calcite** [wt.-%]	**Dolomite/Ank.** [wt.-%]e	**Siderite** [wt.-%]	**Magnesite** [wt.-%]	**Anhydrite** [wt.-%]	**Goethite** [wt.-%]	**Haematite** [wt.-%]	**Pyrite** [wt.-%]	**Clay minerals** [wt.-%]
Opalinus Clay (9)	Sub-unit with silty calcar-eous beds	Mean	0.68	0.05	1.80	0.98	25.8	4.6	2.6	13.5	0.5	1.2	0.0	0.0	0.0	0.0	1.3	49.6
		Median	0.37	0.06	1.68	0.92	27.2	5.1	2.8	14.0	0.0	0.0	0.0	0.0	0.0	0.0	0.7	48.4
		Stdev	0.52	0.02	0.47	0.28	3.8	1.9	1.0	3.9	1.4	1.8	0.0	0.0	0.0	0.0	1.0	8.5
		Min	0.10	0.00	1.29	0.58	20.8	0.0	0.0	7.9	0.0	0.0	0.0	0.0	0.0	0.0	0.2	35.5
		Max	1.49	0.07	2.79	1.50	32.4	6.1	3.6	18.8	4.1	3.9	0.0	0.0	0.0	0.0	2.8	61.9
Opalinus Clay (4)	Upper silty sub-unit	Mean	0.24	0.06	1.76	0.73	28.5	5.0	3.4	12.1	0.4	2.5	0.0	0.0	0.0	0.0	0.4	46.9
		Median	0.25	0.06	1.73	0.71	29.4	5.0	3.4	11.4	0.0	3.1	0.0	0.0	0.0	0.0	0.5	45.9
		Stdev	0.09	0.01	0.22	0.08	3.0	0.4	0.5	1.7	0.8	1.7	0.0	0.0	0.0	0.0	0.2	4.4
		Min	0.12	0.05	1.52	0.67	24.2	4.6	2.8	10.9	0.0	0.0	0.0	0.0	0.0	0.0	0.2	42.9
		Max	0.33	0.07	2.04	0.85	31.1	5.6	4.0	14.5	1.7	3.6	0.0	0.0	0.0	0.0	0.6	53.0
Opalinus Clay (19)	Mixed clay-silt-carbon-ate sub-unit	Mean	0.25	0.07	1.08	0.87	18.5	4.8	2.8	5.8	0.2	3.5	0.0	0.0	0.0	0.0	0.5	63.2
		Median	0.23	0.07	1.10	0.88	16.4	4.9	2.9	5.5	0.0	3.4	0.0	0.0	0.0	0.0	0.4	65.4
		Stdev	0.13	0.01	0.24	0.11	3.9	1.0	0.4	2.2	0.5	2.1	0.0	0.0	0.0	0.0	0.2	4.9
		Min	0.04	0.05	0.69	0.66	14.4	2.9	2.0	3.1	0.0	0.0	0.0	0.0	0.0	0.0	0.1	52.2
		Max	0.60	0.08	1.70	1.07	25.3	6.5	3.3	11.2	1.6	7.4	0.0	0.0	0.0	0.0	1.1	69.0
Opalinus Clay (5)	Clay-rich sub-unit	Mean	0.55	0.07	1.19	0.88	15.8	4.9	2.8	7.6	0.0	2.7	0.0	0.0	0.0	0.0	1.0	64.2
		Median	0.56	0.07	1.19	0.89	15.7	4.7	2.9	7.4	0.0	3.1	0.0	0.0	0.0	0.0	1.0	63.4
		Stdev	0.05	0.00	0.08	0.06	0.7	1.0	0.3	1.6	0.0	1.6	0.0	0.0	0.0	0.0	0.1	2.1
		Min	0.46	0.07	1.10	0.81	15.0	3.6	2.4	5.9	0.0	0.0	0.0	0.0	0.0	0.0	0.9	61.8
		Max	0.61	0.07	1.31	0.95	16.8	6.4	3.2	9.9	0.0	3.8	0.0	0.0	0.0	0.0	1.1	67.4
Staffel-egg Fm. (20)		Mean	1.02	0.05	2.29	1.22	25.5	4.5	2.1	15.8	2.9	0.0	0.0	0.0	0.0	0.0	1.9	45.9
		Median	0.52	0.04	1.88	0.58	24.9	4.5	2.3	9.6	2.3	0.0	0.0	0.0	0.0	0.0	1.0	40.0
		Stdev	1.07	0.06	1.62	1.83	14.6	1.6	0.8	12.8	2.9	0.2	0.0	0.0	0.0	0.0	2.0	15.8
		Min	0.00	0.00	0.12	0.25	5.6	0.0	0.0	1.0	0.0	0.0	0.0	0.0	0.0	0.0	0.0	26.8
		Max	3.44	0.22	7.63	7.04	48.5	7.1	3.3	54.1	8.0	0.9	0.0	0.0	0.0	0.0	6.4	79.1
Klettgau Fm. (10)		Mean	0.08	0.01	4.32	0.26	14.4	8.7	5.1	0.4	32.8	0.0	0.0	0.0	0.0	0.0	0.2	38.1
		Median	0.00	0.00	5.02	0.14	10.2	7.1	4.1	0.0	36.5	0.0	0.0	0.0	0.0	0.0	0.0	39.8
		Stdev	0.16	0.02	3.40	0.23	9.9	4.3	3.8	1.0	26.0	0.0	0.0	0.0	0.0	0.0	0.3	11.8
		Min	0.00	0.00	0.00	0.09	3.5	4.8	0.0	0.0	0.0	0.0	0.0	0.0	0.0	0.0	0.0	17.3
		Max	0.44	0.04	9.61	0.66	28.9	19.4	11.7	2.7	73.7	0.0	0.0	0.0	0.0	0.0	0.8	52.6
Bänker-joch Fm. (14)		Mean	11.1	0.00	1.46	0.25	6.0	3.0	1.0	0.1	10.5	0.0	1.3	46.6	0.0	0.0	0.1	31.9
		Median	13.0	0.00	1.16	0.22	4.6	2.7	0.0	0.0	5.5	0.0	0.0	55.0	0.0	0.0	0.0	27.9
		Stdev	8.87	0.00	1.37	0.21	4.8	3.1	1.4	0.2	11.3	0.0	3.4	37.7	0.0	0.0	0.2	23.6
		Min	0.00	0.00	0.00	0.08	0.0	0.0	0.0	0.0	0.0	0.0	0.0	0.0	0.0	0.0	0.0	0.3
		Max	23.38	0.00	4.17	0.88	13.6	8.3	3.6	0.9	32.0	0.0	12.4	96.9	0.0	0.0	0.6	71.8
Schinz-nach Fm. (5)	All	Mean	0.56	0.00	11.2	0.73	1.5	0.4	0.0	29.8	58.3	0.0	0.0	2.3	0.0	0.0	0.0	7.0
		Median	0.05	0.00	11.2	0.58	1.4	0.0	0.0	0.0	78.3	0.0	0.0	0.0	0.0	0.0	0.0	7.0
		Stdev	0.80	0.00	0.72	0.33	1.0	0.9	0.0	41.6	39.1	0.0	0.0	3.4	0.0	0.0	0.0	2.4
		Min	0.00	0.00	10.2	0.47	0.0	0.0	0.0	0.0	4.0	0.0	0.0	0.0	0.0	0.0	0.0	3.7
		Max	1.80	0.00	12.1	1.31	2.6	1.9	0.0	86.3	93.2	0.0	0.0	7.6	0.0	0.0	0.0	10.2

Tab. 4.2-1: (continued)

Formation (number of analyses)	**Member**		**S** [wt.-%]	**N** [wt.-%]	**C(inorg)** [wt.-%]	**C(org)** [wt.-%]	**Quartz** [wt.-%]	**K-feldspar** [wt.-%]	**Plagioclase** [wt.-%]	**Calcite** [wt.-%]	**Dolomite/Ank.** [wt.-%]e	**Siderite** [wt.-%]	**Magnesite** [wt.-%]	**Anhydrite** [wt.-%]	**Goethite** [wt.-%]	**Haematite** [wt.-%]	**Pyrite** [wt.-%]	**Clay minerals** [wt.-%]
Schinznach Fm. (3)	Stamberg Mb.	Mean	0.92	0.00	11.2	0.87	1.6	0.0	0.0	0.0	85.8	0.0	0.0	3.9	0.0	0.0	0.0	7.8
		Median	0.96	0.00	11.2	0.73	2.3	0.0	0.0	0.0	86.0	0.0	0.0	4.1	0.0	0.0	0.0	7.0
		Stdev	0.90	0.00	0.97	0.38	1.4	0.0	0.0	0.0	7.5	0.0	0.0	3.8	0.0	0.0	0.0	2.2
		Min	0.00	0.00	10.2	0.58	0.0	0.0	0.0	0.0	78.3	0.0	0.0	0.0	0.0	0.0	0.0	6.1
		Max	1.80	0.00	12.1	1.31	2.6	0.0	0.0	0.0	93.2	0.0	0.0	7.6	0.0	0.0	0.0	10.2
Schinznach Fm. (2)	Liedertswil – Kienberg Mb.	Mean	0.02	0.00	11.2	0.52	1.2	1.0	0.0	74.5	17.1	0.0	0.0	0.0	0.0	0.0	0.0	5.7
		Median	0.02	0.00	11.2	0.52	1.2	1.0	0.0	74.5	17.1	0.0	0.0	0.0	0.0	0.0	0.0	5.7
		Stdev	0.03	0.00	0.41	0.08	0.3	1.4	0.0	16.7	18.6	0.0	0.0	0.0	0.0	0.0	0.0	2.9
		Min	0.00	0.00	10.9	0.47	1.0	0.0	0.0	62.7	4.0	0.0	0.0	0.0	0.0	0.0	0.0	3.7
		Max	0.05	0.00	11.5	0.58	1.4	1.9	0.0	86.3	30.2	0.0	0.0	0.0	0.0	0.0	0.0	7.8
Zeglingen Fm. (4)	All	Mean	7.20	0.00	6.83	0.20	3.2	0.0	0.0	0.3	52.2	0.0	0.0	30.6	0.0	0.0	0.0	13.5
		Median	5.05	0.00	7.58	0.13	3.5	0.0	0.0	0.0	58.2	0.0	0.0	21.4	0.0	0.0	0.0	12.3
		Stdev	8.25	0.00	5.47	0.23	2.6	0.0	0.0	0.7	41.6	0.0	0.0	35.0	0.0	0.0	0.0	9.8
		Min	0.72	0.00	0.59	0.00	0.0	0.0	0.0	0.0	4.5	0.0	0.0	3.1	0.0	0.0	0.0	4.9
		Max	18.00	0.00	11.6	0.53	5.9	0.0	0.0	1.3	87.8	0.0	0.0	76.4	0.0	0.0	0.0	24.5
Kaiseraugst Fm. (4)		Mean	0.53	0.00	3.33	0.65	12.5	3.3	3.4	14.7	12.0	0.0	0.0	0.0	0.0	0.0	0.9	52.5
		Median	0.40	0.00	2.01	0.62	14.1	4.2	4.3	10.5	6.9	0.0	0.0	0.0	0.0	0.0	0.6	56.9
		Stdev	0.62	0.00	3.43	0.24	5.6	2.2	2.3	17.2	11.4	0.0	0.0	0.0	0.0	0.0	1.2	17.9
		Min	0.00	0.00	0.95	0.41	4.4	0.0	0.0	0.0	5.0	0.0	0.0	0.0	0.0	0.0	0.0	27.6
		Max	1.33	0.00	8.35	0.96	17.2	4.7	5.0	38.0	29.1	0.0	0.0	0.0	0.0	0.0	2.5	68.8
Dinkelberg Fm. (2)		Mean	0.10	0.00	0.03	0.26	72.2	9.8	0.0	0.0	0.3	0.0	0.0	0.0	0.0	0.0	0.2	16.7
		Median	0.10	0.00	0.03	0.26	72.2	9.8	0.0	0.0	0.3	0.0	0.0	0.0	0.0	0.0	0.2	16.7
		Stdev	0.14	0.00	0.05	0.01	0.3	0.2	0.0	0.0	0.4	0.0	0.0	0.0	0.0	0.0	0.3	1.3
		Min	0.00	0.00	0.00	0.26	72.0	9.6	0.0	0.0	0.0	0.0	0.0	0.0	0.0	0.0	0.0	15.8
		Max	0.20	0.00	0.07	0.27	72.4	10.0	0.0	0.0	0.5	0.0	0.0	0.0	0.0	0.0	0.4	17.7
Weitenau Fm. (3)		Mean	0.04	0.00	0.05	0.37	35.8	29.6	10.4	0.4	0.0	0.0	0.0	0.0	0.0	2.0	0.0	21.5
		Median	0.00	0.00	0.00	0.36	33.7	31.2	14.8	0.0	0.0	0.0	0.0	0.0	0.0	2.1	0.0	23.3
		Stdev	0.07	0.00	0.08	0.11	5.2	3.0	7.9	0.7	0.0	0.0	0.0	0.0	0.0	0.2	0.0	3.6
		Min	0.00	0.00	0.00	0.26	31.9	26.1	1.3	0.0	0.0	0.0	0.0	0.0	0.0	1.7	0.0	17.3
		Max	0.12	0.00	0.14	0.49	41.7	31.5	15.2	1.1	0.0	0.0	0.0	0.0	0.0	2.1	0.0	23.7

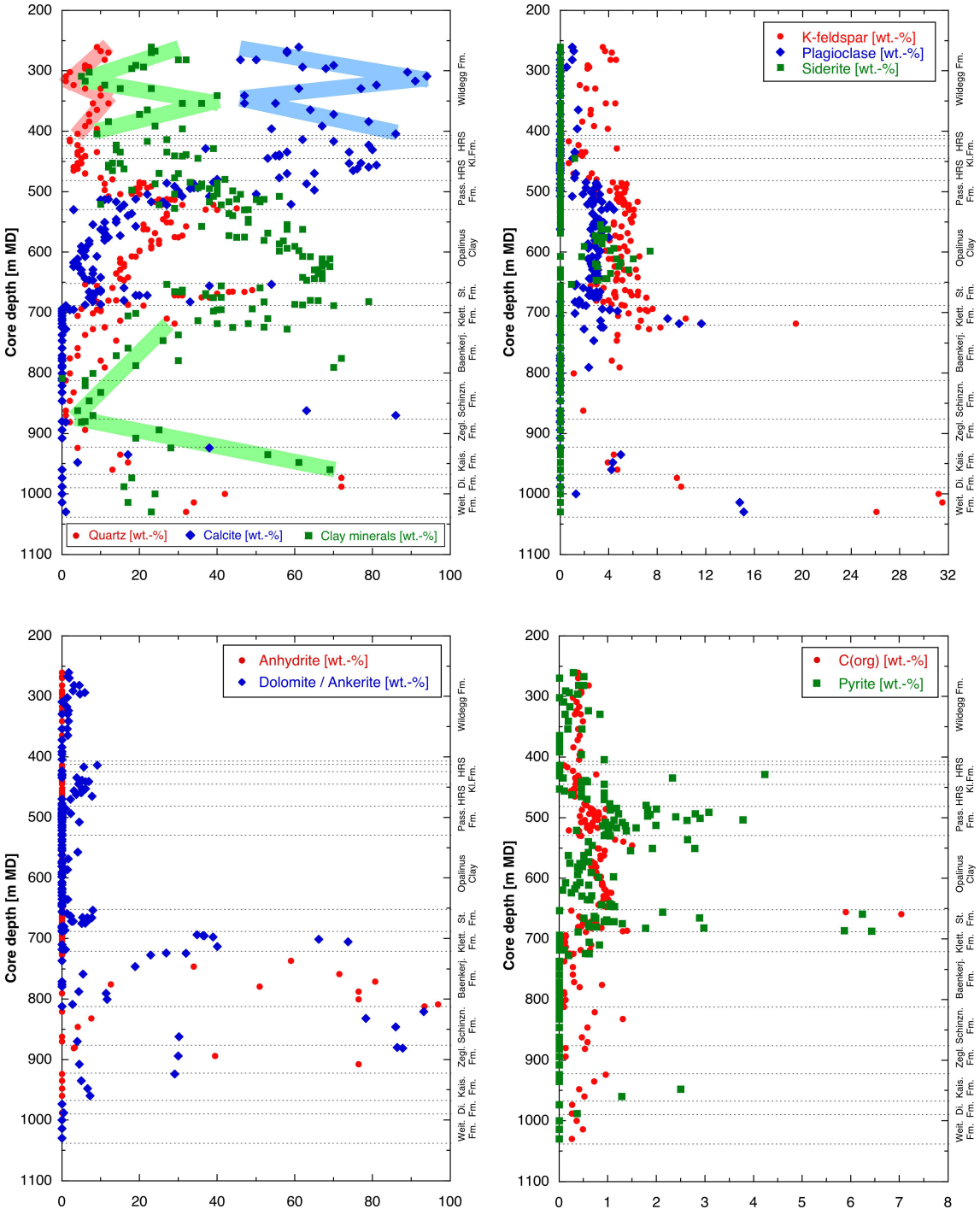

Fig. 4.2-1: Mineral contents in the bulk rock as a function of depth

Observed trends for the main minerals are only indicated for the Malm and Triassic sections, the Dogger and Lias are detailed in Fig. 4.2-4.

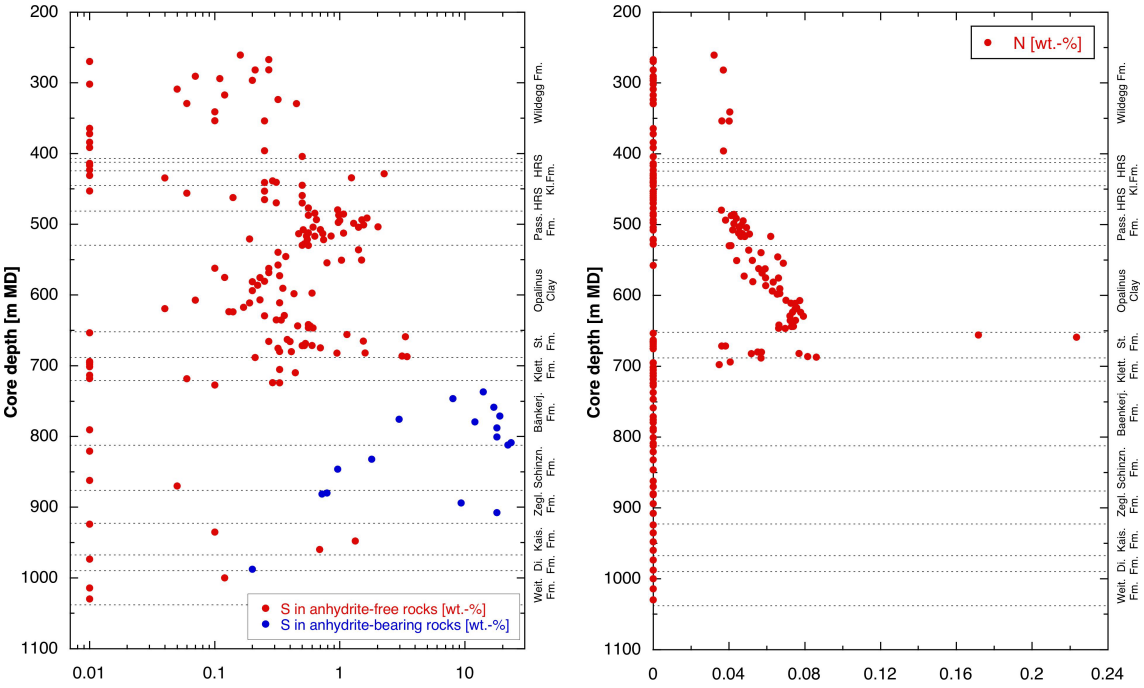

Fig. 4.2-2: Contents of S and N in the bulk rock as a function of depth

S contents below the detection limit of 0.05 wt.-% are represented by data points shown at 0.01 wt.-%. N contents below the detection limit of 0.01 wt.-% are represented by data points shown at 0 wt.-%.

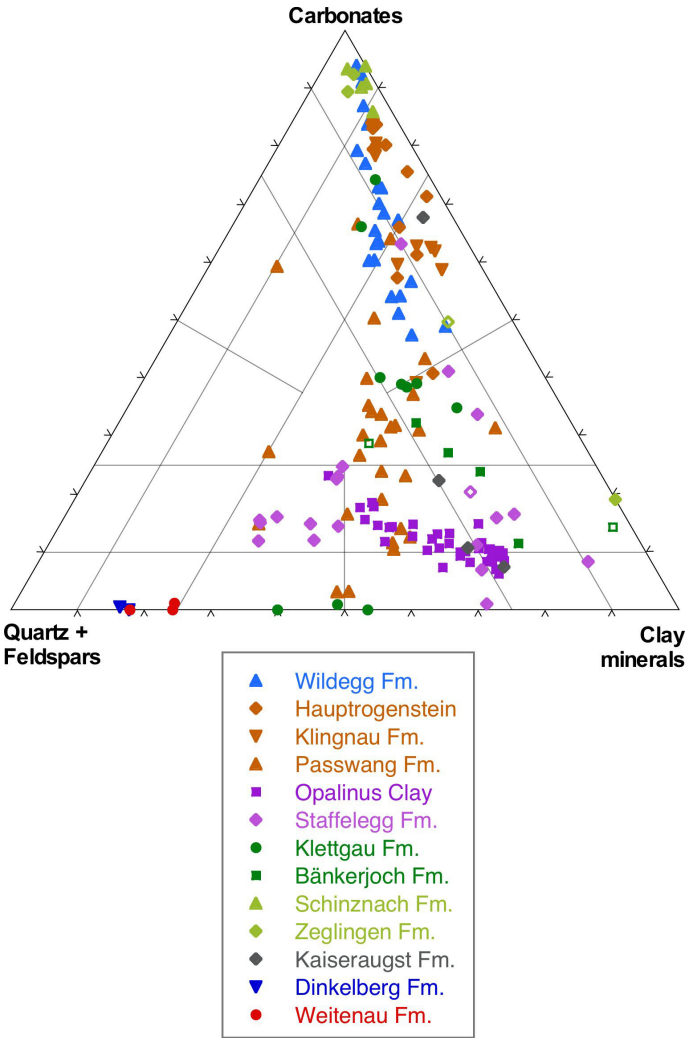

Fig. 4.2-3: Mineralogical composition of studied samples in the Füchtbauer triangle

Open symbols indicate samples containing 10 – 50 wt.-% minerals other than those represented by the Füchtbauer triangle (which are clays, calcite, dolomite/ankerite, siderite, magnesite, quartz, K-feldspar, plagioclase). Samples with > 50% of such minerals are excluded. In the Staffelegg Formation, the additional phases are pyrite and organic C. In case of the Triassic samples, anhydrite is the main additional phase.

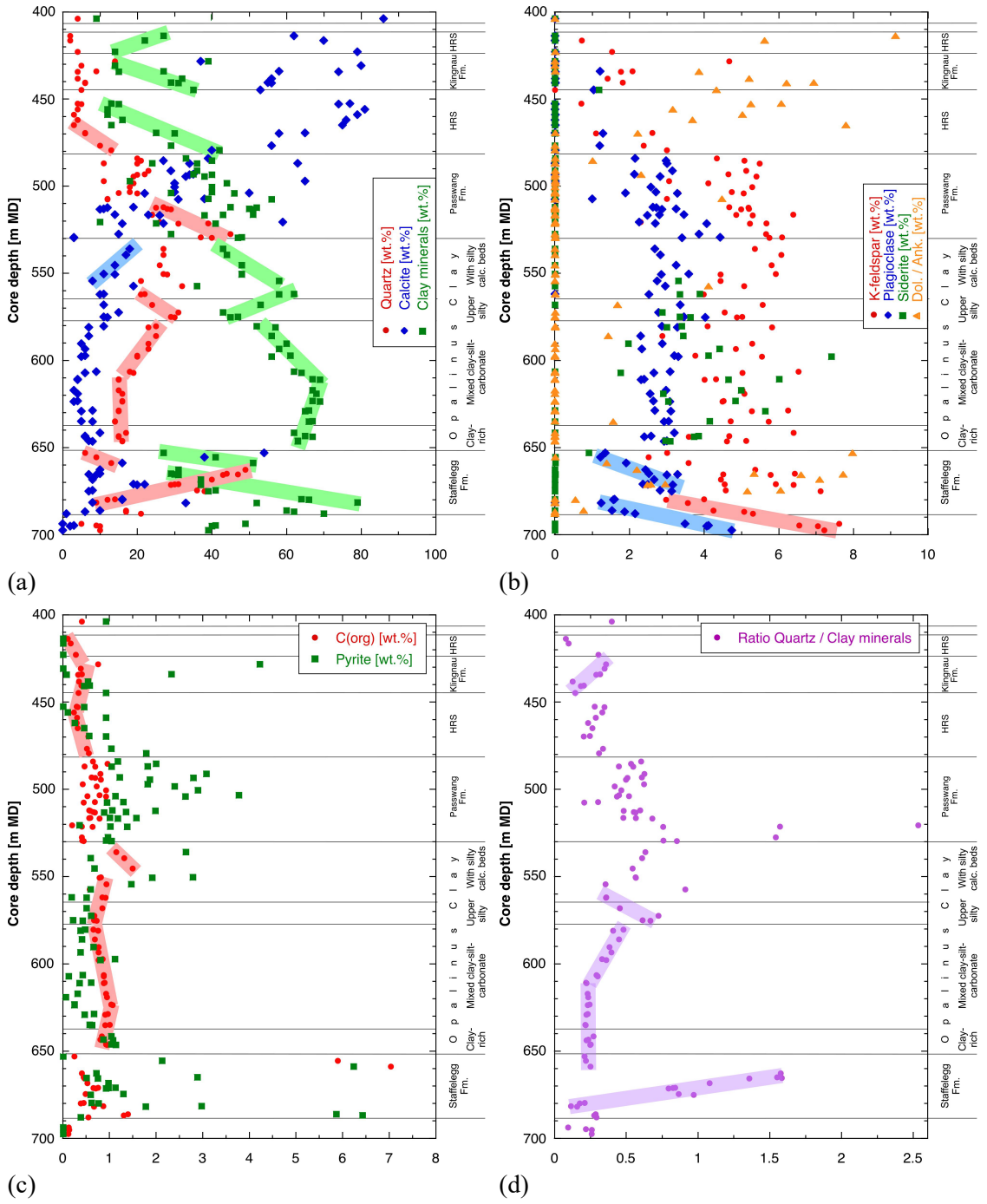

Fig. 4.2-4: Depth trends of mineral contents in the bulk rock in the Lias – Dogger interval
Coloured bars highlight systematic trends.

A closer look at the clay-rich section Staffelegg Formation – Opalinus Clay – Passwang Formation – Hauptrogenstein

The graphs shown in Fig. 4.2-4 indicate observed systematic depth trends of the contents of quartz, feldspars, clay minerals, calcite and C(org), whereas other minerals show no systematic variability.

Staffelegg Formation

- Between about 682 m (within the Schambelen Member) and 660 m (~top of the Frick Member) quartz contents increase sharply upwards, while clay minerals show the reversed trend.
- A sharp break in quartz and clay-mineral contents is found at the base of the Rietheim Member (659 m). In the section Gross Wolf Member–Rietheim Member, both quartz and clay-mineral contents decrease upwards.
- Feldspar contents show a discontinuity at the boundary between the Frick Member and the Schambelen Member (~676–679 m), i.e. at a slightly different position in comparison to the discontinuity of quartz and clay-mineral contents.

Opalinus Clay

Informal sub-units within the Opalinus Clay were defined by Mazurek & Aschwanden (2020) on a regional basis. This scheme was successfully applied to the BOZ1-1 core (Dossier III), and the sub-unit boundaries are included in Fig. 4.2-4.

- The base of the Opalinus Clay correlates with the onset of more homogeneous mineral contents, in contrast to a substantial scatter in the underlying Staffelegg Formation.
- Clay-mineral and quartz contents show a marked discontinuity towards higher values at the base, from where 4 sections with different trends can be identified. The depths at which the trends change correlate approximately with the lithostratigraphically defined sub-units of the Opalinus Clay. As in some other boreholes, the 'Mixed clay-silt-carbonate sub-unit' can be subdivided into two zones with contrasting trends.

Passwang-Formation–Hauptrogenstein

- Within the Passwang Formation, an upward trend of decreasing contents of quartz and feldspars can be identified, even though scatter remains substantial. Calcite tends to increase upwards, but again the trend is poorly defined.
- The lower section of the Hauptrogenstein and the overlying Klingnau Formation each show an upward trend of decreasing clay-mineral contents, with a sharp discontinuity at the base of the Klingnau Formation.

Conclusion

A number of mineralogical discontinuities and changes in depth trends were identified and generally correlate well with the lithostratigraphic subdivision defined in Dossier III.

Quartz and clay-mineral contents show the most pronounced trends and discontinuities in their depth profiles. As the depth trends of quartz and clay minerals are often inverse, the ratio quartz/ clay minerals best highlights the depositional cycles that govern the mineralogical composition, as shown in Fig. 4.2-4d. Last, let us note that the sub-units of the Opalinus Clay are not zones with constant properties but rather zones with constant trends, i.e. depositional cycles.

4.2.2 Clay minerals

A total of 50 mineralogical analyses of the clay fraction were performed in the section Wildegg Formation (Malm) – Bänkerjoch Formation (Keuper). The full dataset is documented in Appendix A, and Tab. 4.2-2 provides formation-specific summaries, normalising the contents of individual clay phases to the sum of all clay minerals.

The identified clay-mineral species include illite, smectite, illite/smectite mixed layers, kaolinite, chlorite and chlorite/smectite mixed layers. The identification of chlorite/smectite mixed layers in all samples is in contrast with previous data from northern Switzerland where this mineral was rarely reported (Mazurek 2017). However, this is not a real difference but due to the improved methodology of the evaluation of X-ray patterns that was applied for the TBO campaign (details in Waber (ed.) 2020). Because the chlorite/smectite mixed-layer phase contains 85 – 95% chlorite layers, its XRD reflections are close to those of pure chlorite. The new methodology also allows to better resolve the fraction of smectite layers in the illite/smectite mixed-layer phase. As seen in Tab. 4.2-2, illite-rich mixed layers dominate, but minor amounts of illite-poorer mixed layers also occur. Given the fact that the contents of mixed-layer phases and the smectite fractions in these are known, the end-member compositions of illite, smectite, chlorite and kaolinite (whether in mixed layers or as a discrete phase) can be calculated and are also listed in Tab. 4.2-2.

Depth trends of the relative proportions of clay minerals are shown graphically in Fig. 4.2-5 for individual clay phases (a) and end-member clays (b). The depth plot of the latter is less noisy than that of the individual clay minerals. Variability of the smectite end-member is limited, except for some high values in the Passwang Formation and one value in the Wildegg Formation. Chlorite varies more strongly, except in the Opalinus Clay.

The relative proportions of the two main end-member clays, namely illite and kaolinite, vary substantially over the profile. The Triassic is characterised by the dominance of the illite end member, while the proportions of kaolinite are low, sometimes below detection. The overlying Dogger – Lias interval will be explored in more detail below. The ratio illite/kaolinite increases systematically upwards in the Wildegg Formation, starting at a minimum in the Klingnau Formation.

The relative proportions of the illite, smectite and kaolinite end members as shown in Fig. 4.2-6 illustrate the homogeneous clay composition in the Opalinus Clay when compared to the overlying units.

Tab. 4.2-2: Mineralogical composition of the clay fraction: formation-specific means, medians, standard deviations and ranges

In some cases, systematic depth trends of clay-mineral contents are observed. This means that in these cases the data do not follow a Gaussian distribution, which is a pre-requisite for the calculation of meaningful standard deviations. In such cases, the ranges (also listed) are more meaningful.

Formation (number of analyses)	**Member**		**Individual clay phases** [wt.-% of clay fraction]										**End-member clays** [wt.-% of clay fraction]			
			Illite	**Ill/Sm ML (85-90)**	**Ill/Sm ML (75-80)**	**Ill/Sm ML (50-70)**	**Ill/Sm ML (20-40)**	**Total Ill/Sm**	**Smectite**	**Kaolinite**	**Chlorite**	**Chl/Sm ML (85-95)**	**Illite**	**Smectite**	**Kaolinite**	**Chlorite**
Wildegg Fm. (9)		Mean	39.7	18.6	10.7	8.6	1.0	38.9	0.17	14.3	1.9	5.0	69.1	10.2	14.3	6.3
		Median	43.1	21.5	4.7	6.7	0.0	36.1	0.00	14.3	1.8	5.9	71.7	8.6	14.3	7.0
		Stdev	6.1	10.0	11.6	9.7	1.7	9.0	0.27	5.2	0.7	2.2	5.1	4.6	5.2	2.4
		Min	29.2	3.8	0.0	2.6	0.0	33.0	0.00	2.9	1.1	0.2	59.2	7.6	2.9	1.3
		Max	46.0	29.6	28.1	34.2	5.0	62.1	0.80	21.6	3.4	7.3	73.7	22.1	21.6	9.9
Hauptrogenstein (all) (4)		Mean	35.2	7.7	3.9	5.2	0.6	17.5	0.35	23.1	9.4	14.5	48.0	5.9	23.1	22.8
		Median	38.8	6.4	3.9	5.2	0.2	16.8	0.20	22.0	7.4	12.7	54.1	6.2	22.0	18.7
		Stdev	13.0	7.5	4.5	0.8	1.0	5.0	0.47	5.4	6.5	4.1	14.7	0.6	5.4	10.2
		Min	17.1	0.0	0.0	4.3	0.0	13.0	0.00	18.0	4.3	12.0	26.1	5.0	18.0	16.1
		Max	46.0	18.0	8.0	6.2	2.1	23.4	1.00	30.2	18.4	20.6	57.8	6.4	30.2	37.7
Upper HRS ('Spatkalk') (1)		Mean	17.1	5.4	0.0	6.2	2.1	13.7	0.00	30.2	18.4	20.6	26.1	6.1	30.2	37.7
Klingnau Fm. (4)		Mean	30.7	14.4	4.4	4.9	0.1	23.8	0.45	24.2	9.4	11.5	49.5	6.4	24.2	19.7
		Median	32.3	17.7	2.8	5.3	0.0	24.1	0.40	25.2	9.4	12.5	50.8	5.9	25.2	20.9
		Stdev	6.8	10.1	5.3	2.0	0.2	4.3	0.44	4.7	4.0	2.4	4.6	1.1	4.7	5.6
		Min	21.3	0.0	0.0	2.2	0.0	19.0	0.00	18.1	5.2	8.0	42.9	5.7	18.1	12.5
		Max	37.0	22.1	12.0	7.0	0.4	28.1	1.00	28.3	13.7	13.0	53.5	8.0	28.3	24.6
Hauptrogenstein (3)	Lower	Mean	41.2	8.5	5.2	4.9	0.1	18.7	0.47	20.7	6.4	12.5	55.3	5.9	20.7	17.8
		Median	43.1	7.4	7.7	5.0	0.0	19.8	0.40	19.8	4.8	12.3	55.0	6.3	19.8	16.3
		Stdev	6.0	9.0	4.5	0.5	0.2	5.3	0.50	3.2	3.2	0.6	2.3	0.8	3.2	2.8
		Min	34.5	0.0	0.0	4.3	0.0	13.0	0.00	18.0	4.3	12.0	53.1	5.0	18.0	16.1
		Max	46.0	18.0	8.0	5.4	0.4	23.4	1.00	24.3	10.0	13.1	57.8	6.4	24.3	21.0
Passwang Fm. (10)		Mean	36.6	13.3	15.8	10.9	0.2	40.2	0.93	11.9	4.6	5.8	66.4	11.8	11.9	9.8
		Median	37.4	13.1	15.1	9.4	0.0	38.9	0.00	10.4	4.9	4.8	68.1	10.4	10.4	9.7
		Stdev	7.3	9.1	13.0	8.9	0.5	13.5	1.50	6.7	1.5	3.2	5.5	5.1	6.7	3.0
		Min	22.7	0.0	0.0	0.0	0.0	16.0	0.00	4.8	1.7	2.4	58.0	6.6	4.8	5.7
		Max	48.0	27.2	42.4	26.8	1.4	65.6	4.20	23.8	6.9	13.0	72.3	22.1	23.8	15.0
Opalinus Clay (12)	All	Mean	28.9	14.2	11.0	2.0	0.1	27.3	0.03	32.2	3.7	7.9	51.1	6.0	32.2	10.7
		Median	29.5	12.7	12.5	2.0	0.0	26.2	0.00	33.4	3.7	7.7	50.5	5.7	33.4	10.3
		Stdev	3.6	8.6	8.1	0.9	0.2	5.3	0.07	3.9	1.0	1.4	3.3	0.8	3.9	1.2
		Min	23.5	4.5	0.0	0.0	0.0	20.3	0.00	23.7	2.1	5.9	47.2	5.0	23.7	9.3
		Max	36.9	31.1	23.6	3.5	0.7	35.4	0.20	37.3	5.1	10.7	59.3	7.8	37.3	13.4
Opalinus Clay (2)	Sub-unit with silty calcar-eous beds	Mean	28.8	18.7	3.8	2.8	0.0	25.2	0.05	33.7	3.7	8.6	49.4	5.6	33.7	11.4
		Median	28.8	18.7	3.8	2.8	0.0	25.2	0.05	33.7	3.7	8.6	49.4	5.6	33.7	11.4
		Stdev	2.7	3.7	1.4	0.8	0.0	4.4	0.07	0.8	0.4	1.2	1.2	0.4	0.8	0.8
		Min	26.9	16.0	2.8	2.2	0.0	22.1	0.00	33.1	3.4	7.7	48.5	5.3	33.1	10.8
		Max	30.7	21.3	4.8	3.3	0.0	28.3	0.10	34.3	3.9	9.4	50.2	5.9	34.3	11.9

Tab. 4.2-2: (continued)

Formation (number of analyses)	**Member**		**Individual clay phases** [wt.-% of clay fraction]										**End-member clays** [wt.-% of clay fraction]			
			Illite	**Ill/Sm ML (85-90)**	**Ill/Sm ML (75-80)**	**Ill/Sm ML (50-70)**	**Ill/Sm ML (20-40)**	**Total Ill/Sm**	**Smectite**	**Kaolinite**	**Chlorite**	**Chl/Sm ML (85-95)**	**Illite**	**Smectite**	**Kaolinite**	**Chlorite**
Opalinus Clay (2)	Upper silty sub-unit	Mean	26.8	15.9	17.6	1.3	0.4	35.2	0.00	27.6	3.6	7.0	55.4	7.3	27.6	9.8
		Median	26.8	15.9	17.6	1.3	0.4	35.2	0.00	27.6	3.6	7.0	55.4	7.3	27.6	9.8
		Stdev	4.6	6.2	3.5	1.8	0.5	0.4	0.00	5.4	2.1	1.5	5.5	0.8	5.4	0.7
		Min	23.5	11.5	15.1	0.0	0.0	34.9	0.00	23.7	2.1	5.9	51.5	6.7	23.7	9.3
		Max	30.0	20.3	20.1	2.6	0.7	35.4	0.00	31.4	5.1	8.0	59.3	7.8	31.4	10.3
Opalinus Clay (6)	Mixed clay-silt-carbonate sub-unit	Mean	30.0	15.2	8.0	2.1	0.0	25.3	0.05	32.7	3.8	8.2	50.8	5.5	32.7	11.0
		Median	29.5	11.6	6.8	2.1	0.0	23.5	0.00	32.6	3.8	7.5	50.9	5.6	32.6	10.6
		Stdev	3.7	10.5	7.0	0.8	0.0	4.7	0.08	4.0	0.9	1.6	2.8	0.3	4.0	1.4
		Min	26.2	5.3	0.0	1.2	0.0	20.3	0.00	28.3	2.3	6.9	47.2	5.0	28.3	9.8
		Max	36.9	31.1	17.2	3.5	0.0	32.6	0.20	37.3	4.8	10.7	53.6	6.0	37.3	13.4
Opalinus Clay (2)	Clay-rich sub-unit	Mean	27.8	5.1	20.8	1.7	0.0	27.6	0.00	34.2	3.5	7.2	49.7	6.4	34.2	9.8
		Median	27.8	5.1	20.8	1.7	0.0	27.6	0.00	34.2	3.5	7.2	49.7	6.4	34.2	9.8
		Stdev	5.4	0.8	4.0	0.1	0.0	5.0	0.00	0.6	0.9	0.8	1.4	1.0	0.6	0.3
		Min	24.0	4.5	17.9	1.6	0.0	24.0	0.00	33.7	2.8	6.6	48.7	5.7	33.7	9.6
		Max	31.6	5.7	23.6	1.8	0.0	31.1	0.00	34.6	4.1	7.7	50.7	7.1	34.6	10.0
Staffelegg Fm. (6)		Mean	36.9	5.5	29.2	1.7	0.1	36.5	0.00	18.2	4.0	4.5	66.0	7.9	18.2	8.0
		Median	38.9	3.5	29.1	1.7	0.0	33.8	0.00	19.2	3.8	4.2	64.9	7.7	19.2	8.1
		Stdev	6.9	6.3	6.4	1.1	0.2	7.5	0.00	3.0	1.2	2.1	4.1	1.3	3.0	2.7
		Min	28.3	0.0	20.4	0.0	0.0	29.5	0.00	12.5	2.8	1.2	62.1	6.4	12.5	4.4
		Max	44.9	17.0	37.5	3.3	0.4	48.4	0.00	20.9	6.0	7.2	73.3	9.9	20.9	12.4
Klettgau Fm. (3)		Mean	53.3	9.3	24.1	1.5	0.3	35.3	0.00	3.8	3.3	3.7	81.6	7.7	3.8	6.8
		Median	58.1	0.8	33.1	0.9	0.0	36.6	0.00	1.2	0.5	3.6	86.9	8.6	1.2	3.7
		Stdev	8.5	15.4	17.9	1.8	0.6	4.1	0.00	5.6	5.3	2.3	10.6	2.0	5.6	7.0
		Min	43.5	0.0	3.5	0.1	0.0	30.7	0.00	0.0	0.0	1.5	69.4	5.4	0.0	1.8
		Max	58.3	27.1	35.8	3.5	1.0	38.5	0.00	10.3	9.4	6.1	88.4	9.0	10.3	14.8
Bänkerjoch Fm. (2)		Mean	53.9	25.4	0.0	1.4	4.2	31.0	0.00	0.4	2.7	12.2	78.4	8.0	0.4	13.3
		Median	53.9	25.4	0.0	1.4	4.2	31.0	0.00	0.4	2.7	12.2	78.4	8.0	0.4	13.3
		Stdev	2.5	2.5	0.0	0.5	0.3	3.3	0.00	0.1	1.1	0.1	0.4	0.5	0.1	1.1
		Min	52.1	23.6	0.0	1.0	4.0	28.6	0.00	0.3	1.9	12.1	78.1	7.6	0.3	12.5
		Max	55.6	27.2	0.0	1.7	4.4	33.3	0.00	0.4	3.5	12.2	78.7	8.3	0.4	14.0

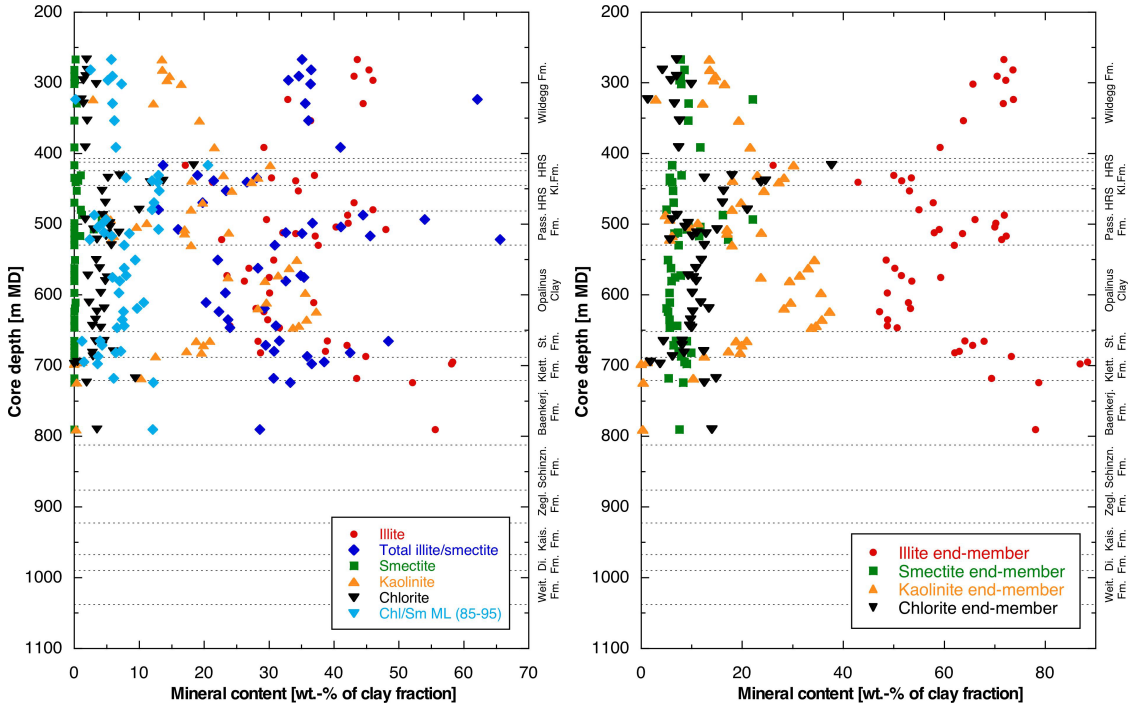

(a) (b)

Fig. 4.2-5: Mineralogical composition of the clay fraction as a function of depth; (a) individual clay minerals, (b) end-member clays

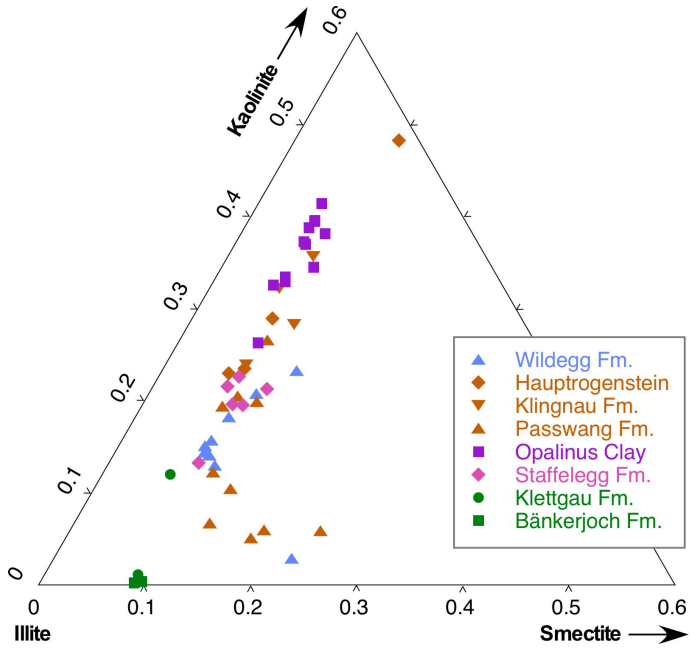

Fig. 4.2-6: Relative mass proportions of illite, smectite and kaolinite end-member clays

A closer look at the clay-rich section Staffelegg Formation – Opalinus Clay – Passwang Formation – Hauptrogenstein

The composition of the clay fraction in this interval shows some depth trends (Figs. 4.2-7 and 4.2-8). Within the Staffelegg Formation, the ratio illite to kaolinite end-member decreases upwards. The relative contents of end-member clays remain remarkably constant throughout the Opalinus Clay, even though the variability is somewhat higher when compared to the profiles from boreholes BUL1-1 and TRU1-1. Substantially more variability is identified in the overlying Passwang Formation–Hauptrogenstein (see also Fig. 4.2-6). A systematic upward decrease of the ratio illite/kaolinite end members is seen in the Hauptrogenstein / Klingnau Formation.

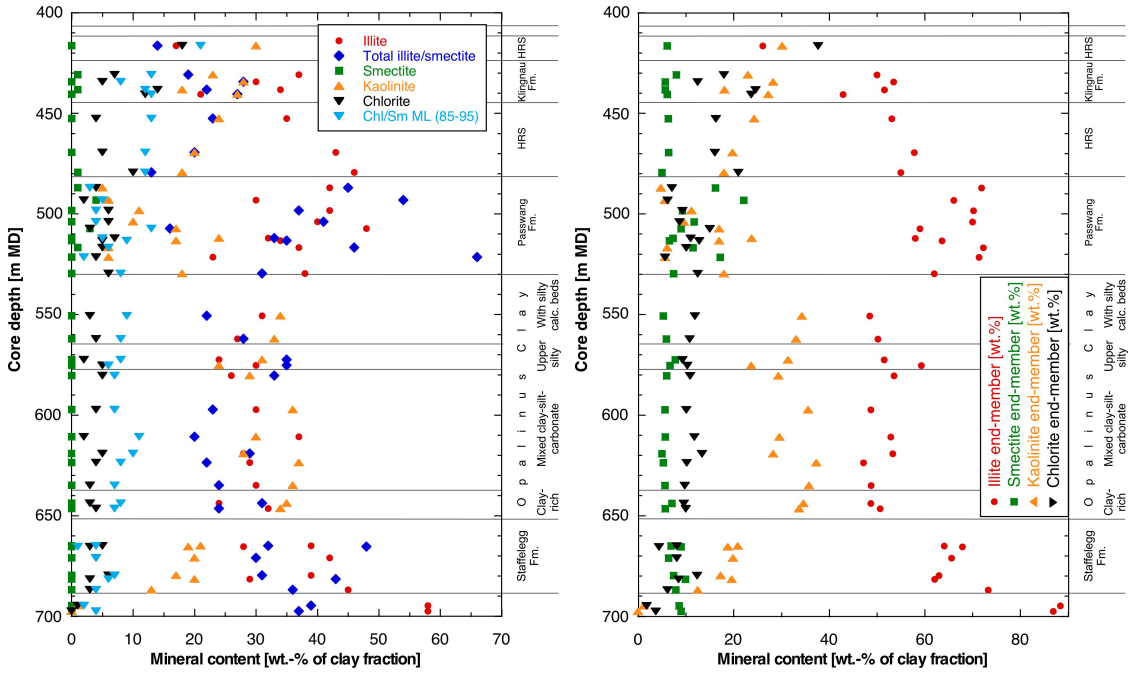

(a) (b)

Fig. 4.2-7: Mineralogical composition of the clay fraction as a function of depth in the Lias – Dogger interval; (a) individual clay minerals, (b) end-member clays

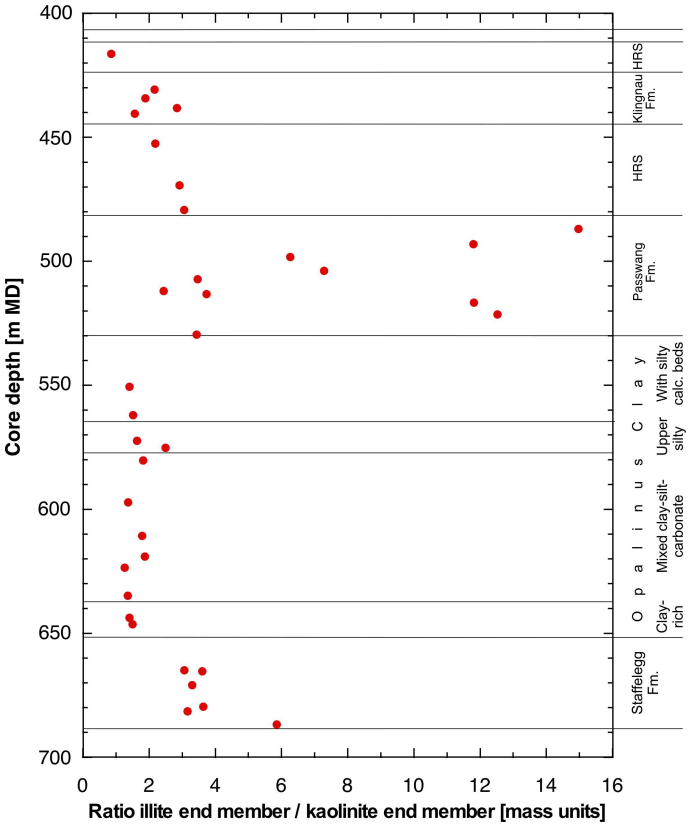

Fig. 4.2-8: Ratio of the illite to kaolinite end-member clays as a function of depth

4.3 Petrophysical parameters

Martin Mazurek, Lukas Aschwanden & Thomas Gimmi

All petrophysical measurements were performed at the University of Bern, and the acquired parameters are listed in Tab. 4.3-1. The formalisms to calculate additional parameters from measured data (such as porosity) are detailed in Waber (ed.) (2020). Formation-specific statistical data are summarised in Tab. 4.3-2, and the full data set is documented in Appendix A. In cases where gravimetric water content was available, but density data were missing, water-loss porosity was calculated assuming a grain density of 2.7 g/cm^3. The uncertainty related to this assumption is small.

Tab. 4.3-1: Analytical programme for petrophysical measurements

	Number of samples
Bulk wet density	126
Grain density	136
Gravimetric water content	164
Water content from isotope mass balance	103
N_2 adsorption (BET external surface + full isotherm)	42

Tab. 4.3-2: Summary of measured and calculated petrophysical data

Listed water contents (wet) are averages of measurements performed on typically 3 sub-samples. n: number of samples per geological unit.

Formation	Member / Sub-unit		Bulk wet density [g/cm³]	Bulk dry density, calculated [g/cm³]	Grain density [g/cm³]	Pycnometer porosity [–]	Gravimetry				Isotope mass bal.			External surface area (BET) [m²/g dry rock]
							Water content (wet) (105 °C) [wt.-%]	Water content (dry) (105 °C) [wt.-%]	Water-loss porosity using bulk wet density [–]	Water-loss porosity using grain density [–]	Water content (wet) based on isotope diff. exch. [wt.-%]	Porosity based on isotope diff. exch. using bulk wet density [–]	Porosity based on isotope diff. exch. using grain density [–]	
Wildegg Fm.		Mean	2.594	2.515	2.705	0.070	3.043	3.150	0.079	0.078	3.090	0.080	0.079	17.54
		Median	2.605	2.529	2.704	0.066	2.879	2.964	0.075	0.074	3.306	0.086	0.085	18.64
		Stdev	0.038	0.063	0.006	0.022	1.037	1.102	0.026	0.025	1.345	0.034	0.033	6.78
		Min	2.526	2.422	2.692	0.023	0.922	0.931	0.025	0.025	0.917	0.025	0.025	5.71
		Max	2.678	2.653	2.717	0.105	4.646	4.872	0.119	0.116	4.857	0.124	0.121	27.83
		n	23	23	23	23	23	23	23	23	14	14	14	9
Haupt-rogenstein	All	Mean	2.589	2.506	2.759	0.090	3.257	3.382	0.083	0.085	3.031	0.079	0.079	7.18
		Median	2.591	2.519	2.745	0.079	2.896	2.982	0.071	0.075	2.962	0.077	0.077	7.18
		Stdev	0.029	0.057	0.050	0.033	1.222	1.330	0.032	0.031	0.692	0.017	0.017	1.02
		Min	2.533	2.400	2.716	0.060	2.107	2.152	0.056	0.056	2.296	0.060	0.061	6.45
		Max	2.642	2.586	2.891	0.170	6.341	6.770	0.163	0.164	4.130	0.106	0.105	7.90
		n	12	12	13	12	13	13	12	13	8	8	8	2
Haupt-rogenstein	'Spatkalk'	Mean	2.558	2.432	2.811	0.134	4.938	5.212	0.126	0.127	3.191	0.082	0.082	7.90
		Median	2.563	2.403	2.818	0.147	5.115	5.391	0.130	0.132				
		Stdev	0.023	0.052	0.085	0.044	1.499	1.655	0.038	0.039				
		Min	2.533	2.400	2.722	0.084	3.359	3.476	0.087	0.086				
		Max	2.579	2.492	2.891	0.170	6.341	6.770	0.163	0.164				
		n	3	3	3	3	3	3	3	3	1	1	1	1
Haupt-rogenstein	Lower sub-unit	Mean	2.599	2.531	2.743	0.075	2.752	2.833	0.069	0.072	3.009	0.078	0.078	6.45
		Median	2.603	2.538	2.743	0.076	2.530	2.596	0.065	0.066	2.735	0.071	0.072	
		Stdev	0.023	0.033	0.024	0.008	0.515	0.546	0.010	0.013	0.744	0.019	0.018	
		Min	2.567	2.479	2.716	0.060	2.107	2.152	0.056	0.056	2.296	0.060	0.061	
		Max	2.642	2.586	2.804	0.090	3.669	3.809	0.088	0.096	4.130	0.106	0.105	
		n	9	9	10	9	10	10	9	10	7	7	7	1
Klingnau Fm.		Mean	2.568	2.462	2.752	0.107	3.821	3.984	0.107	0.098	4.684	0.120	0.119	12.85
		Median	2.578	2.468	2.756	0.108	4.066	4.238	0.108	0.105	4.670	0.121	0.120	14.97
		Stdev	0.021	0.031	0.042	0.017	1.084	1.158	0.015	0.027	0.605	0.015	0.014	4.82
		Min	2.526	2.411	2.703	0.086	1.527	1.551	0.083	0.040	4.095	0.105	0.104	7.33
		Max	2.589	2.501	2.822	0.137	5.024	5.290	0.129	0.130	5.303	0.134	0.131	16.24
		n	7	7	8	7	8	8	7	8	4	4	4	3
Passwang Fm.		Mean	2.527	2.410	2.707	0.110	4.492	4.715	0.117	0.113	4.895	0.126	0.121	25.73
		Median	2.521	2.401	2.707	0.113	4.563	4.781	0.123	0.114	5.267	0.135	0.131	25.83
		Stdev	0.032	0.050	0.012	0.020	1.019	1.107	0.019	0.024	1.679	0.026	0.039	3.71
		Min	2.485	2.348	2.682	0.048	2.096	2.141	0.063	0.055	1.631	0.076	0.043	20.23
		Max	2.618	2.555	2.727	0.137	6.374	6.808	0.137	0.155	8.681	0.152	0.204	31.19
		n	18	18	19	18	27	27	18	27	17	9	17	7
Opalinus Clay	All	Mean	2.522	2.401	2.701	0.111	4.799	5.045	0.121	0.120	5.345	0.135	0.132	31.41
		Median	2.520	2.396	2.702	0.111	4.867	5.115	0.123	0.121	5.345	0.135	0.132	33.33
		Stdev	0.025	0.036	0.012	0.014	0.561	0.616	0.013	0.013	0.653	0.015	0.015	5.34
		Min	2.470	2.340	2.667	0.081	3.179	3.283	0.082	0.082	3.816	0.098	0.097	21.92
		Max	2.567	2.485	2.731	0.130	5.607	5.940	0.139	0.138	6.249	0.156	0.153	37.33
		n	32	32	32	32	32	32	32	32	20	20	20	11

Tab. 4.3-2: (continued)

Formation	Member / Sub-unit		Bulk wet density [g/cm³]	Bulk dry density, calculated [g/cm³]	Grain density [g/cm³]	Pycnometer porosity [–]	Gravimetry				Isotope mass bal.			External surface area (BET) [m²/g dry rock]
							Water content (wet) (105 °C) [wt.-%]	Water content (dry) (105 °C) [wt.-%]	Water-loss porosity using bulk wet density [–]	Water-loss porosity using grain density [–]	Water content (wet) based on isotope diff. exch. [wt.-%]	Porosity based on isotope diff. exch. using bulk wet density [–]	Porosity based on isotope diff. exch. using grain density [–]	
Opalinus Clay	With silty calc. beds	Mean	2.537	2.431	2.695	0.098	4.186	4.371	0.106	0.105	4.826	0.123	0.120	26.51
		Median	2.536	2.424	2.696	0.099	4.375	4.575	0.110	0.109	4.767	0.122	0.119	26.51
		Stdev	0.023	0.034	0.016	0.010	0.491	0.532	0.012	0.011	0.727	0.018	0.016	3.35
		Min	2.507	2.395	2.667	0.081	3.179	3.283	0.082	0.082	3.816	0.098	0.097	24.14
		Max	2.567	2.485	2.719	0.110	4.585	4.805	0.116	0.115	6.032	0.152	0.147	28.88
		n	8	8	8	8	8	8	8	8	6	6	6	2
Opalinus Clay	Upper silty	Mean	2.543	2.433	2.699	0.099	4.318	4.513	0.110	0.109	4.865	0.124	0.121	21.92
		Median	2.550	2.440	2.701	0.095	4.410	4.613	0.112	0.111	4.865	0.124	0.121	
		Stdev	0.019	0.020	0.006	0.008	0.273	0.297	0.007	0.006	0.054	0.001	0.002	
		Min	2.515	2.404	2.691	0.093	3.918	4.078	0.100	0.099	4.826	0.123	0.120	
		Max	2.557	2.448	2.703	0.111	4.533	4.748	0.116	0.113	4.903	0.125	0.122	
		n	4	4	4	4	4	4	4	4	2	2	2	1
Opalinus Clay	Mixed clay-silt-carb.	Mean	2.509	2.379	2.705	0.120	5.182	5.467	0.130	0.129	5.721	0.144	0.141	33.80
		Median	2.511	2.379	2.704	0.124	5.255	5.546	0.131	0.130	5.755	0.145	0.142	35.54
		Stdev	0.023	0.029	0.011	0.010	0.305	0.339	0.007	0.007	0.461	0.011	0.010	4.22
		Min	2.470	2.340	2.687	0.101	4.599	4.821	0.117	0.115	4.961	0.126	0.124	26.13
		Max	2.548	2.431	2.731	0.130	5.607	5.940	0.139	0.138	6.249	0.156	0.153	37.33
		n	16	16	16	16	16	16	16	16	10	10	10	6
Opalinus Clay	Clay-rich	Mean	2.519	2.394	2.701	0.114	4.978	5.239	0.125	0.124	5.502	0.139	0.136	33.88
		Median	2.519	2.393	2.701	0.114	4.939	5.196	0.124	0.123	5.502	0.139	0.136	33.88
		Stdev	0.005	0.006	0.003	0.002	0.115	0.128	0.003	0.003	0.098	0.003	0.002	0.78
		Min	2.514	2.387	2.697	0.111	4.887	5.138	0.123	0.122	5.433	0.137	0.134	33.33
		Max	2.525	2.402	2.704	0.116	5.147	5.426	0.130	0.128	5.571	0.141	0.137	34.44
		n	4	4	4	4	4	4	4	4	2	2	2	2
Staffelegg Fm.		Mean	2.538	2.424	2.686	0.106	4.504	4.727	0.114	0.112	4.981	0.117	0.122	36.44
		Median	2.539	2.436	2.703	0.100	4.103	4.279	0.099	0.102	4.514	0.108	0.113	42.49
		Stdev	0.021	0.044	0.072	0.019	0.990	1.090	0.027	0.023	1.137	0.026	0.026	12.12
		Min	2.505	2.348	2.473	0.081	3.297	3.409	0.085	0.085	3.308	0.086	0.085	21.12
		Max	2.586	2.501	2.740	0.137	6.272	6.692	0.157	0.154	7.144	0.149	0.172	46.89
		n	12	12	19	12	19	19	12	19	13	6	13	5
Klettgau Fm.		Mean	2.536	2.404	2.763	0.130	5.229	5.539	0.132	0.131	5.195	0.132	0.130	39.82
		Median	2.531	2.374	2.778	0.135	5.246	5.536	0.130	0.129	4.726	0.118	0.118	39.82
		Stdev	0.084	0.111	0.057	0.031	1.432	1.596	0.036	0.033	2.035	0.048	0.046	24.87
		Min	2.443	2.286	2.663	0.080	3.251	3.360	0.087	0.086	3.085	0.082	0.082	22.23
		Max	2.672	2.585	2.834	0.181	7.752	8.403	0.192	0.190	8.371	0.207	0.203	57.40
		n	9	9	9	9	10	10	9	10	6	6	6	2
Bänkerjoch Fm.		Mean	2.771	2.701	2.854	0.056	2.843	2.987	0.070	0.073	3.182	0.086	0.082	33.68
		Median	2.835	2.758	2.870	0.026	2.702	2.777	0.072	0.073	2.968	0.082	0.080	38.32
		Stdev	0.161	0.221	0.075	0.055	2.438	2.605	0.062	0.060	2.539	0.067	0.063	31.06
		Min	2.493	2.311	2.745	0.000	0.028	0.028	0.001	0.001	0.231	0.007	0.007	0.56
		Max	2.953	2.952	2.948	0.167	7.311	7.888	0.182	0.180	6.446	0.167	0.160	62.16
		n	13	13	13	13	14	14	13	14	8	8	8	3

Tab. 4.3-2: (continued)

Formation	Member / Sub-unit		Bulk wet density [g/cm³]	Bulk dry density, calculated [g/cm³]	Grain density [g/cm³]	Pycnometer porosity [–]	Gravimetry				Isotope mass bal.			External surface area (BET) [m²/g dry rock]
							Water content (wet) (105 °C) [wt.-%]	Water content (dry) (105 °C) [wt.-%]	Water-loss porosity using bulk wet density [–]	Water-loss porosity using grain density [–]	Water content (wet) based on isotope diff. exch. [wt.-%]	Porosity based on isotope diff. exch. using bulk wet density [–]	Porosity based on isotope diff. exch. using grain density [–]	
Schinznach Fm.	All	Mean					3.442	3.633		0.085	2.544		0.064	
		Median					3.539	3.669		0.090	2.438		0.063	
		Stdev					2.766	2.974		0.067	2.122		0.053	
		Min					0.151	0.151		0.004	0.177		0.005	
		Max					6.953	7.473		0.168	5.122		0.127	
		n	0	0	0	0	5	5	0	5	4	0	4	0
Schinznach Fm.	Stamberg Mb.	Mean					5.232	5.544		0.129	4.173		0.105	
		Median					5.205	5.491		0.129	4.173		0.105	
		Stdev					1.707	1.902		0.039	1.342		0.032	
		Min					3.539	3.669		0.090	3.224		0.083	
		Max					6.953	7.473		0.168	5.122		0.127	
		n	0	0	0	0	3	3	0	3	2	0	2	0
Schinznach Fm.	Leutschenberg Mb./ Kienberg Mb.	Mean					0.757	0.767		0.020	0.915		0.024	
		Median					0.757	0.767		0.020	0.915		0.024	
		Stdev					0.857	0.870		0.023	1.043		0.027	
		Min					0.151	0.151		0.004	0.177		0.005	
		Max					1.363	1.382		0.036	1.652		0.043	
		n	0	0	0	0	2	2	0	2	2	0	2	0
Zeglingen Fm.		Mean					6.313	7.106		0.144	1.400		0.037	
		Median					6.600	7.376		0.152				
		Stdev					6.349	7.249		0.141				
		Min					0.099	0.099		0.003				
		Max					11.95	13.57		0.268				
		n	0	0	0	0	4	4	0	4	1	0	1	0
Kaiser-augst Fm.		Mean					2.931	3.031		0.075	3.164		0.081	
		Median					3.073	3.174		0.079	3.118		0.080	
		Stdev					1.219	1.290		0.030	1.368		0.033	
		Min					1.415	1.435		0.037	1.671		0.044	
		Max					4.162	4.343		0.105	4.748		0.119	
		n	0	0	0	0	4	4	0	4	4	0	4	0
Dinkelberg Fm.		Mean					6.153	6.573		0.150	6.923		0.167	
		Median					6.153	6.573		0.150				
		Stdev					1.679	1.906		0.037				
		Min					4.966	5.225		0.124				
		Max					7.340	7.921		0.176				
		n	0	0	0	0	2	2	0	2	1	0	1	0
Weitenau Fm.		Mean					3.086	3.185		0.079	3.065		0.079	
		Median					3.105	3.204		0.080	2.949		0.076	
		Stdev					0.323	0.344		0.008	0.313		0.008	
		Min					2.753	2.831		0.071	2.827		0.073	
		Max					3.399	3.519		0.087	3.419		0.087	
		n	0	0	0	0	3	3	0	3	3	0	3	0

4.3.1 Water content

The distribution of gravimetric water content in the studied section Malm – Permian is shown in Fig. 4.3-1. Note that the error bars on gravimetric water content reflect the variability among 3 aliquots of the samples, i.e. they are a measure of the lithological heterogeneity of the sample on the cm-scale. The following systematics of water content can be observed in the Triassic – Liassic and in the Malm (the Dogger – Lias section is detailed further below):

- The Kaiseraugst Formation shows a clear trend of water content decreasing upwards.
- In the Schinznach Formation, an upwards increasing trend is identified.
- In the lower part of the Bänkerjoch Formation, the data scatter widely, reflecting the lithological heterogeneity in this section. The upper part of the Bänkerjoch Formation ('Claystone with anhydrite nodules' and 'Cyclic sequence') indicates a trend of increasing water content.
- A cycle of water content decreasing upwards is observed in the interval starting in the uppermost part of the Bänkerjoch Formation and reaching up to the Gansingen Member of the Klettgau Formation.
- Another marked cycle of strongly decreasing water content occurs between base of the Gruhalde Member (Klettgau Formation) and the top of the Staffelegg Formation.
- In the Wildegg Formation, water content varies strongly and systematically – two cycles with upwards increasing trends can be identified (from the base at 407 m to 340 m and from 309 m to 261 m), even though some outliers occur.

Water contents from gravimetry and from isotope diffusive exchange correlate well (Fig. 4.3-2), but the latter shows values that are consistently higher, about $13\%_{rel}$ on the average. Three samples that slightly deviate from the regression line tend to have larger errors, reflecting sample heterogeneity.

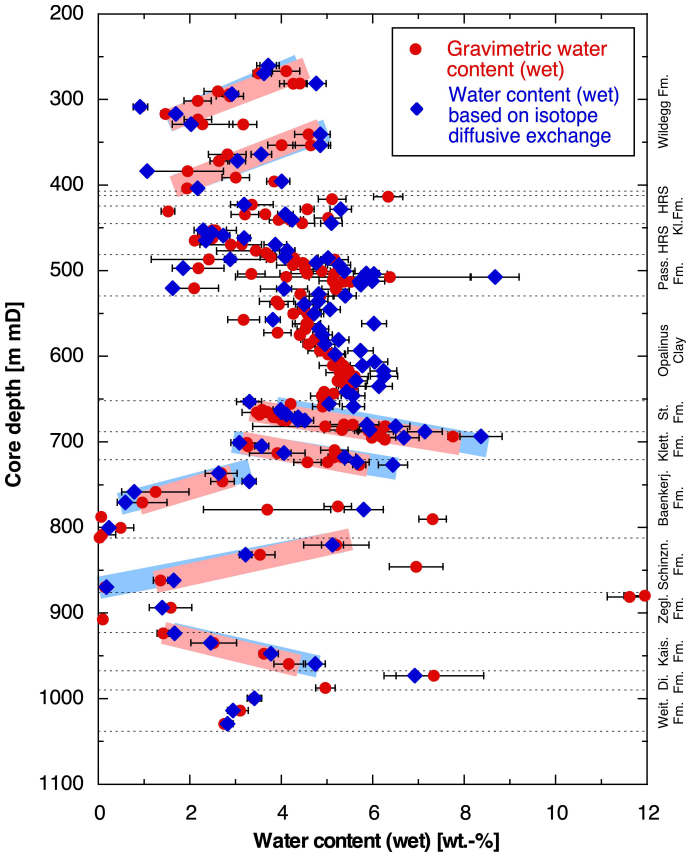

Fig. 4.3-1: Water content as a function of depth

Trends are only indicated for the Malm and Triassic sections, the Dogger and Lias are detailed in Fig. 4.3-3. Black bars for gravimetric water content indicate 1σ variability among 3 aliquots of the same sample. Black bars for water content from isotope diffusive exchange represent the propagated analytical error.

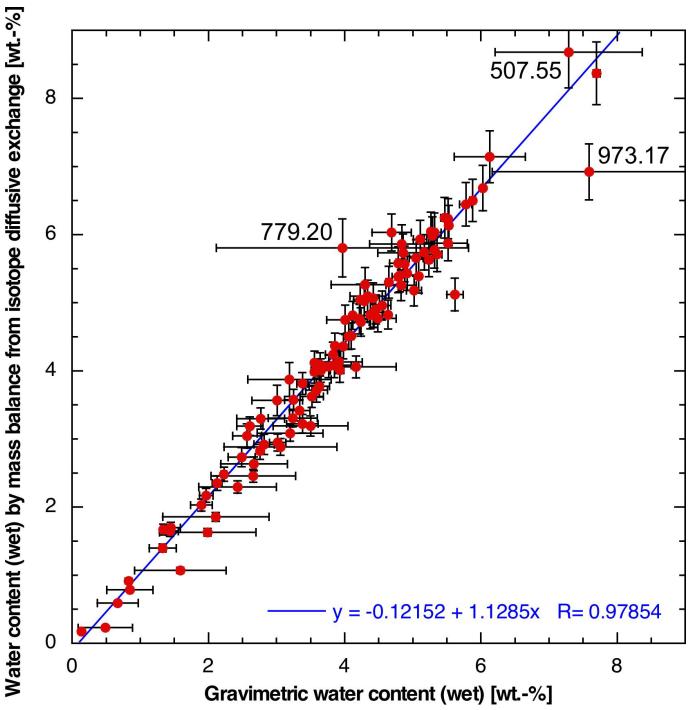

Fig. 4.3-2: Correlation of water contents based on gravimetry and on isotope diffusive exchange

Black bars for gravimetric water content indicate 1σ variability among 2 aliquots of the same sample. Note that only the 2 gravimetric water contents obtained from the aliquots used for the isotope diffusive exchange experiments are considered in this graph, so the correlation refers to identical sample materials. This is particularly important for anhydrite-bearing samples, given the fact that only the anhydrite-poorest portions of such samples were used for diffusive-exchange experiments. Two samples from the Triassic (779.20 m, an anhydrite-clay mixture from the Bänkerjoch Formation, and 973.04 m, a sandstone from the Dinkelberg Formation), slightly fall off the trend and have large errors due to cm-scale heterogeneity. For another sample, 507.55 m from the 'Humphriesi-Schichten', the large error is also due to heterogeneity. Black bars for water content from isotope diffusive exchange represent the propagated analytical error.

A closer look at the clay-rich Lias - Dogger section

As shown in Fig. 4.3-3, water contents in the Lias-Dogger section show several systematic trends with depth. These are similar for gravimetric water content and that obtained from isotope mass balance:

- In the Schambelen Member to Frick Member section of the Staffelegg Formation, a clear upward trend towards lower values is evident.
- In the overlying Gross Wolf Member and Rietheim Member, no systematic trend can be resolved, also due to the limited number of measurements.
- A not overly well defined increasing trend is observed in the basal part of the Opalinus Clay. A maximum is reached in the interval 617 – 635 m, i.e. within the lower part of the 'Mixed clay-silt-carbonate sub-unit'. Above this maximum, a well-defined trend decreasing water content reaches to the top of the 'Upper silty sub-unit'. At this depth, the trend reverses, and values increase towards a maximum at the base of the 'Humphriesi-Schichten' in the centre of the Passwang Formation.

- From here, a decreasing trend is identified until the top of the lower Hauptrogenstein.
- No trend is seen in Klingnau Formation. In the upper Hauptrogenstein ('Spatkalk'), water content increases upwards.

The observed trends of the water content correlate reasonably well with those identified for clay-mineral contents (Section 4.2.1, Fig. 4.2-4). In particular, a positive correlation can be identified with the clay-mineral content and a negative correlation with the ratio quartz/clay minerals. It is evident that a substantial part of the porewater is related to the presence of clay minerals. In detail, some differences exist, given the fact that fabric and degree of cementation also affect porosity and therefore water content.

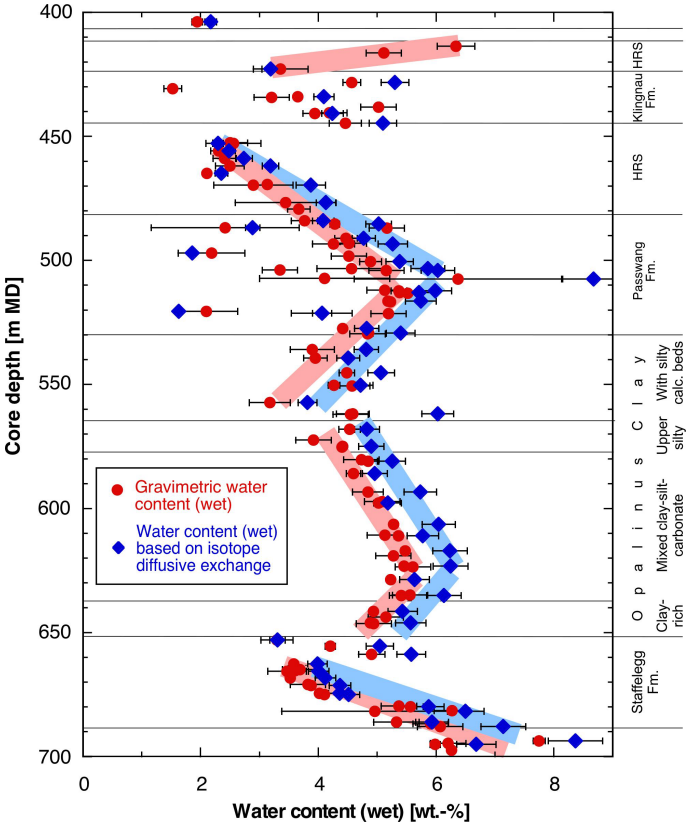

Fig. 4.3-3: Water content (wet) as a function of depth in the Lias – Dogger interval

Black bars for gravimetric water content indicate 1σ variability among 3 aliquots of the same sample. Black bars for water content from isotope diffusive exchange represent the propagated analytical error.

4.3.2 Grain density

The grain-density profile is shown in Fig. 4.3-4. Throughout the Malm, Dogger and Lias units, values are around 2.7 g/cm^3, with only limited scatter. Two outliers (413.63 and 416.35 from the 'Spatkalk') can be explained by the high content of goethite (6 – 11 wt.-%). Some additional outliers occur in the Klingnau Formation, which also contains minor quantities of goethite. One sample from the lower Hauptrogenstein also has an elevated grain density, even though no straightforward mineralogical explanation is at hand. The only other conspicuous excursion is identified in the Rietheim Member of the Staffelegg Formation ('Posidonienschiefer'), where high contents of organic matter (C_{org} = 2.1 – 4.5 wt.-%) lead to markedly lower grain-density values.

In the underlying Triassic section comprising the Klettgau Formation and the Bänkerjoch Formation, values become larger, as does variability. This reflects the lithological heterogeneity, in particular the variable contents of dolomite and anhydrite with their high mineral densities (2.85 and 2.97 g/cm^3, respectively). Fig. 4.3-5 shows the correlation between grain density and dolomite/ankerite contents. Grain density increases linearly with dolomite concentration, and outliers are due to the presence of anhydrite (except in the Hauptrogenstein and the Klingnau Formation, see above).

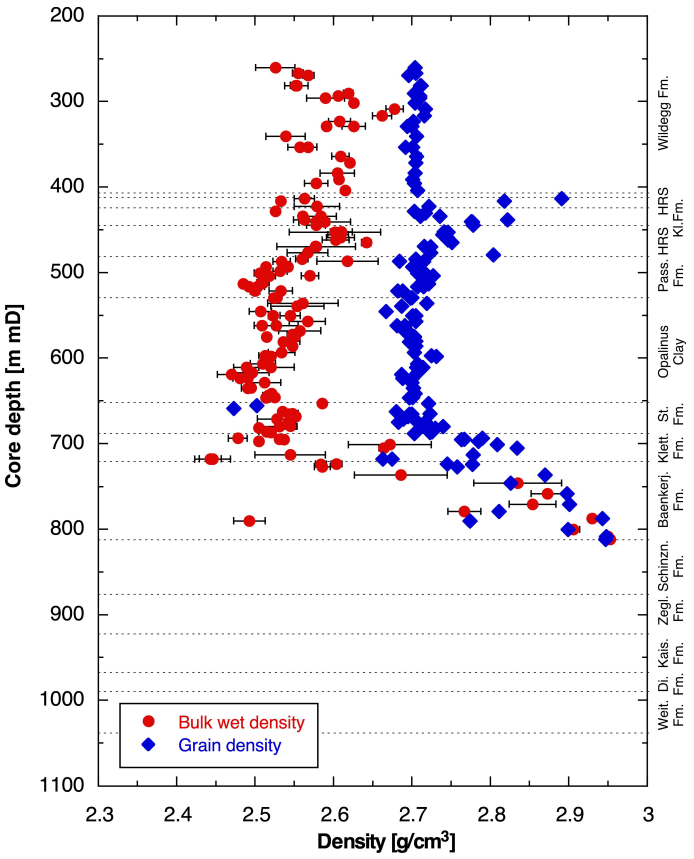

Fig. 4.3-4: Depth profile of bulk wet and grain densities

Black bars for bulk wet density indicate 1σ variability among 3 pieces of the same sample. Analytical error bars for grain density are smaller than the symbol size.

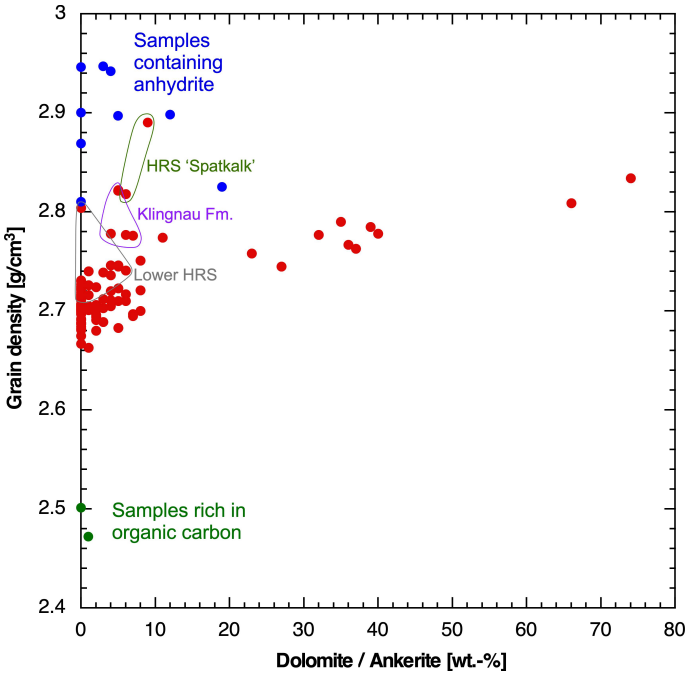

Fig. 4.3-5: Grain density as a function of the contents of dolomite/ankerite

Blue points are from the Bänkerjoch Formation. Green points are from the Rietheim Member of the Staffelegg Formation

4.3.3 Bulk wet density

Data are shown in Fig. 4.3-4 as a function of depth. Large error bars for some samples reflect heterogeneity on the cm-dm scale.

4.3.4 Porosity

Three different approaches were used to constrain rock porosity (for details see Waber (ed.) 2020):

- *Water-loss porosity:* calculation from the gravimetric water content using either bulk wet or grain density.
- *Porosity from isotope diffusive exchange:* calculation from the water content obtained by mass balance using either bulk wet or grain density.
- *Pycnometer porosity:* calculation from bulk dry and grain densities; bulk dry density is calculated from bulk wet density and water content.

Water-loss porosity and porosity from isotope diffusive exchange were calculated using bulk wet density by default. If the latter was not available, grain density was used, by which full water saturation of the pore space is assumed. The graphic in Fig. 4.3-6 shows that the two densities yield near-identical porosities, so the choice of the type of density for the calculation incurs no additional uncertainty.

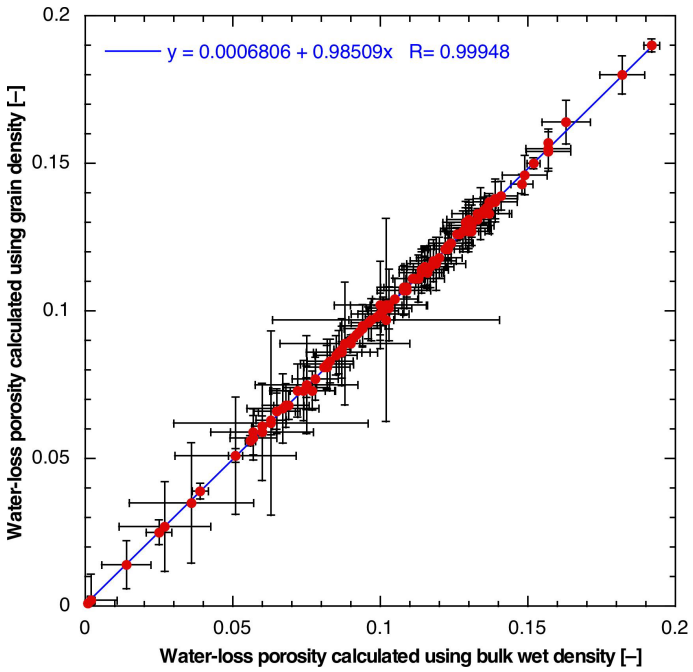

Fig. 4.3-6: Water-loss porosity calculated from gravimetric water content using either bulk wet or grain density

Bars indicate propagated errors, which are dominated by local heterogeneity of water content.

Comparison of porosities obtained by different methods

- An excellent linear correlation is observed between water-loss porosity and porosity from isotope diffusive exchange (Fig. 4.3-7). The latter yields about 15% higher values. The deviation of some samples from the regression line, as well as their large error bars, are explained by cm-scale heterogeneity, as illustrated in Fig. 4.3-9.
- A slightly less good linear correlation is found between pycnometer porosity and porosity from isotope diffusive exchange (Fig. 4.3-8). The latter yields about 19% higher values. Two outliers are explained by sample heterogeneity (see illustrations in Fig. 4.3-9).
- The correlation between water-loss and pycnometer porosity is shown in Fig. 4.3-10. Again, 2 samples fall off the trend (see illustrations in Fig. 4.3-9). Excluding these two outliers yields a slope for the regression line of about 0.89.

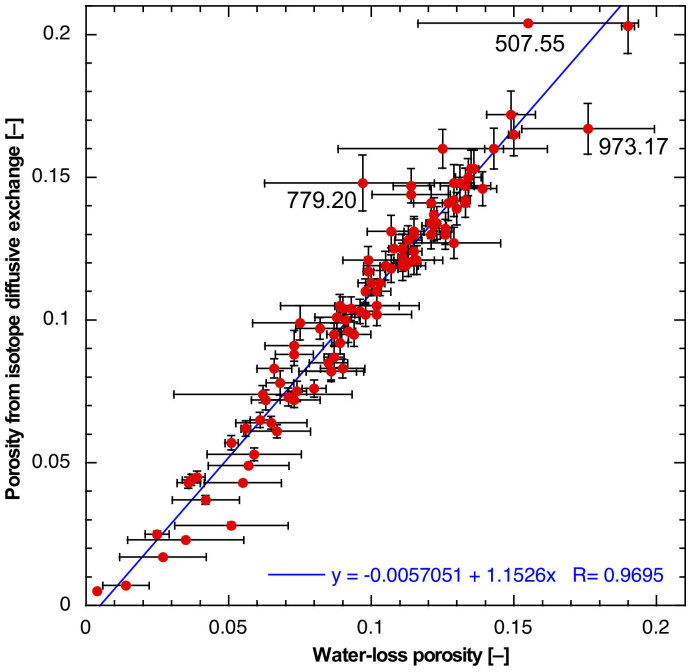

Fig. 4.3-7: Correlation of water-loss porosity and porosity from isotope diffusive exchange

Bars indicate propagated errors. Note that only the gravimetric water contents obtained from the aliquots used for the isotope diffusive exchange experiments are considered for the x-axis of this graph, so the correlation refers to identical sample materials. Three samples falling off the general trend and with large errors are marked (507.55 m, an argillaceous marl from the 'Humphriesi-Schichten', a Fe-oolite; 779.20 m, an anhydrite-clay mixture from the Bänkerjoch Formation; 973.04, a sandstone from the Dinkelberg Formation). All data are included for the calculation of the regression line.

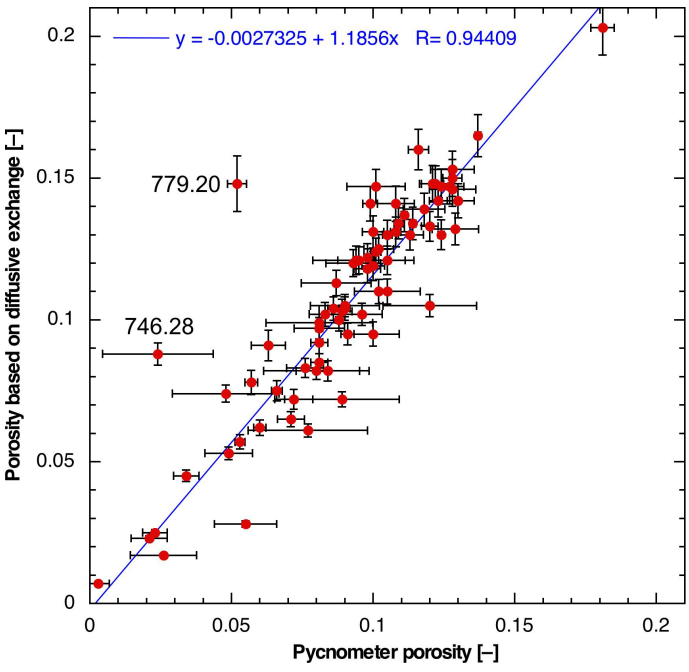

Fig. 4.3-8: Correlation of pycnometer porosity and porosity from isotope diffusive exchange

Bars indicate propagated errors. Indicated outliers were excluded from the regression line.

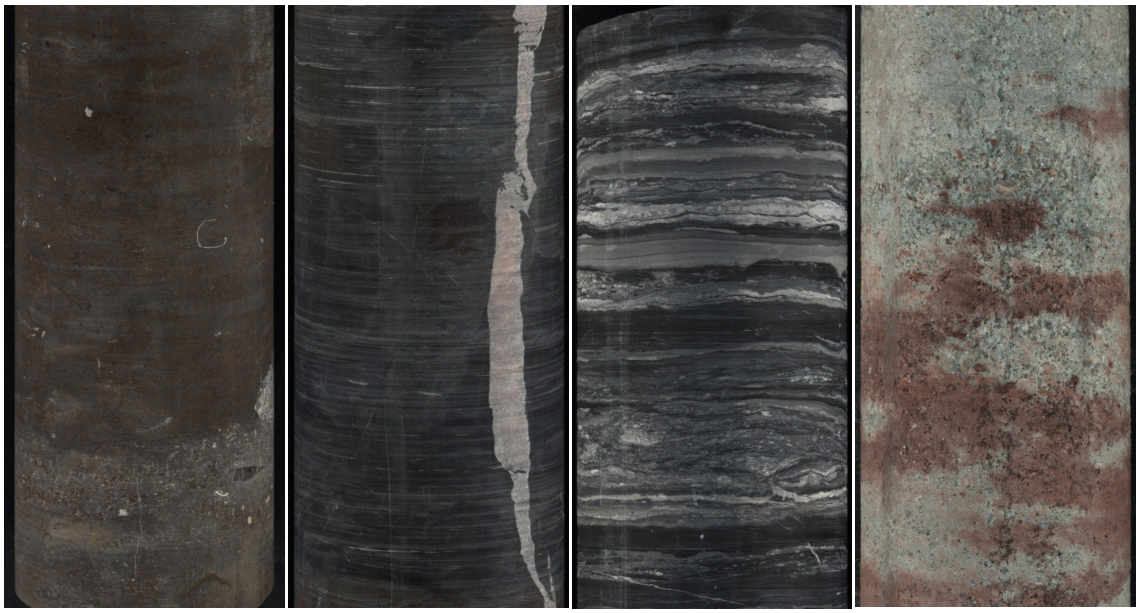

507.55 m ('Humphriesi-Sch.') | 746.28 m (Bänkerjoch Fm.) | 779.20 m (Bänkerjoch Fm.) | 973.17 m (Dinkelberg Fm.)

Fig. 4.3-9: Illustrations of heterogeneous samples

507.55 m: heterogeneous Fe-oolite; 746.28 m: dolomitic claystone with anhydrite veins and nodules; 779.20 m: layered anhydrite-clay mixture; 973.17 m: sandstone. Width of photographs is 10 cm.

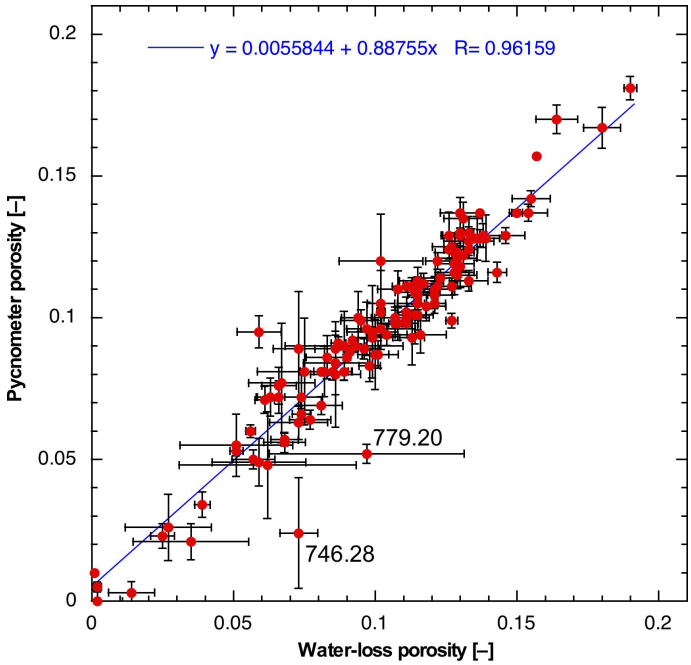

Fig. 4.3-10: Correlation of water-loss and pycnometer porosity

Bars indicate propagated errors. The two indicated outliers were excluded from the regression line.

Depth trends

In Fig. 4.3-11, porosity is shown as a function of depth. The shape of the profile is similar to that of water content (Fig. 4.3-1), including the systematic trends. The comments made on the distribution of water content with depth (Section 4.3.1) also apply to porosity.

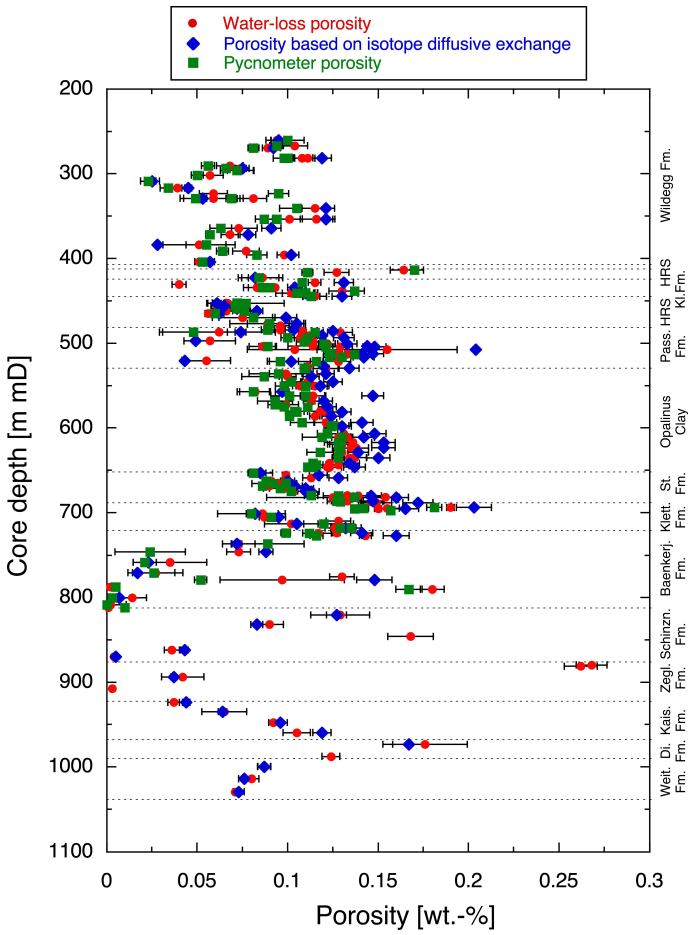

Fig. 4.3-11: Depth trends of porosities obtained by different methods

Porosity as a function of mineralogical composition

The correlation of porosity with clay-mineral content is shown in Fig. 4.3-12. When considering all available data (Fig. 4.3-12a), a general positive correlation can be identified, but scatter is substantial. When only samples from the Malm-Dogger-Lias section are considered, i.e. when the mineralogically and texturally more heterogeneous samples from the Triassic are excluded, a more systematic correlation is obtained (Fig. 4.3-12b). The slope of the data is steeper for clay-mineral contents in the range 0 – 30 wt.-% and becomes flatter at higher clay-mineral contents. Samples 413.63 (Hauptrogenstein, 'Spatkalk') and 507.55 ('Humphriesi-Schichten') are outliers towards higher porosities. These two samples are from brownish condensation horizons, which are known for their particular rock properties.

In the Triassic, a number of highly porous samples with low clay-mineral contents are found in dolomite-rich lithologies of the Schinznach Formation as well as in sandstones of the Dinkelberg Formation. These were affected by diagenetic dissolution to some degree, either during the

process of dolomitisation or at later stages. Thus, their porosity is not the result of compaction and cementation alone. On the other hand, the presence of anhydrite tends to reduce porosity for a given clay-mineral content. Fig. 4.3-13 illustrates that porosity tends to reach values <0.02 for anhydrite-rich samples.

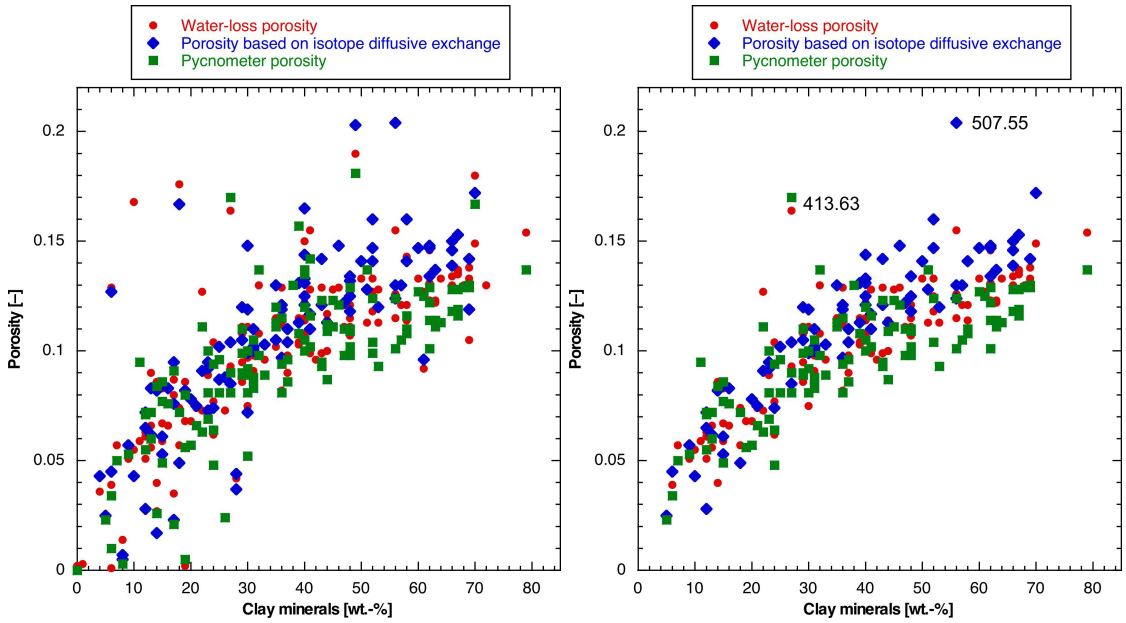

Fig. 4.3-12: Porosity as a function of clay-mineral content. (a) all data, (b) data from the section Malm – Dogger – Lias

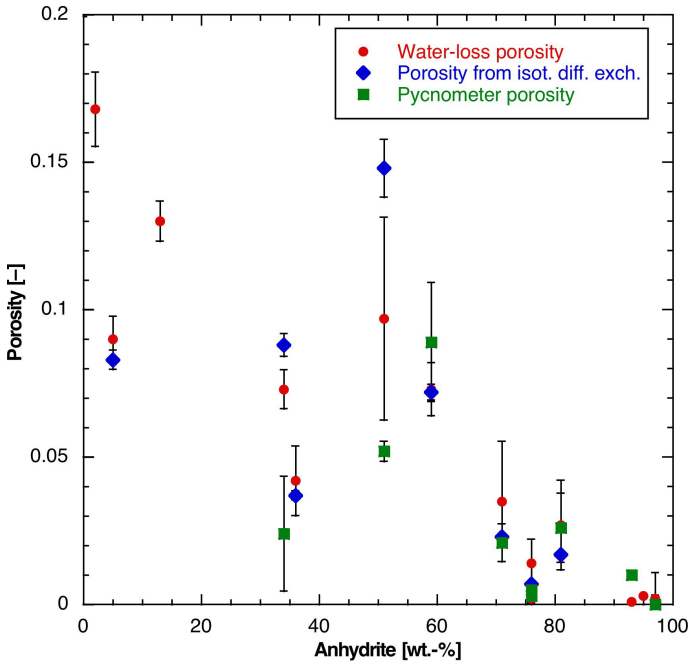

Fig. 4.3-13: Porosity of anhydrite-bearing samples

Bars indicate propagated errors.

4.3.5 Specific surface area and pore size distributions from N_2 ad-/desorption

Thomas Gimmi

Depth trends

The specific surface area S_{BET}[6] varies with the rock formation (Tab. 4.3-2 and Fig. 4.3-14). As N_2 cannot reach any interlayer pores of smectites, S_{BET} represents surfaces of external (non-interlayer) pores. Values in the range of about 20 to 35 m^2/g were generally found for clay-rich units, such as the Passwang Formation, the Opalinus Clay and the upper part of the Staffelegg Formation. Largest values in the range of about 40 to 60 m^2/g are reported for the lower part of the Staffelegg Formation, the upper part of the Klettgau Formation, and partly the Bänkerjoch Formation. This latter formation includes, however, also the lowest value, which was found in the anhydrite sample at 808 m depth. The values scatter between about 5 to 25 m^2/g in the predominantly calcareous lithologies of the Wildegg Formation, the Hauptrogenstein (HRS), and the Klingnau Formation, with a tendency of larger values for calcareous marls compared to limestones. The large range of values found in these formations as well as in the Staffelegg Formation and the Bänkerjoch Formation is linked to the heterogeneity of the clay-mineral contents (Fig. 4.2-1) and of other parameters defining the texture and the pore structure of the sample. Notably, the two samples in the upper HRS ('Spatkalk', 416.35 m) and in the lower HRS (452.61 m), and one sample in the upper part of the Klingnau Fm. (434.29 m) have comparably low values (~ 6 – 8 m^2/g), while two other samples in the lower part of the Klingnau Fm. (at 438.20 m and 440.55 m) show values around 15 m^2/g. A clearly rusty color of the samples was noted in the upper HRS ('Spatkalk') between about 412 and 417 m, and slightly rusty sequences but with a different texture in the lower Klingnau Fm. between ~ 436 and 439 m (see Section 4.2), distinct from the surrounding greyish colors. These local differences point to heterogeneities regarding depositional environment and diagenesis that will also affect the pore structure (but there is no simple relation between color and measured S_{BET}).

Overall, the variation of the specific surface area S_{BET} with depth is related to trends observed in other physical and mineralogical properties of samples from the BOZ1-1 borehole, such as the bulk dry density, the gravimetric water content, the water-loss porosity or the clay-mineral content. Accordingly, clear correlations of specific surface area with these properties are found, as displayed in the following plots.

---

6 The symbol S_{BET} denotes the specific surface are obtained from N_2 adsorption according to the standard method of Brunauer, Emmett & Teller (BET).

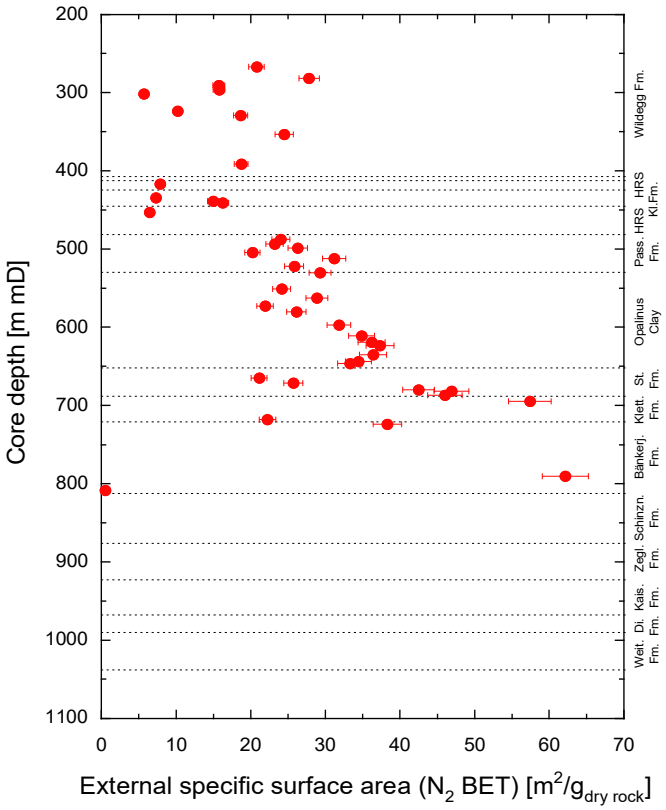

Fig. 4.3-14: Depth profile of specific surface area (S_{BET}) derived from N_2 adsorption

S_{BET} represents external surfaces only. The total specific surface area, including interlayer surfaces, would be larger depending on the smectite content of the sample. Errors resulting from sample preparation and handling are estimated to be ± 5% in general and ± 10% for $S_{BET} < 2$ m^2 g^{-1}, as given by the error bars.

Correlation of S_{BET} with other physical parameters

The relation between S_{BET} and the gravimetric water content relative to the dry sample mass follows an approximately linear trend (Fig. 4.3-15). We see that the largest S_{BET} values in the Lias, Keuper and Dogger (Staffelegg Formation, Klettgau Formation, Bänkerjoch Formation, Opalinus Clay) are all related to comparably large water contents, and the smallest S_{BET} value in the anhydrite sample of the Bänkerjoch Formation (808.61 m) is also related to the smallest water content. This value as well as those at 790.16 m (Bänkerjoch Formation) and 694.72 m (Klettgau Formation) plot above the dashed trend line for all data, whereas those from the upper Hauptrogenstein (416.35 m) and from the lower Klingnau Formation (434.29 m, 438.20 m, 440.55 m), and a value from the Klettgau Formation (717.96 m) plot below the trend line.

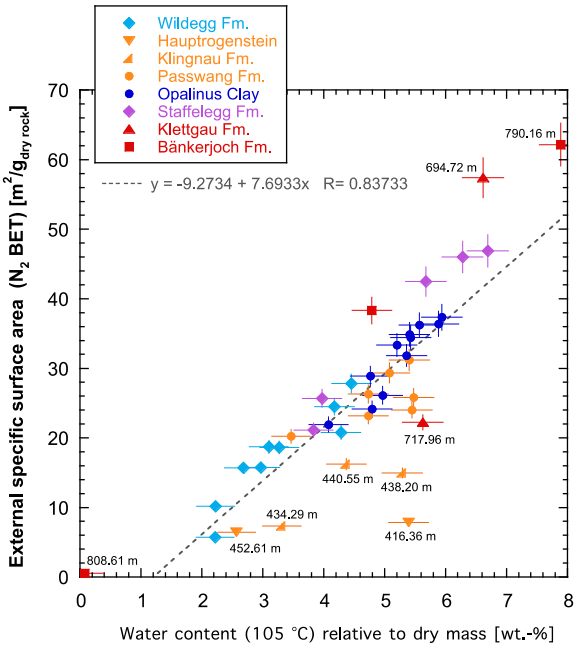

Fig. 4.3-15: Specific surface area (S_{BET}) derived from N_2 adsorption plotted against the gravimetric water content relative to the dry mass of the samples

Error bars show estimated errors for the water content (based on standard deviations of other samples) and estimated errors for S_{BET}.

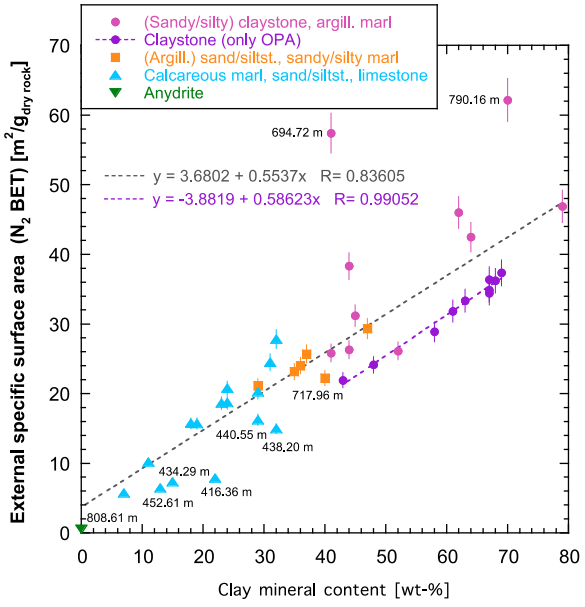

Fig. 4.3-16: Relation between external specific surface area (S_{BET}) derived from N_2 adsorption and content of clay minerals

The samples are assigned to four classes (Opalinus Clay, belonging to the first class, is additionally highlighted) according to their positions in the Füchtbauer diagram (i.e., according to lithological rock types). The linear regression shown in gray is obtained for all samples, while that in purple is specific for the Opalinus Clay samples

The water content is related to the mineral composition of the samples, notably the clay-mineral content, as shown in previous subsections. Accordingly, the specific surface area S_{BET} is also positively correlated with the total content of clay minerals (Fig. 4.3-16), but with some outliers. Especially the two largest S_{BET} values for the samples form the Klettgau Formation (694.72 m) and the Bänkerjoch Formation (790.16 m) plot rather far from the general linear regression. Four different lithological groups are distinguished in this figure, which differ in their ranges of clay-mineral contents. There is some scatter in the first group (claystones, argillaceous marls) that includes the two samples mentioned above. The Opalinus Clay samples, being part of this group, have comparably large clay-mineral contents but comparably lower S_{BET} values. Thus, they plot somewhat below the other samples of this group. They also have a lower scatter when compared to that of all samples in this group. This leads to a clearly higher correlation coefficient for the linear regression just for the Opalinus Clay subgroup. The samples from the Hauptrogenstein, Klingnau Formation and Klettgau Formation that had comparably low S_{BET} when plotted against water content in the previous plot (416.35 m, 434.29 m, 438.20 m, 440.55 m, 717.96 m) also tend to plot below the trend line against the clay content, although less pronounced.

A positive correlation of S_{BET} exists also with the contents of the illite end-member and a weak correlation with those of the smectite end-members (Fig. 4.3-17), whereas no clear correlation with the chlorite or the kaolinite end-member contents is visible. The clear correlation with the illite end-member contents, and possibly also the weak correlation with the smectite end-member content indicates that the dominating clay minerals, illite and illite-smectite, strongly affect the microstructure of the (clayey) samples. The two mentioned samples from the Klettgau Formation (694.72 m) and the Bänkerjoch Formation (790.16 m) plot often as clear outliers compared to the general trend; only in the relation of S_{BET} with the illite content, this Bänkerjoch sample matches approximately the trend given by the other data. The same applies for the mentioned samples from the upper Hauptrogenstein and the Klingnau Formation, and for the two samples from the Wildegg Formation with the lowest S_{BET} of about 6 m^2/g (301.54 m) and 10 m^2/g (323.16 m).

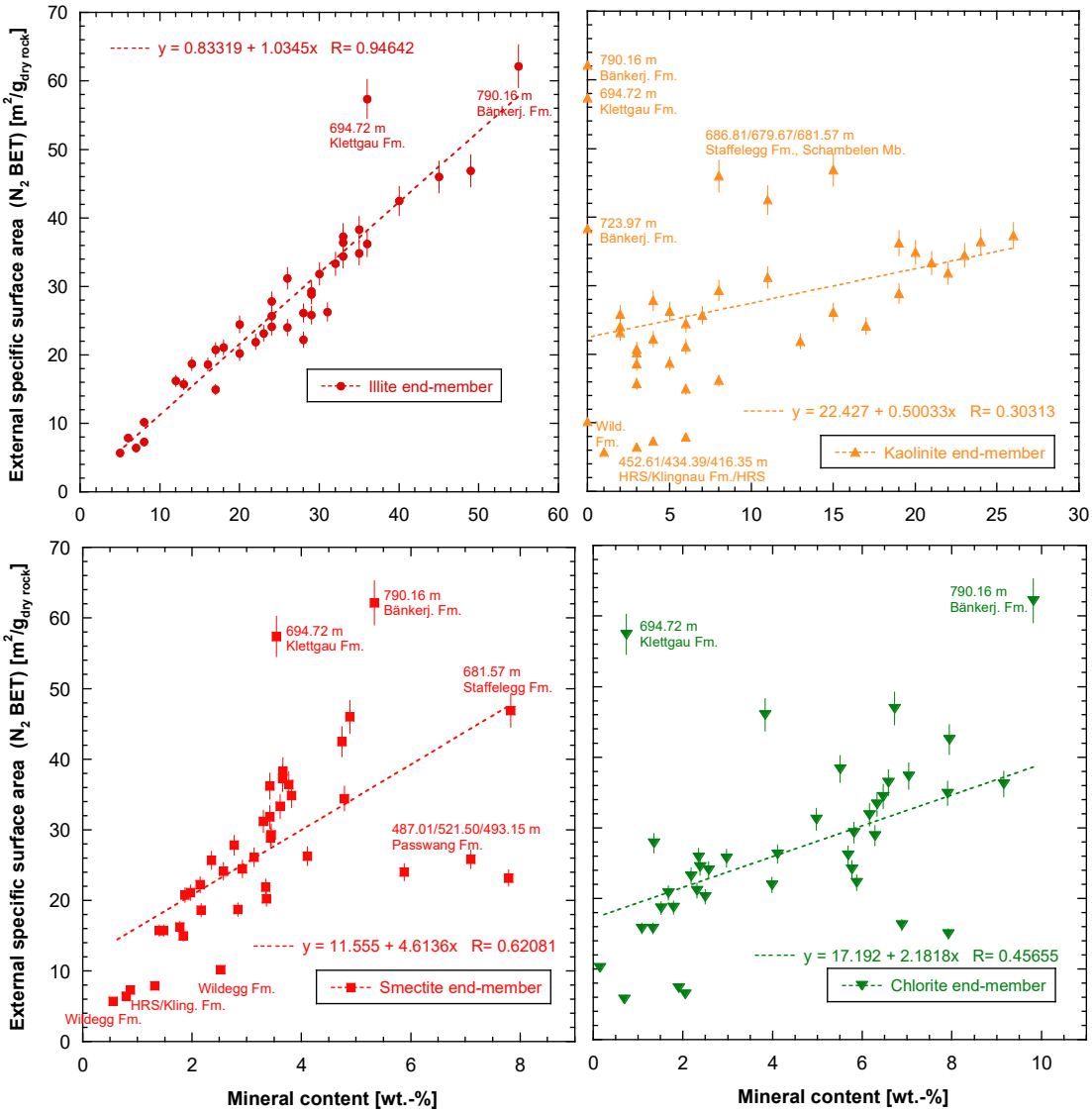

Fig. 4.3-17: Relation between external specific surface area (S_{BET}) derived from N_2 adsorption and contents of specific clay mineral end-members

Average sizes of external pores derived from S_{BET}

Average sizes of external pores were estimated from the specific surface area S_{BET} and the water content per dry mass WC_d as:

$$\overline{r_{ext}} = WC_d/(\rho_w\, S_{BET})$$

with ρ_w the water density taken to be 1 g/mL. This calculation assumes negligible pore volumes in interlayer pores, i.e., it attributes the measured water content to external pores only (which is not appropriate for samples with relevant smectite end-member contents).

From the inverse of the slope of the linear relation in Fig. 4.3-15 (the slope represents S_{BET}/WC_d), we obtain an overall average layer thickness (or radius) of external pores for all samples of 1.3 nm, which corresponds to about 4 to 5 water layers.

Instead of calculating an overall average from the linear regression, it is more interesting to derive an average layer thickness for each sample. Fig. 4.3-18 plots average external pore sizes (attributing all water to external surfaces) for each sample as a function of the gravimetric water content per dry solid mass (a) and as a function of the total clay-mineral content (b). The derived values for the average external layer thickness (or pore radius) are rather small, mostly below 4 nm (average radius of 2.1 nm, median of 1.7 nm). There is a tendency of decreasing values with increasing clay-mineral contents, and thus also with increasing water contents (range of radii of ~ 1 – 3 nm in clay-rich lithologies and of ~ 1.5 – 7 nm in limestones). The limestones and calcareous marls show a comparably large variability, with larger radii for samples from the Wildegg Formation (301.54 m), the Klingnau Formation (434.29 m, 438.20 m, 440.55 m), the lower Hauptrogenstein (452.61 m) and a maximum calculated value of ~ 7 nm (diameter ~ 14 nm) for the sample from the upper Hauptrogenstein (416.35 m). The very argillaceous sandstone/siltstone sample from the Klettgau Formation (717.96 m, Ergolz Member) has also a comparably large value (~ 2.5 nm radius, ~ 5 nm diameter). The anhydrite from the Bänkerjoch Formation (808.61 m) exhibits a rather small radius of ~ 1.4 nm (diameter of ~ 3 nm).

One has to keep in mind that the samples with the largest clay-mineral fractions are very likely those with some interlayer water in smectites. Accordingly, these average external pore sizes represent maximum values for such samples. A correction of average external pore sizes that accounts for the volume of interlayer water based on the smectite end-member content could be made assuming typical smectite particle geometries. However, in view of the involved uncertainties this is not done at present.

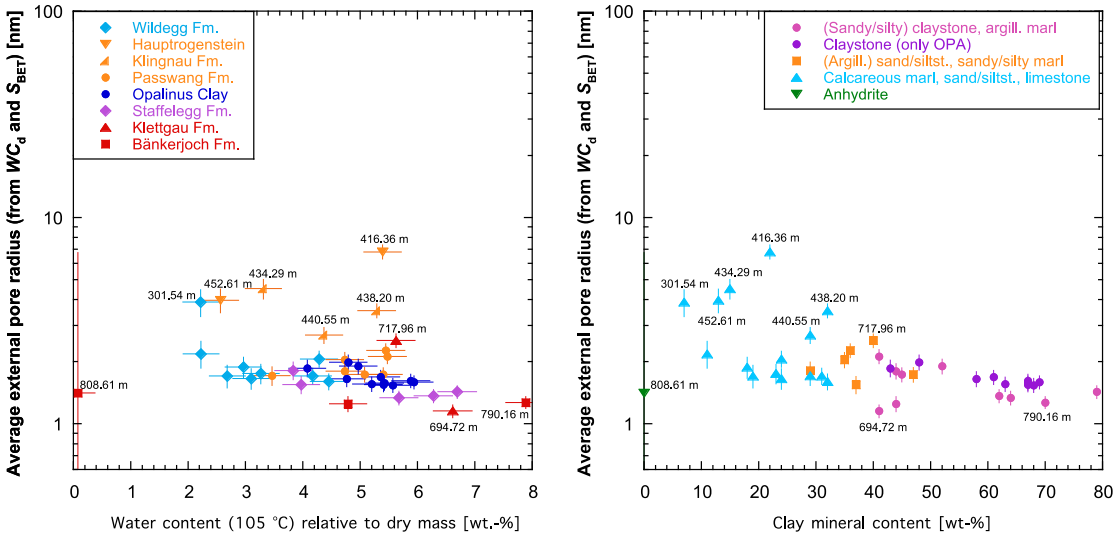

Fig. 4.3-18: Average external pore radius calculated from S_{BET} and the gravimetric water content (assuming insignificant interlayer pore volume) plotted against the gravimetric water content per dry mass of the samples (a) and against the total clay-mineral content (b)

Samples are grouped according to geological units (a) or according to rock lithology (b). Error bars show estimated errors for the water content (based on standard deviations of other samples) and propagated errors for the average external pore radius.

Distribution of external pore sizes derived from N_2 isotherms

Pore size distributions of external pores were derived by the standard BJH algorithm[7] from N_2 ad- and desorption isotherms. The figures in the following present results from N_2 desorption for the samples of the different formations, grouped according to rock lithology. Most samples show more or less prominent peaks at a diameter of about 4 nm in the curves derived from desorption. These peaks are typically related to the closure of the hysteresis of the isotherm and are thus attributed to liquid instabilities (instability of the configuration of liquid nitrogen) rather than to a distinct pore volume in this size range. Such hysteresis is generally interpreted as indicating a relatively complex pore architecture (e.g. Thommes et al. 2015).

Pore size distributions of calcite-rich and clay-poor samples, classified as limestones or calcareous marls according to the Füchtbauer nomenclature, are displayed in Fig. 4.3-19a. The isotherms of these samples are characterised by a comparably small hysteresis (i.e., comparably simple pore architecture) and thus show only a comparably small peak at ~ 4 nm. The majority of these pore size distributions are bimodal, with maxima near 10 – 20 nm and 50 – 60 nm or 100 – 200 nm (left plot of Fig. 4.3-19a). Partly, one of these peaks is more important than the other. For many limestone samples, the peak at the larger size of ~ 100 – 200 nm tends to be more important, while for most calcareous marl samples (281.72 m, 353.36 m, 438.20 m, 440.55 m, 503.67 m) and some limestone samples, the main peak is located near 10 nm and a secondary, less important peak near 60 nm. The greater importance of the smaller pores may partly be related to a marly nature of the samples. The four limestone samples at 323.16 m, 416.35 m, 434.29 m and 452.61 m (Fig. 4.3-19a right plot), in contrast, have a single, but rather broad peak with comparably low intensity (samples at 323.16 m from the Wildegg Formation, 434.29 m from the upper Klingnau Formation and 452.61 m from the lower Hauptrogenstein) or considerable intensity (sample at 416.35 m from the upper Hauptrogenstein) in the range of ~ 10 – 100 nm. These broad peaks at larger sizes are consistent with the comparably small specific external surface areas of these samples and the partly different texture of the cores. The sample at 301.54 m from the Wildegg Formation similarly shows most pores at larger diameters (two peaks at ~ 30 nm and at ~ 200 nm). The reliability of the results can be tested by comparing maximum adsorbed amounts of N_2 at highest N_2 pressures, expressed as wt.-% H_2O, with the samples' water contents (Fig. 4.3-19). In general, the values agree approximately. The limestone samples from 301.54 m, 329.10 m and 391.30 m plot somewhat above the 1:1 line. This could indicate that some pore size fractions (presumably those of large sizes) derived from the N_2 isotherms are slightly overestimated, but it could also be related to heterogeneity at the centimetric scale, because different samples were used to determine the water content and the N_2 isotherms.

Pore size distributions of samples classified as (argillaceous) sandstone/siltstone or sandy/silty marl according to the Füchtbauer nomenclature (Fig. 4.3-18b) are generally relatively broad (when ignoring the peak at ~ 4 nm related to hysteresis closure). The modes, if present, are located near 10 nm and in the range of 40 – 100 nm, similarly as for the limestones and calcareous marls. However, the peaks are relatively flat. In two samples, a more important peak is found near (529.56 m) or below 10 nm (717.96 m), one sample (487.01 m) has two peaks near 10 nm and 100 nm, and the remaining three samples (493.15 m, 665.00 m, 670.95 m) have a slight tendency of a peak at larger sizes (~ 40 – 100 nm) but overall, a rather flat distribution. Most of these samples have maximum amounts of adsorbed N_2 similar or slightly lower than their water contents (Fig. 4.3-19), lending confidence to the derived size distributions.

---

[7] The BJH algorithm developed by Barrett, Joyner & Hallenda evaluates the pore size distribution from N_2 isotherms by considering capillary condensation and surface adsorption.

Pore size distributions of samples classified as (sandy/silty) claystone or argillaceous marl are split into Fig. 4.3-18c and d, with d presenting all Opalinus Clay samples. All samples in the two subfigures show a very significant hysteresis peak at ~ 4 nm, indicating a complex pore architecture, and most of them have an important peak at or below ~ 10 nm and a less important peak between ~ 60 and 100 nm (exceptions: sample 521.50 m from the Passwang Formation and Opalinus Clay sample at 572.43 m, with weak peaks of about equal importance at ~ 15 – 20 nm and ~ 60 nm). The relative contributions of the two peaks to the pore size distribution vary to some degree but compared to the limestone samples and the (argillaceous) sandstone/siltstones or sandy/silty marls, the peak at small pore sizes (at or below ~ 10 nm) is in most cases more important. It furthermore tends to become more important and to move to lower pore sizes with increasing depth: it is located at ~ 10 nm for the uppermost samples at 498.32 m and at 512.03 m, is clearly below 10 nm for all Opalinus Clay samples, and between ~ 4 – 6 nm, partly merging with the hysteresis peak, for the deepest samples. This is mostly related to the increasing clay mineral content with depth. The peak at smallest sizes becomes very important for samples from the Gruhalde Member in the Klettgau Formation (694.72 m) and the samples from the Bänkerjoch Formation (723.97 m and 790.16 m). The latter, classified as claystone with anhydrite nodules or thin-layered anhydrite claystone sequence, respectively, have rather extreme pore size distributions. The maximum adsorbed amount of N_2 is mostly similar or somewhat smaller than the water content (Fig. 4.3-20), lending credibility to the estimated pore size distributions.

The sample at 808.61 m consists of 97% anhydrite. It has a rather small porosity and thus only a very flat peak, located at 30 – 40 nm, and also only a very small hysteresis peak, indicating a comparably simple pore structure. The distribution looks very different from the two other Bänkerjoch samples (723.97 m and 790.16 m) classified as claystones with anhydrite nodules or anhydrite/claystone sequence; those have a strong peak at pore sizes of 5 – 6 nm. As the maximum adsorbed amount of N_2 is much larger than the water content (Fig. 4.3-20, ~ 0.3 H_2O wt.-% vs. 0.079 wt.-%, i.e., factor of 3.8), the estimated pore size distribution may be biased presumably to larger values.

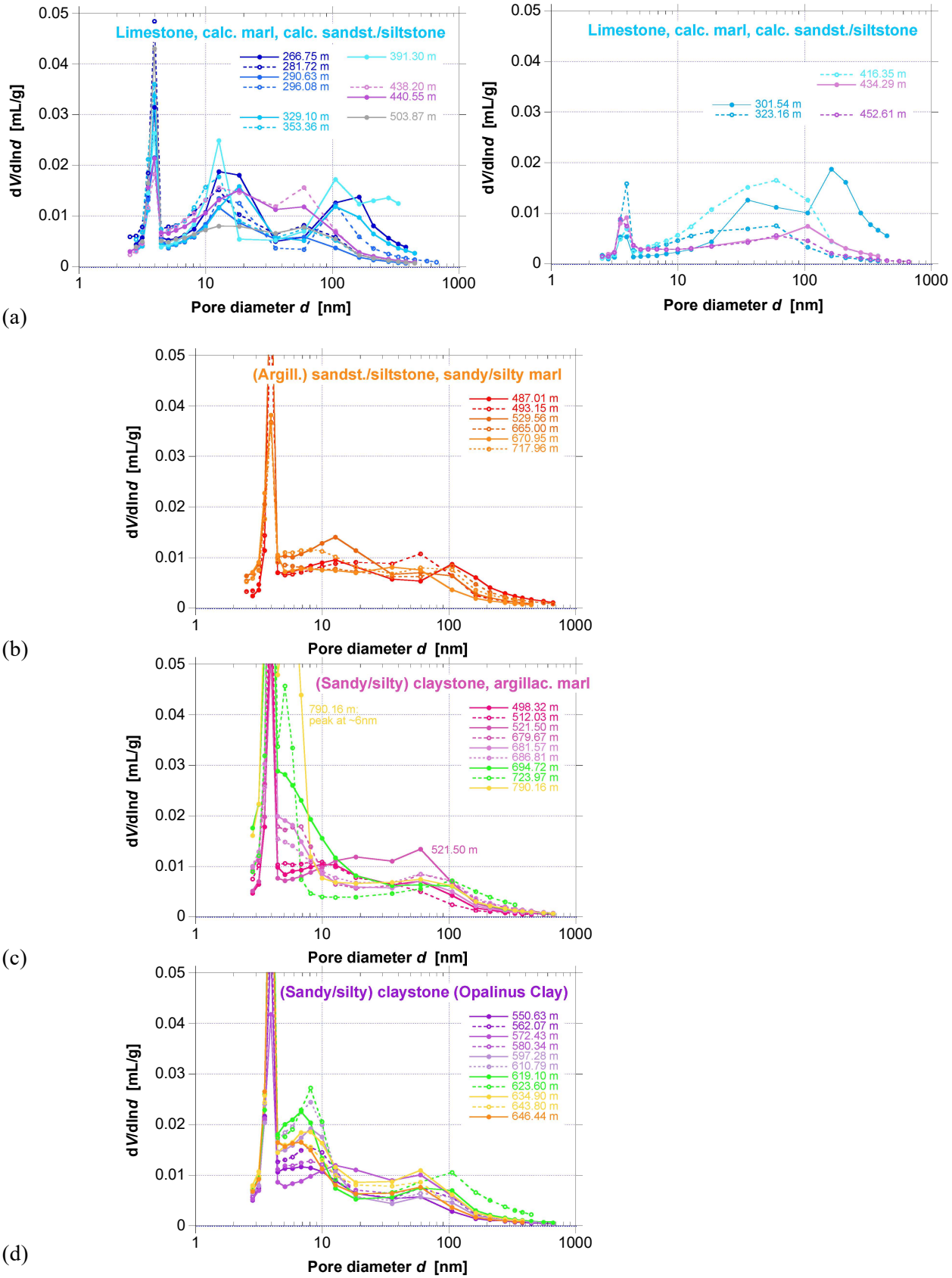

Fig. 4.3-19: (see opposite page)

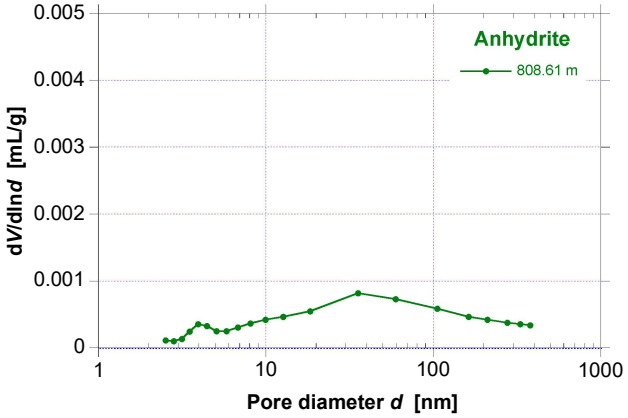

(e)

Fig. 4.3-19: Distribution of (external) pore sizes derived from N_2 desorption

(a) Limestone samples (266.75 m, 290.63 m, 296.08 m, 301.54 m, 323.16 m, 329.10 m, 391.30 m, 416.35 m, 434.29 m, 452.61 m) and calcareous marl samples (281.72 m, 353.36 m, 438.20 m, 440.55 m, 503.87 m), (b) (very argillaceous) sandstone/siltstone samples (529.56 m, 665.00 m, 670.95 m, 717.96 m) and sandy/silty marl samples (487.01 m, 493.15 m), (c) and (d) (sandy/silty) claystone samples and argillaceous marl samples (498.32 m, 694.72 m, 723.97 m), with all Opalinus Clay samples shown in (d), and (e) the anhydrite sample (808.61 m, note the 10 times smaller *y*-axis range compared to the other subfigures)

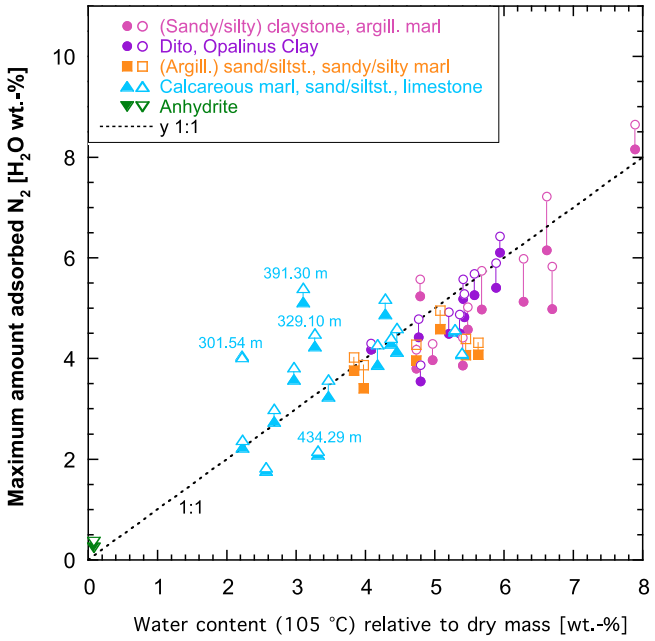

Fig. 4.3-20: Comparison of maximum amount of adsorbed N_2 (recalculated to H_2O wt.-%) with water content per dry sample mass

Open symbols: adsorption, closed symbols: desorption

Average sizes of external pores based on pore size distributions calculated from the N_2 isotherms

Average sizes of external pores cannot only be derived from S_{BET} and the water content as shown above but also from the pore size distribution derived from N_2 isotherms. In both cases, it is assumed that interlayer pore volumes (which are not probed by N_2 adsorption) are insignificant. Radii directly derived by averaging the BJH pore size distributions (Fig. 4.3-21) are larger (average radius of 4 – 5 nm, median of 3 – 4 nm) when compared with the average radii determined from S_{BET} and the gravimetric water content (Fig. 4.3-18) but show the same tendencies: smaller radii (~ 2 – 5 nm) for the claystones and argillaceous marls and larger radii, but with some scatter, for the limestones (~3 – 16 nm), with the largest radii for samples from the Wildegg Formation at 301.54 m and from the upper Hauptrogenstein at 416.35 m. In contrast to the small average pore radius (~ 1.4 nm) estimated from the water content and S_{BET}, the anhydrite sample shows a comparably large average pore radius estimated from the BJH size distribution of ~ 10 – 13 nm. This could mean that a considerable part of the surface S_{BET} is associated with larger pores, i.e., that the size distribution is weighted towards larger sizes in this sample, as it seems evident from the distribution in Fig. 4.3-19. When comparing these numbers, one has to keep in mind, however, that (a) any interlayer pores of smectites are not represented through N_2 adsorption (as for the estimate from S_{BET} and the water content), and (b) the maximum adsorbed N_2 volume partly deviates from the water content of the samples (Fig. 4.3-20), as discussed above. The adsorbed amount of N_2 exceeds the water content by 30% or more for samples from 391.30 m, 301.54 m and 329.10 m, and even much more for the anhydrite sample at 808.10 m. For these samples, the reported average sizes derived from the N_2 isotherm may overestimate true average sizes, unless the differences are related to heterogeneities at the centimeter scale, as different subsamples were used for the two measurements.

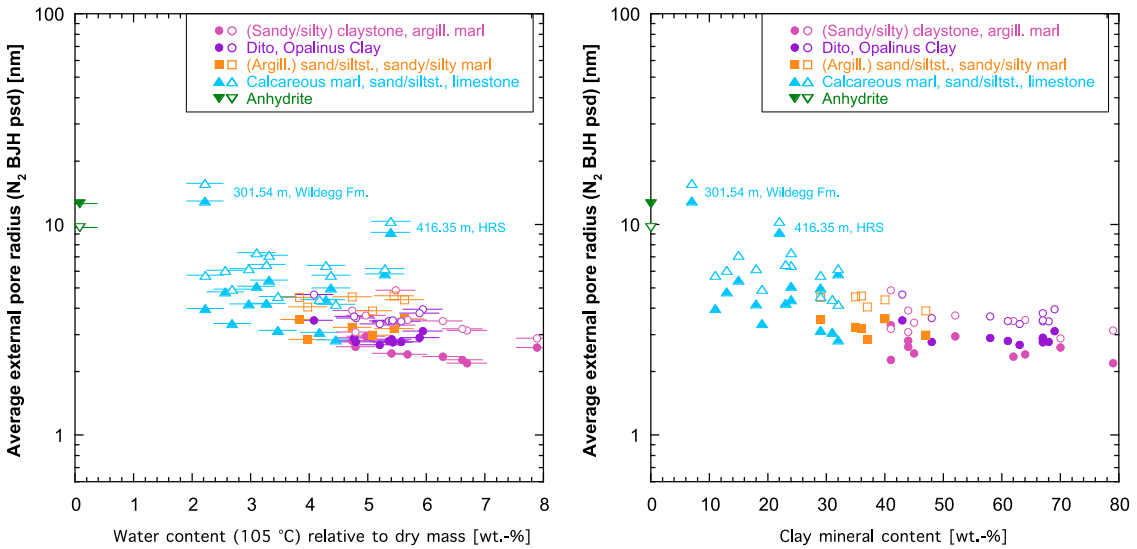

(a) (b)

Fig. 4.3-21: Average external pore radius (assuming insignificant interlayer pore volume) based on the BJH pore size distribution from the N_2 isotherms (closed symbols: adsorption; open symbols: desorption) plotted against the gravimetric water content per dry mass of the samples (a) and against the total clay-mineral content (b)

Samples are grouped according to rock lithology. Error bars show estimated errors for the water content per dry mass (based on standard deviations of other samples).

4.4 Data from aqueous extraction tests

Carmen Zwahlen

Aqueous extraction (AqEx) tests are a simple but useful method to improve the understanding of the porewater – rock system across a sequence of sedimentary rocks if carried out at regular intervals. In this section, we present the data from aqueous extraction tests performed on wet and dry rock sample at a solid to liquid ratio of approximately 1. The aqueous extraction tests on dried regular water content subsamples were carried out to reduce the uncertainty regarding the variability of the water content within a core sample. The data are discussed further in Chapter 5. The full dataset can be found in Appendix A and details about the method are given in Section 3.3 and Waber (ed.) (2020).

4.4.1 Sample material and overview of analytical work

A total of 103 moisture-preserved drill core samples (PW and AD) from the Malm to the Rotliegend and 31 dried drill core samples from the Malm to the Bänkerjoch Formation were subjected to aqueous extraction tests. Additionally, the data of the extract solutions were used to model the mineral saturation states and the partial pressure of CO_2. These parameters were calculated with the PHREEQC Version 3 code (Parkhurst & Appelo 2013) and the PSI/Nagra thermodynamic database (Thoenen et al. 2014) assuming a temperature of 25 °C.

Tab. 4.4-1: Summary of analytical work performed on samples for aqueous extraction tests from the different geological formations (excluding duplicate and post-mortem extracts of AD and SQ experiments; *cf.* Sections 4.7.4 and 4.6.5)

Sample type: PW: porewater sample, AD: Advective displacement sample, SQ: Sqeezing samples, OD: outdiffusion samples, RS: Rock salt, AqEx: aqueous extraction tests, S/L: solid to liquid ratio.

Group	**Formation**	**Sample type**	**AqEx at S/L 1, pH, Alkalinity, Cations, Anions**
Malm	Wildegg Fm.	PW	17
Dogger	Hauptrogenstein	PW, AD, OD	17
Dogger	Klingnau Fm.	PW, OD	6
Dogger	Passwang Fm.	PW, AD, OD	24
Dogger	Opalinus Clay	PW, AD	26
Lias	Staffelegg Fm.	PW, AD	9
Keuper	Klettgau Fm.	PW, AD, SQ	8
Keuper	Bänkerjoch Fm.	PW, SQ	9
Muschelkalk	Schinznach Fm.	PW	5
Muschelkalk	Zeglingen Fm.	PW, RS	6
Muschelkalk	Kaiseraugst Fm.	PW	4
Buntsandstein	Dinkelberg Fm.	PW	2
Rotliegend	Weitenau Fm.	PW	3
Total		PW, AD, OD, SQ	134

4.4.2 Aqueous extraction tests at a S/L of 1

Ion concentrations in aqueous extracts have a limited significance if they are not recalculated to porewater concentrations, either to the measured water content or to the water content corrected for anion exclusion. For chemically conservative compounds, this recalculation is established in Chapter 5. Thus, in this section only ion ratios (and Br and Cl profiles) are presented, as they are independent of the recalculation formalisms.

4.4.2.1 Contamination by drilling fluid

During sample preparation, approximately 1.5 cm of rim material is removed from the drill core samples to avoid contamination by the drilling fluid. However, in porous and permeable rocks such as e.g. dolostones or sandstones, the drilling fluid might reach the central parts of the drill core. This was already observed in a few samples from the BUL1-1, TRU1-1 and MAR1-1 boreholes (Mazurek et al. 2021, Aschwanden et al. 2021, Mäder et al. 2021).

The drilling fluid was a potassium silicate mud down to the upper part of the Zeglingen Formation and a NaCl drilling mud below. The K-silicate drilling mud is highly alkaline, characterised by a high Si and K concentration (ca. 40 g/L Si, 70 g/L K, mostly balanced by OH) and only a small portion is required to affect an entire aqueous extract. The K-silicate drilling mud contains SO_4, Cl and Na concentrations that do not differ much from porewater concentrations and thus bear much less potential to contaminate the aqueous extracts (drilling mud ca. 9 g/L SO_4, 0.4 g/L Cl and 1.7 g/L Na). There is no analytical information on the Na-Cl drilling mud, however, this drilling mud bears the potential to modify the Na and Cl concentration of the porewater in certain samples.

In this borehole, we identified four samples from the Schinznach and Zeglingen Formation that show evidence for contamination by the K-Si-drilling fluid for selective components (Tab. 4.4-2). All these samples exhibit a high K concentration that correlates directly with the water content. The Na/K ratio in these samples is below 1.5, which is difficult to reach through evolving marine porewater in the corresponding formations, or by later processes. Additionally, half of the contaminated samples have elevated alkalinity and pH values pointing towards contamination by the drilling fluid (Tab. 4.4-2). All four contaminated samples are dolostones with a high porosity and likely elevated matrix permeability allowing percolation of the drilling fluid to central parts of the drill core sample.

For Br and Cl, the maximum estimated proportion of contamination lies within the analytical uncertainty except for the sample from the Zeglingen Formation (at 881 m depth), where the contamination might exceed 20%. For Na and SO_4, the estimated proportion of contamination is higher than the analytical uncertainty in most or half of the contaminated samples, respectively. This estimation of the extent of contamination is based on the K concentration of the drilling mud and assumes that all measured K in the aqueous extracts derives from the drilling mud. All samples that show indications for contamination by the drilling fluid in the presented ion concentration are highlighted with red circles in the following figures.

Additionally, all AD samples exhibit Na/K ratios that are below the neighbouring PW samples resulting from twice as much K (Fig. 4.4-5). The excess K results likely from the drilling fluid, but the extent of contamination is minor and too low to affect any other ion concentrations. Therefore, these samples are not further mentioned in Tab. 4.4-2.

We identified one sample from the Zeglingen (at 879 m depth) and two samples from the Dinkelberg Formation that are likely contaminated by the NaCl drilling mud (Tab. 4.4-2). In these samples halite crystals were detected by XRD, which is likely a secondary feature. These samples are circled with a dashed red line in all figures, even though the amount of contamination cannot be estimated due to the lack of drilling mud analysis from that depth.

Tab. 4.4-2: List of 7 samples and their geochemical characteristics which classify them as contaminated by the drilling fluid

The K-Si drilling fluid is characterised by a high pH, alkalinity and a high K concentration. The Na-Cl drilling fluid is characterised by a high Cl and Na concentration.

Depth [m]	**Formation**	**Member**	**WC_{wet}** [%]	**K** [mg/L]	**Na/K** [mol/mol]	**pH**	**Alk** [meq/L]	**Cl** [mg/L]	**Na** [mg/L]
820.53	Schinznach Fm.	Stamberg Mb.	5.205	545	0.3	8.1	1.3	169	106
831.86	Schinznach Fm.	Stamberg Mb.	3.539	195	1.2	8.2	0.6	235	139
846.00	Schinznach Fm.	Stamberg Mb.	6.953	1'869	0.2	10.1	4.0	354	261
879.74	Zeglingen Fm.	'Dolomitzone'	11.952	410	26.4	7.8	4.6	9'542	6'360
881.21	Zeglingen Fm.	'Dolomitzone'	11.618	4'518	0.01	10.8	79.5	182	39
973.17	Dinkelberg Fm.		7.34	33.1	39	7.9	1.1	1'114	759
987.48	Dinkelberg Fm.		4.966	197	43.6	7.9	2.5	7'489	5'052

4.4.2.2 Anions

The Cl concentrations in the aqueous extracts range from 2.6 to 9'542 mg/L and reach maximum values in the Schinznach and Dinkelberg Formation. The Br concentrations vary from below the limit of detection to 0.94 mg/L in the Schinznach Formation.

Most samples from the Passwang and upper Opalinus Clay exhibit a molar Br/Cl ratio close to the seawater ratio. The samples from the Wildegg Formation to the Hauptrogenstein and the Bänkerjoch Formation plot above the seawater ratio. The remaining samples from the upper Opalinus Clay to the Weitenau Formation plot substantially below the seawater ratio (Fig. 4.4-1). There are three samples from the Zeglingen and Dinkelberg Formation that are not shown on Fig. 4.4-1 due to exceptionally high Cl values (contaminated by the drilling fluid).

The depth profile of the Br/Cl ratio (Fig. 4.4-2) displays a smooth trend with decreasing Br/Cl ratios from the Wildegg Formation to the base of the Klettgau Formation. Note, that most dry extracts in the Passwang Formation have often lower ratios compared to the wet extracts. The Br/Cl ratios increase in the Bänkerjoch Formation and reach similarly high values as the highest samples of the Wildegg Formation. Subsequently, the ratios drop sharply to much lower values and increase again towards the base of the Schinznach Formation. The samples from the top of the Zeglingen Formation to the base of the Weitenau Formation follow roughly the trend set by overlying units and scatter around 0.4, however, the sample at 881 m depth has a higher value but is contaminated by drilling fluid. The rock salt sample at 915 m depth exhibits a Br/Cl ratio of 0.02 and fits well with the low ratio observed in PW samples in the Zeglingen Formation.

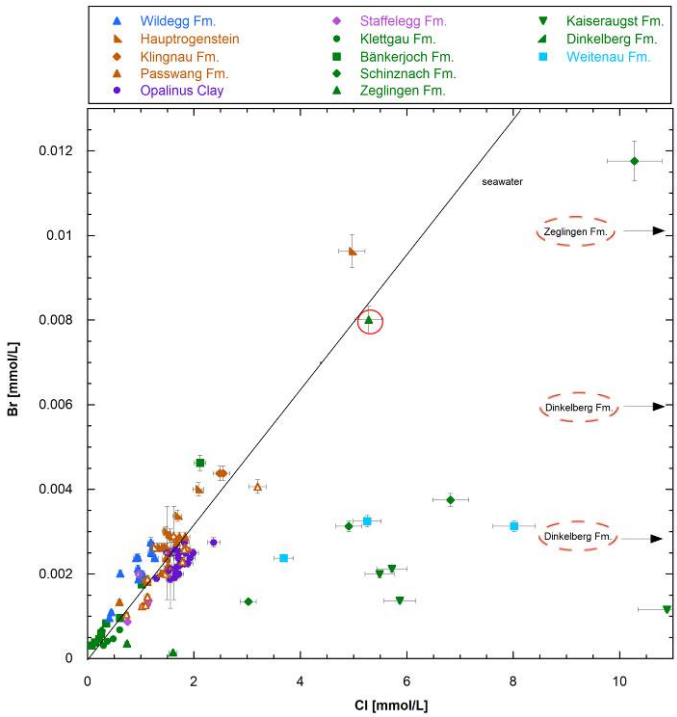

Fig. 4.4-1: Molar Br versus Cl concentrations in aqueous extracts at a S/L ratio of about 1

'Dry' aqeous extract samples are shown with empty symbols. Samples where the contamination by the drilling fluid likely exceeds the analytical uncertainty are circled in red. Samples with an uncertain amount of contamination are marked with a dashed red circle.

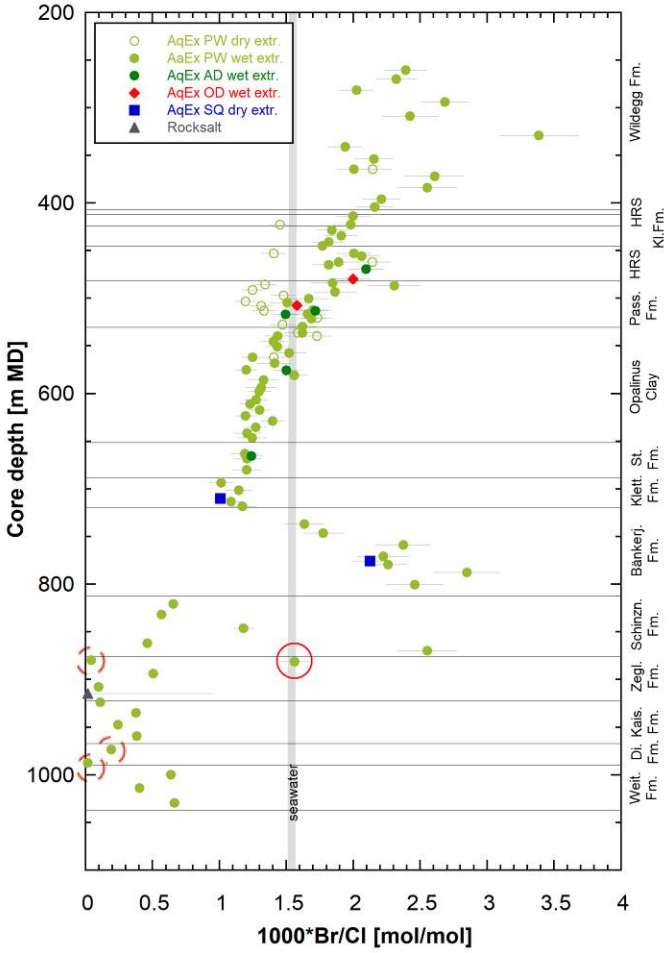

Fig. 4.4-2: Depth profile of the molar Br/Cl ratio in aqueous extracts at a S/L ratio of about 1

Samples where the contamination by the drilling fluid likely exceeds the analytical uncertainty are circled in red. Samples with an uncertain amount of contamination are marked with a dashed red circle.

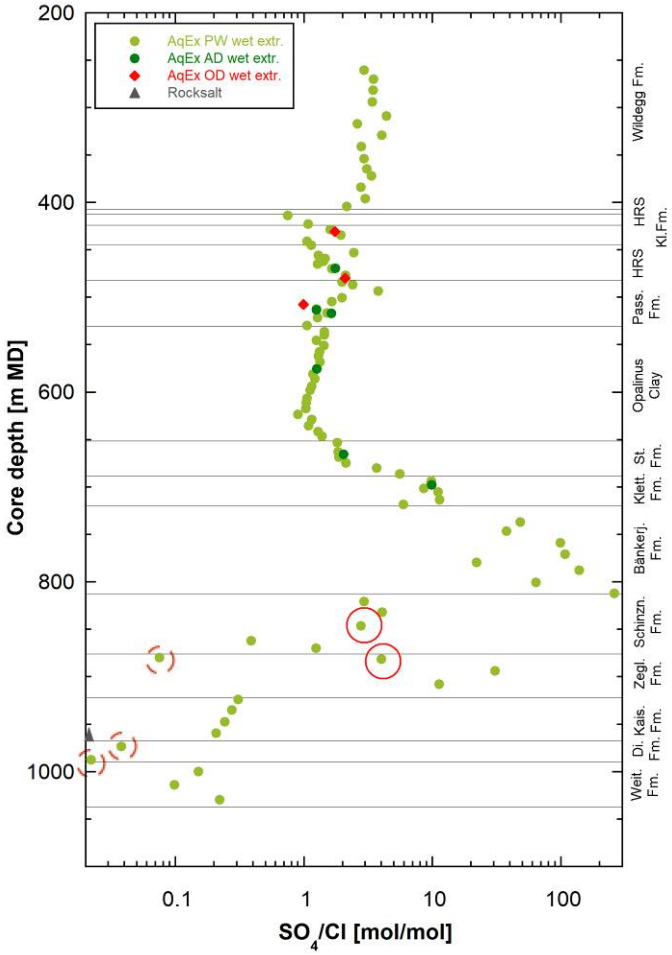

Fig. 4.4-3: Depth profile of SO_4/Cl molar concentration ratio in aqueous extracts at a S/L ratio of about 1

Samples where the contamination by the drilling fluid likely exceeds the analytical uncertainty are circled in red. Samples with an uncertain amount of contamination are marked with a dashed red circle.

The SO_4 concentration varies between 31.0 and 445 mg/L with the exception of anhydrite-bearing samples from the Bänkerjoch, Schinznach and Zeglingen Formation where concentrations range from 1'340 up to 4'329 mg/L. The depth profile of the SO_4/Cl ratio in aqueous extract solutions shows a continuous decrease across the Wildegg Formation and a step-like change to a sample with much lower ratio due to higher Cl concentrations in the top Hauptrogenstein. Subsequently, the ratio increases towards the upper part of the Passwang Formation and continues with a smooth decreasing trend to the lower part of the Opalinus Clay. Towards the base of the Bänkerjoch Formation, the ratio increases and reaches maximum values in anhydrite-bearing samples. The Schinznach and Zeglingen Formation exhibit lower SO_4/Cl ratios with a large scatter over a couple of orders of magnitude. The ratios in the Zeglingen Formation are higher than the low ratio measured in the rock salt samples. The ratios decrease smoothly across the Kaiseraugst Formation, drop in the Dinkelberg Formation, and are a bit higher again in the Weitenau Formation.

The F concentrations in aqueous extracts range between 0.2 and 8.4 mg/L across the whole depth profile (not shown) with the highest values being in the Klingnau, Hauptrogenstein, and Passwang Formation. The alkalinity varies between 0.2 and 5.0 meq/L when excluding the contaminated sample (alkalinity affected by OH). The pH is fairly constant from the Wildegg to the Klettgau Formation and continues with more scatter and lower values from the Bänkerjoch Formation down to the Weitenau Formation. The values range from 6.4 up to 9.5, disregarding the two likely contaminated samples with an even high pH (Tab. 4.4-2).

4.4.2.3 Cations

The Na concentrations in the aqueous extracts vary between 7 and 838 mg/L with maximum values reached in the Bänkerjoch Formation with the exception of two samples in the Dinkelberg and Zeglingen Formation reaching > 5'000 mg/L. The Na/Cl ratios show little variability throughout the Malm and Dogger section of the depth profile. The ratios increase in the Staffelegg Formation until reaching a maximum in the Klettgau and Bänkerjoch Formation. The Na/Cl ratios decrease throughout the Bänkerjoch Formation towards constant low values in the Schinznach and Zeglingen Formation, except for an outlier in the Zeglingen Formation with a high Na and low Cl concentration. The ratios in the lower part of the profile align with that of the rock salt samples.

The K concentrations range from 2.9 mg/L up to 197 mg/L in the Dinkelberg Formation, disregarding the contaminated samples. The Na/K ratios present a complex depth profile with the highest ratios in the Klettgau Formation. The very low Na/K ratios observed in the Schinznach and Zeglingen Formations are indicative for drilling fluid contamination (elevated K) as discussed in detail in Section 4.4.2.1. All AD samples plot below the neighbouring PW samples and exhibit twice the K concentration. This additional K arises most likely from the drilling fluid and it could be that some small particles from the rim were mixed into aqueous extraction material. However, the extent of contamination is not large enough to affect other ion concentrations (see Section 4.4.2.1). The K concentration of the rock salt is below the limit of detection, which leads to minimum ratios of 6500 far from the measured PW samples.

The Sr concentrations range between 0.025 and 16.4 mg/L and maximum values are measured in the Hauptrogenstein and Bänkerjoch Formation. The Sr/Cl ratios (not shown) plot in a narrow range throughout the Malm and Dogger sections with a couple of outliers. In the underlying formations, the Sr/Cl ratios increase up to a maximum in the Bänkerjoch Formation with a subsequent decrease to lower values in the Schinznach and Zeglingen Formation. This can be explained by the release of Sr from the dissolution of anhydrite or celestite during aqueous extraction. Celestite was not detected in any anhydrite-bearing sample but was observed in the same lithologies in another borehole (BUL1-1).

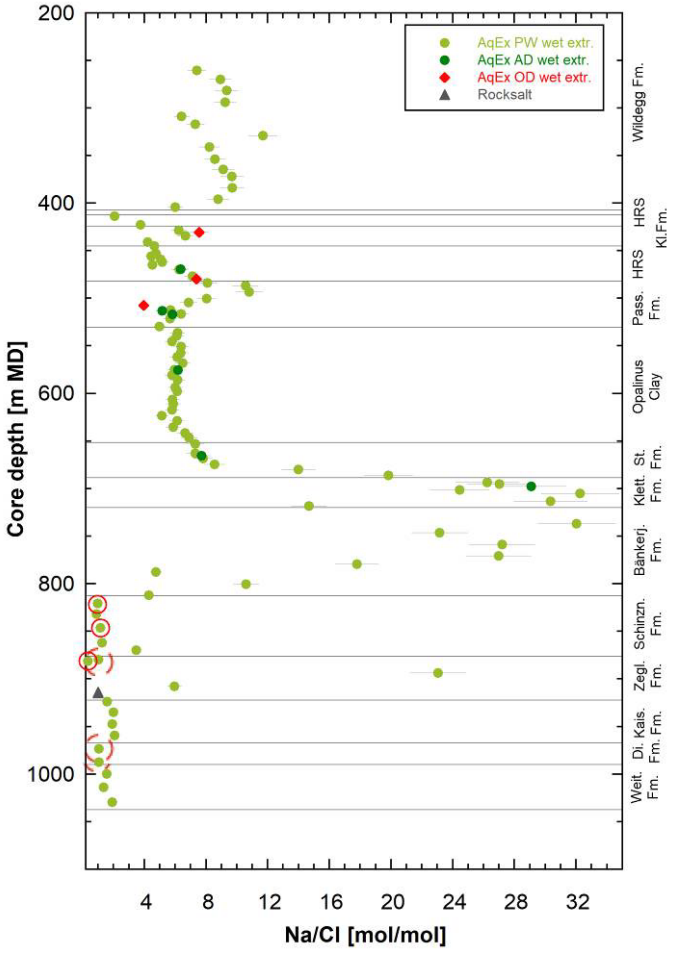

Fig. 4.4-4: Depth profile of the Na/Cl molar concentration ratio in aqueous extracts at a S/L ratio of about 1

The samples with red circles show indications of contamination by the drilling fluid exceeding the analytical uncertainty. Samples with an uncertain amount of contamination are marked with a dashed red circle.

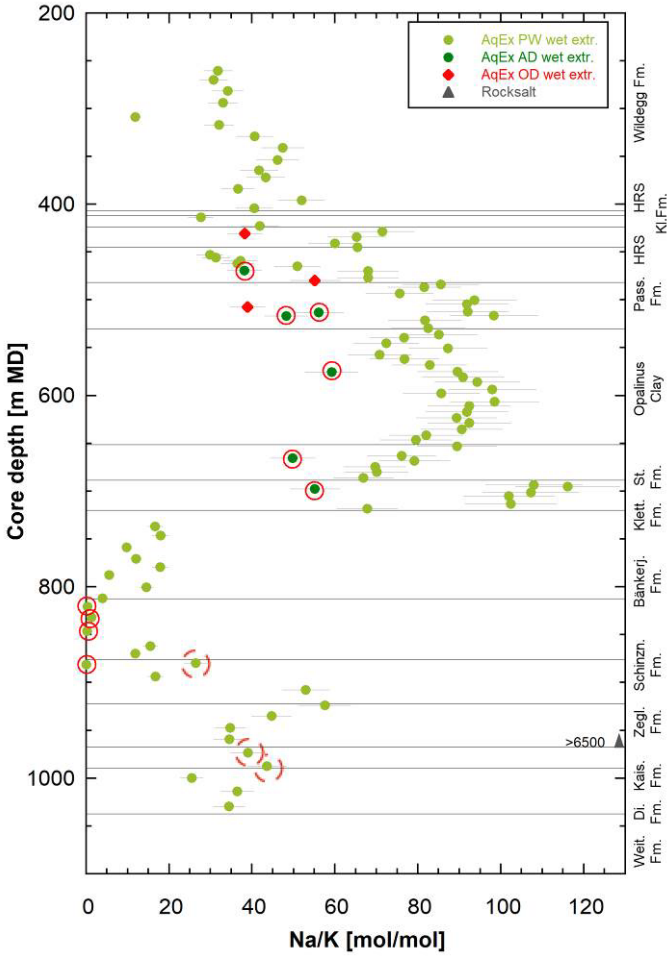

Fig. 4.4-5: Depth versus Na/K molar concentration ratio in aqueous extracts at a S/L ratio of about 1

The samples with red circles show indications of contamination by the K-silicate drilling fluid (low apparent ratios). Note that AD samples show lower Na/K ratios compared to neighbouring samples due to minor contamination by the drilling fluid. Samples with an uncertain amount of contamination are marked with a dashed red circle.

4.4.2.4 Saturation indices

The charge balance of the aqeous extracts lies within 5% for most samples and two samples (at 870 and 894 m depth) show a charge imbalance of 6%. Most aqueous extract solutions from the Malm, Dogger and Lias are saturated or close to saturation with respect to calcite, but mostly undersaturated with respect to dolomite (disordered and ordered) (Tab. 4.4-3). The saturation indices for calcite vary from the Klettgau to the Weitenau Formation from -1.5 to 1.9, with distinct oversaturation and undersaturation reached in many samples from all these formations. Calcite oversaturation is expected for anhydrite-bearing samples where dissolution of Ca-sulphate is producing excess Ca that cannot be precipitated as calcite due to the limiting amount of hydrogencarbonate. All samples that are considerably undersaturated with respect to calcite do not contain detectable amounts of calcite with the exception of samples at 308, 452, 464, 623, 862, 870, 924 and 935 m depth, which contain 94, 74, 56, 4, 63, 86, 38 and 17 wt% calcite, respectively, despite showing an undersaturation of -0.2 to -0.4. This might be caused by calcite

dissolution during the aqueous extraction leading to a P_{CO2} level below atmospheric concentrations and a subsequent decrease in pH due to CO_2 equilibration by in-gassing during filtration and titration. Contamination by K, Na, SO_4 and Si from drilling muds (sections above) is not expected to significantly affect calculations, except in case of pH and alkalinity (total titrated alkalinity interpreted as carbonate alkalinity for speciation calculations), or where significant additional K uptake may liberate Ca-Mg-Sr-K-Na and other cations from the clay exchanger.

The sulphate minerals gypsum, anhydrite and celestite are undersaturated by 0 to 3 orders of magnitude in all extract solutions with the exception of all samples from the Bänkerjoch Formation, one sample from the Schinznach and two samples from the Zeglingen Formation. These exceptions contain anhydrite and are saturated with respect to gypsum and close to saturation or saturated with respect to anhydrite. Two anhydrite-bearing samples from the Bänkerjoch Formation reached celestite saturation even though they lack detectable levels of celestite in the XRD analysis.

Tab. 4.4-3: Saturation indices for calcite, dolomite (disordered and ordered), gypsum, anhydrite and celestite at a S/L 1, pH and partial pressure of CO_2

Mineral saturation indices were calculated with the PHREEQC Version 3 code (Parkhurst & Appelo 2013) and the PSI/Nagra thermodynamic database (Thoenen et al. 2014) assuming a temperature of 25° C. Fm/Gr stands for Formation/Group, Ma for Malm, Hr for Hauptrogenstein, Kl for Klingnau, Pa for Passwang, OPA for Opalinus Clay, St for Staffelegg, Kl for Klettgau, Bä for Bänkerjoch, Sc for Schinznach, Ze for Zeglingen, Ka for Kaiseraugst, Di for Dinkelberg, We for Weitenau, S/L for solid/liquid, Cc for calcite, Do for Dolomite ordered or disordered, Gy for gypsum, An for Anhydrite and Ce for Celestite. Most dolomite SI in the Kaiseraugst and Dinkelberg Formation lack due to Mg concentrations below the limit of detection.

Fm	**Depth** [m]	**S/L**	**SI Cc**	**SI Do (dis)**	**SI Do (ord)**	**SI Gy**	**SI An**	**SI Ce**	**pH**	**P_{CO2}**
Ma	260.58	0.92	0.09	-0.50	0.05	-1.99	-2.21	-0.77	8.55	-3.48
Ma	269.63	0.92	0.03	-0.65	-0.10	-2.05	-2.28	-0.83	8.53	-3.45
Ma	281.50	0.91	0.04	-0.61	-0.06	-2.11	-2.34	-0.81	8.59	-3.49
Ma	293.74	0.95	0.09	-0.50	0.05	-2.10	-2.32	-1.96	8.63	-3.56
Ma	308.63	0.98	-0.34	-1.53	-0.98	-1.82	-2.05	-0.57	8.10	-3.42
Ma	316.92	0.97	0.01	-0.72	-0.17	-2.39	-2.62	-2.34	8.83	-3.95
Ma	328.88	0.96	0.11	-0.52	0.03	-2.39	-2.61	-2.23	8.87	-3.81
Ma	340.77	0.91	0.02	-0.69	-0.14	-2.15	-2.37	-2.03	8.54	-3.36
Ma	353.59	0.91	-0.03	-0.79	-0.24	-2.16	-2.38	-2.01	8.48	-3.29
Ma	364.26	0.94	0.02	-0.69	-0.14	-2.17	-2.40	-2.02	8.53	-3.35
Ma	371.91	0.95	0.09	-0.56	-0.01	-2.20	-2.42	-2.03	8.65	-3.50
Ma	383.83	0.96	0.23	-0.37	0.18	-2.71	-2.93	-2.58	9.14	-4.17
Ma	395.73	0.93	0.09	-0.56	-0.01	-2.15	-2.37	-2.02	8.63	-3.45
Ma	403.83	0.95	0.03	-0.69	-0.14	-2.10	-2.33	-1.96	8.61	-3.64
Hr	413.63	0.86	0.28	-0.21	0.34	-1.26	-1.48	-1.20	7.78	-2.53
Hr	422.84	0.92	-0.06	-1.02	-0.47	-2.22	-2.45	-2.14	8.51	-3.48
Kl	428.29	0.90	0.05	-0.68	-0.13	-2.55	-2.78	-2.45	8.78	-3.53
Kl	430.71	0.97	0.11	-0.63	-0.08	-2.87	-3.09	-2.80	9.04	-3.95
Kl	434.07	0.94	0.05	-0.73	-0.18	-2.33	-2.55	-1.90	8.66	-3.45
Kl	440.78	0.93	0.60	0.40	0.95	-2.31	-2.53	-2.10	9.17	-4.00
Hr	444.67	0.91	0.12	-0.58	-0.03	-2.32	-2.54	-2.21	8.60	-3.30
Hr	452.84	0.94	-0.24	-1.29	-0.74	-1.55	-1.77	-0.12	7.94	-3.06
Hr	455.84	0.96	-0.02	-0.85	-0.30	-2.24	-2.46	-1.91	8.51	-3.43
Hr	458.94	0.94	-0.11	-1.05	-0.50	-2.00	-2.22	-1.62	8.15	-2.97
Hr	461.92	0.94	-0.04	-0.89	-0.34	-2.36	-2.59	-2.11	8.52	-3.37
Hr	464.91	0.95	-0.22	-1.07	-0.52	-2.47	-2.69	-1.81	8.49	-3.40
Hr	469.40	0.93	0.28	-0.26	0.29	-2.47	-2.69	-2.34	9.01	-3.84
Hr	469.63	0.93	-0.10	-1.12	-0.57	-2.48	-2.70	-2.44	8.56	-3.31
Hr	476.74	0.92	0.08	-0.76	-0.21	-2.54	-2.76	-2.33	8.93	-3.84
Pa	479.33	0.92	0.10	-0.67	-0.12	-2.71	-2.93	-2.57	9.09	-3.93
Pa	484.00	0.93	0.16	-0.52	0.03	-2.88	-3.11	-2.78	9.22	-4.04
Pa	486.79	0.95	0.38	-0.32	0.23	-3.00	-3.22	-3.00	9.51	-4.42
Pa	493.38	0.92	0.04	-0.79	-0.24	-2.40	-2.62	-1.65	8.89	-3.73
Pa	500.50	0.90	0.18	-0.58	-0.03	-2.78	-3.00	-2.72	9.10	-3.87
Pa	504.10	0.90	0.14	-0.66	-0.11	-2.76	-2.99	-2.63	9.05	-3.81
Pa	507.30	0.93	-0.03	-0.94	-0.39	-2.17	-2.40	-1.89	8.29	-2.89
Pa	512.26	0.89	0.13	-0.65	-0.10	-2.83	-3.05	-2.67	9.04	-3.77
Pa	513.25	0.90	0.33	-0.32	0.23	-2.66	-2.89	-2.66	9.24	-4.12
Pa	516.50	0.90	-0.04	-0.95	-0.40	-2.83	-3.05	-2.70	8.91	-3.65
Pa	516.72	0.89	0.06	-0.79	-0.24	-2.86	-3.09	-2.66	9.29	-4.24
Pa	521.28	0.91	0.07	-0.77	-0.22	-2.84	-3.06	-2.74	9.00	-3.77
Pa	529.34	0.89	-0.06	-1.04	-0.49	-2.82	-3.04	-2.73	8.81	-3.54

Tab. 4.4-3: (continued)

Fm/Gr	**Depth** [m]	**S/L**	**SI Cc**	**SI Do (dis)**	**SI Do (ord)**	**SI Gy**	**SI An**	**SI Ce**	**pH**	**$\log_{10} P_{CO2}$** [bar]
OPA	535.94	0.93	0.06	-0.83	-0.28	-2.67	-2.89	-2.50	8.81	-3.50
OPA	539.35	0.92	-0.10	-1.14	-0.59	-2.66	-2.88	-2.51	8.63	-3.29
OPA	545.37	0.93	-0.01	-1.01	-0.46	-2.64	-2.86	-2.54	8.62	-3.23
OPA	550.41	0.91	-0.12	-1.16	-0.61	-2.78	-3.00	-2.67	8.70	-3.37
OPA	557.38	0.93	0.01	-0.90	-0.35	-2.86	-3.08	-2.58	8.84	-3.54
OPA	561.85	0.90	-0.08	-1.10	-0.55	-2.77	-2.99	-2.63	8.68	-3.31
OPA	568.09	0.91	0.33	-0.27	0.28	-2.85	-3.08	-2.68	9.20	-3.89
OPA	575.04	0.93	0.28	-0.38	0.17	-2.80	-3.03	-2.63	9.13	-3.82
OPA	575.26	0.91	-0.10	-1.13	-0.58	-2.81	-3.03	-2.59	8.66	-3.26
OPA	580.97	0.91	0.10	-0.75	-0.20	-2.79	-3.01	-2.63	8.86	-3.48
OPA	585.95	0.92	0.11	-0.72	-0.17	-2.81	-3.03	-2.66	8.87	-3.49
OPA	593.35	0.90	0.10	-0.74	-0.19	-2.82	-3.04	-2.67	8.84	-3.44
OPA	597.80	0.94	-0.06	-1.00	-0.45	-2.88	-3.10	-2.68	8.74	-3.34
OPA	606.46	0.89	0.11	-0.70	-0.15	-2.84	-3.06	-2.67	8.88	-3.48
OPA	611.02	0.88	-0.11	-1.15	-0.60	-2.84	-3.06	-2.68	8.60	-3.16
OPA	617.10	0.90	-0.08	-1.09	-0.54	-2.82	-3.05	-2.63	8.63	-3.19
OPA	623.28	0.89	-0.29	-1.45	-0.90	-2.72	-2.94	-2.52	8.32	-2.87
OPA	628.69	0.89	-0.04	-1.00	-0.45	-2.83	-3.05	-2.64	8.74	-3.35
OPA	635.13	0.87	-0.07	-1.13	-0.58	-2.87	-3.09	-2.71	8.74	-3.37
OPA	641.48	0.89	-0.01	-1.01	-0.46	-2.85	-3.07	-2.69	8.82	-3.46
St	646.22	0.92	-0.14	-1.28	-0.73	-2.83	-3.06	-2.69	8.67	-3.30
St	653.10	0.92	-0.06	-0.98	-0.43	-2.71	-2.93	-2.47	8.85	-3.61
St	662.65	0.92	-0.16	-1.29	-0.74	-2.96	-3.19	-2.83	8.95	-3.74
St	665.40	0.93	0.15	-0.53	0.02	-2.88	-3.10	-2.64	9.30	-4.17
St	668.39	0.95	-0.01	-0.84	-0.29	-3.01	-3.23	-2.89	9.09	-3.84
St	674.60	0.91	-0.14	-1.18	-0.63	-2.89	-3.11	-2.84	8.84	-3.55
St	679.90	0.89	-0.06	-0.97	-0.42	-2.79	-3.02	-2.76	8.83	-3.47
St	686.20	0.90	-0.05	-0.97	-0.42	-2.77	-2.99	-2.78	8.85	-3.50
Kl	693.72	0.86	-0.05	-0.82	-0.27	-2.57	-2.80	-2.55	9.02	-3.85
Kl	695.15	0.89	-0.02	-0.78	-0.23	-2.72	-2.94	-2.71	9.15	-4.00
Kl	697.51	0.88	0.29	-0.19	0.36	-2.47	-2.70	-2.46	9.10	-3.82
Kl	701.15	0.93	-0.01	-0.75	-0.20	-2.87	-3.09	-2.92	9.32	-4.26
Kl	705.04	0.93	0.13	-0.43	0.12	-2.86	-3.08	-2.74	9.43	-4.39
Kl	713.28	0.93	-0.09	-0.81	-0.26	-2.86	-3.08	-2.88	9.28	-4.24
Kl	718.19	0.90	-0.61	-1.91	-1.36	-2.84	-3.06	-2.89	8.91	-4.01

Tab. 4.4-3: (continued)

Fm/Gr	Depth [m]	S/L	SI Cc	SI Do (dis)	SI Do (ord)	SI Gy	SI An	SI Ce	pH	$\log_{10} P_{CO2}$ [bar]
Bä	736.78	0.95	-0.55	-2.22	-1.67	0.11	-0.12	0.00	7.29	-3.09
Bä	746.28	0.95	0.43	-0.28	0.27	0.26	0.04	-0.17	7.85	-3.32
Bä	758.55	0.97	0.50	-0.25	0.30	0.13	-0.09	0.02	7.99	-3.53
Bä	770.74	0.98	-1.47	-4.29	-3.74	0.10	-0.13	-0.16	6.41	-2.33
Bä	779.20	0.93	-0.18	-1.15	-0.60	0.23	0.01	-0.13	7.36	-2.86
Bä	787.44	0.99	-1.23	-4.80	-4.25	0.09	-0.13	-0.15	6.52	-2.37
Bä	800.47	0.98	0.63	-0.71	-0.16	0.14	-0.08	-0.14	8.08	-3.63
Bä	811.83	1.00	-1.35	-5.49	-4.94	0.09	-0.13	-0.26	6.48	-2.42
Sc	820.53	0.90	0.35	0.10	0.65	-0.57	-0.80	-0.63	8.07	-3.25
Sc	831.86	0.93	0.70	-0.06	0.49	0.21	-0.01	-0.37	8.17	-3.76
Sc	846.00	0.86	1.82	2.10	2.65	-0.73	-0.96	-0.92	10.14	-5.52
Sc	861.91	0.97	-0.15	-0.24	0.31	-2.35	-2.57	-2.45	8.55	-3.81
Sc	869.79	0.99	-0.41	-1.56	-1.01	-2.82	-3.04	-2.86	8.37	-3.69
Ze	879.74	0.79	0.94	1.00	1.55	-0.35	-0.57	-0.62	7.80	-2.52
Ze	881.21	0.79	1.86	3.39	3.94	-2.39	-2.61	-2.55	10.78	-5.34
Ze	893.76	0.97	0.29	-0.78	-0.23	0.00	-0.23	-0.16	8.03	-3.69
Ze	907.62	1.01	0.36	-1.53	-0.98	-0.02	-0.24	-0.28	8.06	-3.75
Ka	923.87	0.99	-0.20	-1.08	-0.53	-1.94	-2.16	-1.96	8.4	-3.58
Ka	934.88	0.95	-0.15			-2.92	-3.14	-2.81	8.79	-3.61
Ka	947.60	0.94	-0.12			-2.82	-3.05	-2.76	8.71	-3.55
Ka	959.60	0.89	-0.02			-2.84	-3.06	-2.73	8.56	-3.21
Di	973.17	0.86	-0.37	-1.86	-1.31	-2.10	-2.32	-1.74	7.94	-3.19
Di	987.48	0.90	-0.13	-1.38	-0.83	-1.80	-2.01	-1.72	7.87	-2.82
We	999.55	0.93	0.02			-3.05	-3.28	-2.76	9.04	-4.06
We	1013.84	0.93	-0.16			-2.97	-3.19	-2.65	8.85	-3.97
We	1029.34	0.94	0.22			-3.16	-3.38	-2.70	9.38	-4.41

4.4.3 Chloride and bromide concentrations in bulk porewater

The formalisms to recalculate Cl and Br concentrations in aqueous extracts to concentrations in bulk porewater (free + bound water) are given in Waber (ed.) (2020). In clay-free rocks, this recalculation to water content delivers the porewater concentrations of Cl and Br directly, assuming a limited contribution from fluid inclusions. In clay-bearing rocks, this recalculation additionally has to account for the anion-exclusion effect in order to result in porewater concentrations. The derivation of the Cl and Br accessible porosity proportion and calculation of porewater concentrations is established in Chapter 5.

The recalculation of Cl and Br concentrations in aqueous extracts to concentrations in bulk porewater (Figs. 4.4-6 to 4.4-9) requires the knowledge of the water content of the rocks, which is obtained by calculating the average of three gravimetric water contents (one regular sample and two subsamples used for diffusive-exchange experiments). Additional aqueous extraction tests were carried out on selected dried regular water content subsamples from Malm to Lias in order to reduce the uncertainty regarding the variability of the water content within a core sample.

The depth profiles of Cl and Br concentrations in bulk porewater cover a large range of 0.2 to 55 g/kg_{H2O} and 0.5 to 89 mg/kg_{H2O}, respectively, disregarding the likely contaminated samples

(Figs. 4.4-6 to 4.4-9). The AD, SQ and OD aqueous extract samples fit well into the concentration profile of the PW aqueous extracted samples. In the Br profile, the dry aqueous extracts show lower concentrations compared to the wet extracts. No such difference between dry and wet extracts is seen in the Cl data obtained by RWI. The differences for Br may be related to oxidation processes (e.g., organic matter), but this is not proven at the moment.

Both, the Cl and Br concentrations, present constant values from the Malm to the top of the Opalinus Clay with the exception of a couple of positive excursions in the Hauptrogenstein and an increasing trend in the lower Passwang Formation. There is a general decreasing trend from the Opalinus Clay down to the bottom of the Klettgau Formation (Figs. 4.4-6 to 4.4-9), reaching minimum values there. At greater depths, the Cl concentrations increase towards the bottom of the Schinznach Formation. At the top and bottom of the Zeglingen Formation there are very high Cl concentrations which drop to much lower values in the middle of the Formation. This can be explained by a change to a NaCl drilling fluid at the top of the Zeglingen Formation and the presence of rock salt at the bottom of the Formation. The Kaiseraugst and Weitenau Formation present similar Cl concentrations as the Schinznach Formation. The Dinkelberg Formation has the highest Cl concentrations, however, these samples are likely affected by the Na-Cl drilling fluid (Section 4.4.2.1).

The Br concentrations differ at greater depth from the Cl concentrations and reach maximum values in the bottom of the Bänkerjoch Formation. Subsequently, the Br concentrations drop drastically and increase again towards the bottom of the Schinznach Formation. Further below the Br concentrations scatter around lower values similar to the ones observed in the Malm.

At this stage, these observed trends should be treated with care because the recalculated Cl and Br concentrations still need to be corrected for anion accessibility, which, as mentioned above, is further investigated in Chapter 5.

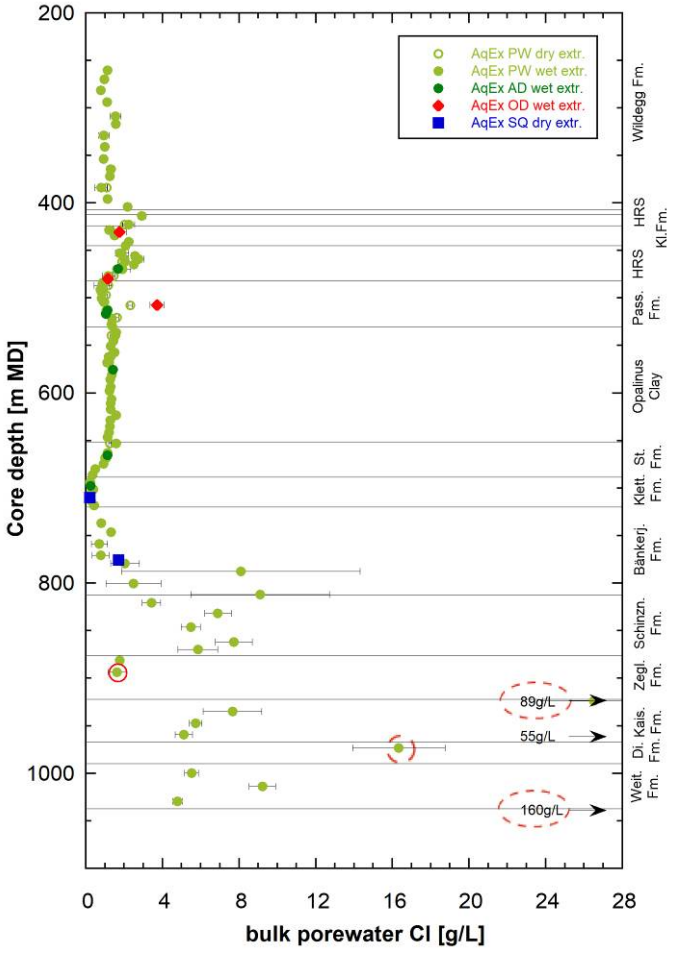

Fig. 4.4-6: Bulk porewater Cl concentrations versus depth from aqueous extracts

Samples where the contamination by the drilling fluid likely exceeds the analytical uncertainty are circled in red. Samples with an uncertain amount of contamination are marked with a dashed red circle.

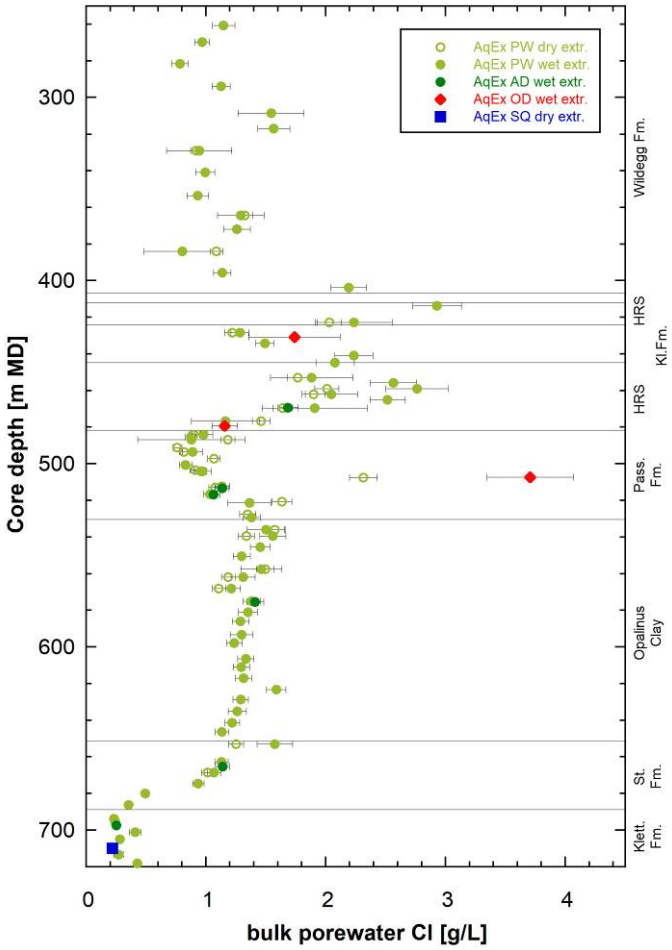

Fig. 4.4-7: Bulk porewater Cl concentrations versus depth from aqueous extracts from the Malm to the Klettgau Formation

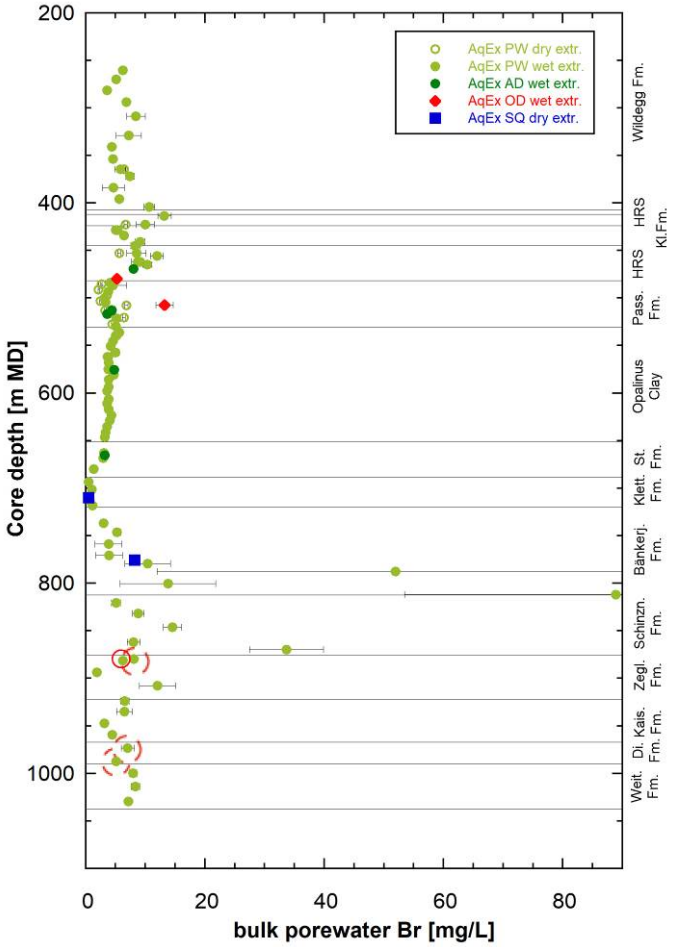

Fig. 4.4-8: Bulk porewater Br concentrations versus depth from aqueous extracts

Samples where the contamination by the drilling fluid likely exceeds the analytical uncertainty are circled in red. Samples with an uncertain amount of contamination are marked with a dashed red circle.

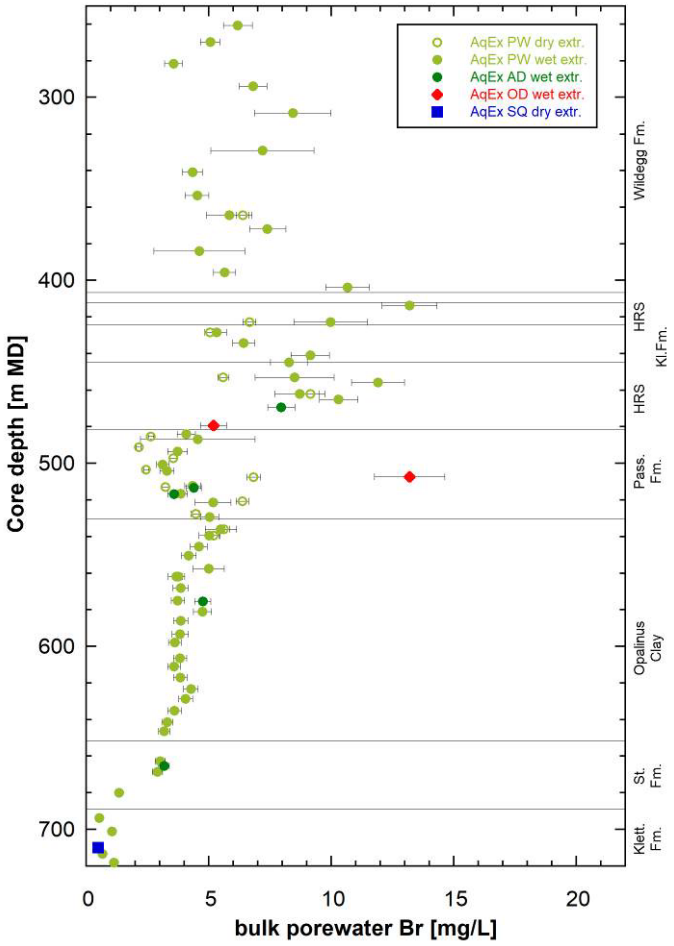

Fig. 4.4-9: Bulk porewater Br concentrations versus depth from aqueous extracts from the Malm to the Klettgau Formation

4.4.4 Cl-isotopes in AqEx solutions

The stable isotopes signature of Cl in aqueous extract solutions, expressed as $\delta^{37}Cl$ relative to the SMOC standard, carries information about the origin of Cl. Thus, Cl isotope ratios may be used to some degree to discern the origin of Cl between seawater and rock salt dissolution. Over long periods of time, however, Cl-isotopes fractionate through Cl diffusion across low-permeability rocks (e.g. Gimmi & Waber 2004).

In the Malm, Passwang Formation, Opalinus Clay and top Staffelegg Formation, the $\delta^{37}Cl$ values from AqEx solutions are almost constant below modern seawater values and vary within the analytical error, except for one sample from the Hauptrogenstein that extends to lower values (Fig. 4.4-10). At the bottom of the Staffelegg Formation a higher value is measured followed by a low $\delta^{37}Cl$ isotopic value in the Klettgau Formation. The in- and decreasing trends observed in Cl bulk porewater concentrations in the Bänkerjoch and Schinznach Formation are also reflected in the $\delta^{37}Cl$ isotopic signature in these Formations. The lowermost values in the Schinznach Formation overlap with the measurements from the rock salt of the Zeglingen Formation in BUL1-1.

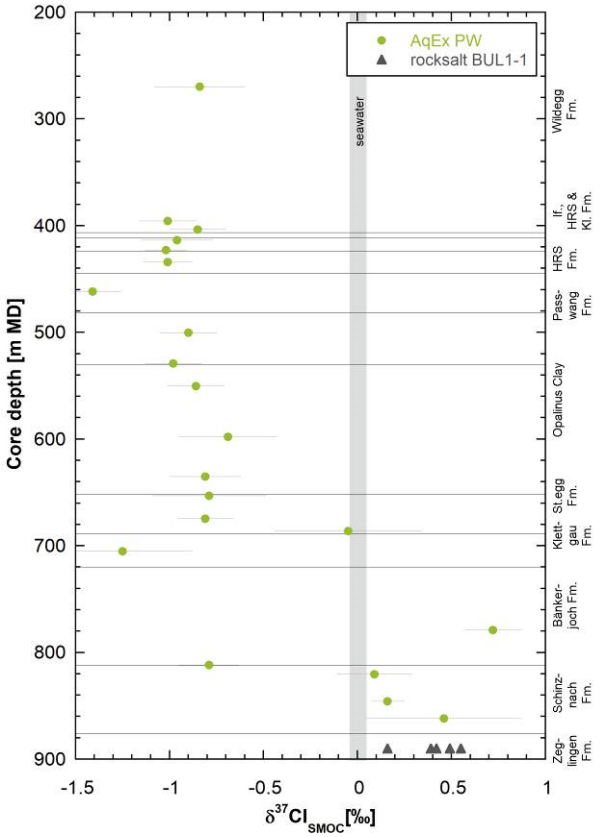

Fig. 4.4-10: Cl isotopes, expressed as $\delta^{37}Cl$, in AqEx solutions of rocks vs. depth from the Malm to the Muschelkalk and in rock salt samples from the Zeglingen Formation in BUL1-1

Shortly before printing this report, the analysis of rock salt sample BOZ1-1 914.80 m, became available (analysis by Hydroisotop GmbH): -0.01 ± 0.20 ‰-SMOC.

4.5 Cation-exchange extraction data

Paul Wersin

Six samples used for advective displacement experiments (AD samples) were analysed at Uni Bern with the nickel ethylenediamine (Ni-en) extraction method to determine the cation exchange capacity (CEC) and the composition of the clay exchanger (for methodology see Waber (ed.) 2020). Material from end pieces above and below the AD core was mixed to obtain a representative sample for Ni-en extraction. A larger number of samples were studied by the team at PSI using the CsCl extraction method (Marques Fernandes & Baeyens *in prep.*). The objective of the Ni-en extraction study was (i) to help to analyse the AD data (Section 4.7) and (ii) to compare and verify the PSI study with an alternative method (see Section 5.6). In this section, only data from Uni Bern are presented.

The CEC can be derived in two ways: (1) From the consumption of the index cation (Ni in this case) during extraction and (2) from the sum of extracted cations (ΣCAT). Note that the latter includes (i) the exchangeable cations, (ii) cations dissolved in the porewater and (iii) cations released from potentially dissolving minerals (e.g. carbonates, sulphates) during extraction. Thus, in principle, the CEC derived from the sum of cations requires correction from contributions of (ii) and (iii). Corrected CEC and exchangeable cation data are discussed in Section 5.6, where the

data from Uni Bern is also compared with that of PSI. The analysis does not include ammonium, NH_4^+, known to be present in small but measurable amounts (e.g. 1.8 to 3.2 mg/L in aqueous extracts, at S/L ≈ 1, Section 4.7).

Tab. 4.5-1 shows the Ni consumption and extracted cation data (Na, K, Ca, Mg, Sr, Ba, Fe) for solid/liquid ratios (S/L) around 1[8]. Anion data (Cl, Br, SO_4, NO_3) is depicted in Tab. 4.5-2. Note that Ni nitrate was added to the samples, which explains the high NO_3 contents.

Tab. 4.5-1: Cation data from Ni-en extracts at a S/L ratio around 1 (Uni Bern data)

Type	**Depth**	**Formation**	**S/L**	**Na**	**K**	**Ca**	**Mg**	**Sr**	**Ba**	**Fe**	**ΣCAT**	**Ni cons.**
	[m]		[g/g]	[meq/kg$_{dry\ rock}$]								
AD	469.40	Hauptrogenstein	0.934	24.1	3.9	22.4	10.0	0.3	0.001	< 0.002	60.7	56.2
AD	513.25	Passwang Fm.	0.910	60.4	5.9	49.4	19.2	0.9	0.003	< 0.002	135.8	137.4
AD	516.72	Passwang Fm.	0.845	63.3	8.6	58.1	22.6	1.1	0.003	< 0.002	153.7	160.7
AD	575.26	Opalinus Clay	0.867	53.7	5.2	37.7	14.4	0.7	0.011	0.005	111.7	107.3
AD	665.40	Staffelegg Fm.	0.873	35.7	4.6	24.9	11.5	0.4	0.011	< 0.002	77.0	84.2
AD	697.51	Klettgau Fm.	0.820	57.7	7.9	44.4	22.7	0.5	0.005	< 0.002	133.2	141.0

Tab. 4.5-2: Anion data from Ni-en extracts at a S/L ratio around 1 (Uni Bern data)

Type	**Depth**	**Formation**	**S/L**	**F**	**Cl**	**Br**	**NO_3** [a]	**SO_4**
	[m]		[g/g]	[meq/kg$_{dry\ rock}$]				
AD	469.40	Hauptrogenstein	0.934	0.015	1.5	< 0.002	229.9	4.1
AD	513.25	Passwang Fm.	0.910	0.014	2.0	0.002	1084.9	3.1
AD	516.72	Passwang Fm.	0.845	0.012	1.7	0.003	1274.4	3.8
AD	575.26	Opalinus Clay	0.867	0.007	1.7	0.002	330.4	2.9
AD	665.40	Staffelegg Fm.	0.873	0.012	1.2	< 0.002	322.2	3.3
AD	697.51	Klettgau Fm.	0.820	0.012	0.5	< 0.002	780.9	6.1

[a] Nitrate is part of the added Ni-en stock solution

The CEC derived from Ni consumption of the AD samples varies in the range 84 – 161 meq/kg$_{rock}$, similar to the uncorrected sum of cations. The depth profiles of Ni consumption and ΣCAT data both show consistent trends (Fig. 4.5-1). The CEC data show a positive correlation with clay mineral content (Fig. 4.5-2), but with some scatter. The scatter in CEC is further discussed in Section 5.6.2.

Na and Ca are the main extracted cations, followed by Mg and K (Tab. 4.5-1). The Ca/Na ratio (eq/eq) is constant for the five samples down to the Staffelegg Formation, with values of 0.7 – 0.9. Mg correlates with Ca, thus the ratio (Ca+Mg)/Na shows the same trend as the Ca/Na ratio. The K/Na ratio exhibits a rather narrow range of 0.10 – 0.16 for all samples. The Sr/Na ratio ranges from 0.009 to 0.015 within the sampled rock sequence.

[8] A water mass equal to the mass of the wet rock was added, leading to S/L (mass of dry rock /[mass of added water + porewater]) slightly below 1.

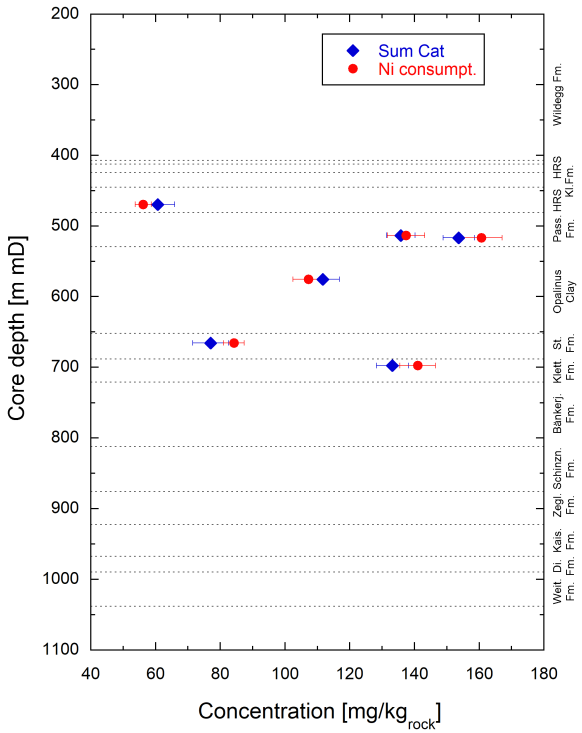

Fig. 4.5-1: Depth profile of Ni consumption and sum of cations (uncorrected)

Errors reflect propagated analytical uncertainties.

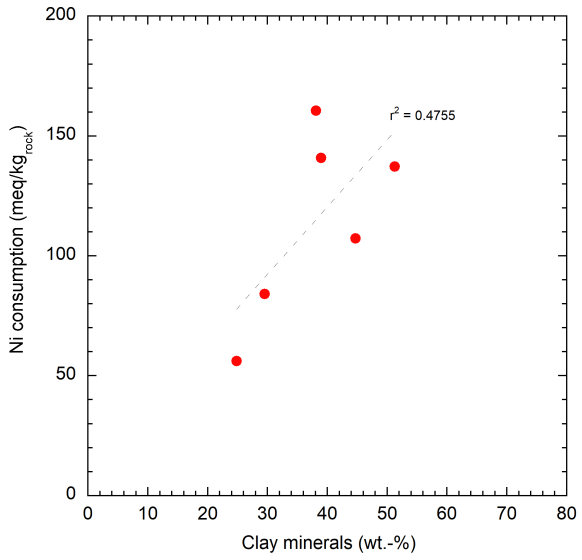

Fig. 4.5-2: Ni consumption vs. clay-mineral content

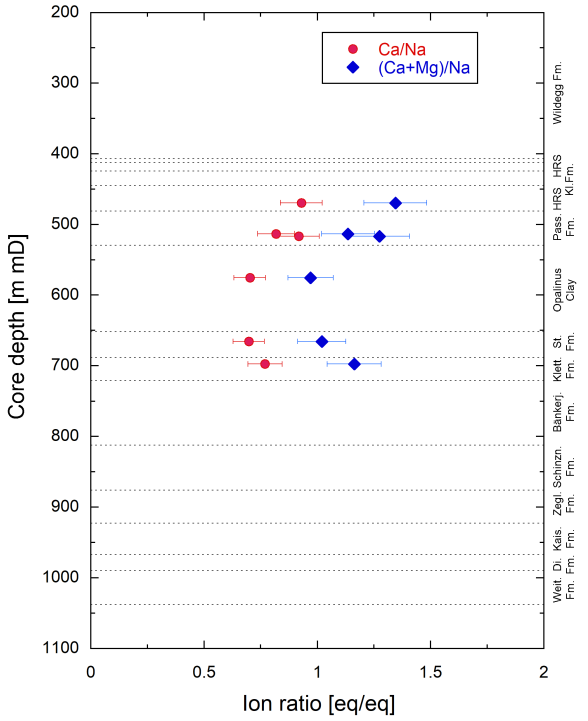

Fig. 4.5-3: Depth profiles of Ca/Na and (Ca+Mg)/Na ratios in Ni-en extracts

Errors reflect propagated analytical uncertainties

Speciation calculations on the Ni-en extracts were carried out with the PHREEQC Version 3 code (Parkhurst & Appelo 2013) and the PSI/Nagra thermodynamic database (Thoenen et al. 2014) assuming a temperature of 25 °C. The ethylene diamine complexes were taken from the MINTEC database (Allison et al. 1991) and included in the calculations. The concentration of ethylene diamine in the extracts, which was not analysed, was constrained by charge balance. The dissolved carbonate concentration (not measured) was constrained by assuming calcite equilibrium. The calculated TIC values are low, in the range of 0.05 – 0.15 mM (Tab. 4.5-3). The calculated partial pressures of CO_2 (P_{CO2}) and saturation indices for selected minerals are depicted in Tab. 4.5-3. The Ni-en extracts are clearly undersaturated with regard to the carbonate minerals dolomite and strontianite. They are also undersaturated with regard to the sulphate minerals gypsum and celestite, but either close to saturation or oversaturated with regard to barite.

Tab. 4.5-3: Calculated saturation indices of selected minerals, TIC log$P(CO_2)$ for Ni-en extract solutions

Calcite saturation was assumed in the calculations.

Type	**Depth** [m]	**Formation**	**LogP(CO_2)** [bar]	**TIC** [mol/kg]	**Gypsum**	**Celestite**	**Barite**	**Dolomite (ord)**	**Dolomite (dis)**	**Strontianite**
AD	469.40	Hauptrogenstein	-4.85	1.13E-04	-1.30	-1.10	-0.13	-0.23	-0.78	-1.06
AD	513.25	Passwang Fm.	-4.97	7.29E-05	-1.19	-0.87	-0.02	-0.28	-0.83	-0.95
AD	516.72	Passwang Fm.	-5.25	5.35E-05	-1.11	-0.78	-0.06	-0.28	-0.83	-0.93
AD	575.26	Opalinus Clay	-4.55	1.28E-04	-1.34	-1.02	0.49	-0.29	-0.84	-0.94
AD	665.40	Staffelegg Fm.	-4.57	1.50E-04	-1.42	-1.14	0.61	-0.21	-0.76	-0.98
AD	697.51	Klettgau Fm.	-4.88	8.86E-05	-1.02	-0.91	0.38	-0.16	-0.71	-1.15

4.6 Data from squeezing experiments

Martin Mazurek

A set of 10 samples from the interval Passwang-Formation – Bänkerjoch Formation were subjected to porewater squeezing. The mineralogical composition of the samples is listed in Tab. 4.6-1. The following observations can be made:

- Clay-mineral contents are ≥ 37 wt.-% for all samples.
- Sample 709.84 from the Klettgau Formation contains no resolvable carbonates (traces below detection cannot be excluded).
- Sample 775.39 from the Bänkerjoch Formation contains abundant magnesite and anhydrite – within the TBO squeezing campaign, this is a novelty.
- Except for the two Triassic samples, calcite is generally the main carbonate mineral.

Tab. 4.6-1: Mineralogical composition of samples subjected to squeezing experiments

tr: trace, empty field: mineral not identified.

Depth [m]	**Formation**	**Member**	**S** [wt.-%]	**C(inorg)** [wt.-%]	**C(org)** [wt.-%]	**Quartz** [wt.-%]	**K-feldspar** [wt.-%]	**Plagioclase** [wt.-%]	**Calcite** [wt.-%]	**Dolomite / Ank.** [wt.-%]	**Siderite** [wt.-%]	**Magnesite** [wt.-%]	**Anhydrite** [wt.-%]	**Pyrite** [wt.-%]	**Clay minerals** [wt.-%]
494.48	Passwang Fm.	Rothenfluh Mb.	1.00	3.94	0.82	19	5	3	33					1.9	38
516.27	Passwang Fm.	Waldenburg and lower part of Brüggli Mb.	0.54	1.66	0.59	24	6	3	14					1.0	51
554.36	Opalinus Clay	'Sub-unit with silty calcareous beds'	0.79	1.29	0.94	21	4	3	8		3			1.5	58
590.32	Opalinus Clay	'Mixed clay-silt-carbonate sub-unit'	0.35	0.83	0.77	23	5	3	5		2			0.7	60
607.13	Opalinus Clay	'Mixed clay-silt-carbonate sub-unit'	0.07	0.95	0.88	19	5	3	6		2			0.1	64
629.09	Opalinus Clay	'Mixed clay-silt-carbonate sub-unit'	0.25	1.15	0.91	15	5	3	5		6			0.5	65
643.35	Opalinus Clay	'Clay-rich sub-unit'	0.46	1.18	0.81	15	5	3	6		4			0.9	65
671.15	Staffelegg Fm.	Frick Mb.	0.52	2.95	0.66	30	5	2	22	3				1.0	37
709.84	Klettgau Fm.	Ergolz Mb.	0.44	<0.02	0.66	27	10	9						0.8	53
775.39	Bänkerjoch Fm.	'Thin-layered anhydrite claystone sequence'	2.98	1.76	0.88	2				tr		12	13		72

4.6.1 Mass recovery

The water masses obtained by squeezing are listed in Tab. 4.6-2 and shown graphically in Fig. 4.6-1 as a function of the squeezing pressure. The total mass recovery broadly correlates with the initial water content of the sample (Fig. 4.6-2). The latter was measured at CRIEPI on the cut-off materials adjacent to the squeezed rock pieces. Samples yielded first water aliquots at 200 MPa, except for 2 samples where 300 – 400 MPa were required to extract the first waters. On the other hand, no evident correlation is found between mass recovery and the contents of clay or other minerals. Thus, other sample characteristics, such as microfabric, must play a role regarding squeezability.

Given the fact that for 8 samples, a sufficient water mass was obtained in the pressure range 200 – 400 MPa, the experiments were terminated at this pressure, i.e. no waters were squeezed at the highest pressure of 500 MPa. Two samples yielded limited amounts of water and so were squeezed up to the highest pressure.

Tab. 4.6-2: Water masses squeezed at different pressure steps

The initial water content was measured at CRIEPI on cut-off materials adjacent to the squeezed core, and this value was used here to calculate the initial mass of porewater in the sample. "-": pressure step not applied.

Depth [m]	**Formation**	**Initial sample mass (CRIEPI)** [g]	**Initial wet water content (CRIEPI)** [wt.-%]	**Mass of porewater prior to squeezing (CRIEPI)** [g]	**Mass squeezed at P =**						**Total mass squeezed** [g]
					100 MPa [g]	**150 MPa** [g]	**200 MPa** [g]	**300 MPa** [g]	**400 MPa** [g]	**500 MPa** [g]	
494.48	Passwang Fm.	387.03	4.17	16.14	0	-	1.27	1.79	1.09	-	4.15
516.27	Passwang Fm.	419.23	6.47	27.12	0	-	2.93	1.89	1.05	-	5.87
554.36	Opalinus Clay	426.95	5.07	21.65	0	-	1.45	1.54	0.93	-	3.92
590.32	Opalinus Clay	426.80	4.26	18.18	0	-	1.64	1.70	0	-	3.34
607.13	Opalinus Clay	407.22	5.08	20.69	0	-	0.94	1.50	1.63	-	4.07
629.09	Opalinus Clay	438.73	5.02	22.02	0	-	1.72	1.55	1.29	-	4.56
643.35	Opalinus Clay	428.04	4.94	21.15	0	-	1.33	1.72	1.32	-	4.37
671.15	Staffelegg Fm.	447.60	3.50	15.89	0	-	0	0	0.26	0.95	1.21
709.84	Klettgau Fm.	427.90	5.23	22.38	0	0	0	0.44	1.17	1.00	2.61
775.39	Bänkerjoch Fm.	434.64	5.81	25.25	0	0	1.31	1.60	-	-	2.91

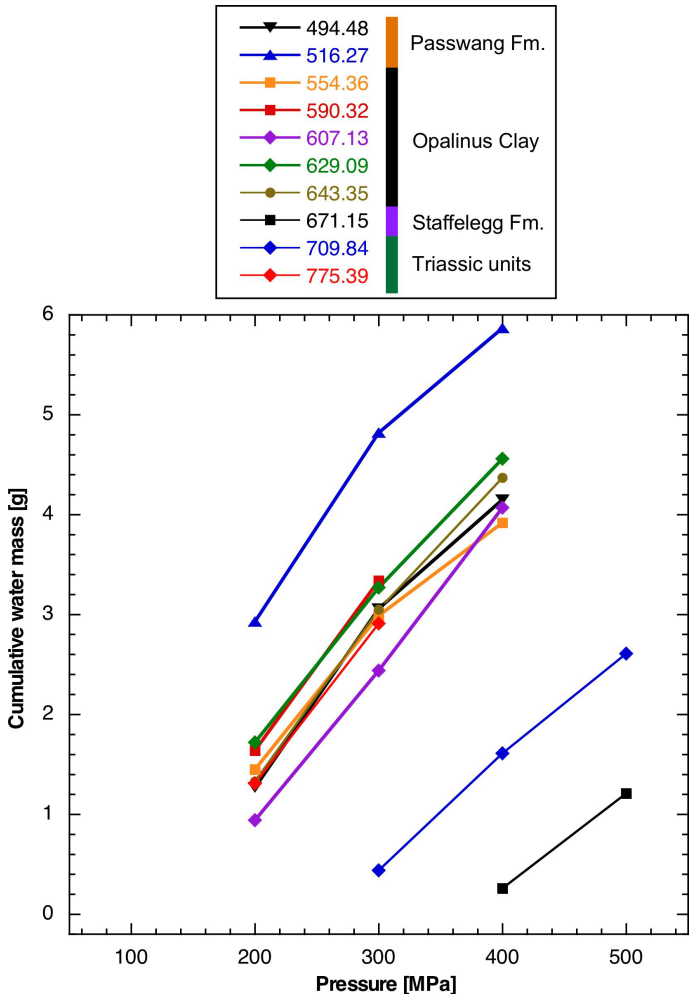

Fig. 4.6-1: Cumulative water masses obtained by squeezing as a function of the squeezing pressure

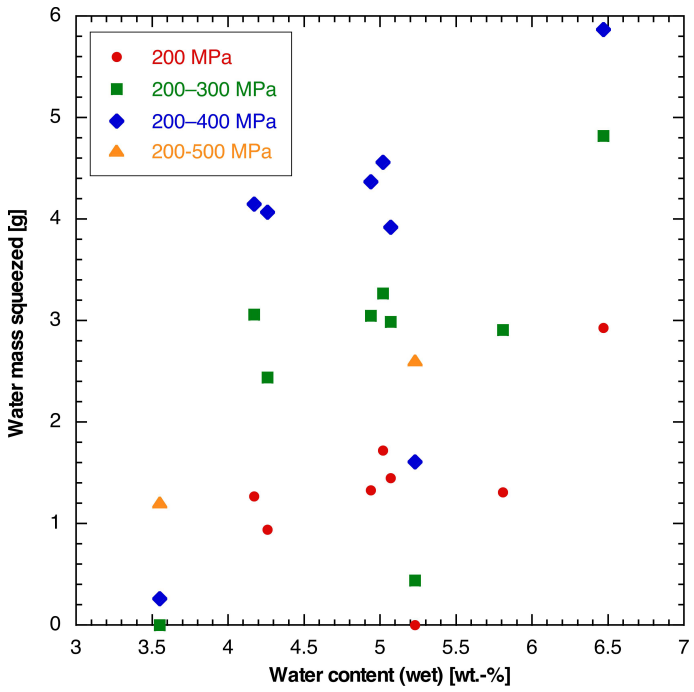

Fig. 4.6-2: Correlation of the original water content and the cumulative water mass obtained by squeeezing

4.6.2 Chemical composition of squeezed waters

Given the fact that the effects of artefacts (ion filtration, enhanced mineral dissolution) increase with squeezing pressure, only waters obtained during the first two pressure steps were analysed (sample 709.84: three pressure steps). The first squeezed aliquots yielded > 0.9 g water in most cases, from which a complete data set (major-ion composition, TIC/TOC, pH, water isotopes) could be obtained. For samples 671.15 and 709.84, which were difficult to squeeze, < 0.5 g were obtained at the first pressure step (400 and 300 MPa, respectively), resulting in incomplete data sets and an increased uncertainty. However, sufficient water was squeezed at higher pressures.

The chemical compositions of squeezed waters are listed in Tab. 4.6-3 and shown graphically as a function of squeezing pressure in Fig. 4.6-3. Na is by far the most abundant cation. In the lowermost, magnesite-bearing sample 775.39, Mg content of around 2 g/L is more than a factor 20 higher than in any other sample. In the Dogger, Cl and SO_4 (expressed in mass units) have comparable concentrations. Towards the Lias and Keuper, Cl contents decrease and SO_4 contents increase substantially. The lowermost sample 775.39 from the Bänkerjoch Formation has by far the highest salinity and SO_4 content, the latter reflecting its high content of anhydrite.

The concentrations of monovalent ions Na, K, Cl and Br generally decrease with squeezing pressure, likely due to ion-filtration effects that become important at higher pressures (Mazurek et al. 2015). NO_3 shows deviations in both directions with pressure. Ca and Mg remain near-constant with pressure or deviate slightly towards higher concentrations (with some exceptions). Ca and Mg contents in the carbonate-free sample 709.84 remain particularly constant. SO_4 concentrations evolve only weakly with increasing squeezing pressure.

As discussed in Mazurek et al. (2015) and Rufer & Mazurek (2018), the composition of the first water aliquot recovered from a sample is considered to be closest to that of the porewater, and these analyses are highlighted by bold print in Tab. 4.6-3. For samples 671.15 and 709.84, the first aliquots produced only small masses of water, so the water retrieved at the next higher pressure was chosen for further considerations. F concentrations, in particular in the first squeezed aliquots, are contaminated by F leached from the fiberglass filters and so are not representative of the porewater. For clarity, the subset of the data that is considered to be useful for further interpretation is summarised in Tab. 4.6-4.

Tab. 4.6-3: Chemical composition of squeezed waters: full data set

Bold print indicates the selected ("best") aliquots. F concentrations, in particular in the first squeezed aliquots, are contaminated by F leached from the fiberglass filters and so are not representative of the porewater. n.a.: no analysis. Data for sample 516.27 are less certain due to possible contamination by drilling mud (see Section 4.6.3) and therefore listed in italics.

Depth [m]	**Formation**	**Pressure** [MPa]	**Squeezing time** [d]	**Mass squeezed** [g]	**Na** [mg/L]	**NH_4** [mg/L]	**K** [mg/L]	**Ca** [mg/L]	**Mg** [mg/L]	**Sr** [mg/L]	**F** [mg/L]	**Cl** [mg/L]	**Br** [mg/L]	**NO_3** [mg/L]	**SO_4** [mg/L]	**pH**	**TIC** [mg/L]	**TOC** [mg/L]	**TDS** [mg/L]	**Charge balance** [%]
494.48	Passwang Fm.	**200**	**2**	**1.27**	**2779**	**n.a.**	**48.6**	**360**	**96**	**15.4**	**10.7**	**2343**	**8.9**	**6.17**	**3364**	**8.92**	**18.0**	**111.5**	**9235**	**3.5**
		300	3	1.79	2161	n.a.	27.5	325	85	14.9	5.6	1778	6.9	3.60	3013	8.98	11.3	63.3	7541	1.7
516.27	Passwang Fm.	**200**	**3**	**2.93**	***1639***	***< 10***	***65.5***	***183***	***50***	***10.2***	***9.5***	***1496***	***4.9***	***3.28***	***1814***	***9.24***	***<10***	***70.0***	***5395***	***3.1***
		300	3	1.89	*1015*	*< 10*	*11.7*	*220*	*66*	*11.4*	*4.5*	*998*	*3.4*	*3.60*	*1362*	*9.20*	*11.8*	*29.5*	*3785*	*2.8*
554.36	Opalinus Clay	**200**	**3**	**1.45**	**2600**	**n.a.**	**42.0**	**284**	**79**	**13.0**	**11.5**	**2458**	**7.5**	**5.78**	**2565**	**8.99**	**22.4**	**114.7**	**8295**	**3.8**
		300	3	1.54	2034	n.a.	21.1	289	80	13.3	5.3	1941	6.2	2.39	2372	8.97	19.2	61.2	6923	1.9
590.32	Opalinus Clay	**200**	**4**	**1.64**	**2699**	**n.a.**	**43.5**	**293**	**72**	**11.3**	**11.5**	**2623**	**7.9**	**6.97**	**2576**	**9.02**	**23.0**	**128.8**	**8590**	**3.3**
		300	6	1.70	2156	n.a.	22.4	296	73	11.6	5.2	2068	6.2	2.29	2385	8.75	23.8	64.2	7210	2.2
607.13	Opalinus Clay	**200**	**2**	**0.94**	**2618**	**< 10**	**46.6**	**279**	**70**	**8.2**	**14.7**	**2690**	**7.5**	**6.02**	**2212**	**9.00**	**17.5**	**146.4**	**8186**	**4.1**
		300	3	1.50	2530	< 10	31.7	241	71	8.6	6.8	2437	7.0	7.09	2433	8.36	21.4	89.5	7972	2.9
629.09	Opalinus Clay	**200**	**3**	**1.72**	**2582**	**< 10**	**45.6**	**259**	**74**	**9.7**	**10.0**	**2591**	**6.6**	**8.77**	**2459**	**8.79**	**24.6**	**135.5**	**8304**	**2.1**
		300	3	1.55	1974	< 10	23.2	266	77	9.0	5.7	1954	5.2	5.83	2185	8.74	20.3	69.1	6677	1.7
643.35	Opalinus Clay	**200**	**2**	**1.33**	**2481**	**< 10**	**41.1**	**250**	**69**	**10.2**	**13.1**	**2427**	**7.0**	**6.41**	**2552**	**8.97**	**17.7**	**156.5**	**8102**	**1.3**
		300	3	1.72	1983	< 10	26.2	278	72	9.7	6.1	1834	4.8	7.87	2326	8.93	13.1	66.7	6679	2.5
671.15	Staffelegg Fm.	400	3	0.26	2648	< 10	47.1	242	48	< 5	15.1	1897	3.8	10.45	3219	n.a.	n.a.	n.a.	8131	4.3
		500	**4**	**0.95**	**3012**	**< 10**	**51.6**	**377**	**73**	**9.6**	**10.6**	**1894**	**4.7**	**10.93**	**4312**	**8.90**	**15.4**	**90.2**	**9924**	**4.0**
709.84	Klettgau Fm.	300	2	0.44	2693	< 10	42.2	384	94	< 10	11.8	675	< 1.6	43.99	5554	8.79	n.a.	n.a.	9498	3.2
		400	**2**	**1.17**	**2848**	**< 10**	**60.5**	**396**	**94**	**< 10**	**8.4**	**585**	**< 1.6**	**17.01**	**6198**	**9.05**	**36.7**	**93.9**	**10490**	**1.2**
		500	3	1.00	2510	< 10	44.0	377	92	< 10	6.5	455	< 1.6	7.65	5610	8.88	36.4	51.2	9339	1.3
775.39	Bänkerjoch Fm.	**200**	**4**	**1.31**	**6030**	**< 10**	**169.4**	**463**	**2012**	**< 10**	**9.9**	**4096**	**19.3**	**11.34**	**16198**	**8.49**	**65.7**	**105.7**	**29458**	**-0.4**
		300	2	1.60	5304	< 10	128.9	549	1943	9.9	6.9	3618	17.7	7.53	15334	8.44	58.7	64.6	27282	-0.6

Tab. 4.6-4: Chemical composition of squeezed waters: summary of selected analyses to be used for interpretation

Data for sample 516.27 are less certain due to possible contamination by drilling mud (see Section 4.6.3) and therefore listed in italics.

Depth [m]	**Formation**	**Pressure** [MPa]	**Squeezing time** [d]	**Mass squeezed** [g]	**Na** [mg/L]	**K** [mg/L]	**Ca** [mg/L]	**Mg** [mg/L]	**Sr** [mg/L]	**Cl** [mg/L]	**Br** [mg/L]	**NO_3** [mg/L]	**SO_4** [mg/L]	**pH**	**TIC** [mg/L]	**TOC** [mg/L]
494.48	Passwang Fm.	200	2	1.27	2779	48.6	360	96	15.4	2343	8.9	6.17	3364	8.92	18.0	111.5
516.27	Passwang Fm.	200	3	2.93	*1639*	*65.5*	*183*	*50*	*10.2*	*1496*	*4.9*	*3.28*	*1814*	*9.24*	*<10*	*70.0*
554.36	Opalinus Clay	200	3	1.45	2600	42.0	284	79	13.0	2458	7.5	5.78	2565	8.99	22.4	114.7
590.32	Opalinus Clay	200	4	1.64	2699	43.5	293	72	11.3	2623	7.9	6.97	2576	9.02	23.0	128.8
607.13	Opalinus Clay	200	2	0.94	2618	46.6	279	70	8.2	2690	7.5	6.02	2212	9.00	17.5	146.4
629.09	Opalinus Clay	200	3	1.72	2582	45.6	259	74	9.7	2591	6.6	8.77	2459	8.79	24.6	135.5
643.35	Opalinus Clay	200	2	1.33	2481	41.1	250	69	10.2	2427	7.0	6.41	2552	8.97	17.7	156.5
671.15	Staffelegg Fm.	500	4	0.95	3012	51.6	377	73	9.6	1894	4.7	10.93	4312	8.90	15.4	90.2
709.84	Klettgau Fm.	400	2	1.17	2848	60.5	396	94	< 10	585	< 1.6	17.01	6198	9.05	36.7	93.9
775.39	Bänkerjoch Fm.	200	4	1.31	6030	169.4	463	2012	< 10	4096	19.3	11.34	16198	8.49	65.7	105.7

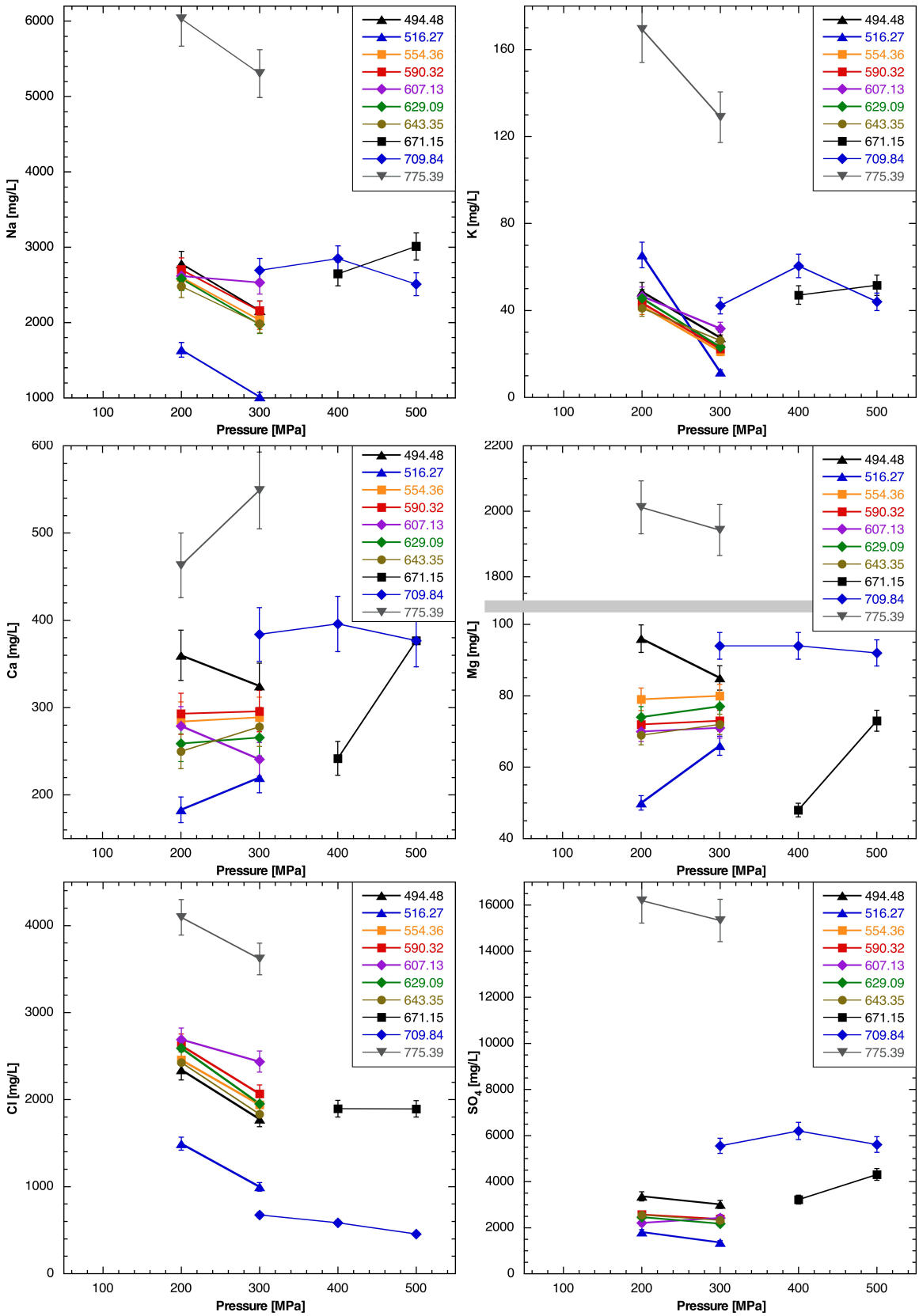

Fig. 4.6-3: Ion concentrations in squeezed waters as a function of squeezing pressure

Bars indicate analytical errors of ion-chromatography analysis. Grey bar in the plot for Mg separates two y-axis ranges.

4.6.3 Depth trends

Profiles with depth for various pore-water constituents are shown in Fig. 4.6-4. The following observations can be made:

- Na and K show no systematic variability in the Passwang Formation and the Opalinus Clay. Concentrations become slightly higher in the Staffelegg and Klettgau Formations, and a massive increase is identified in the Bänkerjoch Formation.
- In the Triassic units, Ca and Mg show increasing concentrations with depth.
- The Cl profile is flat in the Dogger, but concentrations decrease substantially towards the minimum in the Klettgau Formation, before rising again in the Bänkerjoch Formation.
- The SO_4 profile is flat in the Opalinus Clay (values around 2.5 g/L), below which a sharp rise starts towards a value of 16 g/L in the Bänkerjoch Formation.
- The Br/Cl ratio decreases systematically from the Passwang Formation (where it is close to that of current seawater) to the Staffelegg Formation. A substantially higher ratio is identified in the Bänkerjoch Formation.
- The SO_4/Cl ratio decreases downwards to reach a minimum in the lower part of the Opalinus Clay, followed by a sharply increasing trend towards the Triassic. Thus, the shapes of the Br/Cl and SO_4/Cl profiles are similar. However, all SO_4/Cl ratios are much higher than the seawater value of 0.052.
- In the depth profile, sample 516.27 has relatively high K, relatively low Na, Ca, Mg and Cl contents, in addition to a high pH. This may be due to some degree of contamination by the K silicate drilling mud (see Tab. 2-5). However, the relatively low SO_4 and TOC concentrations are not in line with this proposition, given the high contents of these solutes in the drilling mud. Major-ion data from this sample are considered less certain and marked as such in Tabs. 4.6-3 and 4.6-4.

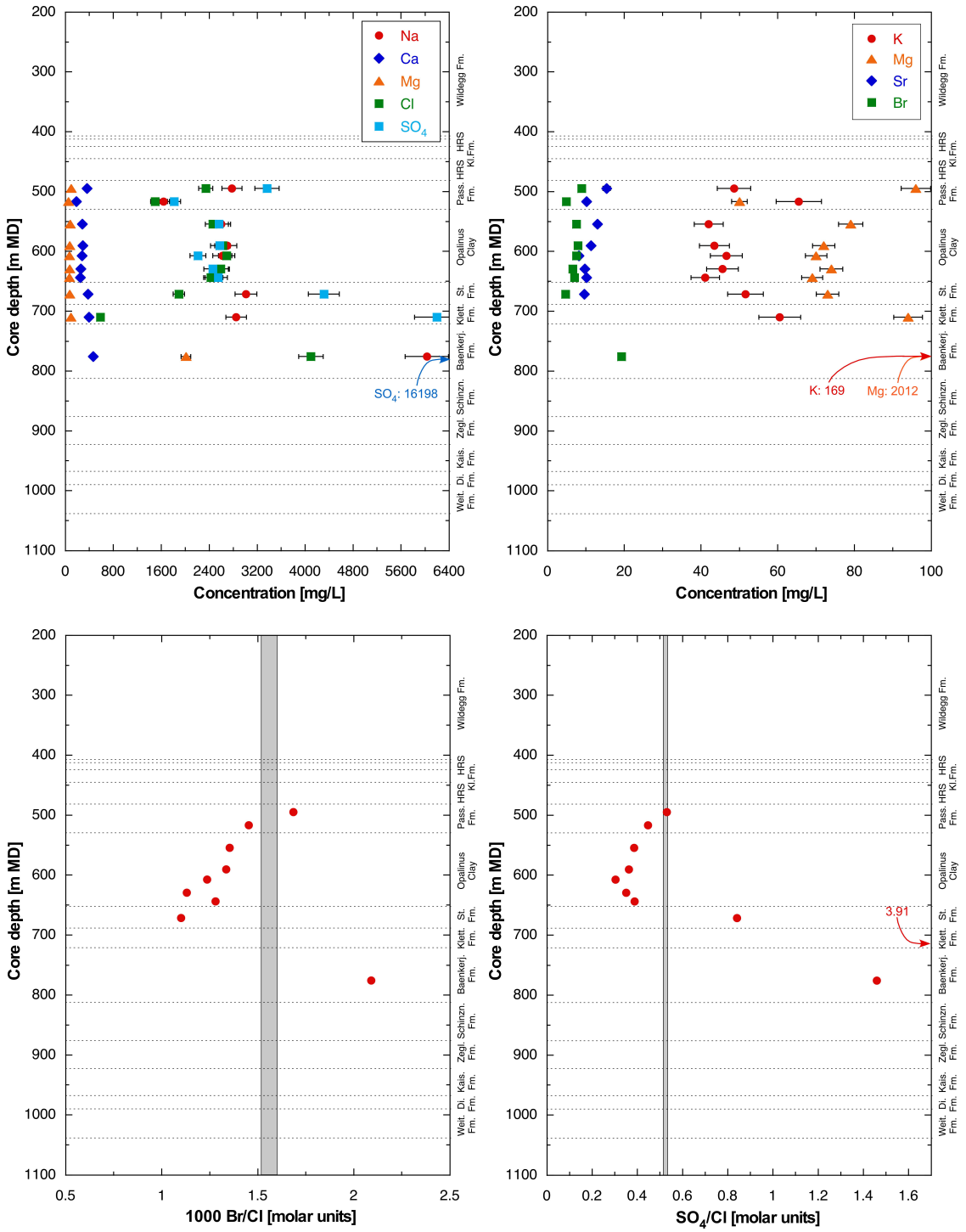

Fig. 4.6-4: Depth trends of ion concentrations and ion ratios in squeezed waters

Only the selected aliquots are shown for each sample. Bars indicate analytical errors of ion-chromatography analysis. Grey rectangles represent current seawater ratios.

4.6.4 Geochemical modelling and mineral saturation states

Mineral saturation indices for squeezed waters were calculated using PhreeqC V3 and the PSI/Nagra thermodynamic data base at 25 °C (Thoenen et al. 2014) and are shown in Tab. 4.6-5.

- Squeezed waters are strongly oversaturated with respect to calcite and dolomite, a feature already known from previous studies (e.g. Mazurek et al. 2015). The oversaturation is possibly due to the fact that mineral solubility at high pressures during squeezing is higher than at atmospheric pressure. Further, outgassing of CO_2 during the squeezing process increases the pH and the saturation indices of calcite and dolomite (Tournassat et al. 2015). Further outgassing my take place in the headspace of the sample vials during sample storage. The comparatively low calculated $P(CO_2)$ suggest that some outgassing may have taken place, which also affects pH. However, this nevertheless does not markedly affect the obtained major-ion composition due to the large buffering capacity of the rock-water system in clay-rich lithologies. Last, lattice defects in carbonate minerals induced by deformation during squeezing might increase the solubility of these minerals. On the other hand, outgassing into the external atmosphere during sample storage in glass vessels is not considered to contribute to the low $P(CO_2)$. Such a process should also be seen by higher δ values of water isotopes, which is not the case (see Section 4.8), but this depends on the mode of water loss (via a gas phase, or via a liquid film). In Section 5.5.1, an attempt is made to restore the outgassing by model calculations assuming equilibrium with calcite.
- For the same reasons, all squeezed waters are oversaturated with respect to magnesite. The oversaturation is highest in sample 775.39, the only one actually containing magnesite.
- Saturation indices for strontianite decrease with depth. Slight oversaturation is observed for the Dogger units, evolving towards slight resaturation in the footwall.
- The waters are close to saturation or slightly undersaturated with respect to celestite. They are undersaturated with respect to gypsum in samples from the Dogger and Liassic but close to saturation in the underlying Triassic units. Note that sample 775.39 actually contains anhydrite.
- Using the data from Tab. 4.6-3, squeezed waters are strongly oversaturated with respect to fluorite, which is a consequence of the contamination of F concentrations by the filter material. Therefore, no F data are listed in Tab. 4.6-4.

Tab. 4.6-5: Mineral saturation indices for squeezed waters

Bold print indicates the selected ("best") aliquots. n.d.: no data. Data for sample 516.27 are less certain due to possible contamination by drilling mud (see Section 4.6.3) and therefore listed in italics.

Depth [m]	**Formation**	**Pressure** [MPa]	**pH**	**TIC** [M]	**log (P_{CO2})**	**SI Calcite**	**SI Aragonite**	**SI Dolomite (ordered)**	**SI Dolomite (disordered)**	**SI Strontianite**	**SI Magnesite**	**SI Gypsum**	**SI Anhydrite**	**SI Celestite**	**SI Fluorite**
494.48	Passwang Fm.	**200**	**8.92**	**1.51E-03**	**-4.17**	**1.28**	**1.13**	**2.30**	**1.75**	**0.36**	**0.70**	**-0.23**	**-0.45**	**0.13**	**1.05**
		300	8.98	9.48E-04	-4.43	1.11	0.97	1.96	1.41	0.23	0.53	-0.26	-0.49	0.12	0.48
516.27	Passwang Fm.	**200**	***9.24***	***n.d.***								***-0.60***	***-0.82***	***-0.13***	***0.81***
		300	*9.20*	*9.86E-04*	*-4.64*	*1.30*	*1.15*	*2.40*	*1.85*	*0.47*	*0.78*	*-0.56*	*-0.78*	*-0.12*	*0.30*
554.36	Opalinus Clay	**200**	**8.99**	**1.88E-03**	**-4.15**	**1.37**	**1.23**	**2.51**	**1.96**	**0.49**	**0.82**	**-0.39**	**-0.61**	**-0.01**	**1.06**
		300	8.97	1.61E-03	-4.18	1.32	1.18	2.41	1.86	0.44	0.77	-0.37	-0.60	0.01	0.42
590.32	Opalinus Clay	**200**	**9.02**	**1.93E-03**	**-4.17**	**1.41**	**1.27**	**2.54**	**1.99**	**0.46**	**0.81**	**-0.38**	**-0.60**	**-0.07**	**1.07**
		300	8.75	2.00E-03	-3.83	1.24	1.09	2.19	1.64	0.29	0.63	-0.37	-0.59	-0.06	0.42
607.13	Opalinus Clay	**200**	**9.00**	**1.47E-03**	**-4.27**	**1.28**	**1.14**	**2.29**	**1.74**	**0.21**	**0.69**	**-0.44**	**-0.66**	**-0.25**	**1.29**
		300	8.36	1.80E-03	-3.46	0.74	0.60	1.28	0.73	-0.25	0.21	-0.46	-0.68	-0.19	0.55
629.09	Opalinus Clay	**200**	**8.79**	**2.07E-03**	**-3.87**	**1.22**	**1.07**	**2.21**	**1.66**	**0.25**	**0.68**	**-0.44**	**-0.66**	**-0.14**	**0.91**
		300	8.74	1.70E-03	-3.89	1.13	0.99	2.06	1.51	0.12	0.60	-0.43	-0.65	-0.18	0.47
643.35	Opalinus Clay	**200**	**8.97**	**1.49E-03**	**-4.22**	**1.21**	**1.06**	**2.18**	**1.63**	**0.28**	**0.65**	**-0.44**	**-0.66**	**-0.10**	**1.13**
		300	8.93	1.10E-03	-4.30	1.12	0.97	1.97	1.42	0.12	0.53	-0.39	-0.61	-0.12	0.54
671.15	Staffelegg Fm.	400	n.d.	n.d.								-0.38	-0.60		1.22
		500	**8.90**	**1.29E-03**	**-4.21**	**1.17**	**1.03**	**1.94**	**1.39**	**0.03**	**0.45**	**-0.14**	**-0.36**	**-0.02**	**1.03**
709.84	Klettgau Fm.	300	8.79	n.d.								-0.06	-0.28		1.08
		400	**9.05**	**3.09E-03**	**-4.01**	**1.61**	**1.47**	**2.91**	**2.36**		**0.98**	**-0.04**	**-0.26**		**0.77**
		500	8.88	3.06E-03	-3.80	1.48	1.33	2.66	2.11		0.86	-0.07	-0.29		0.55
775.39	Bänkerjoch Fm.	**200**	**8.49**	**5.63E-03**	**-3.20**	**1.26**	**1.11**	**3.46**	**2.91**		**1.88**	**0.10**	**-0.11**		**0.48**
		300	8.44	5.02E-03	-3.19	1.25	1.11	3.35	2.80	-0.04	1.78	0.17	-0.04	0.15	0.25

4.6.5 Water content and aqueous extraction of squeezed core material

After the squeezing experiment, each core was dried at 105 °C, from which the mass of water remaining in the sample was obtained. The dry core was then subjected to aqueous extraction, from which the mass of Cl remaining in the sample could be calculated. The results are summarised in Tab. 4.6-6. Given the fact that oven-drying was performed with air, some degree of rock oxidation occurred. Therefore, results are only given for the conservative constituents Cl and Br.

Tab. 4.6-6: Water contents and results of aqueous-extraction tests on previously squeezed samples

Depth [m]	**Formation**	**Water content (wet) of squeezed sample** [wt.-%]	**Mass of porewater in squeezed sample** [g]	**Aqueous extraction of squeezed sample**				
				Mass of dry rock [g]	**Mass of added water** [g]	**S/L** [g/g]	**Cl** [$mg/L_{extract\ solution}$]	**Br** [$mg/L_{extract\ solution}$]
494.48	Passwang Fm.	3.78	14.46	29.89	29.86	1.001	23.3	0.12
516.27	Passwang Fm.	5.37	22.20	29.90	29.82	1.003	37.5	0.13
554.36	Opalinus Clay	4.03	17.04	29.82	29.82	1.000	43.5	0.12
590.32	Opalinus Clay	3.88	16.42	30.07	29.81	1.009	41.5	0.10
607.13	Opalinus Clay	3.86	15.57	29.43	29.79	0.988	39.2	0.10
629.09	Opalinus Clay	4.04	17.55	29.87	29.81	1.002	45.2	0.11
643.35	Opalinus Clay	3.94	16.69	29.84	29.78	1.002	37.6	0.09
671.15	Staffelegg Fm.	3.13	13.96	30.58	29.80	1.026	29.6	0.07
709.84	Klettgau Fm.	4.39	18.68	30.05	29.96	1.003	10.8	0.02
775.39	Bänkerjoch Fm.	5.39	23.27	30.61	29.92	1.023	95.8	0.47

4.6.6 Chloride-accessible porosity

Combining the data for squeezed waters (Tab. 4.6-3) and for the samples after squeezing (Tab. 4.6-6) permits the reconstruction of the total Cl and water inventories, therefore also the initial Cl concentrations in the bulk porewater. Assuming that the squeezed water represents the composition of the anion-accessible water, the Cl-accessible porosity fraction f_{Cl} can be calculated. The formalism is detailed in Mazurek et al. (2021).

The volume of the water remaining in the sample after squeezing is obtained from the water content of the squeezed core, assuming a porewater density of 1 g/cm^3. Note that the formalism also assumes that the dead volume of the squeezing system is negligible. While the dead volume is indeed likely small, a sensitivity calculation was performed on its impact. Assuming a dead volume of 1 mL results is an anion-accessible porosity fraction that is 0.01 – 0.04 higher than the value without consideration of a dead volume. The most strongly expressed shift is found in samples where only a small water volume was squeezed, while it becomes insignificant for samples with a good water yield.

The Cl-accessible porosity fraction is finally obtained from

$$f_{Cl} = \frac{C_{Cl\ in\ bulk\ pore\ water}}{C_{Cl\ in\ squeezed\ water}}$$

The resulting Cl-accessible porosity fractions are listed in Tab. 4.6-7 and shown as a function of the clay-mineral content in Fig. 4.6-5. The mean value for f_{Cl} is 0.45, which is at the lower end of the range reported for boreholes BUL1-1, TRU1-1, MAR1-1, Schlattingen-1 and the Mont Terri Rock Laboratory (Mazurek et al. 2021, Aschwanden et al. 2021, Mäder et al. 2021, Mazurek et al. 2015, Pearson et al. 2003).

The results cover a limited range of 0.41 – 0.50 for the chloride-accessible porosity fraction for clay-rich samples (excluding the samples from the Passwang Formation and the Staffelegg Formation yields the range 51 – 72 wt.-% clay minerals), despite quite a range of experimental bounding parameters: squeezed first aliquots of 5 - 11% of the porewater inventory, and a Cl concentration range of 0.6 – 4.1 g/L. This attests a certain robustness to the method.

Tab. 4.6-7: Cl-accessible porosity fractions derived from squeezing and aqueous-extraction experiments

The masses of Cl and water needed for the calculation are also listed.

Depth [m]	**Formation**	**Member**	**Total mass of squeezed Cl** [mg]	**Mass of Cl in aq. extract of squeezed core** [mg]	**Porewater mass squeezed** [g]	**Water mass remaining in squeezed core** [g]	**Cl-accessible porosity fraction f_{Cl}** [-]
494.48	Passwang Fm.	Rothenfluh Mb.	6.16	8.57	4.15	14.46	0.34
516.27	Passwang Fm.	Waldenburg and lower part of Brüggli Mb.	6.27	14.61	5.87	22.20	0.50
554.36	Opalinus Clay	'Sub-unit with silty calcareous beds'	6.55	17.68	3.92	17.04	0.47
590.32	Opalinus Clay	'Mixed clay-silt-carbonate sub-unit'	7.82	16.73	3.34	16.42	0.47
607.13	Opalinus Clay	'Mixed clay-silt-carbonate sub-unit'	6.18	15.39	4.07	15.57	0.41
629.09	Opalinus Clay	'Mixed clay-silt-carbonate sub-unit'	7.48	18.80	4.56	17.55	0.46
643.35	Opalinus Clay	'Clay-rich sub-unit'	6.38	15.26	4.37	16.69	0.42
671.15	Staffelegg Fm.	Frick Mb.	2.29	12.47	1.21	13.96	0.51
709.84	Klettgau Fm.	Ergolz Mb.	1.44	4.38	2.61	18.68	0.47
775.39	Bänkerjoch Fm.	'Thin-layered anhydrite claystone sequence'	11.16	38.27	2.91	23.27	0.46

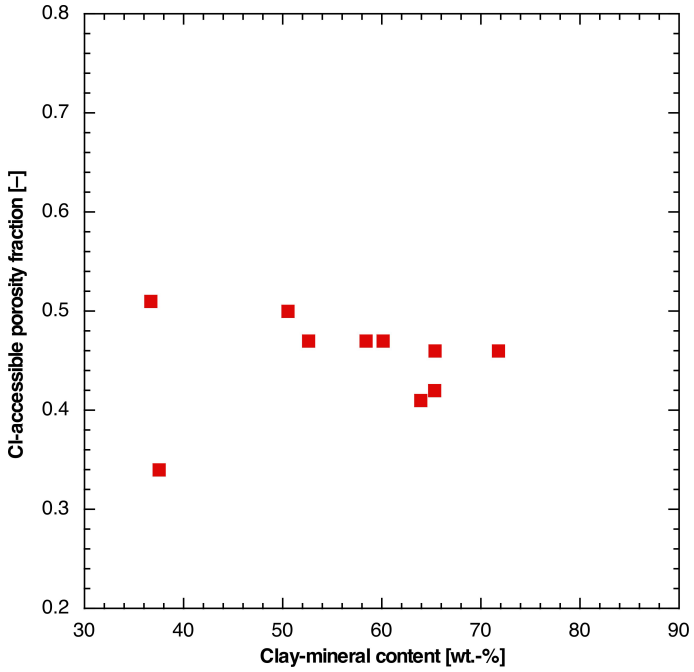

Fig. 4.6-5: Cl-accessible porosity fractions derived from squeezing experiments as a function of the clay-mineral content

4.6.7 Stable isotopic composition of squeezed water

Results of stable water-isotope analyses are listed in Tab. 4.6-8 and shown as a function of depth in Fig. 4.6-6. The following observations can be made:

- Within any sample, the variation of the δ values with squeezing pressure is small (often within analytical error). In most cases, the δ values become slightly more negative with increasing pressure.
- Sample 516.27 shows somewhat lower δ values when compared to the adjacent samples, in particular for $\delta^{18}O$. This could be due to contamination by drilling mud, as already suspected for major ions (Section 4.6-3). The data for this sample are therefore considered less certain.
- $\delta^{18}O$ values decrease systematically with depth between the Passwang Formation and a minimum in the Klettgau Formation. The underlying sample from the Bänkerjoch Formation has a slightly higher value.
- $\delta^{2}H$ values remain constant within error in the Dogger-Lias section, which is a clear difference to the systematic trend of $\delta^{18}O$. As for $\delta^{18}O$, a minimum is observed in the Klettgau Formation.
- In a plot $\delta^{18}O$ vs. $\delta^{2}H$ (Fig. 4.6-7), the shallower samples are located on the right side of the global ($\delta^{2}H = 8\ \delta^{18}O + 10$; Craig 1961) and the local ($\delta^{2}H = 7.55\ \delta^{18}O + 4.8$; Kullin & Schmassmann 1991) meteoric water lines. With depth, they come progressively closer to the meteoric water lines. The Triassic samples lie slightly to the left of the meteoric water lines.
- The same information is illustrated in Fig. 4.6-8 by the depth trend of deuterium excess ($\delta^{18}O - 8\ \delta^{2}H$), which increases systematically with depth until the Klettgau Formation.

Tab. 4.6-8: Stable isotopic composition of squeezed waters

The aliquots selected for interpretation are shown in bold. Data for sample 516.27 are less certain due to possible contamination by drilling mud (see Section 4.6.3) and therefore listed in italics.

Depth [m]	**Formation**	**Pressure** [MPa]	**$\delta^{18}O$** [‰ VSMOW]	**$\delta^{2}H$** [‰ VSMOW]	**D excess** [‰]
494.48	Passwang Fm.	**200**	**-4.39**	**-39.8**	**-4.7**
		300	-4.53	-40.5	-4.2
516.27	Passwang Fm.	**200**	***-4.81***	***-40.3***	***-1.8***
		300	*-5.23*	*-41.9*	*-0.1*
554.36	Opalinus Clay	**200**	**-4.67**	**-38.4**	**-1.1**
		300	-4.85	-39.7	-0.9
590.32	Opalinus Clay	**200**	**-4.99**	**-38.5**	**1.4**
		300	-5.04	-38.6	1.7
607.13	Opalinus Clay	**200**	**-5.38**	**-39.3**	**3.8**
		300	-5.29	-38.8	3.5
629.09	Opalinus Clay	**200**	**-5.65**	**-39.3**	**5.9**
		300	-5.81	-39.8	6.7
643.35	Opalinus Clay	**200**	**-6.06**	**-39.5**	**9.0**
		300	-6.18	-39.9	9.6
671.15	Staffelegg Fm.	400	-6.18	-39.9	9.6
		500	**-6.17**	**-39.7**	**9.7**
709.84	Klettgau Fm.	300	-7.14	-44.3	12.8
		400	**-7.23**	**-44.5**	**13.3**
		500	-7.27	-45.0	13.1
775.39	Bänkerjoch Fm.	**200**	**-6.82**	**-42.3**	**12.3**
		300	-6.90	-42.4	12.8

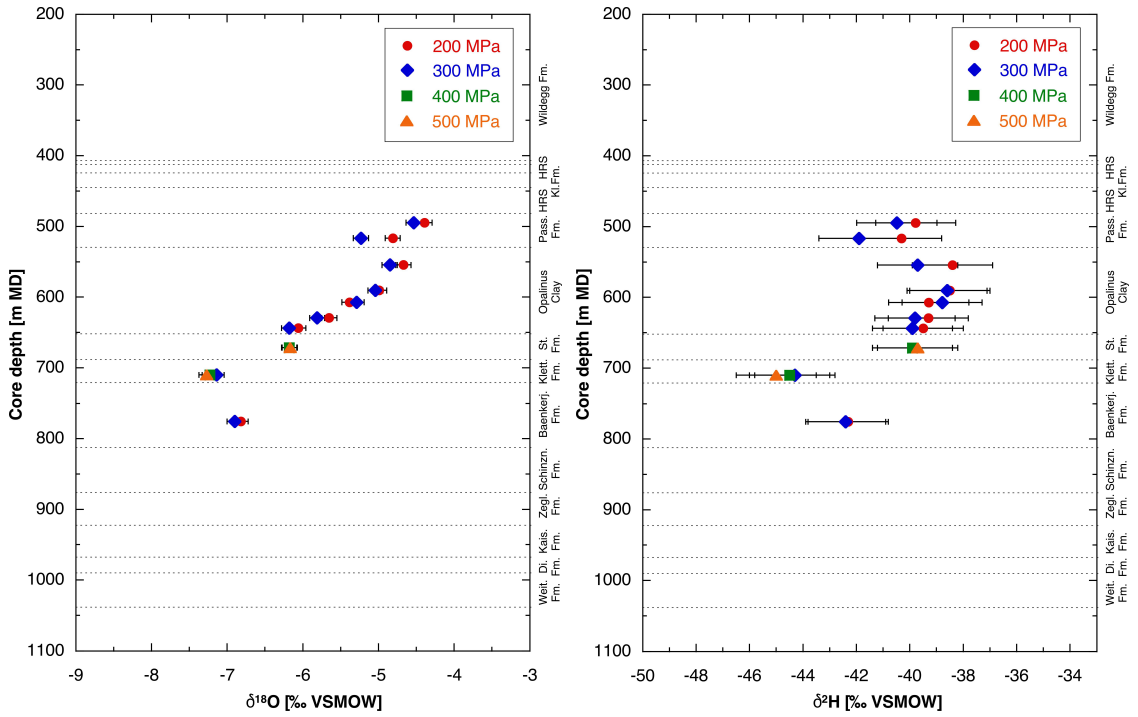

Fig. 4.6-6: Depth trends of $\delta^{18}O$ and $\delta^{2}H$ in squeezed waters

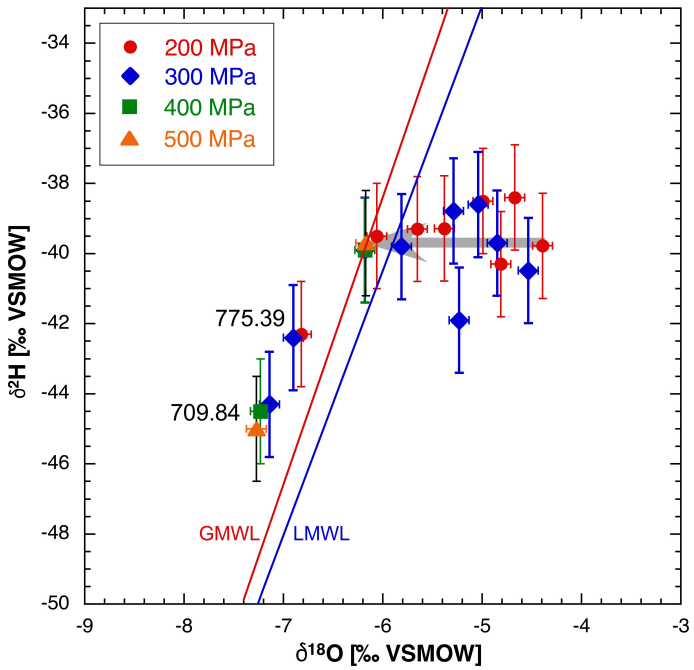

Fig. 4.6-7: Plot of $\delta^{18}O$ vs. $\delta^{2}H$ for squeezed waters

Grey arrow indicates trend with depth in the section Passwang Formation – Staffelegg Formation. GMWL: Global Meteoric Water Line, LMWL: Local Meteoric Water Line.

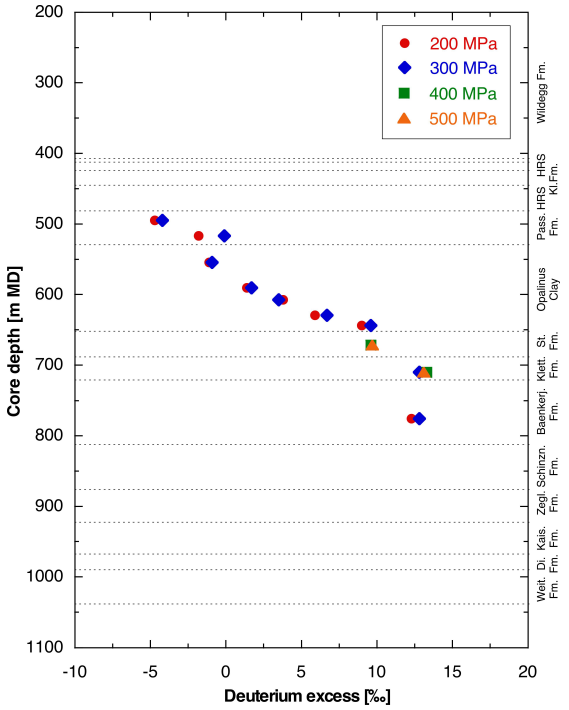

Fig. 4.6-8: Depth trend of deuterium excess in squeezed waters

4.7 Data from advective displacement experiments

Carmen Zwahlen, Mirjam Kiczka, Andreas Jenni, Urs Mäder

Advective displacement (AD) experiments are a methodology for a comprehensive physico-chemical characterisation, including porewater chemistry and certain transport properties (details in method report, Waber (ed.) 2020). This section presents a data summary, more details where important, and short discussions where appropriate. The full data sets are provided in Appendix B. Integration of the data into context and depth profiles is included in Chapter 5.

Six samples from the clay-rich Dogger to Keuper units were processed. All except one experiment were successful, subjected to a similar analytical program, with differences mainly related to the duration of each experiment (numbers of sampled fluid aliquots). The extent of pre and post-mortem characterisation of core material was optimised based on gained experience from former BUL1-1, TRU1-1 and MAR1-1 investigations. The duration of the percolation period was 57-161 days, transporting 0.4 – 0.8 pore volumes of fluid.

The salinity of porewater in this borehole is significantly lower than in all previous TBO boreholes. A feature not observed in the boreholes BUL1-1 and TRU1-but in some experiments for MAR1-1 and BOZ1-1 are very high nitrate concentrations eluted initially during advective displacement. At BOZ1-1, this is particularly the case for the sample from the Hauptrogenstein and this is discussed in Section 4.7.5.4, and further below.

4.7.1 Sample material and overview of analytical work

The drill core samples (Fig. 4.7-1) span more than 200 m of clay-rich confining units and host rock (469 – 698 m depth), from the Passwang Formation ('Brauner Dogger') to the Staffelegg Formation and include one sample from the overlaying Hauptrogenstein and the underlaying Klettgau Formation.

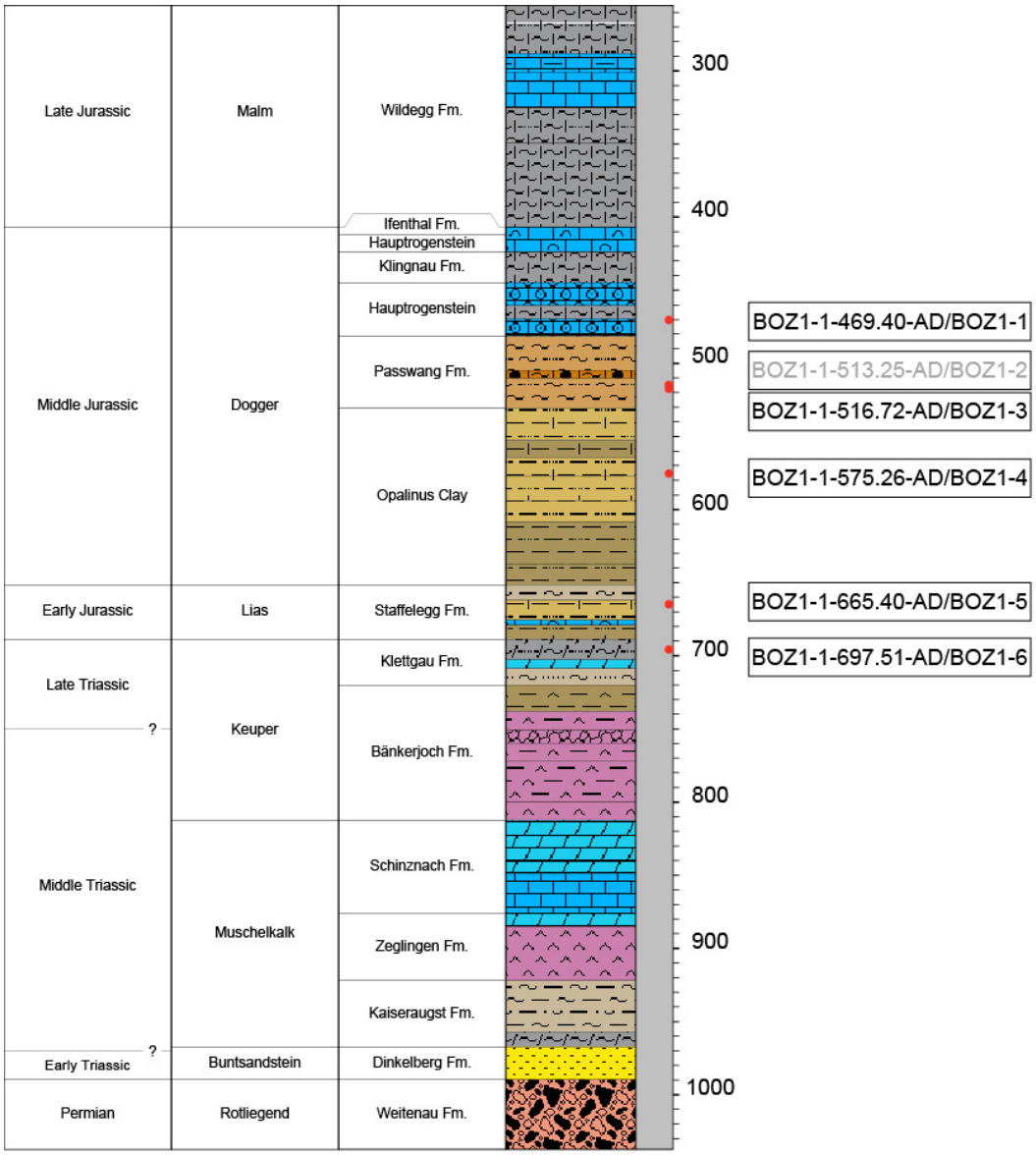

Fig. 4.7-1: Location of samples used for advective displacement experiments (red dots)

Short labels are consecutively numbered laboratory abbreviations. The failed experiment, BOZ1-2, is marked in gray.

X-ray computed tomography (CT) was performed on a medical scanner (Waber (ed.) 2020) for sample selection (Fig. 4.7-2), detection of disturbing features (fractures, pyrite accumulations, macro-fossils, etc.). Dry cutting was used for obtaining a central core segment for AD experiments (yellow in Fig. 4.7-2), and adjacent 1 or 2 discs for accompanying characterisation (green in Fig. 4.7-2). The central core segment was turned on a lathe from 95 mm to 80 mm diameter. Tab. 4.7-1 lists all analytical work performed on the six samples.

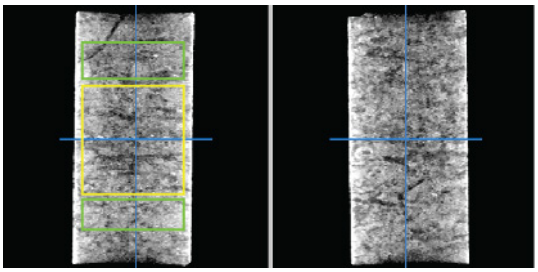

BOZ1-1-469.40-AD (Hauptrogenstein) (BOZ1-1)

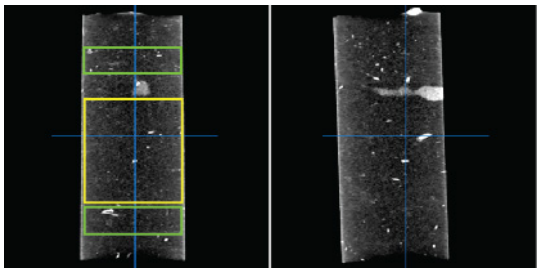

BOZ1-1-513.25-AD (Passwang Fm. / Brüggli Mb.) (BOZ1-2, failed)

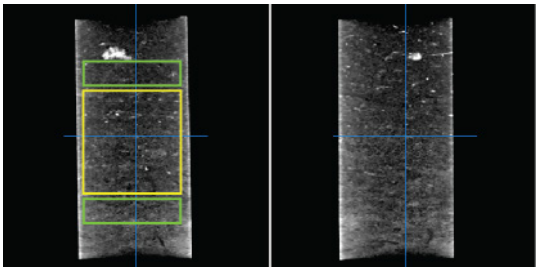

BOZ1-1-516.72-AD (Passwang Fm. / Brüggli Mb.) (BOZ1-3)

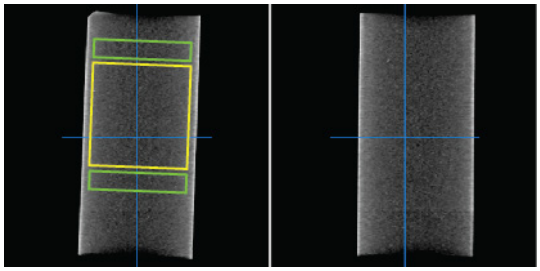

BOZ1-1-575.26-AD (Opalinus Clay) (BOZ1-4)

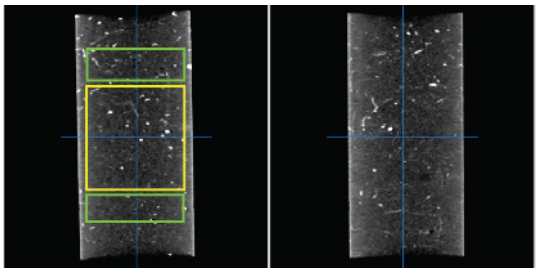

BOZ1-1-665.40-AD (Staffelegg Fm. / Frick Mb.) (BOZ1-5)

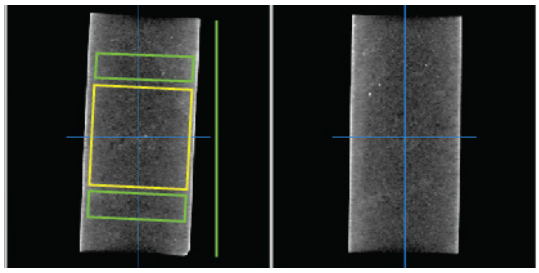

BOZ1-1-697.51-AD (Klettgau Fm.) (BOZ1-6)

Fig. 4.7-2: X-ray CT images of AD samples

Central sections parallel to core axis at right angle. Grey scale range setting is 1700-2500 HU. Yellow segments are used for advective displacement, green segments for pre-characterisation. Low X-ray absorbance represents clay/quartz-rich sections (darker grey), slightly lighter grey indicates carbonate-richer parts, siderite is brighter, and pyrite is white (strongest absorbance). Black lines/gaps represent fractures.

Tab. 4.7-1: Summary of analytical work perfomed on samples for advective displacement experiments

Parameter	**BOZ1-1**	**BOZ1-2**	**BOZ1-3**
Sample ID RWI	BOZ1-1-469.40-AD	BOZ1-1-513.25-AD	BOZ1-1-516.72-AD
Lab sample ID	BOZ1-1xx-AD	BOZ1-2xx-AD	BOZ1-3xx-AD
Depth [m]	469.40	513.25	516.72
Geol. unit	Hauptrogenstein	Passwang Fm.	Passwang Fm.
Member / sub-unit	'Spatkalk'	Waldenburg Mb. / Brueggli Mb.	Waldenburg Mb. / Brueggli Mb.
AD_exp	y	n	y
Pre_WC	1+1	1+1	1+1
Pre_M	y	y	y
Pre_V,A,L	y	y	y
Pre_Min	1+1	1	1+1
Pre_Clay	1+1	1	1+1
Pre_AqEx	1+1	1+1	1+1
Pre_Ni-en	ave	ave	ave
Post_WC	5	n	5
Post_M	y	n	y
Post_V,A,L	y	n	y
Post_AqEx	3	n	2
Post_Ni-en	n	n	n
Abras_Drilling_Fl	n	n	n

Parameter	**BOZ1-4**	**BOZ1-5**	**BOZ1-6**
Sample ID RWI	BOZ1-1-575.26-AD	BOZ1-1-665.40-AD	BOZ1-1-697.51-AD
Lab sample ID	BOZ1-4xx-AD	BOZ1-5xx-AD	BOZ1-6xx-AD
Depth [m]	575.26	665.40	697.51
Geol. unit	Opalinus Clay	Staffelegg Fm.	Klettgau Fm.
Member / sub-unit	'Upper silty sub-unit'	Frick Mb.	Gruhalde Mb.
AD_exp	y	y	y
Pre_WC	1+1	1+1	1+1
Pre_M	y	y	y
Pre_V,A,L	y	y	y
Pre_Min	1	1	1
Pre_Clay	1	1	1
Pre_AqEx	1+1	1+1	1+1
Pre_Ni-en	ave	ave	ave
Post_WC	5	5	5
Post_M	y	y	y
Post_V,A,L	y	y	y
Post_AqEx	5	2	2
Post_Ni-en	n	n	n
Abras_Drilling_Fl	n	n	n

y: yes = done; n: no = not done; integer numbers refer to the number of samples processed; +: samples from above (left number) and below (right number) a core were processed; 2: duplicate samples; Pre: sample pre-characterisation; Post: post-mortem characterisation; WC: water content; M: mass; V,A,L: core volume, sectional area and length; Min: mineralogy; Clay: clay mineralogy; AqEx: aqueous extracts; Ni-en: cation selectivity with Ni-en method; Post_WC: post-mortem water content determined along a profile with 5 segments; AD_exp: complete analysis of fluid sample aliquots collected during advective displacement.

4.7.2 Conditions of advective displacement experiments

Sample preparation was performed according to Waber (ed.) (2020). The overview table (Tab. 4.7-2) presents some experiment specific parameters such as sample processing dates, storage time and other characteristic times like arrival of first fluid drop and its electric conductivity. Numbers of samples taken and analysed are listed as well as average pressures for confining and injection. The number of pore volumes percolated are based on the water content determined from pre-characterisation. Infiltration pressure was set to 47 – 48 bar for the artificial porewater (APW), pressuriesed by He. The hydraulic gradients are large, 5'000 – 6'000 m_{H2O}/m (sample dimensions are in Tab. 4.7-4). Experiments were started within 3 – 38 days of sample delivery. The time until arrival of a first fluid drop at the electric conductivity cell (outflow, before sampling syringe) was 3 – 12 days after start of infiltration.

Confining pressure was set to 58 – 60 bar, pressurised by Ar on water except for BOZ1-6 where Kr was used instead of Ar. The gas collected in gas-tight glass vials (with needle and septum) prior to the arrival of the first fluid drop, as well as the head space in selected syringes containing gas and fluid, was analysed by mass spectrometry (Entracers GmbH and Hydroisotop GmbH, results in Appendix B). In addition, the density of the gas could be derived from high-precision weighing. Assuming all O_2 originates from air that is present at the core surface, in filters and in dead-space (entrapped during preparation), the air proportion in the gas is calculated and all air components (mainly N_2) are subtracted from the measurements. The results are summarised below:

- Apart from air (and He used as carrier gas), Ar (or Kr in case of Kr-pressurised confining fluid) dominates the exfiltrating gas composition, especially at early times. Ar content is far above compositions observed in other gas measurements (e.g., Schlattigen borehole). The Ar and Kr must therefore originate from the confining system, although it is unclear how these gases penetrate the core insulation (inner Teflon tape, outer Latex double sleeve). From literature it is clear that Latex is not strictly gas-tight and it may be envisaged that Ar/Kr dissolves into Latex at the outer interface, permeates across the latex membrane, and exsolves again and migrates towards the low-pressure outflow. The sleeve appears to become much gas tight with time, because gas outflow is observed to rapidly decrease with time. The interaction of noble gases with the porewater chemistry is expected to be negligible. There is no indication from the isotopic composition that confining water did also penetrate into the sample core.
- At later infiltration stages, but still before APW breakthrough, gas exfiltration decreases and N_2 dominates the gas composition. These very small amounts of N_2 are inferred to originate from the initial porewater present in the sample cores.

Approaching APW breakthrough, the low density (relative to air) of the minor volumes of exfiltrating gas indicates the expected presence of He, which is used to pressurise the infiltrating APW and dissolves therein in the infiltration tank at approximately 47 bar infiltration pressure. The pore pressure in the core decreases from 47 bar at the bottom to 1 bar at the top, where the degassing He is caught in the sampling syringe. Some He may also get trapped in the pore space of the core samples. This effect is expected to be small, because the total weight of the cores increases during the experiment (Tab. 4.7-4).

Tab. 4.7-2: Conditions of advective displacement experiments

Parameter	**BOZ1-1**	**BOZ1-2**	**BOZ1-3**
Depth [m]	469.40	513.25	516.72
Geol. unit	Hauptrogenstein	Passwang Fm.	Passwang Fm.
Drilled	23.05.2020	30.06.2020	30.06.2020
Delivered	29.06.2020	06.07.2020	06.07.2020
Prep_AD	02.07.2020	09.07.2020	10.08.2020
Injection	03.07.2020	AD experiment failed	11.08.2020
First drop	06.07.2020		23.08.2020
Days to first drop	2.6		11.8
Initial gas [mL]	10.0		0.1
End_AD	15.10.2020		19.01.2021
Duration [d]	103.8		160.7
Pore-volumes	0.6		0.7
EC_initial (22 °C) [mS/cm]	19.2		16.3
Filter	PEEK	PEEK	PEEK
AD-samples	9		13
AD-samp_chem	7		13
AD-samp_isotopes	7		13
in-line pH	4		7
P_Conf [bar]	59		58
P_Inf [bar]	48		47
Gradient [mH_2O/m]	5'470		5'485

Tab. 4.7-2: (continued)

Parameter	**BOZ1-4**	**BOZ1-5**	**BOZ1-6**
Depth [m]	575.26	665.40	697.51
Geol. unit	Opalinus Clay	Staffelegg Fm.	Klettgau Fm.
Drilled	22.07.2020	27.07.2020	01.09.2020
Delivered	27.07.2020	03.08.2020	07.09.2020
Prep_AD	10.08.2020	18.08.2020	15.10.2020
Injection	11.08.2020	19.08.2020	16.10.2020
First drop	19.08.2020	24.08.2020	25.10.2020
Days to first drop	8.3	4.9	8.8
Initial gas [mL]	3.2	3.4	2.7
End_AD	19.01.2021	15.10.2020	19.01.2021
Duration [d]	160.7	56.8	94.7
Pore-volumes	0.8	0.4	0.5
EC_initial (22 °C) [mS/cm]	13.5	11.7	14.3
Filter	PEEK	PEEK	PEEK
AD-samples	13	6	10
AD-samp_chem	11	6	9
AD-samp_isotopes	11	6	9
in-line pH	7	4	6
P_Conf [bar]	59	60	59
P_Inf [bar]	47	47	47
Gradient [mH_2O/m]	5'534	5'348	5'309

4.7.3 Mineralogy and petrophysical properties

For each core, the mineralogy was determined on the sum of subsamples cut adjacent to the core segment used for the AD experiments (Tab. 4.7-1). Results are summarised in Tab. 4.7-3 and plotted in Section 4.2. Samples cover a range of clay-mineral contents of 25 – 51 wt.-%, calcite contents of 0 – 65 wt.-%, and quartz contents of 6 – 47 wt.-%. Most samples contain pyrite, between 0.4 and 1.2 wt.-%, only in BOZ1-6 no pyrite was detected (Klettgau Formation). Of the clays, the dominant minerals are illite (8 – 23 wt.-%), illite/smectite mixed layers (5 – 18 wt.-%), and kaolinite (0 – 10.6 wt.-%). The ratio of (illite/smectite+smectite)/(total_clay) is rather uniform in the samples from the Passwang to Klettgau Formations in the range of 0.35 – 0.48, but 0.2 for the sample from the Hauptrogenstein.

Carbon, sulphur and nitrogen analyses are also included. Pyrite contents are moderately low, because pyrite-rich lithologies were avoided based on X-ray CT characterisation (Fig. 4.7-2). More details, including end-member clays, are included in Appendix A.

The calculation of the initial corrected water content is based on the assumption, that the desaturation of the sample material from the pre analysis is the same as determined for the post-mortem core. The saturation state of the core is calculated based on the post-mortem water content

and the initial and final core volume and mass. Thus, water related to the regularly observed slight core expansion was explicitly taken into account. The core volume increases by 0.1 – 1.1% (Tab. 4.7-4) during AD experiments, accompanied by a water uptake of 3.2 – 5.7 g. Accounting for volume expansion, there remains a small water uptake that must reflect an initially small volume of unsaturated porosity, ranging from 0.8 to 2.7 ml, or a saturation ratio in the range of 0.93 – 0.99. Therefore, the initial state is essentially saturated for all samples within measurement uncertainty.

Tab. 4.7-3: Mineralogy of advective displacement samples, including C, S and N analyses

Average values of subsamples (see text).

Parameter	**Unit**	**BOZ1-1**	**BOZ1-2**	**BOZ1-3**
Depth	[m]	469.40	513.25	516.72
Geol. unit		Hauptrogenstein	Passwang Fm.	Passwang Fm.
S	[wt.-%]	0.3	0.5	0.6
C(inorg)	[wt.-%]	6.8	1.2	3.1
C(org)	[wt.-%]	0.6	0.7	0.8
N	[wt.-%]	b.d.	0.05	0.05
Quartz	[wt.-%]	6	29	26
K-feldspar	[wt.-%]	3	5	5
Plagioclase	[wt.-%]	b.d.	3	2
Calcite	[wt.-%]	65	10	26
Dolomite / Ankerite	[wt.-%]	b.d.	b.d.	b.d.
Siderite	[wt.-%]	b.d.	b.d.	b.d.
Anhydrite	[wt.-%]	b.d.	b.d.	b.d.
Celestite	[wt.-%]	b.d.	b.d.	b.d.
Pyrite	[wt.-%]	0.6	0.9	1.2
Clay minerals	**[wt.-%]**	**25**	**51**	**38**
Illite	[wt.-%]	11	17	14
Illite/smectite ML (85-90)	[wt.-%]	2	10	9
Illite/smectite ML (75-80)	[wt.-%]	2	8	5
Illite/smectite ML (50-70)	[wt.-%]	1	b.d.	2
Illite/smectite ML (20-40)	[wt.-%]	0.2	b.d.	1.0
Smectite	[wt.-%]	b.d.	b.d.	0.4
Kaolinite	[wt.-%]	4.9	8.7	2.3
Chlorite	[wt.-%]	1.2	2.6	1.9
Chl/Sm ML (85-95)	[wt.-%]	1.2	2.6	1.9
Total illite/smectite	[wt.-%]	**5**	**18**	**18**
(tot_ill/sm+sm)/(total_clay)		0.20	0.35	0.48
(tot_ill+ill/sm+sm)/(total_clay)		0.63	0.69	0.85

b.d.: below detection

Tab. 4.7-3: (continued)

Average values of subsamples (see text).

Parameter	**Unit**	**BOZ1-4**	**BOZ1-5**	**BOZ1-6**
Depth	[m]	575.26	665.40	697.51
Geol. unit		Opalinus Clay	Staffelegg Fm.	Klettgau Fm.
S	[wt.-%]	0.2	0.3	b.d.
C(inorg)	[wt.-%]	1.6	1.7	3.6
C(org)	[wt.-%]	0.7	0.5	0.1
N	[wt.-%]	0.07	b.d.	0.04
Quartz	[wt.-%]	30	47	10
K-feldspar	[wt.-%]	5	5	7
Plagioclase	[wt.-%]	4	3	5
Calcite	[wt.-%]	12	7	b.d.
Dolomite / Ankerite	[wt.-%]	b.d.	8	39
Siderite	[wt.-%]	4	b.d.	b.d.
Anhydrite	[wt.-%]	b.d.	b.d.	b.d.
Celestite	[wt.-%]	b.d.	b.d.	b.d.
Pyrite	[wt.-%]	0.4	0.5	b.d.
Clay minerals	**[wt.-%]**	**45**	**30**	**39**
Illite	[wt.-%]	13	8	23
Illite/smectite ML (85-90)	[wt.-%]	9	5	b.d.
Illite/smectite ML (75-80)	[wt.-%]	7	9	13
Illite/smectite ML (50-70)	[wt.-%]	b.d.	b.d.	1
Illite/smectite ML (20-40)	[wt.-%]	b.d.	b.d.	b.d.
Smectite	[wt.-%]	b.d.	b.d.	b.d.
Kaolinite	[wt.-%]	10.6	5.5	b.d.
Chlorite	[wt.-%]	2.3	1.0	b.d.
Chl/Sm ML (85-95)	[wt.-%]	2.3	1.0	b.d.
Total illite/smectite	[wt.-%]	**16**	**14**	**14**
(tot_ill/sm+sm)/(total_clay)		0.35	0.48	0.37
(tot_ill+ill/sm+sm)/(total_clay)		0.65	0.77	0.95

b.d.: below detection

A plethora of petrophysical parameters can be derived from sample dimensions, mass, water content, and changes in these parameters determined before and after an AD experiment (Tab. 4.7-4). These quantities include porosity, bulk density, grain density, water uptake during the experiments, and unsaturated porosity (saturation ratio). The relationships are given in Waber (ed.) (2020). Note that the water content determined for pre-characterisation is based on 2 sub-samples adjacent to the AD core segment.

Tab. 4.7-4: Core dimensions and derived petrophysical parameters

Parameter	**Unit**	**BOZ1-1**	**BOZ1-2**	**BOZ1-3**	**BOZ1-4**	**BOZ1-5**	**BOZ1-6**
Depth	[m]	469.40	513.25	516.72	575.26	665.40	697.51
Geol. unit		Hauptrogenstein	Passwang Fm.	Passwang Fm.	Opalinus Clay	Staffelegg Fm.	Klettgau Fm.
Pre_Core_M	**[g]**	**1'112.71**	**1'057.86**	**1'069.99**	**1'076.24**	**1'119.07**	**1'116.55**
Pre_Core_DM	[cm]	8.02	8.01	8.01	8.01	8.02	8.02
Pre_Core_L	[cm]	8.55	8.45	8.52	8.49	8.70	8.83
Pre_Core_A	[cm^2]	50.50	50.38	50.38	50.44	50.55	50.50
Pre_Core_V	[cm^3]	431.79	425.67	429.39	427.97	439.90	445.74
Post_Core_M	**[g]**	**1'117.29**	**n.m.**	**1'075.71**	**1'080.45**	**1'122.28**	**1'121.71**
Post_Core_DM	[cm]	8.03	n.m.	8.03	8.02	8.02	8.04
Post_Core_L	[cm]	8.59	n.m.	8.58	8.52	8.71	8.86
Post_Core_A	[cm^2]	50.59		50.61	50.49	50.55	50.75
Post_Core_V	[cm^3]	434.60		434.28	430.20	440.37	449.62
Delta_M	**[g]**	**4.58**		**5.72**	**4.21**	**3.21**	**5.16**
Delta_Core_DM	[cm]	0.007		0.018	0.004	0.000	0.020
Delta_Core_L	[cm]	0.041		0.058	0.035	0.009	0.033
Delta_Core_A	[cm^2]	0.085		0.233	0.054	0.003	0.249
Delta_Core_V	[cm^3]	**2.814**		**4.896**	**2.234**	**0.470**	**3.886**
Delta_Core_V-%	[%]	0.652		1.140	0.522	0.107	0.872
Pre_Bulk_WD	**[g/cm^3]**	**2.577**	**2.485**	**2.492**	**2.515**	**2.544**	**2.505**
Post_Bulk_WD	**[g/cm^3]**	**2.571**		**2.477**	**2.511**	**2.549**	**2.495**
Delta_Bulk_WD	[g/cm^3]	-0.006		-0.015	-0.003	0.005	-0.010
Delta_Bulk_WD-%	[%]	-0.239		-0.599	-0.130	0.180	-0.406
Pre_GD	**[g/cm^3]**	**2.716**	**2.721**	**2.715**	**2.703**	**2.700**	**2.785**
Post_GD	**[g/cm^3]**	**2.724**		**2.726**	**2.717**	**2.709**	**2.804**
Delta_GD	[g/cm^3]	0.009		0.011	0.014	0.009	0.018
Corr_Pre_GD	**[g/cm^3]**	**2.712**		**2.720**	**2.703**	**2.690**	**2.794**

_L: length; _A: area; _V: volume; _M: mass; WD: wet density; GD: grain density; n.m.: not measured

Tab. 4.7-4: (continued)

Parameter	**Unit**	**BOZ1-1**	**BOZ1-2**	**BOZ1-3**	**BOZ1-4**	**BOZ1-5**	**BOZ1-6**
Depth	[m]	469.40	513.25	516.72	575.26	665.40	697.51
Geol. unit		Hauptrogenstein	Passwang Fm.	Passwang Fm.	Opalinus Clay	Staffelegg Fm.	Klettgau Fm.
Pre_WCw		**0.0313**	**0.0552**	**0.0523**	**0.0440**	**0.0361**	**0.0627**
Post_WCw		**0.0346**		**0.0583**	**0.0477**	**0.0368**	**0.0686**
Delta_WCw		0.0033		0.0061	0.0036	0.0007	0.0060
Corr_Pre_WCw		**0.0306**		**0.0533**	**0.0439**	**0.0340**	**0.0643**
Pre_H2O_Core	**[g]**	**34.87**	**58.41**	**55.91**	**47.39**	**40.37**	**69.96**
Post_H2O_Core	**[g]**	**38.65**		**62.73**	**51.49**	**41.28**	**76.98**
Delta_H2O_Core	[g]	3.78		6.82	4.10	0.91	7.02
Corr_Pre_H2O_Core	**[g] or [mL]**	**34.07**		**57.01**	**47.28**	**38.07**	**71.82**
Unsat_Vol	[g] or [mL]	1.76		0.82	1.98	2.74	1.27
Pore_Vol_tot	[mL]	35.83		57.84	49.26	40.81	73.09
Sat_ratio		**0.95**		**0.99**	**0.96**	**0.93**	**0.98**
Pre_Poro_WL		**0.0808**	**0.1372**	**0.1302**	**0.1107**	**0.0918**	**0.1569**
Post_Poro_WL		**0.0889**		**0.1445**	**0.1197**	**0.0937**	**0.1712**
Delta_Poro_WL		0.0082		0.0142	0.0090	0.0020	0.0143
Delta_Poro_WL-%	[%]	10.12		10.93	8.09	2.14	9.09
Corr_Pre_Poro_WL		**0.0789**		**0.1328**	**0.1105**	**0.0865**	**0.1611**
Corr_Pre_Poro_tot		**0.0830**		**0.1347**	**0.1151**	**0.0928**	**0.1640**
Delta_Corr_Poro_WL-%		-2.29		1.97	-0.23	-5.71	2.66

WCw: water content rel. to wet mass; _WL: water loss

There are significant differences in water content measured in adjacent samples (pre-characterisation) and in the core itself (post-mortem) of 3 – 10% (solid and dashed line in Fig. 4.7-3), which are reduced to a much lower range of 2 – 6% if accounting for core expansion (solid and dotted line in Fig. 4.7-3). This leads to small differences in the bulk wet density, the water-loss porosity and the grain density (assuming saturated conditions) derived from pre-characterisation and post-mortem data.

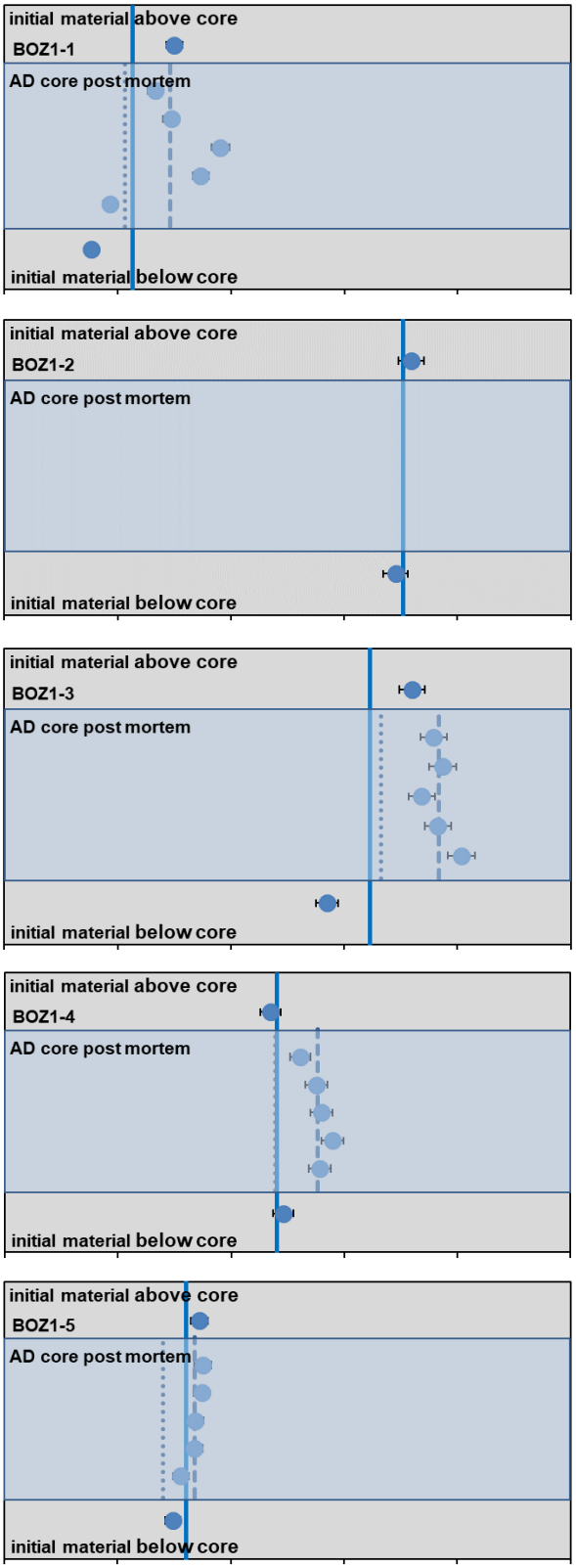

(see opposite site)

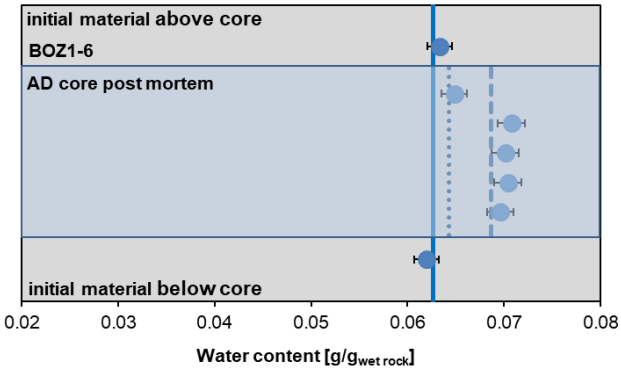

Fig. 4.7-3: Details of water content measurements before and after AD experiments

BOZ1-1 = BOZ1-1-469.40-AD (Hauptrogenstein); BOZ1-2 = BOZ1-1-513.25-AD (Passwang Fm.); BOZ1-3 = BOZ1-1-516.72-AD (Passwang Fm.); BOZ1-4 = BOZ1-1-575.26-AD (Opalinus Clay); BOZ1-5 = BOZ1-1-665.40-AD (Staffelegg Fm.); BOZ1-6 = BOZ1-1-697.51-AD (Klettgau Fm.). Vertical lines indicate the average for pre-characterisation (solid line), average of post-mortem characterisation (dashed line) and the calculated corrrected initial water content (dotted line). Error bars refer to measurement uncertainty of 2%.

4.7.4 Aqueous extracts, CEC and cation selectivity of AD samples

Aqueous extracts, CEC and cation selectivity determinations were carried out within the pre-characterisation and post-mortem analysis (except BOZ1-2: experiment failed - no post-mortem analysis). Detailed analyses are provided in Appendix B. Methods are the same as used for other core samples (Waber (ed.) 2020), with the exception of sample masses for water content that may have been smaller than used for regular core sample analysis. Averaged data – also used for integrative data plots – are presented in this section. Averaging refers to aqueous extraction measurements of pieces above and below the segment used for the AD experiments (indicated in Fig. 4.7-2 and Tab. 4.7-5). For CEC/ cation selectivity, the pieces were combined in equal proportions and analysed as one sample.

All averaged aqueous extract solutions (Tab. 4.7-5) from pre-characterisation processed at S/L ≈ 1 contain low concentrations of NH_4 (up to 3.2 mg/L) and NO_3 (0.74 – 1.65 mg/L). Iodide content was analysed in one sample, but not detected. The factor (1/WCw·L/Sw) refers to the scaling factor required to scale aqueous concentrations for conservative components to porewater concentrations (i.e. at water content). Characteristic molar ion ratios (Tab. 4.7-6) do not follow a systematic trend with depth, except for the Br/Cl ratio, which decreases with depth. The Cl and Br concentrations above and below the segment used for the AD experiment vary within the analytical uncertainty.

Tab. 4.7-5: Composition of aqueous extract solutions from pre-characterisation

Parameter	**Unit**	**BOZ1-1**	**BOZ1-2**	**BOZ1-3**
Depth	[m]	469.40	513.25	516.72
Geol. unit		Hauptrogenstein	Passwang Fm.	Passwang Fm.
averaging		top+base (1+1)	top+base (1+1)	top+base (1+1)
$1/WC_w*L/S_w$		33.59	19.10	20.58
Rock wet	[g]	29.92	30.19	29.87
Water	[g]	30.16	30.16	30.40
WC_w	[g/g_{wet}]	0.031	0.055	0.052
S/L (S_d/(L+PW))		0.932	0.896	0.886
pH at Titration		9.01	9.24	9.29
Na	[mg/L]	210	199	196
NH_4	[mg/L]	2.69	2.78	3.22
K	[mg/L]	9.34	6.03	6.91
Ca	[mg/L]	4.90	3.68	2.06
Mg	[mg/L]	1.155	0.588	0.446
Sr (OES)	[mg/L]	0.119	0.066	0.059
Ba (OES)	[mg/L]	< 0.025	< 0.025	< 0.025
F	[mg/L]	5.19	5.82	4.27
Cl	[mg/L]	51	59	52
Br	[mg/L]	0.24	0.23	0.18
NO_3	[mg/L]	0.91	1.65	1.04
SO_4	[mg/L]	241	201	230
I	[mg/L]	< 0.4	n.a.	n.a.
Alk (tit)	[meq/L]	2.97	2.92	2.58
Alk as HCO_3	[mg/L]	181.0	178.2	157.5
TOC	[mg/L]	10.05	11.15	11.25
TIC	[mg/L]	31.8	32.3	30.6
lactate	[mg/L]	< 2	< 2	< 2
acetate	[mg/L]	3.65	3.14	3.10
propionate	[mg/L]	< 2	< 2	< 2
formate	[mg/L]	< 2	< 2	< 2

n.a.: not analysed

Tab. 4.7-5: (continued)

Parameter	**unit**	**BOZ1-4**	**BOZ1-5**	**BOZ1-6**
Depth	[m]	575.26	665.40	697.51
Geol. unit		Opalinus Clay	Staffelegg Fm.	Klettgau Fm.
averaging		top+base (1+1)	top+base (1+1)	top+base (1+1)
$1/WC_w*L/S_w$		23.82	28.90	17.20
Rock wet	[g]	30.26	30.04	30.08
Water	[g]	30.40	30.21	30.52
WC_w	[g/g_{wet}]	0.044	0.036	0.063
$S/L (S_d/(L+PW))$		0.912	0.925	0.870
pH at Titration		8.66	9.30	9.10
Na	[mg/L]	237	197	279
NH_4	[mg/L]	1.87	1.78	2.29
K	[mg/L]	6.81	6.71	8.61
Ca	[mg/L]	2.61	2.14	3.73
Mg	[mg/L]	0.532	0.459	1.007
Sr (OES)	[mg/L]	0.080	0.066	0.069
Ba (OES)	[mg/L]	< 0.025	0.025	< 0.025
F	[mg/L]	2.67	4.03	4.71
Cl	[mg/L]	59	39	15
Br	[mg/L]	0.20	0.11	< 0.16
NO_3	[mg/L]	0.74	1.17	0.67
SO_4	[mg/L]	202	217	394
I	[mg/L]	n.a.	n.a.	n.a.
Alk (tit)	[meq/L]	4.58	3.00	4.06
Alk as HCO_3	[mg/L]	279.5	166.3	224.0
TOC	[mg/L]	16.50	7.05	9.30
TIC	[mg/L]	54.2	32.7	44.1
lactate	[mg/L]	< 2	< 2	< 20
acetate	[mg/L]	3.44	2.93	< 20
propionate	[mg/L]	< 2	< 2	< 20
formate	[mg/L]	< 2	< 2	< 20

n.a.: not analysed

Tab. 4.7-6: Cation ratios and details of carbon system in aqueous extract solutions from pre-characterisation

Parameter	**Unit**	**BOZ1-1**	**BOZ1-2**	**BOZ1-3**	**BOZ1-4**	**BOZ1-5**	**BOZ1-6**
Depth	[m]	469.40	513.25	516.72	575.26	665.40	697.51
Geol. unit		Hauptrogenstein	Passwang Fm.	Passwang Fm.	Opalinus Clay	Staffelegg Fm.	Klettgau Fm.
Br/Cl*1000	[mol/mol]	2.10	1.72	1.49	1.50	1.24	Br < 0.16
SO_4/Cl	[mol/mol]	1.75	1.25	1.63	1.26	2.03	9.83
Ca/Mg	[mol/mol]	2.57	3.79	2.80	2.97	2.83	2.24
Ca/Sr	[mol/mol]	90	123	76	71	71	118
(Ca+Mg)/(Na+K)	[eq/eq]	0.026	0.021	0.012	0.012	0.012	0.015
Alk (tit)	[meq/L]	2.97	2.92	2.58	4.58	3.00	4.06
TIC	[meq/L]	2.65	2.69	2.55	4.51	2.72	3.67
acetate	[meq/L]	0.062	0.053	0.053	0.058	0.050	< 0.3
TOC	[mg/L]	10.1	11.2	11.3	16.5	7.1	9.3
acetate (as C)	[mg/L]	1.48	1.28	1.26	1.40	1.19	< 8.14

Tab. 4.7-7 shows that the aqueous extract solutions are at or exceed calcite saturation and are oversaturated with respect to dolomite except for sample BOZ1-4 which is just below calcite saturation and far from dolomite saturation. Extracts are distinctly undersaturated with respect to sulphates and strontianite. TIC was used as input for the carbon system, because the titrated alkalinity would also include acetate. However, the calculated alkalinity agrees well with the measured one due to low acetate concentrations in this borehole.

Tab. 4.7-7: Saturation indices calculated for aqueous extract solutions from pre-characterisation

Parameter	**unit**	**BOZ1-1**	**BOZ1-2**	**BOZ1-3**	**BOZ1-4**	**BOZ1-5**	**BOZ1-6**
Depth	[m]	469.40	513.25	516.72	575.26	665.40	697.51
Geol. unit		Hauptrogen-stein	Passwang Fm.	Passwang Fm.	Opalinus Clay	Staffelegg Fm.	Klettgau Fm.
Charge	[eq/kg_w]	2.2E-04	-7.3E-05	-4.7E-04	6.2E-05	-5.4E-06	-2.0E-04
%-Error		1.14	-0.40	-2.60	0.29	-0.03	-0.80
Acetate	[eq/kg_w]	6.2E-05	5.3E-05	5.3E-05	5.8E-05	5.0E-05	<3.0E-04
Ionic strength	[mol/kg_w]	1.22E-02	1.14E-02	1.17E-02	1.28E-02	1.13E-02	1.68E-02
tot_alk	[eq/kg]	2.90E-03	3.09E-03	3.00E-03	4.68E-03	3.14E-03	4.07E-03
pH		9.01	9.24	9.29	8.66	9.30	9.10
log$P(CO_2)$	[bar]	-3.85	-4.09	-4.17	-3.25	-4.15	-3.82
SI(calcite)		0.27	0.35	0.11	-0.10	0.16	0.29
SI(dolomite)		0.26	0.27	-0.08	-0.54	0.02	0.36
SI(gypsum)		-2.46	-2.67	-2.87	-2.81	-2.88	-2.47
SI(celestite)		-2.34	-2.66	-2.67	-2.59	-2.64	-2.46
SI(strontianite)		-0.87	-0.90	-0.94	-1.14	-0.85	-0.96
SI(anhydrite)		-2.69	-2.89	-3.10	-3.03	-3.11	-2.70

Nagra PSI 2012 thermodynamic data base, calculated in PHREEQC for 25 °C, using ordered dolomite; kgw = kg water; charge = Σ(cation charge) - ıΣ(anion charge)ı ; %-error = 100*charge / (Σ(cation charge) + ıΣ(anion charge)ı).

Aqueous extracts of all cores were also produced after termination of the experiments. A thin disc (10 – 21 mm) from the top and base of each core was processed according to the protocols used for pre-characterisation. In BOZ1-1 and BOZ1-4 profiles of 3 and 5 samples, respectively, were processed. The base of the core represents the inlet of the artificial porewater, whereas the top represents the outflow to sampling. The two may yield different results depending on the overall progress of fluid percolation (different concentrations in inlet sample compared to outlet), and averaging is therefore meaningless.

Results (Tab. 4.7-8) show that Br (not present in the APW) was effectively flushed out of each core in all inlets and most of the outlets, whereas other minor anionic components were buffered to some extent (e.g., F, NO_3). The Br bulk porewater concentration profile in BOZ1-4 illustrates a smooth trend from 0.9 mg/L at the outlet to concentrations below the detectiom limit at the inlet (Tab. 4.7-8 and Fig. 4.7-17).

The Cl concentrations scaled to bulk porewater in the post-mortem aqueous extracts increase from top to bottom (or remain constant in BOZ1-3) as expected from the higher Cl concentration in the APW. The Cl profile measured in BOZ1-4 shows a smoth increase also when scaled up to bulk porewater concentrations (Tab. 4.7-8 and Fig. 4.7-17).

The initially observed acetate and TOC were partially or completely flushed out except for BOZ1-1 and BOZ1-5 where TOC concentrations increased. The cation concentrations increased in general and need to be interpreted in more detail considering ion-exchange processes. The Sr concentrations decreased, except in BOZ1-1. A more in-depth analysis will be required to reconcile differences between extracts from pre-characterisation and post-mortem analysis.

Calculation of speciation and saturation indices (Tab. 4.7-9) of the aqueous extract solutions from Tab. 4.7-8 are close to calcite saturation, mostly below dolomite saturation except for BOZ1-6 and the top of BOZ1-1 which are saturated with respect to dolomite, and BOZ1-4 which is distinctly undersaturated with respect to calcite and dolomite. All extracts are distinctly undersaturated with respect to sulphates and strontianite. TIC was used as input for the carbon system.

Cation exchange capacities and cation selectivities determined by the Ni-en method (Waber (ed.) 2020) were performed on one precombined sample from the two samples used for aqueous extracts. The results are also presented and interpreted in Section 4.5. Tab. 4.7-10 shows uncorrected (for porewater contribution and mineral dissolution/precipitation) capacities of 61 – 154 meq/kg (dry rock) with errors of up to ~ ± 6%. Ni consumptions is up to 8% higher than the sum of cations, whereas for the BOZ1-1 and BOZ1-4 samples Ni consumption was slightly lower. Ammonium was not measured but is expected to be present on the exchanger judged by the presence of up to 3 mg/L of NH4 in the aqueous extracts performed at the same S/L ratio (Tab. 4.7-5).

The low or non-detectable Br concentrations agree well with the concentrations in aqueous extracts. Interestingly, the SO_4/Cl ratios are significantly and systematically lower in the Ni-en solutions compared to the aqueous extracts, suggesting that there is either a sulphate source in the aqueous extracts, which does not dissolve in the Ni-en solutions, or a sink in the Ni-en solutions (complexation).

The cation occupancies (selectivities) derived from Ni-en extracts and applying a correction for the porewater contribution are presented in Section 4.5.

Tab. 4.7-8: Composition of aqueous extract solutions from post-mortem characterisation

Parameter	**Unit**	**BOZ1-1**			**BOZ1-3**	
Depth	[m]	469.40			516.72	
Geol. unit		Hauptrogenstein Fm.			Passwang Fm.	
Averaging		top post-mortem	mid post-mortem	base post-mortem	top post-mortem	base post-mortem
$1/WC_w*L/S_w$		30.78	26.92	34.86	18.42	17.80
Rock wet	[g]	30.69	30.07	30.56	30.25	30.22
Water	[g]	30.44	30.44	30.31	30.51	30.63
WC_w	[g/g_{wet}]	0.033	0.039	0.029	0.058	0.060
S/L (S_d/(L+PW))		0.943	0.914	0.951	0.883	0.875
pH at Titration		9.00	8.69	8.53	9.48	9.21
Na	[mg/L]	226	233	233	237	228
NH_4	[mg/L]	3.26	2.81	2.94	3.16	2.19
K	[mg/L]	14.30	12.00	14.20	6.67	5.96
Ca	[mg/L]	6.85	5.93	6.98	2.58	2.25
Mg	[mg/L]	1.520	1.460	1.740	0.590	0.558
Sr (OES)	[mg/L]	0.177	0.157	0.177	<0.025	<0.025
Ba (OES)	[mg/L]	<0.025	<0.025	<0.025	<0.025	<0.025
F	[mg/L]	4.72	5.54	4.62	3.89	3.61
Cl	[mg/L]	73	82	79	131	132
Br	[mg/L]	<0.16	<0.16	<0.16	0.04	<0.016
NO_3	[mg/L]	45.70	65.70	41.50	3.84	0.85
SO_4	[mg/L]	234	237	244	242	201
Alk (tit)	[meq/L]	2.76	2.64	2.72	1.91	2.26
Alk as HCO_3	[mg/L]	146.0	148.7	156.6	116.5	137.9
TOC	[mg/L]	21.80	16.40	15.40	5.52	<5
TIC	[mg/L]	28.7	29.3	30.8	20.6	26.1
lactate	[mg/L]	<20	<20	<20	0.520	0.330
acetate	[mg/L]	<20	<20	<20	1.79	0.62
propionate	[mg/L]	<20	<20	<20	<0.2	<0.2
formate	[mg/L]	<20	<20	<20	0.350	<0.2

Tab. 4.7-8: (continued)

Parameter	**Unit**	**BOZ1-4**					**BOZ1-5**		**BOZ1-6**	
Depth	[m]	575.26					665.40		697.51	
Geol. unit		Opalinus Clay					Staffelegg Fm.		Klettgau Fm.	
Averaging		top post-mortem	mid1 post-mortem	mid2 post-mortem	mid3 post-mortem	base post-mortem	top post-mortem	base post-mortem	top post-mortem	base post-mortem
$1/WC_w*L/S_w$		22.72	22.31	22.00	21.35	21.77	28.02	28.85	16.39	15.40
Rock wet	[g]	30.59	30.12	30.21	30.53	30.49	30.07	30.73	30.07	30.34
Water	[g]	30.63	30.50	30.45	30.41	30.29	30.51	30.48	30.01	30.41
WCw	[g/gwet]	0.046	0.048	0.048	0.049	0.048	0.038	0.036	0.065	0.070
S/L (S_d/(L+PW))		0.911	0.898	0.902	0.910	0.914	0.915	0.939	0.880	0.868
pH at Titration		8.54	8.61	8.61	8.45	8.74	9.16	8.94	9.01	8.76
Na	[mg/L]	254	258	262	266	266	211	215	338	327
NH4	[mg/L]	1.91	1.41	1.41	1.48	1.30	2.35	2.23	2.69	2.10
K	[mg/L]	6.48	6.31	6.49	6.63	6.45	7.70	7.83	11.50	10.70
Ca	[mg/L]	2.99	2.82	2.90	2.94	3.04	2.33	2.52	4.91	4.38
Mg	[mg/L]	0.641	0.603	0.624	0.664	0.722	0.538	0.610	1.370	1.290
Sr (OES)	[mg/L]	< 0.025	< 0.025	< 0.025	< 0.025	< 0.025	0.063	0.067	< 0.025	< 0.025
Ba (OES)	[mg/L]	< 0.025	< 0.025	< 0.025	< 0.025	< 0.025	< 0.025	< 0.025	< 0.025	< 0.025
F	[mg/L]	2.38	2.49	2.39	2.48	2.45	4.04	3.59	4.51	3.99
Cl	[mg/L]	111	110	118	122	136	80	119	126	162
Br	[mg/L]	0.04	0.04	0.03	0.02	< 0.016	< 0.16	< 0.16	0.02	< 0.016
NO_3	[mg/L]	2.76	2.54	1.58	1.09	0.76	7.20	1.51	0.54	0.42
SO_4	[mg/L]	198	194	191	194	191	213	173	376	287
Alk (tit)	[meq/L]	3.50	4.11	4.09	3.97	4.08	2.68	2.66	4.04	3.86
Alk as HCO_3	[mg/L]	213.6	250.8	249.6	242.2	248.9	142.5	145.5	246.5	235.5
TOC	[mg/L]	8.27	7.59	< 5	6.58	< 5	11.40	10.60	< 5	< 5
TIC	[mg/L]	50.0	48.1	49.9	45.9	47.1	28.0	28.6	43.6	47.6
lactate	[mg/L]	< 0.2	< 0.2	< 0.2	< 0.2	1.130	< 20	< 20	< 0.2	0.360
acetate	[mg/L]	2.52	2.40	1.72	1.62	0.58	< 20	< 20	1.32	0.57
propionate	[mg/L]	< 0.2	< 0.2	< 0.2	< 0.2	< 0.2	< 20	< 20	< 0.2	< 0.2
formate	[mg/L]	0.310	0.290	0.280	0.270	0.210	< 20	< 20	< 0.2	< 0.2

Tab. 4.7-9: Saturation indices calculated for aqueous extract solutions obtained post-mortem

Parameter	**Unit**	**BOZ1-1**		
Depth	[m]	469.40		
Geol. unit		Hauptrogenstein		
Position		top post-mortem	mid post-mortem	base post-mortem
Charge	[eq/kg_w]	3.0E-04	-1.4E-04	2.9E-04
%-Error		1.42	-0.64	1.34
Acetate	[eq/kg_w]	< 3.0E-04	< 3.0E-04	< 3.0E-04
Ionic strength	[mol/kg_w]	1.31E-02	1.35E-02	1.35E-02
tot_alk	[eq/kg]	2.64E-03	2.56E-03	2.65E-03
pH		9.00	8.69	8.53
log$P(CO_2)$	[bar]	-3.89	-3.55	-3.37
SI(calcite)		0.36	0.02	-0.04
SI(dolomite)		0.41	-0.22	-0.34
SI(gypsum)		-2.34	-2.38	-2.30
SI(celestite)		-2.19	-2.24	-2.17
SI(strontianite)		-0.76	-1.09	-1.17
SI(anhydrite)		-2.56	-2.61	-2.52

b.d.: below detection; Nagra PSI 2012 thermodynamic data base, calculated in PHREEQC for 25 °C, using ordered dolomite; kgw = kg water; charge = Σ(cation charge) - ׀Σ(anion charge)׀ ; %-error = 100*charge / (Σ(cation charge) + ׀Σ(anion charge)׀).

Tab. 4.7-9: (continued)

Parameter	**Unit**	**BOZ1-3**	
Depth	[m]	516.72	
Geol. unit		Passwang Fm.	
Position		top post-mortem	base post-mortem
Charge	[eq/kg_w]	-3.5E-04	-2.4E-04
%-Error		-1.61	-1.19
Acetate	[eq/kg_w]	3.0E-05	1.1E-05
Ionic strength	[mol/kg_w]	1.35E-02	1.26E-02
tot_alk	[eq/kg]	2.18E-03	2.48E-03
pH		9.48	9.21
log$P(CO_2)$	[bar]	-4.57	-4.16
SI(calcite)		0.19	0.03
SI(dolomite)		0.09	-0.19
SI(gypsum)		-2.77	-2.88
SI(celestite)		-5.44	-5.49
SI(strontianite)		-3.74	-3.84
SI(anhydrite)		-3.00	-3.10

Sr in BOZ1-3 is below detection limit, values based on arbitrary Sr concentration of 0.0001; b.d.: below detection; Nagra PSI 2012 thermodynamic data base, calculated in PHREEQC for 25 °C, using ordered dolomite; kgw = kg water; charge = Σ(cation charge) - ׀Σ(anion charge)׀ ; %-error = 100*charge / (Σ(cation charge) + ׀Σ(anion charge)׀).

Tab. 4.7-9: (continued)

Parameter	**unit**	**BOZ1-4**				
Depth	[m]	575.26				
Geol. unit		Opalinus Clay				
Position		top post-mortem	mid1 post-mortem	mid2 post-mortem	mid3 post-mortem	base post-mortem
Charge	[eq/kg_w]	-1.7E-04	2.1E-04	9.9E-05	5.0E-04	-2.8E-05
%-Error		-0.74	0.93	0.42	2.16	-0.12
Acetate	[eq/kg_w]	4.3E-05	4.1E-05	2.9E-05	2.7E-05	9.8E-06
Ionic strength	[mol/kg_w]	1.36E-02	1.35E-02	1.37E-02	1.37E-02	1.40E-02
tot_alk	[eq/kg]	4.27E-03	4.13E-03	4.28E-03	3.89E-03	4.09E-03
pH		8.54	8.61	8.61	8.45	8.74
log$P(CO_2)$	[bar]	-3.17	-3.26	-3.24	-3.11	-3.40
SI(calcite)		-0.18	-0.16	-0.13	-0.31	-0.02
SI(dolomite)		-0.69	-0.64	-0.59	-0.93	-0.31
SI(gypsum)		-2.76	-2.79	-2.79	-2.77	-2.78
SI(celestite)		-5.51	-5.51	-5.52	-5.51	-5.53
SI(strontianite)		-4.20	-4.14	-4.13	-4.32	-4.03
SI(anhydrite)		-2.98	-3.01	-3.01	-2.99	-3.00

Sr in BOZ1-4 is below detection limit, values based on arbitrary Sr concentration of 0.0001; b.d.: below detection; Nagra PSI 2012 thermodynamic data base, calculated in PHREEQC for 25 °C, using ordered dolomite; kgw = kg water; charge = Σ(cation charge) - ǀΣ(anion charge)ǀ ; %-error = 100*charge / (Σ(cation charge) + ǀΣ(anion charge)ǀ).

Tab. 4.7-9: (continued)

Parameter	**unit**	**BOZ1-5**		**BOZ1-6**	
Depth	[m]	665.40		697.51	
Geol. unit		Staffelegg Fm.		Klettgau Fm.	
Position		top post-mortem	base post-mortem	top post-mortem	base post-mortem
Charge	[eq/kg_w]	2.0E-05	1.1E-04	-1.0E-04	1.1E-05
%-Error		0.11	0.58	-0.34	0.04
Acetate	[eq/kg_w]	< 3.0E-04	< 3.0E-04	2.2E-05	9.7E-06
Ionic strength	[mol/kg_w]	1.19E-02	1.16E-02	1.93E-02	1.78E-02
tot_alk	[eq/kg]	2.63E-03	2.57E-03	3.98E-03	4.17E-03
pH		9.16	8.94	9.01	8.76
log$P(CO_2)$	[bar]	-4.07	-3.82	-3.73	-3.42
SI(calcite)		0.03	-0.10	0.32	0.12
SI(dolomite)		-0.22	-0.47	0.44	0.05
SI(gypsum)		-2.83	-2.86	-2.38	-2.50
SI(celestite)		-2.66	-2.70	-5.34	-5.42
SI(strontianite)		-1.06	-1.20	-3.89	-4.05
SI(anhydrite)		-3.06	-3.08	-2.61	-2.73

Sr in BOZ1-6 is below detection limit, values based on arbitrary Sr concentration of 0.0001; b.d.: below detection; Nagra PSI 2012 thermodynamic data base, calculated in PHREEQC for 25 °C, using ordered dolomite; kgw = kg water; charge = Σ(cation charge) - ǀΣ(anion charge)ǀ ; %-error = 100*charge / (Σ(cation charge) + ǀΣ(anion charge)ǀ).

Tab. 4.7-10: Composition of Ni-en extract solutions and related parameters from pre-characterisation

Parameter	**Unit**	**BOZ1-1**	**BOZ1-2**	**BOZ1-3**	**BOZ1-4**	**BOZ1-5**	**BOZ1-6**
Depth	[m]	469.40	513.25	516.72	575.26	665.40	697.51
Geol. unit		Hauptrogenstein	Passwang Fm.	Passwang Fm.	Opalinus Clay	Staffelegg Fm.	Klettgau Fm.
Averaging		1 averaged sample	1 averaged sample	1 averaged sample	1 averaged sample	1 averaged sample	1 averaged sample
$1/WC_w*L/S_w$		33.09	18.77	21.31	25.07	30.53	18.24
Rock wet	[g]	29.82	30.62	30.24	30.27	29.81	29.83
Solution	[g]	29.98	30.05	32.10	32.08	31.76	32.21
WC_w	[g/g_{wet}]	0.03	0.06	0.05	0.04	0.04	0.06
S/L (S_d/(L+PW))		0.93	0.91	0.85	0.87	0.88	0.82
pH (initial)		8.27	8.27	8.27	8.27	8.27	8.24
Ni (initial)	[mg/L]	5'936	5'858	5'993	5'993	6'197	5'818
pH (final)		8.52	8.41	8.53	8.27	8.37	8.41
Na	[mg/L]	518	1'264	1'229	1'070	716	1'088
K	[mg/L]	143	210	283	174	156	252
Mg	[mg/L]	113	212	232	152	122	226
Ca	[mg/L]	420	901	984	656	435	730
Sr	[mg/L]	12.9	36.1	40.5	26.4	16.0	18.2
Ba	[mg/L]	0.089	0.188	0.156	0.628	0.652	0.266
Fe	[mg/L]	< 0.05	< 0.05	< 0.05	0.12	< 0.05	< 0.05
Ni	[mg/L]	4215	1870	1708	3027	3830	2106
F	[mg/L]	0.27	0.24	0.19	0.12	0.20	0.19
Cl	[mg/L]	50	64	50	53	36	14
Br	[mg/L]	< 0.16	0.18	0.22	0.17	< 0.16	< 0.16
NO_3	[mg/L]	13'312	12'648	12'328	12'865	13'025	12'881
SO_4	[mg/L]	183	135	154	120	137	240
TDS	[mg/L]	18'966	17'341	17'009	18'143	18'474	17'555

kg_d = kg dry rock

Tab. 4.7-10: (continued)

Parameter	**Unit**	**BOZ1-1**	**BOZ1-2**	**BOZ1-3**	**BOZ1-4**	**BOZ1-5**	**BOZ1-6**
Depth	[m]	469.40	513.25	516.72	575.26	665.40	697.51
Geol. unit		Hauptrogenstein	Passwang Fm.	Passwang Fm.	Opalinus Clay	Staffelegg Fm.	Klettgau Fm.
Averaging		1 averaged sample	1 averaged sample	1 averaged sample	1 averaged sample	1 averaged sample	1 averaged sample
charge %-error	[%]	-4.65	-5.38	-3.93	-2.80	-3.92	-8.15
Na	[meq/kg_d]	24.1	60.4	63.3	53.7	35.7	57.7
K	[meq/kg_d]	3.9	5.9	8.6	5.2	4.6	7.9
Mg	[meq/kg_d]	10.0	19.2	22.6	14.4	11.5	22.7
Ca	[meq/kg_d]	22.4	49.4	58.1	37.7	24.9	44.4
Sr	[meq/kg_d]	0.31	0.90	1.10	0.69	0.42	0.51
Ba	[meq/kg_d]	0.001	0.003	0.003	0.011	0.011	0.005
Fe	[meq/kg_d]	< 0.002	< 0.002	< 0.002	0.005	< 0.002	< 0.002
SumCat	[meq/kg_d]	60.7	135.8	153.7	111.7	77.0	133.2
SumCat_err	[meq/kg_d]	2.48	5.73	6.36	4.78	3.22	5.50
Ni_cons	[meq/kg_d]	56.2	137.4	160.7	107.3	84.2	141.0
Ni_cons_err	[meq/kg_d]	5.20	4.40	4.80	5.10	5.50	4.90
Br/Cl	[mol/mol*1000]	-	1.25	1.96	1.43	-	-
SO_4/Cl	[mol/mol]	1.36	0.78	1.14	0.84	1.41	6.47

kg_d = kg dry rock

4.7.5 Chemical and isotopic evolution of displaced porewater aliquots

An artificial porewater (APW) composition was injected to force advective displacement. The outflow of each experiment was continuously sampled in small syringes (Waber (ed.) 2020). These syringe aliquots were analysed for chemical and water isotopic composition. Hydraulic conductivity was evaluated for each sampled aliquot (Darcy's law), and any expelled gas was also recorded, although gas-tightness is commonly good, but cannot be ensured for a syringe sampling system. Most data for each experiment are included in tables and graphs in this section, and more details are provided in Appendix B.

According to the method of advective displacement (Mäder 2018), it is expected that the first few sampled aliquots are of similar composition and represent the displaced porewater from the sample core. After this, a gradual breakthrough of the injected APW should be observed, until full breakthrough of conservative components (e.g. Cl, Br), given enough time.

4.7.5.1 Artificial porewater used for advective displacement

In the absence of constraining data, an artificial porewater composition (Tab. 4.7-11) was chosen that was based on work performed for the deep geothermal well in Schlattingen (advective displacement experiments detailed in Mäder & Waber 2017). The composition was calculated with PHREEQC for 25 °C, to be saturated with respect to calcite and dolomite, and a partial pressure of CO_2 of $10^{-2.2}$ bar. This partial pressure was imposed by bubbling with an Ar/CO_2 gas mixture during mixing and again when the fluid reservoir was filled before the experiments started. A recipe with the appropriate amounts of PA-grade chemicals is given in Tab. 4.7-12.

Deuterium was added as a water tracer for advective-diffusive transport, aiming for a δ^2H of approximately +100 ‰ (VSMOW). There is no Br contained in the APW and therefore bromide-breakout can be used as an anionic tracer in the case of significant Br concentrations in the porewater. If the Cl concentration in the APW is significantly different from the displaced early aliquots, Cl breakthrough forms an additional anionic tracer for transport.

All five successful experiments were fed from PFA-coated fluid tanks containing the APW from the same batch 3. The pressurised head space of the tanks was filled with He after bubbling with the Ar/CO_2 gas mixture mentioned above. The composition of the APW is therefore identical for all experiments.

Tab. 4.7-11: Composition and recipe for the artificial porewater

Parameter	**Unit**	**Recipe**	**Calculated ***	**Measured**	**Compounds**
pH		7.19		7.38	
Na	[mg/L]	3'989	3'988	4'059	$NaCl$; $NaHCO_3$; Na_2SO_4
NH_4	[mg/L]			< 10	
K	[mg/L]	79.4	79.3	78.7	KCl
Ca	[mg/L]	503	504	506	$CaCl_2 \cdot 2H_2O$
Mg	[mg/L]	226	226	208	$MgCl_2 \cdot 6H2O$
Sr(OES)	[mg/L]			< 0.25	
Ba	[mg/L]			< 0.25	
Si	[mg/L]			< 2.5	
Al	[mg/L]			0.279	
F	[mg/L]			< 1.6	
Cl	[mg/L]	5'992	5'986	5'826	$CaCl_2 \cdot 2H_2O$; KCl; $MgCl_2 \cdot 6H_2O$
Br	[mg/L]			< 1.6	
NO_3	[mg/L]			5.25	
SO_4	[mg/L]	2305	2303	2132	Na_2SO_4
I	[mg/L]			n.m	
TOC	[mg/L]			7.4	
TIC	[mg/L]	29.3	29.32	28.0	$NaHCO_3$
lactate	[mg/L]			< 20	
acetate	[mg/L]			< 20	
propionate	[mg/L]			< 20	
formate	[mg/L]			< 20	
$\delta^{18}O$	[‰ VSMOW]		-11.43	-11.52	
$\delta^{2}H$	[‰ VSMOW]	100	91.9	90.8	D_2O

* calculated from the weighed-in chemical compounds; pH measured; CO_2-Ar bubbling not taken into account

Tab. 4.7-12: Recipe for the artificial porewater for a 2-litre batch

Parameter	**Unit**		**Recipe**		
Chemical	**Manufacturer**	**Grade**	[g/kg_w]	[$g/2kg_w$]	**weighed in** [g/2L]
$NaHCO_3$	Merck	p.a.	0.2051	0.4101	0.4102
$CaCl_2 \cdot 2H_2O$	Merck	p.a.	1.8465	3.6930	3.6944
KCl	Merck	p.a.	0.1514	0.3029	0.3026
$MgCl_2 \cdot 6H_2O$	Merck	p.a.	1.8907	3.7814	3.7827
$NaCl$	Merck	p.a.	7.1916	14.3831	14.3838
Na_2SO_4	AnalaR NORAMAPUR	Ph.Eur.	3.4089	6.8177	6.8114
D_2O (100 %)	Roth	> 99.8% D	0.0310	0.0620	0.0607

4.7.5.2 Physical conditions, hydraulic conductivity, sampling, and pore volume equivalents

All core samples were subjected to 57 – 61 bar hydraulic confining pressure, and an infiltration pressure of initially around 48 bar set by a He headspace. The infiltration pressure was gradually decreasing with time (displaced APW, and any small He leak), and was replenished repeatedly until the end of the experiments. The pressure range covered 44 – 49 bar.

Temperature conditions were stable without diurnal fluctuations, ranging seasonally from 21.5 to 25.5 °C. Critical temperature-sensitive measurements, such as electric conductivity, pH and hydraulic conductivity, were temperature-compensated, either intrinsically or explicitly (details in Waber (ed.) 2020).

Hydraulic conductivity referenced to 25 °C was evaluated for all sampled aliquots based on sample mass and Darcy's law (detailed data in Appendix B, method in Waber (ed.) 2020). Earliest aliquots commonly show low apparent hydraulic conductivities due to the expulsion of gas from the dead volume in the outflow, and any small unsaturated volume in the sample core itself. All cores (Fig. 4.7-4) share an increasing hydraulic conductivity, followed by a slight decrease to a steady-state value, if sufficient run-time was provided. The exceptionally low conductivity of BOZ1-1 at 0.55 pore volume is likely associated with the observed clogging of the filter due to extensive observed calcite precipitation. The values for the early conductivity and that measured towards the end of the experiments (Tab. 4.7-13) span a narrow range from $1.0\text{-}3.6 \cdot 10^{-13}$ m/s with the exception of BOZ1-1 at the end of the experiment with 1.1×10^{-14} m/s. This conductivity refers to a direction perpendicular to bedding and a sample length of 8 – 9 cm, measured at very large hydraulic gradients (Tab. 4.7-2). A gradual but rather minor decrease after an early maximum value may be due to slow sample consolidation, and this was also observed in earlier work (Mäder 2018). These latter values are considered most representative for in-situ conditions, although the confining stress of 60 bar (6 MPa) in the experiments is still considerably less than the lithostatic stresses at 500 – 1'000 m depth.

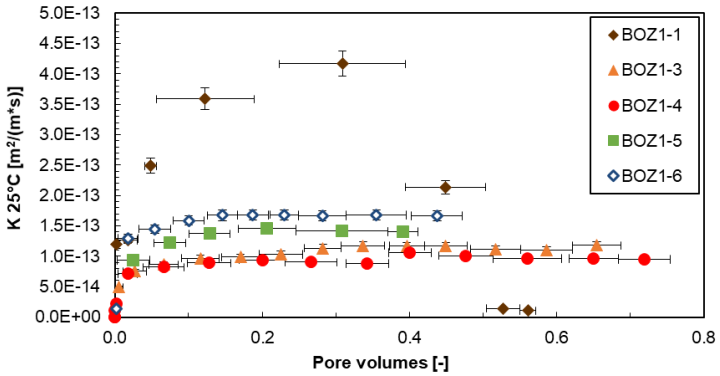

Fig. 4.7-4: Evolution of hydraulic conductivity during advective displacement experiments

BOZ1-1 = BOZ1-1-469.40-AD (Hauptrogenstein); BOZ1-3 = BOZ1-1-516.72-AD (Passwang Fm.); BOZ1-4 = BOZ1-1-575.26-AD (Opalinus Clay); BOZ1-5 = BOZ1-1-665.40-AD (Staffelegg Fm.); BOZ1-6 = BOZ1-1-697.51-AD (Klettgau Fm.). Pore volume fractions relate to transport time based on water content. Experiment duration is 57 – 161 days. Horizontal length of symbol bar covers the sampling interval, vertical bars are an estimate of combined uncertainties.

BOZ1-1 (Hauptrogenstein) was selected as an additional sample when it was realised that parts of this formation are quite marly (25 wt.-% clay, 65 wt.-% calcite for this sample) and because no groundwater could be sampled (formation considered as aquifer more to the west). It is also unusual in several other aspects, namely a coarse texture (mm-cm scale) of distribution of marly portions, limestone components and concretions / shell fragments. It also contains abundant interparticle macro-pores (~ 3 wt.-% water content, ~ 8 vol.-% water-loss porosity), but that are not well connected as evident by a relatively low hydraulic conductivity of ~ 4×10^{-13} m/s. The observed deacrease in hydraulic conductivity after 0.3 pore volumes of percolation (Fig. 4.7-4) was inferred to be related to an observed precipitation of calcite at the outleft port where a small titanium filter disc is protecting the capillary tube from particulate matter. The experiment shows an anomalous hydraulic behaviour, and the interpretation of the geochemical evolution will be limited by this.

Tab. 4.7-13: Hydraulic conductivity of AD samples

Parameter	**Unit**	**BOZ1-1**	**BOZ1-3**	**BOZ1-4**	**BOZ1-5**	**BOZ1-6**
Depth	[m]	469.40	516.72	575.26	665.40	697.51
Geol. unit		Hauptrogenstein	Passwang Fm.	Opalinus Clay	Staffelegg Fm.	Klettgau Fm.
Early_K (25 °C)	[m/s]	3.59E-13	9.89E-14	8.90E-14	1.37E-13	1.68E-13
Late_K (25 °C)	[m/s]	*1.09E-14* *	1.18E-13	9.52E-14	1.40E-13	1.67E-13

* This value is not considered reliable and should not be used (see text)

The time axis for all data representations of sequential fluid aliquots is converted to pore volume fractions by dividing the cumulative sample mass (volume) by the water content of the core. In this way, experiments with very different hydraulic conductivities or different water contents can be represented in a meaningful way for transport. There may be some minor ambiguities in case where water contents from pre-characterisation deviate from the true water content of a sample core, or if a significant initial unsaturated porosity fraction would be present. The chosen approximation is sufficient for a visual presentation of data.

Sampled aliquots (mass) plotted versus pore volume fraction (time) provides an overview of all syringe samples taken for all five AD experiments (Fig. 4.7-5). Up to 15 samples were collected for some of the experiments.

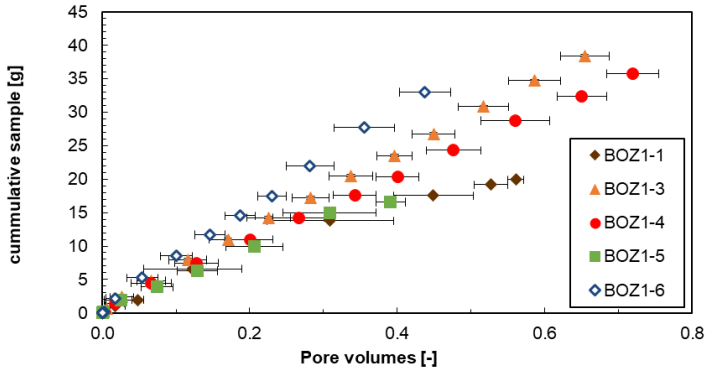

Fig. 4.7-5: Sampling schedule and sample volumes taken

BOZ1-1 = BOZ1-1-469.40-AD (Hauptrogenstein); BOZ1-3 = BOZ1-1-516.72-AD (Passwang Fm.); BOZ1-4 = BOZ1-1-575.26-AD (Opalinus Clay); BOZ1-5 = BOZ1-1-665.40-AD (Staffelegg Fm.); BOZ1-6 = BOZ1-1-697.51-AD (Klettgau Fm.). Each data point represents a syringe aliquot taken, with the horizontal bar indicating the duration for sampling, here converted to pore volume fraction percolated. Different slopes reflect different volumetric flow rates scaled by porosity.

4.7.5.3 Inline measurement of electric conductivity and pH

Electric conductivity (EC) was continuously monitored in all experiments (Fig. 4.7-6; Waber (ed.) 2020 for method). Conductivity cells were initially calibrated but may show a drift to varying extent over time due to electrode corrosion, commonly resulting in low apparent readings. Therefore, electric conductivity values are only meant to provide an indication of salinity but are not used quantitatively.

The electric conductivities generally show a local maximum in the early percolated pore volumes ranging from 10 to 19 mS/cm (22 °C laboratory reference). The injected artificial porewater has a higher conductivity compared to the displaced porewater. The value of the APW is gradually approached with progress of advective displacement if sufficient run-time is provided. Experiment BOZ1-1 shows an anomalous behaviour with EC values rising well above the injected APW at the same time as the nitrate concentration increases (Fig. 4.7-19).

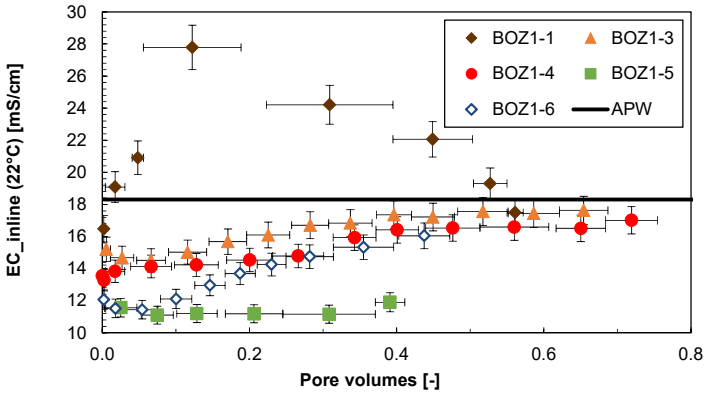

Fig. 4.7-6: Evolution of electric conductivity (22 °C) during advective displacement experiments

BOZ1-1 = BOZ1-1-469.40-AD (Hauptrogenstein); BOZ1-3 = BOZ1-1-516.72-AD (Passwang Fm.); BOZ1-4 = BOZ1-1-575.26-AD (Opalinus Clay); BOZ1-5 = BOZ1-1-665.40-AD (Staffelegg Fm.); BOZ1-6 = BOZ1-1-697.51-AD (Klettgau Fm.). Pore volume fractions relate to transport time based on water content. Experiment duration is 57 – 161 days. Horizontal length of symbol bar covers the sampling interval, vertical bars are an estimate of combined uncertainties.

The aim was to measure pH inline three times before/after sampling of the first four aliquots, and less frequently at later times (method in Waber (ed.) 2020). Measurements took 12 – 24 hrs in most cases, to ensure that the dead volume of the very small flow-through pH cell was sufficiently flushed given the very slow flow rates of the experiments. The micro-electrode was left installed in the flow-through cell and was checked before and after each pH measurement period with a standard solution. The initial calibration was made at pH 7 and 9, and simple drift checks and corrections were made with a standard solution at pH 7. The electrode slope was examined from time to time and was found to remain remarkably stable. In most cases, drift corrections over 12 – 24 hrs were ≤ 0.1 pH units. The overall uncertainty is difficult to assess because these small electrodes may respond to manipulations at the flow-through cell (response to small strains) and also small gas bubbles may temporarily affect readings. It is estimated that an error of ± 0.2 pH units is appropriate for most measurements. pH values of early aliquots are tabulated below (Tab. 4.7-14).

These in-line pH measurements (Fig. 4.7-7) are rather tricky and require careful handling of the equipment. Criteria to accept a value include a small drift and a reasonably well-defined pH-plateau, as well as a stable non-zero electric conductivity (no gas bubbles). It cannot be excluded that for long measurement durations some effect from out-gassing or in-gassing may influence the readings. The measurements for each experiment span a range of less than 0.65 pH units and point to a systematic trend over the duration of each experiment, thus indicating that random errors or disturbed signals are not a dominant feature. The in-line pH from BOZ1-1 form an exception and vary over 0.8 pH units likely due to the calcite precipitation towards the end of the experiment. More details are discussed further below.

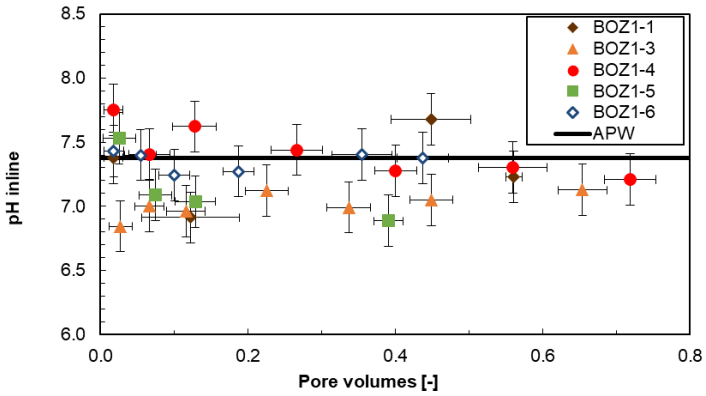

Fig. 4.7-7: Evolution of inline pH during advective displacement experiments

BOZ1-1 = BOZ1-1-469.40-AD (Hauptrogenstein); BOZ1-3 = BOZ1-1-516.72-AD (Passwang Fm.); BOZ1-4 = BOZ1-1-575.26-AD (Opalinus Clay); BOZ1-5 = BOZ1-1-665.40-AD (Staffelegg Fm.); BOZ1-6 = BOZ1-1-697.51-AD (Klettgau Fm.). Pore volume fractions relate to transport time based on water content. Experiment duration is 57 – 161 days. Horizontal length of symbol bar covers the sampling interval, vertical bars are an estimate of combined uncertainties.

4.7.5.4 Evolution of major and minor components

Evolution of concentrations with progress of percolation are shown in Figs. 4.7-8 to 4.7-13. Select analytical data for the first two aliquots sampled (liquid) are summarised in Tab. 4.7-14 further below, with full details in Appendix B. The composition of the earliest aliquots displaced from the core samples are the most representative for the pore fluid extracted, and this is highlighted and interpreted in a separate Section 4.7.5.5.

From the displaced **major components**, **SO_4** is the only one initially more concentrated in the outflow than in the injected APW (Fig. 4.7-8). The concentrations of the other **major components Cl, Na Ca and Mg** are initially below the APW. BOZ1-1 forms an exception and elutes concentrations above the APW for all major components disregarding Cl. All concentrations tend to converge to APW concentrations with progress of percolation, attesting to an ion-exchanger population in situ that is compatible with ion ratios in the APW (but different in ionic strength). BOZ1-1 presents a more complicated pattern of ion concentrations along the course of the experiment. Elevated Ca, Na and Mg in in this experiment compensates for the exceptionally high nitrate, both decreasing with ongoing percolation (also see Tab. 4.7-10). In this case, nitrate forms a major component and is a carrier for anion charge along with chloride and sulphate. BOZ1-4 is the sole sample with major ion concentrations that form an early plateau, whereas in the remaining experiments there is an initial drop in major ion concentrations or a constant rise towards the APW.

The same information as depicted in Fig. 4.7-8 is summarised for select components for all five experiments (Fig. 4.7-9). A choice was made to use average compositions of the first two analysed aliquots to best represent the porewater composition. The resulting porefluid compositions are summarised in Tab. 4.7-15 (Section 4.7.5.5) and are also used in the integrative plots in Chapter 5.

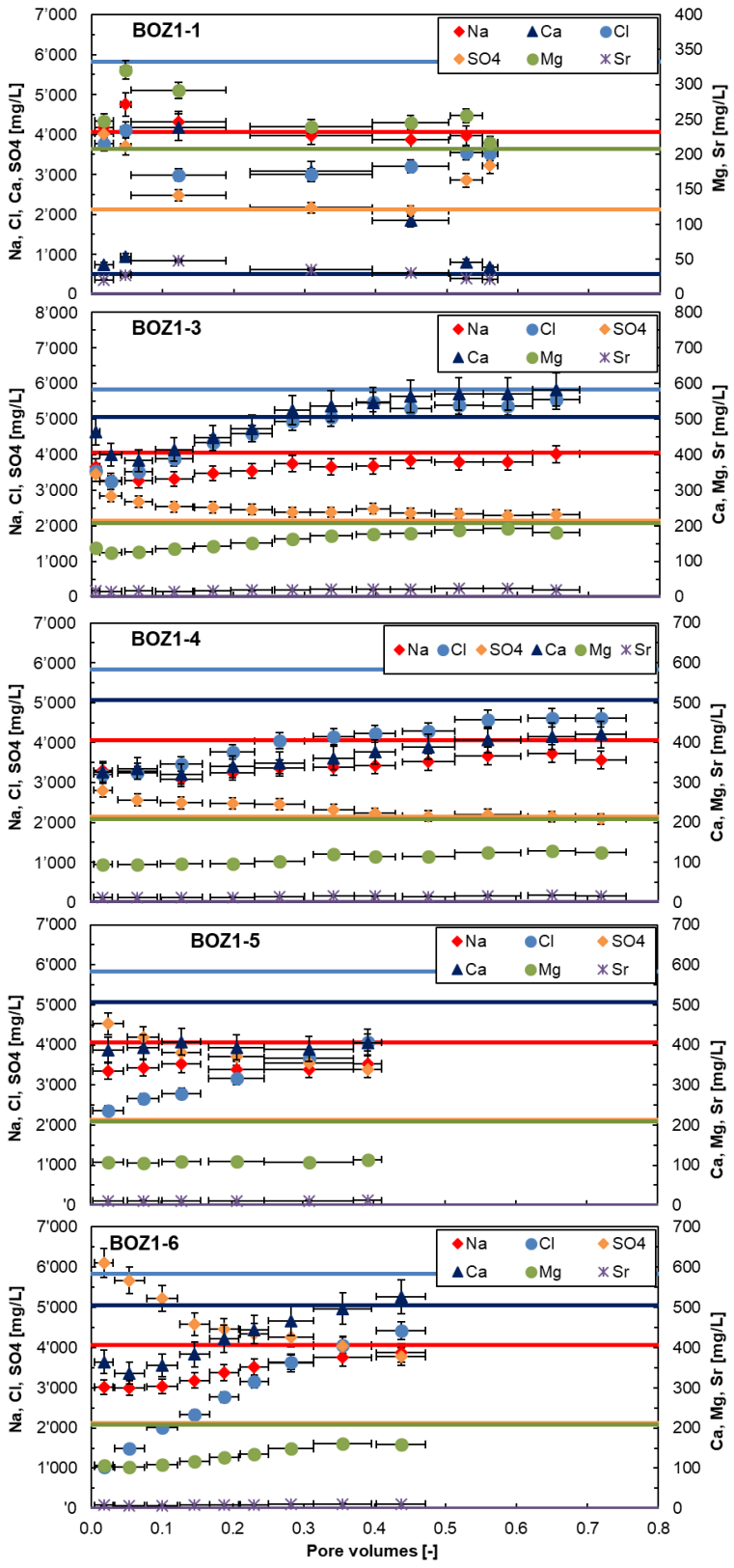

Fig. 4.7-8: Evolution of major components during advective displacement experiments

For legend see Fig. 4.7-9.

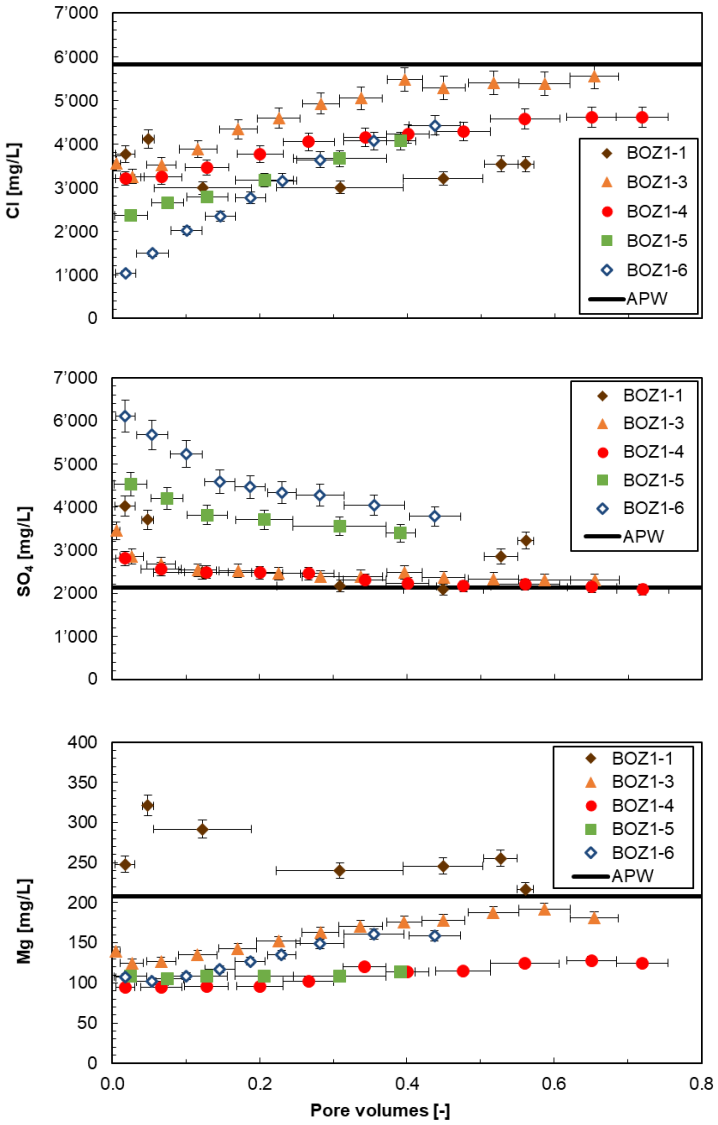

Fig. 4.7-9: Evolution of Cl, SO_4 and Mg during advective displacement experiments

BOZ1-1 = BOZ1-1-469.40-AD (Hauptrogenstein); BOZ1-3 = BOZ1-1-516.72-AD (Passwang Fm.); BOZ1-4 = BOZ1-1-575.26-AD (Opalinus Clay); BOZ1-5 = BOZ1-1-665.40-AD (Staffelegg Fm.); BOZ1-6 = BOZ1-1-697.51-AD (Klettgau Fm.). Pore volume fractions relate to transport time based on water content. Experiment duration is 57 – 161 days. Horizontal length of symbol bar covers the sampling interval, vertical bars are an estimate of combined uncertainties. Horizontal lines represent the composition of the injected APW.

Of the **minor components (Br, NO_3, K, Sr, Si)**, only potassium is present in the injected APW. Its evolution shows a smooth trend towards the APW concentration with a slight decrease at the end of most experiments (Fig. 4.7-10). BOZ1-1 forms an exception and presents a drastic increase in potassium concentrations followed by a constant decrease towards the APW, similar to the patterns observed for the major cations Ca, Mg and Na (Fig. 4.7-10). The Sr concentrations present patterns analogous to the major cations and potassium despite not being present in the APW. Bromide is gradually decreasing in all experiments until being almost completely flushed out

(details in Fig. 4.7-11). This can be used as a reversed breakthrough of an anionic tracer (see below). Dissolved silica elutes almost at constant concentations at 3 – 6 mg/L with the exception of the first aliquot of BOZ1-3 with Si concentrations of 10 mg/L. This aliquot includes also an elevated K concentration and is likely affected by the potassium silicate drilling fluid. Note, that this aliquot includes the very first few drops in contrast to other experiments, where these are discarded due to potential disturbances. It is therefore not included in the calculation of the representative early aliquot (Tab. 4.7-14).

Nitrate is a major component in the early aliquots of the experiment BOZ1-1 (Hauptrogenstein). For this sample, the maximum values reach up to 16 g/L in the third aliquot, followed by a regular decrease (Fig. 4.7-10, Tab. 4.7-14, Appendix B). The elution behaviour of NO_3 in the remaining experiments (Fig. 4.7-10, Tab. 4.7-14, Appendix B) provides early values up to 980 mg/L, and a decrease to below the limit of detection at the end of the experiments with the exception of BOZ1-5 which remains at 43 mg/L after 0.4 pore volumes. The origin of nitrate is still unknown, but a reactive nitrogen phase is suspected (associated with solid organic matter), which is not mobilised during comparably short and anaerobic aqueous extracts. However, aqueous extracts of post-mortem samples from BOZ1-1 (Hauptrogenstein) show nitrate concentrations up to 66 mg/L (Tab. 4.7-8). Ammonium (NH_4) is near or below a detection limit of 10 mg/L in all exfiltrated sample aliquots except for BOZ1-1, where concentrations reach up to 95 mg/L.

Ba and Al were measured by ICP-OES but remain below detection limits of 0.025 – 0.5 mg/L for Ba and 0.25 – 2.5 mg/L for Al depending on dilution factors. A few aliquots from BOZ1-1 have detectable Ba and Al concentrations ranging from 0.3 to 0.9 mg/L and 0.3 to 0.5 mg/L, respectively.

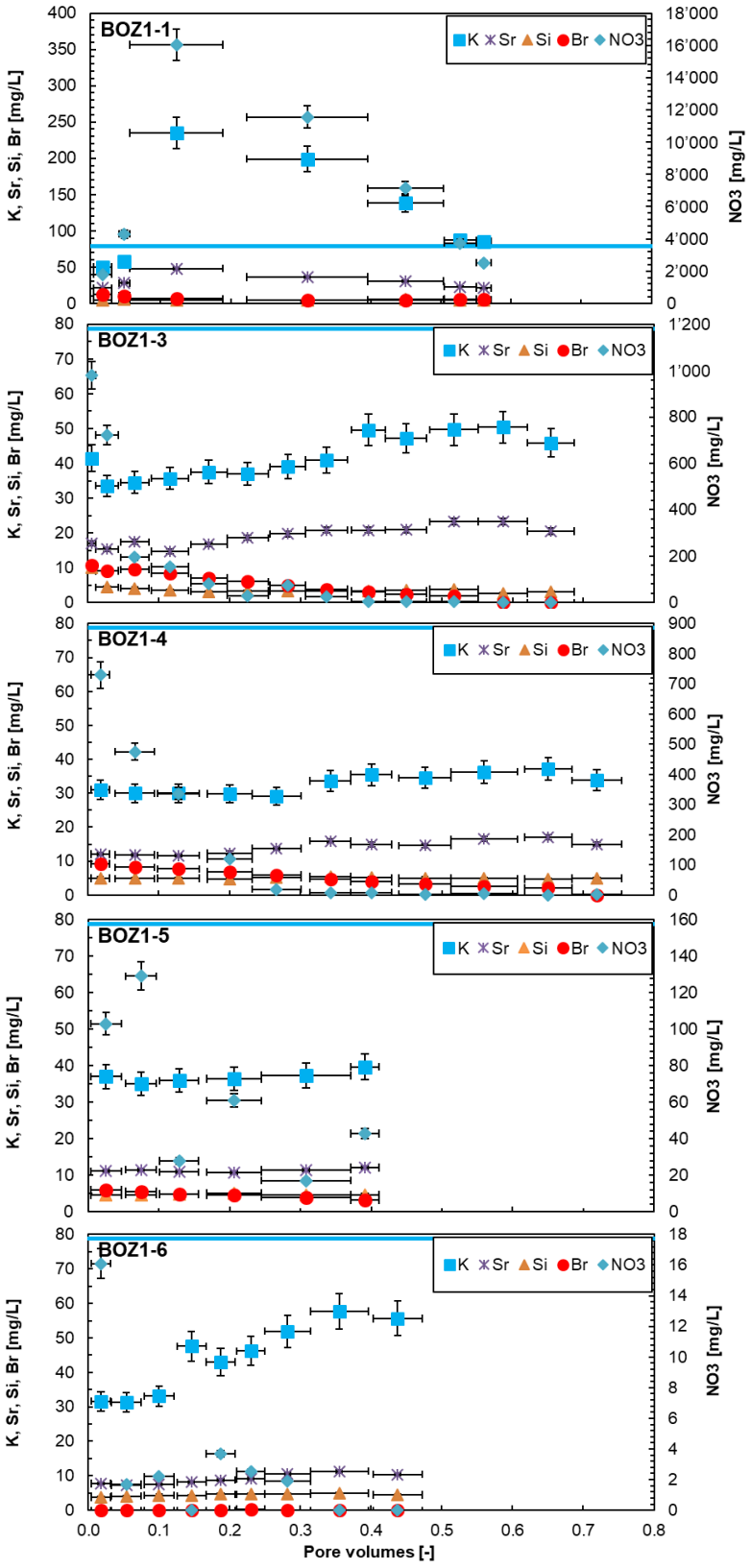

Fig. 4.7-10: Evolution of minor components during advective displacement experiments

For legend see Fig. 4.7-9. Horizontal lines represent the composition of the injected APW for K (0 for others).

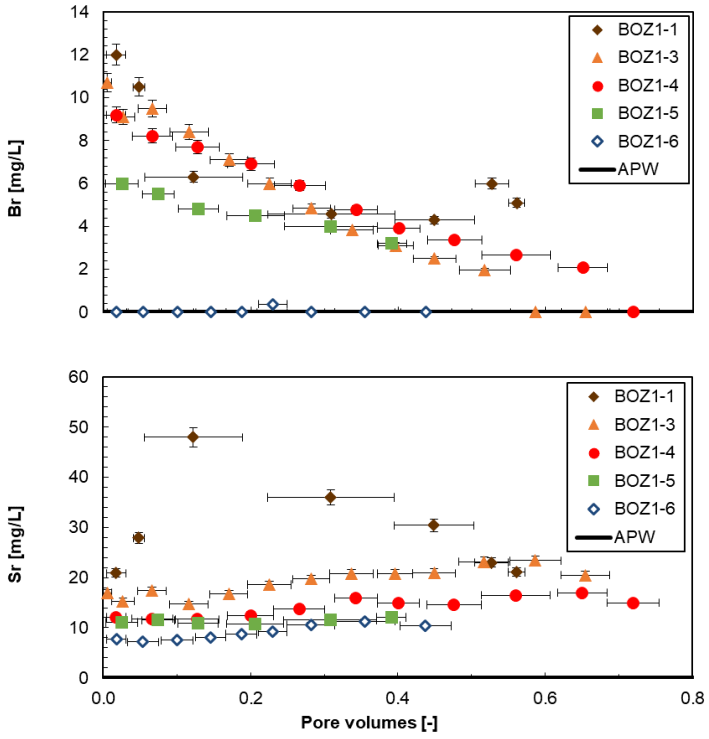

Fig. 4.7-11: Evolution of selected minor components during advective displacement experiments

BOZ1-1 = BOZ1-1-469.40-AD (Hauptrogenstein); BOZ1-3 = BOZ1-1-516.72-AD (Passwang Fm.); BOZ1-4 = BOZ1-1-575.26-AD (Opalinus Clay); BOZ1-5 = BOZ1-1-665.40-AD (Staffelegg Fm.); BOZ1-6 = BOZ1-1-697.51-AD (Klettgau Fm.). Pore volume fractions relates to transport time based on water content. Experiment duration is 57 – 161 days. Horizontal length of symbol bar covers the sampling interval, vertical bars are an estimate of combined uncertainties. Br and Sr in the APW are 0. Br concentrations below detection are plotted at 0.

The **carbon system (TIC, TOC, TC, lmwoa)** shares as a common feature that relatively large TOC concentrations are eluted initially (81-210 mg/L) that gradually decrease to 18 – 78 mg/L with progressive percolation (Fig. 4.7-12, Tab. 4.7-14 shows averages of first 2 aliquots). BOZ1-1 forms an exception and elutes values up to 1'524 mg/L, decreasing to 181 mg/L after 0.4 pore volumes. TOC clearly dominates the dissolved carbon inventory (TC) at early times. The high TOC concentrations in BOZ1-1 and BOZ1-6 can be explained to some extent by low-molecular-weight organic acids (LMWOA), namely acetate and in case of BOZ1-1 also propionate. In these cores acetate concentrations of up to 277 and 194 mg/L (Fig. 4.7-12 show acetate as carbon equivalents, Fig. 4.7-13 in mg/L) were measured, respectively. In the remaining three experiments, acetate was below the limit of detection.

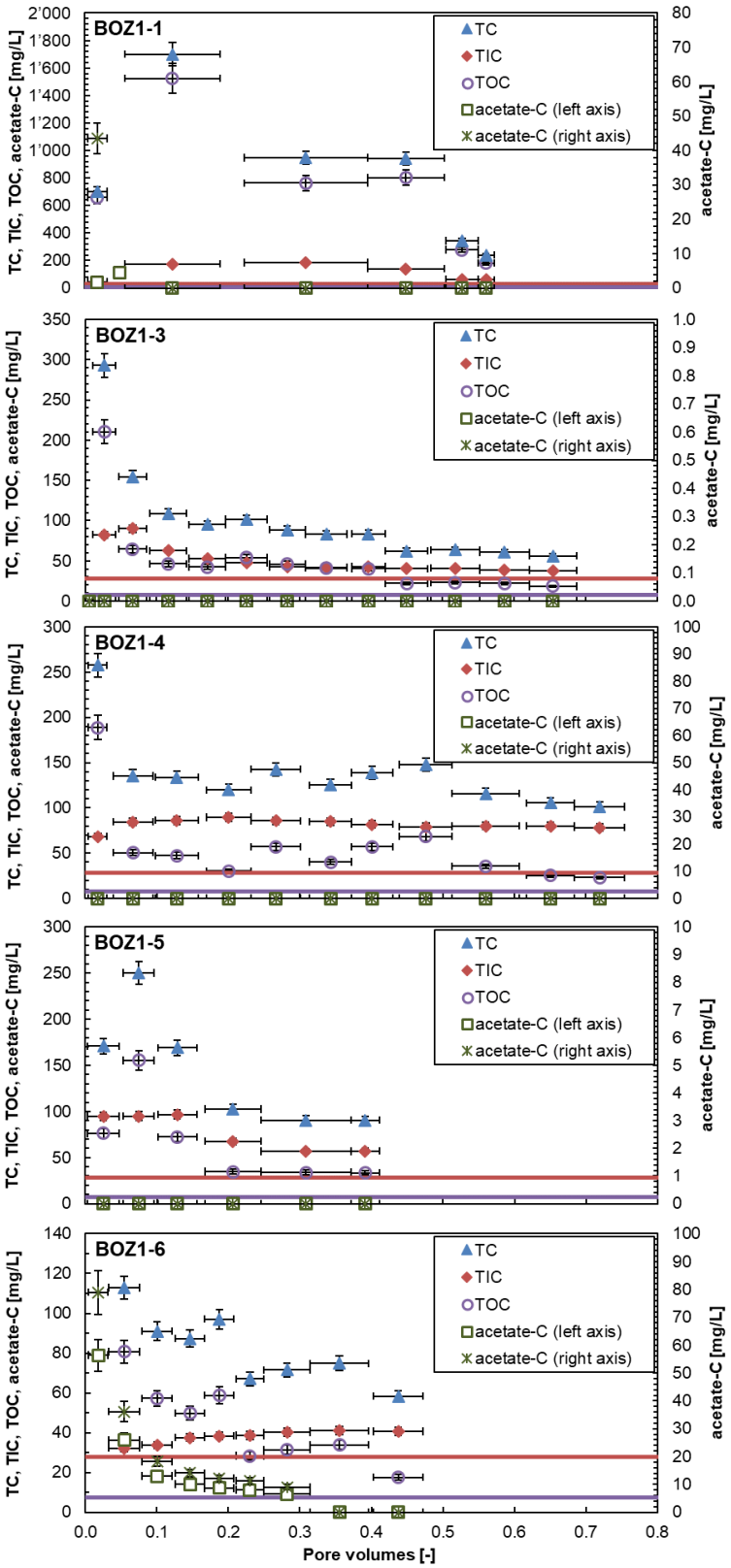

Fig. 4.7-12: Evolution of carbon system during advective displacement experiments

For legend see Fig. 4.7-9.

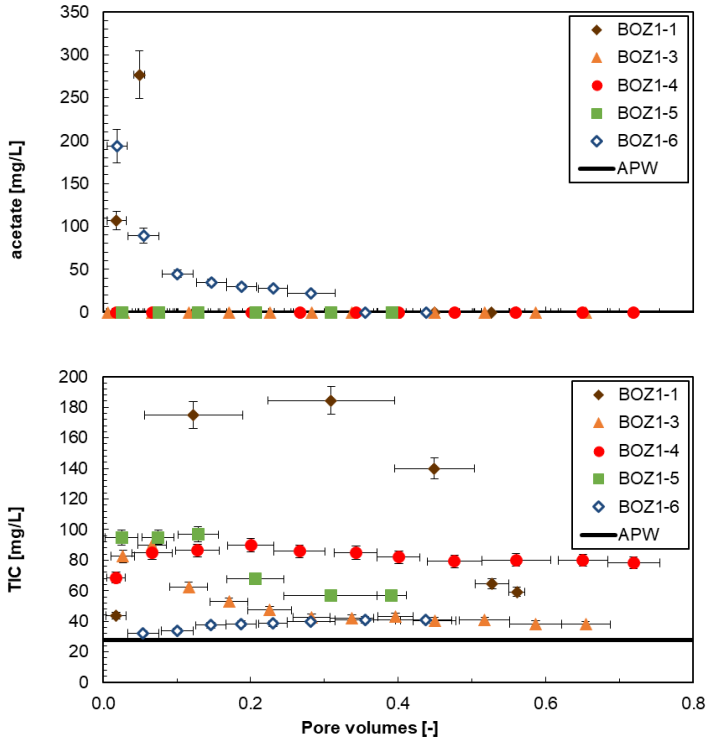

Fig. 4.7-13: Evolution of select carbon components during advective displacement experiments

BOZ1-1 = BOZ1-1-469.40-AD (Hauptrogenstein); BOZ1-3 = BOZ1-1-516.72-AD (Passwang Fm.); BOZ1-4 = BOZ1-1-575.26-AD (Opalinus Clay); BOZ1-5 = BOZ1-1-665.40-AD (Staffelegg Fm.); BOZ1-6 = BOZ1-1-697.51-AD (Klettgau Fm.). Pore volume fractions relate to transport time based on water content. Experiment duration is 57 – 161 days. Horizontal length of symbol bar covers the sampling interval, vertical bars are an estimate of combined uncertainties. Horizontal lines represent the composition of the injected APW. Concentrations below detection (acetate) are plotted at 0.

Aqueous extracts (Tab. 4.7-5) imply TOC values 160 – 400 mg/L when scaled to porewater content, which covers the range observed in the early aliquots. Aqueous extracts carried out post-mortem (Tab. 4.7-8) show a clear depletion of TOC compared to the initial state with the exception of BOZ1-1 where concentrations almost doubled. The observation of TOC depletion is similar to previous work with samples from the Schlattingen-1 geothermal well (Mäder & Waber 2017) and also TBO boreholes BUL1-1 (Mazurek et al. 2021), TRU1-1 (Aschwanden et al. 2021) and MAR1-1 (Mäder et al. 2021).TIC elutes initially at much lower concentrations than TOC, but covers a wide range of concentrations, and trends for each experiment are dissimilar to some extent (Figs. 4.7-12 and 4.7-13). Microbial activity might influence TIC/TOC, either in the syringe itself (i.e. during sampling/ storage) or at the surface of the core sample, whereby a part of organic carbon might be oxidised to inorganic carbon, e.g. coupled with sulphate reduction.

The **measurement of pH** was performed in-line between some of the sampling intervals (setup in Waber (ed.) 2020) and in the laboratory when syringe aliquots were prepared/preserved for analysis. The latter was done in most cases very shortly after sampling (one to a few hours), or after a few days of cold storage. The total range covered for all samples, in-line and laboratory, is 6.8 – 7.8 (Fig. 4.7-14), both showing similar spreads. In BOZ1-3, BOZ1-5 and BOZ1-6 there

is a systematic offset between the in-line and laboratory measured pH with the in-line pH presenting lower values. An exceptional value is the laboratory pH of 8.4 from the first sample in BOZ1-3, which is likely affected by the drilling fluid. This first aliquot is usually discarded but was analysed in this case.

The in-line pH series define relatively smooth trends with percolation progress, but not a very systematic behaviour. The spread in the in-line values is relatively small, ranging from 0.2 – 0.6 pH units with the exception of BOZ1-1, which shows variations of 0.8 pH units. The laboratory measured pH presents some increasing and decreasing trends with variations of 0.2 – 0.6 pH units. The calculated partial pressure of CO_2 is larger than atmospheric in the aliquots, and this bears the potential for outgassing and resultant supersaturation with respect to calcite, and a possibility for some loss of Ca and TIC by precipitation.

It should be noted that in the sample with the large initial nitrate concentrations (BOZ1-1) there is some uncertainty regarding the generation of this dissolved nitrate. Depending on the processes, this could also affect pH values. While the pH may still be representative of the porewater of the experiment, it may deviate from the undisturbed state.

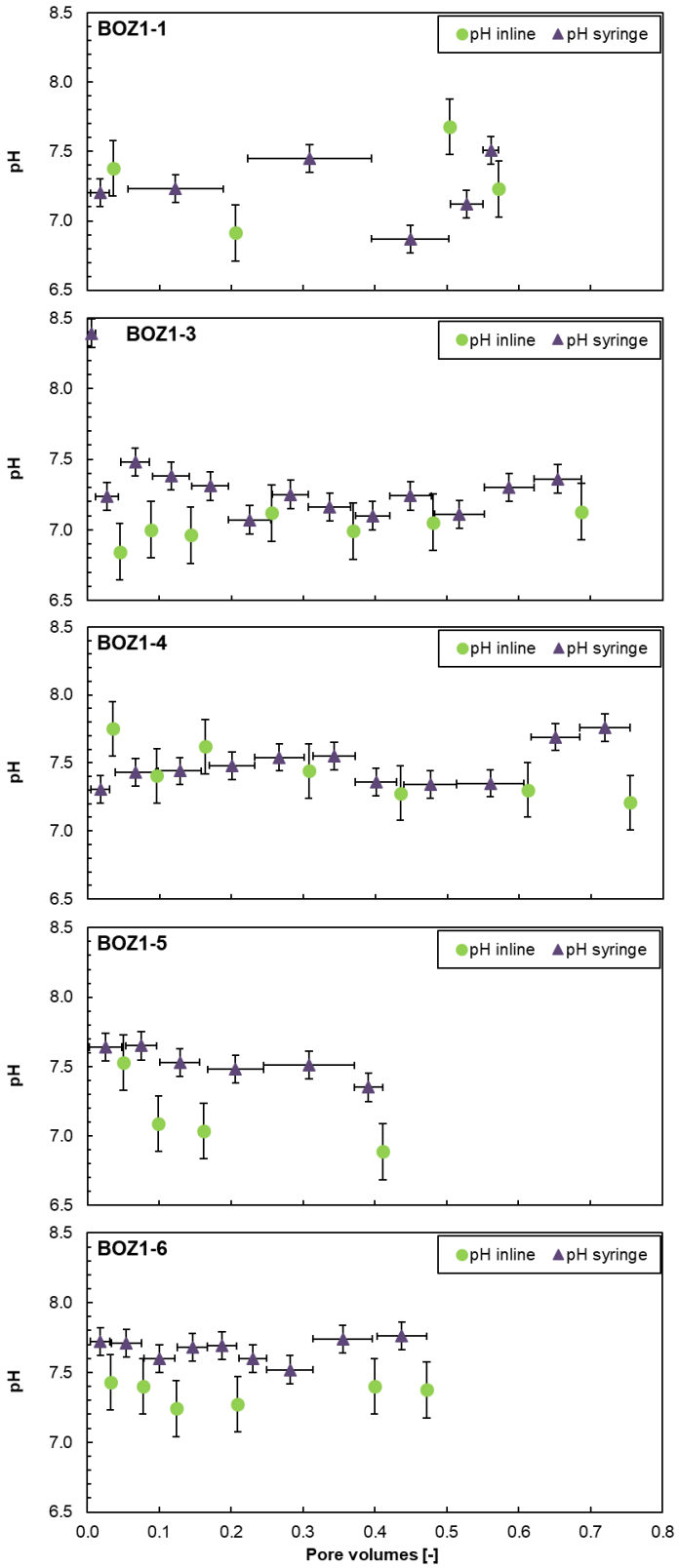

Fig. 4.7-14: Evolution of pH during advective displacement experiments

For legend see Fig. 4.7-4.

4.7.5.5 Early displaced aliquots representing the porewater composition

Early displaced aliquots were generally obtained by averaging the first two measured samples (Tab. 4.7-14). Note, that in experiment BOZ1-3, the very first few drops were analysed, in contrast to the general procedure of discarding them due to potential disturbances. Therefore, and because of indications for drilling fluid contamination, this sample was not considered for the derivation of the average early displaced aliquot. The first two sample aliquots from BOZ1-1 have much higher Cl but much lower nitrate concentrations than all later aliquots of this experiment. Therefore, these first two sample aliquots are considered to be unaffected by nitrate interferences.

Interpretation of these early displaced aliquots as being representative of the in situ porewater, contained in the core at the time of the experiment, requires integration and interpretation of the entire data set supported with geochemical calculations. Comprehensive reactive transport simulations are expected to further restrict the initial porewater compositions, as well as the transport properties of the cores. Only speciation calculations are included in this data report for the early compositions. Speciation calculations for all individual syringes are provided in Appendix B. The laboratory pH values were used for the speciation calculations. TIC was used as a constraint for inorganic carbon.

Tab. 4.7-14: Composition of earliest aliquots from advective displacement experiments

Parameter		**BOZ1-1**	**BOZ1-3**	**BOZ1-4**
Depth	[m]	469.40	516.72	575.26
Sample ID RWI		BOZ1-1-469.40-AD	BOZ1-1-516.72-AD	BOZ1-1-575.26-AD
Lab sample ID		BOZ1-1xx-AD	BOZ1-3xx-AD	BOZ1-4xx-AD
Geol. unit		Hauptrogenstein	Passwang Fm.	Opalinus Clay
pH inline	[-]	7.38	6.92	7.58
pH lab	[-]	7.20	7.36	7.37
Na	[mg/L]	4'459	3'271	3'291
NH_4	[mg/L]	< 10	10	< 10
K	[mg/L]	53.65	34.05	30.50
Ca	[mg/L]	841	391	331
Mg	[mg/L]	285	126	94.9
Sr	[mg/L]	24.4	16.4	12.0
Ba	[mg/L]	< 0.25	< 0.25	< 0.25
Si	[mg/L]	4.54	4.27	4.91
Al	[mg/L]	0.429	< 0.5	< 0.5
F	[mg/L]	2.31	< 1.6	< 1.6
Cl	[mg/L]	3'940	3'383	3'224
Br	[mg/L]	11.3	9.3	8.705
NO_3	[mg/L]	3052	459	603
SO_4	[mg/L]	3'860	2'758	2'681
TOC	[mg/L]	659.2	137.5	119.8
TIC	[mg/L]	43.6	86.3	76.7
lactate	[mg/L]	< 20	< 20	< 20
acetate	[mg/L]	192	< 20	< 20
propionate	[mg/L]	< 20	< 20	< 20
formate	[mg/L]	< 20	< 20	< 20
$\delta^{18}O$	[‰VSMOW]	-4.72	-5.03	-5.68
$\delta^{2}H$	[‰VSMOW]	-42.0	-42.5	-44.4

Tab. 4.7-14: (continued)

Parameter		**BOZ1-5**	**BOZ1-6**
Depth	[m]	665.40	697.51
Sample ID RWI		BOZ1-1-665.40-AD	BOZ1-1-697.51-AD
Lab sample ID		BOZ1-5xx-AD	BOZ1-6xx-AD
Geol. unit		Staffelegg Fm.	Klettgau Fm.
pH inline	[-]	7.31	7.41
pH lab	[-]	7.64	7.72
Na	[mg/L]	3'393	3'011
NH_4	[mg/L]	< 10	< 10
K	[mg/L]	36.05	31.45
Ca	[mg/L]	391	350
Mg	[mg/L]	107	105
Sr	[mg/L]	11.3	7.47
Ba	[mg/L]	< 0.5	< 0.25
Si	[mg/L]	4.61	3.93
Al	[mg/L]	< 0.5	< 2.5
F	[mg/L]	< 1.6	2.275
Cl	[mg/L]	2'507	1'262
Br	[mg/L]	5.75	< 1.6
NO_3	[mg/L]	116	8.9
SO_4	[mg/L]	4'365	5'888
TOC	[mg/L]	115.8	80.7
TIC	[mg/L]	94.9	32.2
lactate	[mg/L]	< 20	< 20
acetate	[mg/L]	< 20	141.45
propionate	[mg/L]	< 20	< 20
formate	[mg/L]	< 20	< 20
$\delta^{18}O$	[‰VSMOW]	-6.52	-7.21
$\delta^{2}H$	[‰VSMOW]	-42.9	-45.6

The speciation calculations (Tab. 4.7-15) reveal a cation charge surplus (positive 'Charge', not observed in BOZ1-6) that is not large and partially explained by significant TOC concentrations that were not included in the speciation (as acetate). TIC was used as constraint for inorganic carbon. The aliquots are all significantly oversaturated with respect to calcite and also dolomite. Such oversaturation may result from shifts in pH linked to potential outgassing of CO_2 during sampling and storage. Alternatively, the large TOC (and TC) contents pose analytical difficulties to obtain TIC, and associated errors may be larger than commonly assigned to TIC measurements.

Saturation is reached or exceeded for celestite in all samples except for a slight undersaturation calculated in BOZ1-4 and BOZ1-6. For gypsum, saturation is only reached in the upper most sample (Hauptrogenstein, BOZ1-1) and andydrite is undersaturated in all samples. The implication is that the ion-activity products ($[Sr]\cdot[SO_4]$) and ($[Ca]\cdot[SO_4]$) are controlling factors, but this does not necessarily mean that these minerals are also present in the core before the experiments. There are larger SO_4 and Sr concentrations in the the early aliquots than in the APW (Figs. 4.7-8 and 4.7-11), but Ca is eluted initially below APW concentrations. BOZ1-1 forms an exception with Ca concentrations slightly above the APW leading to gypsum saturation. Note that the first two aliquots in this core are still low in nitrate and therefore most likely undisturbed by nitrate interferences.

A more in-depth analysis and interpretation will have to be carried out, including reconstructions by geochemical modelling.

Tab. 4.7-15: Saturation state of earliest aliquots from advective displacement experiments

Parameter	**unit**	**BOZ1-1**	**BOZ1-3**	**BOZ1-4**	**BOZ1-5**	**BOZ1-6**
Depth	[m]	469.40	516.72	575.26	665.40	697.51
Geol. unit		Hauptrogenstein Fm.	Passwang Fm.	Opalinus Clay	Staffelegg Fm.	Klettgau Fm.
Charge	[eq/kg_w]	1.7E-02	6.3E-03	6.0E-03	5.8E-03	-3.0E-03
%-Error		3.78	2.00	1.93	1.86	-1.08
Acetate	[eq/kg_w]	3.3E-03	< 3.4E-4	< 3.4E-4	< 3.4E-4	2.4E-03
Ionic strength	[mol/kg_w]	0.28	0.19	0.18	0.20	0.19
tot_alk	[eq/kg_w]	3.4E-03	6.9E-03	6.1E-03	7.8E-03	2.7E-03
pH (Lab)		7.20	7.36	7.37	7.64	7.72
log$P(CO_2)$		-2.04	-1.87	-1.93	-2.10	-2.64
SI(calcite)		0.33	0.52	0.41	0.78	0.29
SI(dolomite-o)		0.51	0.87	0.60	1.31	0.37
SI(dolomite-d)		-0.04	0.32	0.05	0.76	-0.18
SI(gypsum)		0.06	-0.28	-0.35	-0.15	-0.10
SI(celestite)		0.25	0.06	-0.08	0.03	-0.05
SI(strontianite)		-0.76	-0.41	-0.58	-0.31	-0.92
SI(anhydrite)		-0.15	-0.50	-0.57	-0.37	-0.32

Nagra PSI 2012 thermodynamic data base, calculated in PHREEQC for 25 °C; dolomite-o: ordered dolomite; dolomite-d: disordered dolomite; charge = Σ(cation charge) - |Σ(anion charge)| ; %-error = 100*charge / (Σ(cation charge) + |Σ(anion charge)|).

4.7.5.6 Initial values and evolution of stable water isotope composition

Common to all five experiments (Fig. 4.7-15) is a relatively smooth evolution of $\delta^{18}O$ towards the APW value with progress of percolation. Unlike some major chemical components (e.g. chloride), the breakthrough trend starts immediately with the first sample aliquot and only in BOZ1-6 a plateau is visible within the first 0.15 pore volumes. The perculated porevolume is limited in all experiments and therefore no complete breakthrough of the APW is reached.

The behaviour for $\delta^{2}H$ is distinctly different and shows initially a reverse trend towards more negative values that goes through a minimum at 0.15 – 0.5 pore volumes with the exception of BOZ1-6 that shows a constant increase towards the APW values. The extent of breakthrough is much less compared to $\delta^{18}O$ for reasons that may not be intuitively obvious and are not yet resolved in detail, however, a couple of hypotheses are discussed below (Section 4.7.7; Fig. 4.7-18).

One explanation might be a difference in isotopic fractionation during partial or full equilibration between the anion-accessible and anion-inaccessible porewater (Horita et al. 1995, Sheppard & Gilg 1996). Another hypothesis is that there is an effect from dry cutting the core surfaces during sample preparation. This may induce evaporation of small amounts of porewater in the close vicinity of the cut surfaces, thus, enriching the residual porewater in heavy isotopes. Percolation would then first yield isotopically heavy signatures, which are then gradually mixed with the unaffected porewater signature, and increasingly also affected by the breakthrough of the traced

APW (ca. +100 ‰ V-SMOW for δ^2H and -11.5 ‰ V-SMOW for $\delta^{18}O$). This would explain the observed trends for δ^2H. In case of the oxygen isotopes, the APW is significantly lighter than the in-situ porewater and accordingly, the trend of $\delta^{18}O$ will always decrease as a function of replaced pore volumes (i.e. first by mixing with the non-evaporated and heavier porewater and later with the APW). This could explain the apparent immediate breakthrough behaviour. The suspected evaporation effect on $\delta^{18}O$ would be less compared to δ^2H due to the prevalence of kinetic isotope fractionation during evaporation. In laboratory experiments a slope of $a = 4.34$ was observed for the relationship $\delta^2H = a\ \delta^{18}O\text{-}c$ (Cappa et al. 2003). In the δ^2H vs. $\delta^{18}O$ plot (Fig. 4.7-16) the early samples of the experiment, prior to the start of APW breakthrough follow a trend with a similar slope. However, the early aliquots are isotopically lighter than neighbouring isotopic exchange experiments (Fig. 5.7-1), contradicting the potential evaporation effect.

The high concentrations of TOC may also influence the water isotopic system, or any microbial activity, as well as any precipitation of hydrous minerals that may be induced by advective displacement. These effects could explain the initial drop in isotopic values and are in agreement with the difference to the isotopic exchange experiments.

The stable isotope composition in $\delta^{18}O$ vs δ^2H coordinates (Fig. 4.7-16) displays a slightly curved data array for each experiment extending from the earliest and isotopically light (δ^2H) or heaviest ($\delta^{18}O$) extracts towards the APW isotopic composition. Earliest aliquots of the experiments (on right side of arrays) define a trend distinctly below the global meteoric water line, but plot rather on the GMWL with increasing sample depth.

The observed differences between $\delta^{18}O$ and δ^2H concerning the extents of breakthrough are discussed in more details in Section 4.7.7 and compared to other data sources in Chapter 5.

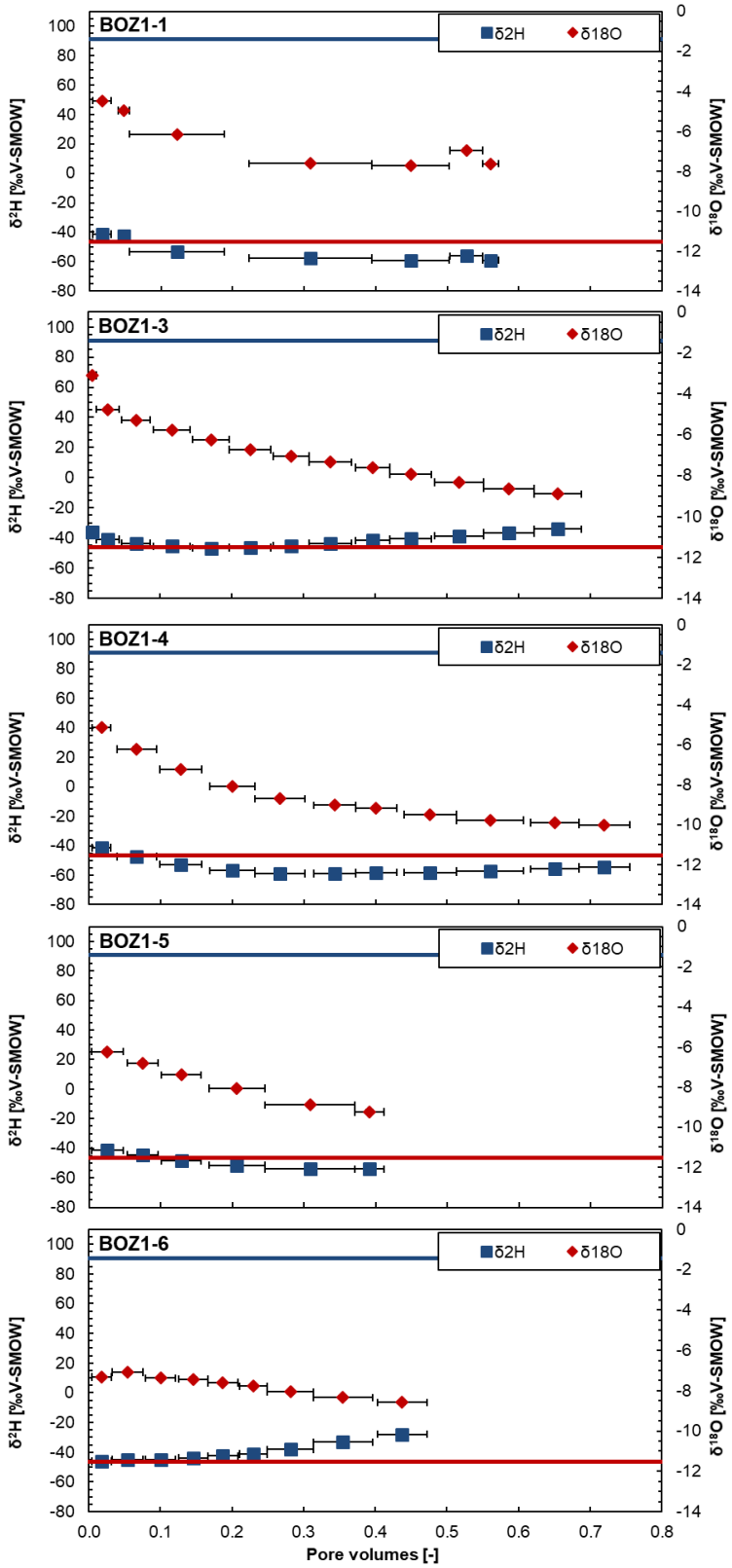

Fig. 4.7-15: Evolution of δ^2H and $\delta^{18}O$ during advective displacement experiments

For legend see Fig. 4.7-4. Horizontal length of symbol bar covers the sampling interval. Measurement errors are 1.5 ‰ for δ^2H and 0.1 ‰ for $\delta^{18}O$.

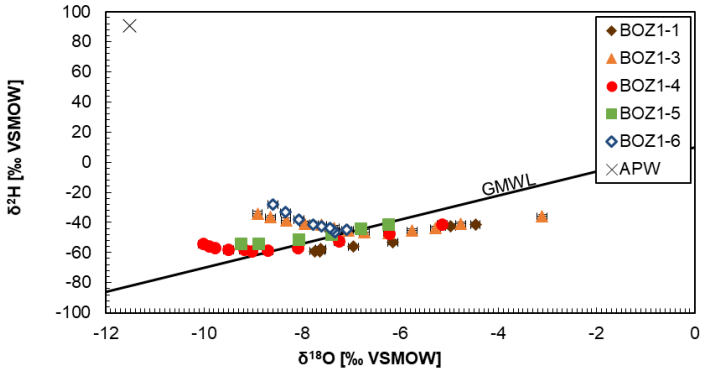

Fig. 4.7-16: Stable isotope composition of aliquots from advective displacement experiments

BOZ1-1 = BOZ1-1-469.40-AD (Hauptrogenstein); BOZ1-3 = BOZ1-1-516.72-AD (Passwang Fm.); BOZ1-4 = BOZ1-1-575.26-AD (Opalinus Clay); BOZ1-5 = BOZ1-1-665.40-AD (Staffelegg Fm.); BOZ1-6 = BOZ1-1-697.51-AD (Klettgau Fm.). Measurement errors are 1.5 ‰ for δ^2H and 0.1 ‰ for $\delta^{18}O$. GMWL is the global meteoric water line. 1st aliquots are located the furthest to the right, and evolve towards the left.

4.7.6 Derivation of anion-accessible porosity

There are several ways by which chloride and bromide accessible porosity fractions may be obtained. The principle is the same: namely the ratio between the anion concentration obtained from aqueous extracts up-scaled to bulk porewater content divided by that obtained from earliest aliquots from the percolation experiments (discussion in Waber (ed.) 2020 and Mäder 2018). There are some variants depending on how water contents were measured and averaged, or how inferred water losses and volume changes may be corrected. In the case where a full or well-advanced breakthrough in chloride is captured, such a ratio may also be obtained by post-mortem aqueous extracts (top and base) and the latest aliquots sampled before the end of the experiments (for the outlet / top), or the injected APW (for the inlet / base). Normally, bromide drops below detection and only the chloride data can be evaluated for post-mortem datasets. The bromide data commonly is more 'noisy'. Fig. 4.7-17 visualises for the BOZ1-4 sample (Opalinus Clay) the evolution of porewater Cl and Br concentrations from the initial state to a post-mortem profile and how it relates to the Cl and Br concentrations in sampled aliquots and in the APW. The different variants of calculating the intial and final accessible porosity fractions induce a range of Cl and Br concentrations when upscaled to the respective accessible porosity fractions (orange bars in Fig. 4.7-16). For Br, the accessible porosity fraction derived from the initial dataset was applied for the scaling of post-mortem aqueous extracts.

The top two data lines (Tab. 4.7-16) list the average concentrations (Cl, Br) for the first two displaced aliquots as shown in Tab. 4.7-14. The third line lists the concentration of Cl in the last syringe sampled (for post-mortem evaluation). The following three lines list different Cl concentrations up-scaled to water content: for the sample from above the AD core (_upscaled_top), for the sample from below (_upscaled_base) and a corrected and averaged value (top and base). The correction compensates for a small amount of water loss (unsaturated volume) commonly observed and evaluated from a measured net water uptake. The net water uptake is the measured water uptake (mass gain of the core during the experiment) corrected for a commonly measured small volume increase during the experiment (Section 4.7.3 and Tab. 4.7-4). The correction hinges on the assumption that sample treatment for the AD core and the off-cuts share the same history (core handling, storage, sample preparation) and therefore also potentially underwent similar water losses. These corrections are rather small, with small net water uptakes, except for

BOZ1-5 where a low water content results in a correction of 7% relative. The following three lines contain the same data for Br. The observed range in up-scaled concentrations is an indication of heterogeneity, mainly in clay-mineral content. A homogeneous sample with respect to the degree of anion-exclusion should yield the same up-scaled Cl and Br concentrations, despite differences in water content. A consistent proportion of anion-accessible porosity would then be evaluated regardless of choosing a sample from the top or from the base as a reference for the early displaced aliquots. The two data lines for Cl suffixed with _p-m are the up-scaled chloride concentrations evaluated post-mortem from aqueous extracts from the top of the core (outlet to sampling) and the base of the core (APW inlet).

The final data block (Tab. 4.7-16) lists the accessible porosity fraction obtained by various combinations and averaging. The first four lines list values that are derived without accounting for the net water uptake. Shaded in blue are the 'best' values for chloride after applying a correction for net water uptake as mentioned above. The data line below is the same for bromide. The last two data lines represent the post-mortem evaluations of the top of the core (outlet) and the base of the core (inlet).

There is good agreement and a rather high degree of consistency among the different ways of evaluation and data derived from pre-characterisation. The post-mortem characterisation for Cl is consistent in itself (not so for BOZ1-1) but yield higher values for the chloride-accessible porosity fraction compared to the pre-characterisation. This can be explained by an increase in the salinity over the course of the experiment, leading to a higher anion accessibility at the end of the experiment (contraction of the width of the diffuse layer next to negatively charged surfaces). The inconsistency in post-mortem values calculated for BOZ1-1 might arise from the disturbances by the large nitrate concentration, the anomalous hydraulic behaviour (Fig. 4.7-4) with an increasingly low hydraulic conductivity along with the low total percolation volume of less than 0.6, and hence the post-mortem aqueous extracts are not comparable to the last aliquot or the APW.

The anion exclusion effects calculated for Br approximate the ones calculated for Cl but are consistently smaller (in BOZ1-6 Br is b.d.), which results in larger bromide-accessible porosity fractions compared to chloride. A good explanation for this is lacking, because good agreement was obtained in many previous experiemnts (but not all), e.g. from BUL1-1, TRU1-1, MAR1-1 and the Schlattingen-1 geothermal well.

The experiment with Opalinus Clay shows calculated pre-characterisation accessible porosity fractions for chloride of 0.42 (and 0.53 for bromide). The pre-characterisation value for Cl is consistent with earlier work from Opalinus Clay (BUL1-1, TRU1-1 and MAR1-1) despite the significant difference in salinities. The post-mortem values for Cl range between 0.53 and 0.55 relate to APW salinity and are higher than values from earlier work at comparable salinities (BUL1-1 and MAR1-1). The reason for this is not yet resolved, but the observed salinity-dependence of the chloride-accessible porosity fraction is thought to be relevant, and it is also observed systematically in all other samples (Tab. 4.7-16, row shaded in blue v.s. the two last rows).

Chloride accessible porosity fractions calculated for the pre-characterisation of the two samples with lower clay-mineral content (25 – 38 wt.-%) from the 'Brauner Dogger' vary from 0.31 to 0.41 for chloride and 0.38 to 0.68 for bromide. The post-mortem values for Cl of the sample from the Passwang Formation are 0.40 to 0.44 but are unreliable for the Hauptrogenstein as discussed above. The sample from the Staffelegg Formation (30 wt.-% clay) yield anion accessible porosity fractions for the pre-characterisation of 0.42 and 0.52 for chloride and bromide, respectively. The

corresponding post-mortem values for Cl are between 0.55 and 0.59. The sample from the Klettgau Formation with 39 wt.-% clay shows a very low chloride-accessibility porosity fraction of 0.20 in pre-characterisation and much higher values of 0.43 to 0.47 in post-mortem analysis.

The accuracy is limited by the basic assumptions underlying the approach and by sample heterogeneity to some degree, mainly in clay-mineral content. The combined measurement uncertainties are dominated by the analytical error associated with Cl and Br concentrations but are probably not more than ± 10% for chloride.

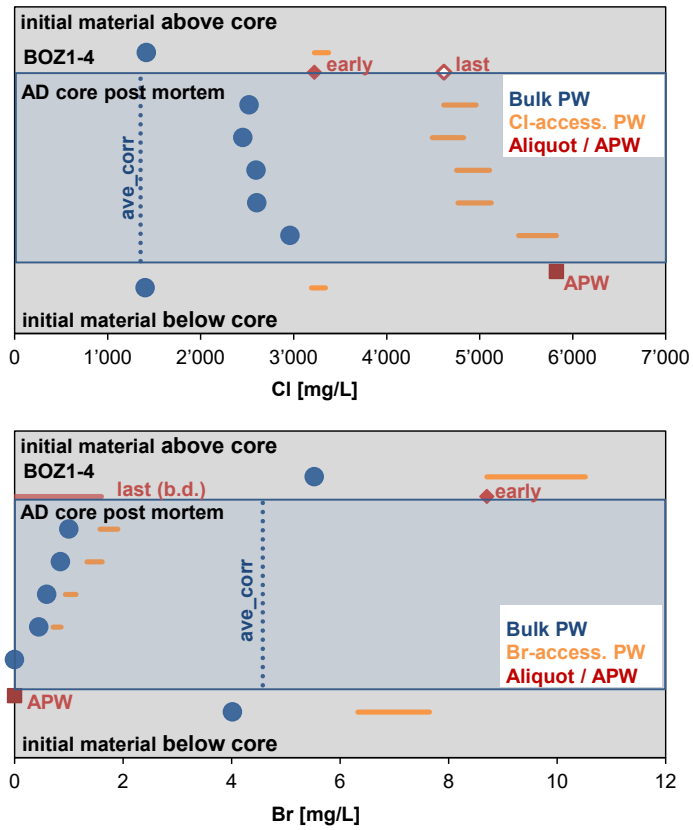

Fig. 4.7-17: Cl and Br concentrations from aqueous extracts up-scaled to bulk porewater and Cl/Br accessible porewater concentrations for the initial material and post-mortem profile of AD experiment BOZ1-4 (BOZ1-1-575.26-AD, Opalinus Clay)

Aliquots and APW used for the derivation of the accessible porosity fractions are indicated in red. The orange bar indicates the range of Cl and Br concentration obtained for the range of accessible porosity fractions (Tab. 4.7-16). For Cl, the upscaling for the initial/early samples and post-mortem samples were done with the corresponding dataset, whereas for Br only accessible porosity fractions based on pre-aqueous extracts and the early aliquot were calculated and used for scaling of both, initial and post-mortem profile.

Tab. 4.7-16: Chloride and bromide-accessible porosity fractions

Parameter	**Unit**	**BOZ1-1**	**BOZ1-3**	**BOZ1-4**	**BOZ1-5**	**BOZ1-6**
Depth	[m]	469.40	516.72	575.26	665.40	697.51
Geol. unit		Hauptrogenstein	Passwang Fm.	Opalinus Clay	Staffelegg Fm.	Klettgau Fm.
Cl-AD_ave (1-2)	[mg/L]	3'940	3'383	3'224	2'507	1'262
Br-AD_ave (1-2)	[mg/L]	11.25	9.30	8.71	5.75	
Cl_AD_last	[mg/L]	3'528	5'541	4'615	4'063	4'421
Cl-AqEx-upscaled_top	[mg/L]	1'577	1'033	1'417	1'113	257
Cl-AqEx-upscaled_base	[mg/L]	1'822	1'099	1'403	1'164	252
Cl-AqEx-upscaled_ave_corr	[mg/L]	**1'622**	**1'054**	**1'353**	**1'062**	**250**
Br-AqEx-upscaled_top	[mg/L]	7.18	3.44	5.52	3.08	bd
Br-AqEx-upscaled_base	[mg/L]	8.94	3.75	4.01	3.27	bd
Br-AqEx-upscaled_ave_corr	[mg/L]	7.67	3.55	4.57	2.97	bd
Cl-AqEx-upscaled_top_p-m	[mg/L]	2'247	2'413	2'522	2'239	2'065
Cl-AqEx-upscaled_base_p-m	[mg/L]	2'740	2'349	2'961	3'434	2'495
Cl-AqEx_top / Cl-AD_ave		0.40	0.31	0.44	0.44	0.20
Br-AqEx_top / Br-AD_ave		0.64	0.37	0.63	0.54	bd
Cl-AqEx_ave / Cl-AD_ave		0.43	0.32	0.44	0.45	0.20
Br-AqEx_ave / Br-AD_ave		0.72	0.39	0.55	0.55	bd
Cl-AqEx_ave_corr / Cl-AD_ave		**0.41**	**0.31**	**0.42**	**0.42**	**0.20**
Br-AqEx_ave_corr / Br-AD_ave		0.68	0.38	0.53	0.52	bd
Cl_AqEx_p-m_top / Cl_last_AD		*0.64*	0.44	0.55	0.55	0.47
Cl_AqEx_p-m_base / Cl_APW		*0.47*	0.40	0.51	0.59	0.43

Preferred values are shaded in blue; empty cells: no sample taken due to limited core size; n.m.: not measured; b.d.: below detection; BOZ1-1 values in *italic* are uncertain due nitrate disturbances and the low hydraulic conductivity.

4.7.7 Transport properties marked by breakthrough of δ^2H, $\delta^{18}O$, Cl and Br

There are four components that can be used to elucidate transport properties by their breakthrough behaviour, namely Cl, Br, and the water isotopes δ^2H and $\delta^{18}O$. Chloride is a good tracer in the experiments BOZ1-3, BOZ1-4, BOZ1-5 and BOZ1-6, because the APW is distinctly more saline than the in-situ porewater. Bromide is a break-out tracer that is gradually flushed out of the core (no Br in the APW). Again, as a full break-out is approached, bromide concentrations tend to fall below the detection limit. Water tracers also feature a considerable contrast between the in-situ porewater (Tab. 4.7-15) and the APW.

For comparison (Fig. 4.7-18) all breakthrough data are normalised to 1 and bromide is inverted to mimic a breakthrough behaviour. The normalised breakthrough of chloride, for example, is given by $1-(Cl-Cl_{APW})/(Cl_{PW}-Cl_{APW})$, where Cl_{PW} refers to the value of the early aliquots representing the in-situ porewater composition (Tab. 4.7-14).

Chloride breakthrough is comparable to bromide in BOZ1-5, slightly faster in BOZ1-3 and slower in BOZ1-4 (BOZ1-6 Br is below detection). A similar behaviour was illustrated in earlier work by Mäder (2018), where a slightly faster breakthrough for Br was observed. BOZ1-1 shows initial Cl concentrations increasing towards the APW but then deceasing rapidly, away from the APW concentration before rising again, and this is not in line with a normal conservative breakthrough behaviour. In this sample very high nitrate concentrations may have disturbed a normal breakthrough, and Cl may not behave as a conservative tracer. Bromide breakthrough cannot be tracked beyond the percolation progress where it drops below detection (seemingly missing points in Fig. 4.7-18). There is some ambiguity in dealing with data scatter that may be present in the first few syringe compositions (e.g. Br, Cl), and the choice made to define the initial value that is used for normalisation of breakthrough curves. Different choices may shift curves somewhat, but this is a minor effect for these relatively smooth data trends.

Fig. 4.7-19 illustrates the breakthrough behaviour of the Br/Cl molal ratio vs. time (pore volume fraction). Plotting the ratio removes some of the data scatter of the individual data series and illustrates similarities between the different experiments and thus also highlights any differences. BOZ1-1 is the only experiment that does not plot on a set of nearly parallel curves. This is also the experiment with the largest nitrate elution (production) as illustrated in the lower graph of Fig.4.7-19, but it is not entirely clear if this is really the cause for the somewhat aberrant trend. The trends of decreasing Br/Cl ratios are mainly caused by the washing out of bromide (no Br in the injected APW), the increase in Cl concentrations towards the APW and to a minor extent by the small observed difference of Br transport vs. Cl transport properties (mentioned above).

$\delta^{18}O$ is expected to break through more slowly compared to the anions Br and Cl, and this is observed in BOZ1-3 and BOZ1-6. In BOZ1-4 and BOZ1-5 the $\delta^{18}O$ breakthrough is faster compared to the other tracers. δ^2H displays an anomalous behaviour during the early breakthrough, possibly for reasons discussed in Section 4.7.5. Deuterium lags considerably behind oxygen; this is currently not understood.

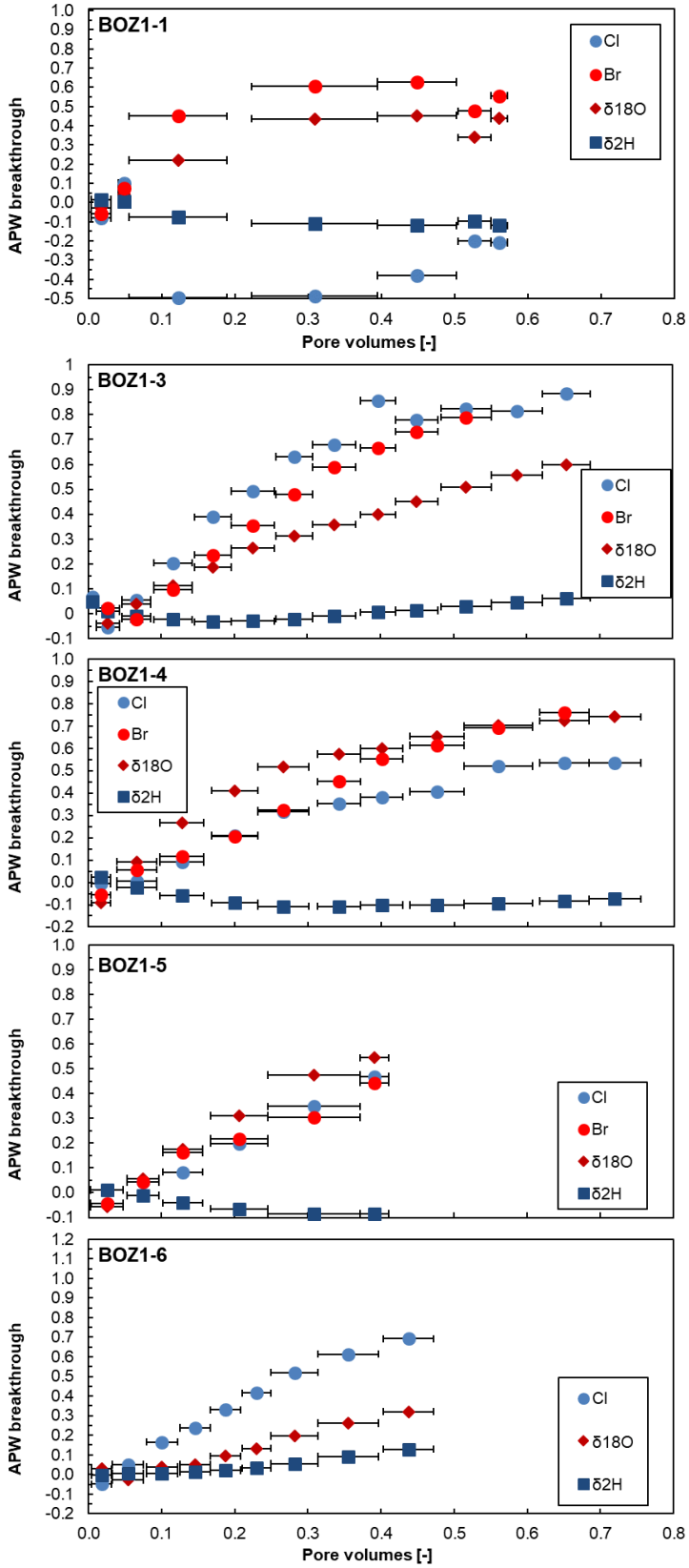

Fig. 4.7-18: Breakthrough of Cl, Br, δ^2H and $\delta^{18}O$ during advective displacement experiments

For legend see Fig. 4.7-4. Horizontal length of symbol bar covers the sampling interval.

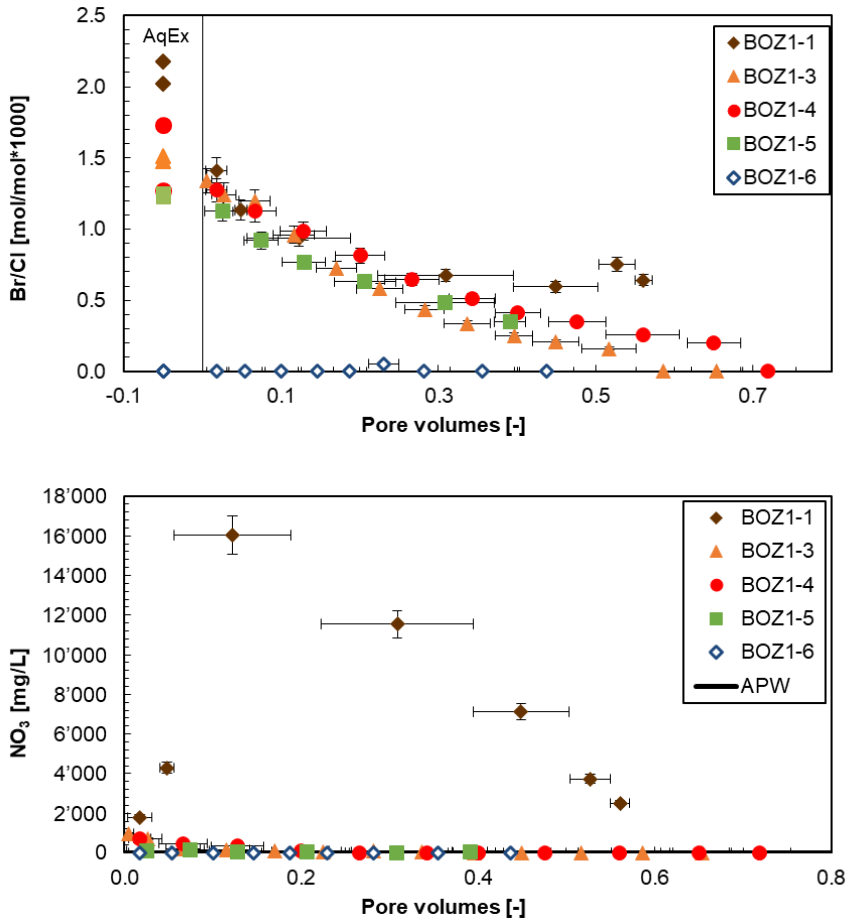

Fig. 4.7-19: Breakthrough of Cl/Br and NO_3 during advective displacement experiments

Data on left side (top graph, 'Aq Ex') are the ratios measured in the aqueous extracts perfomed for pre-characterisation. Ratios plotted at 0 correspond to later aliquots where Br concentration drops below detection. BOZ1-1 = BOZ1-1-469.40-AD (Hauptrogenstein); BOZ1-3 = BOZ1-1-516.72-AD (Passwang Fm.); BOZ1-4 = BOZ1-1-575.26-AD (Opalinus Clay); BOZ1-5 = BOZ1-1-665.40-AD (Staffelegg Fm.); BOZ1-6 = BOZ1-1-697.51-AD (Klettgau Fm.).; APW = artificial porewater. Pore volume fractions relate to transport time based on water content. Horizontal length of symbol bar covers the sampling interval.

4.7.8 Concluding remarks and open issues

Five technically successful advective displacement experiments were conducted on samples from the Dogger units, lower Liassic and Keuper, especially focussing on the derivation of constraints for a representative porewater composition, and with less emphasis on transport properties. Thus, experimental duration was in general shorter than for BUL1-1 (Mazurek et al. 2021). Nevertheless, a systematic and consistent dataset on petrophysical and geochemical properties was obtained not only of value for the specific site characterisation but also for interpretation of porewater chemistry and chloride / bromide accessible porosity fractions across all TBO drilling sites. Data from one experiment with a sample from the Hauptrogenstein (BOZ1-1) is not considered reliable due to its anomalous hydraulic behaviour, and a very large nitrate production at early times.

Advective displacement experiments on samples from the clay-rich confining units supplied a large amount of systematic, consistent and plausible data on petrophysical and geochemical properties of high quality. Samples covered a clay-mineral content of 25 – 45 wt.-% (without failed BOZ1-2), with similar proportions of (illite/smectite + smectite) compared to total clay, and a derived anion-accessible porosity fraction of 0.20 – 0.55 for chloride and 0.38 – 0.68 for bromide. The post-mortem calculated anion-accessible porosity fraction is consistently higher compared to the pre-characterisations, likely due to considerable difference in ionic strength between the porewater and the APW. The hydraulic conductivities are similar for all core samples tested but porosities differ and thus also volumetric fluxes induced by identical head gradients.

Earliest displaced aliquots are representative of the porewater contained in the sample cores but possibly subject to some artefacts. This sampled porewater differs from the in situ porewater due to issues of drilling, unloading, handling and storage. While derived Cl and Br concentrations are robust with respect to such artefacts, the sulphate system in all aliquots appears to be controlled by celestite equilibrium. This either implies that such a control is imposed by these minerals being initially present, or that a disturbance causes to reach such a solubility-product control. In the latter case, the reconstruction of the porewater sulphate concentration is more challenging, and also influences the carbonate system and clay-exchanger complex by ways of interdependent thermodynamic mass-action equilibria.

Like in all earlier work, there are unusually high concentrations of TOC mobilised in the earliest aliquots, decreasing gradually to values more in line with aqueous extracts, but still at significant concentrations. Remarkably, early aliquots of the core from the Hauptrogenstein show large nitrate concentrations (1'803 – 4'300 mg/L) that increases further to 16'000 mg/L before gradually decreasing at later sampling times, a feature not observed in samples from BUL1-1 and TRU1-1 but in two samples of MAR1-1. Corresponding aqueous extracts from post-mortem samples show still increased nitrate concentrations. The origin of this nitrate is likely the kerogenous solid organic matter, but the mechanisms of its mobilisation or liberation are not known. There is relatively little data and experience to compare such findings.

An interesting feature – not yet well understood – is the observed delayed breakthrough of deuterium ($\delta^{2}H$ traced in the APW) compared to $\delta^{18}O$ that elutes more regularly as expected for a water tracer. It is unclear if this observation is related to the elevated amount of nitrate measured in the sampled aliquots.

An initial decreasing trend of deuterium isotopic signatures in early displaced aliquots is suspected to be either caused by different fractionation during partial or full equilibration between the anion accessible and anion inaccessible pore space, or the result of minor evaporation from the surface during dry cutting of the core. Alternatively – or in addition – a very early but limited APW breakthrough along a preferential flow path (unsaturated core surface) might lead to an initial increase in deuterium, but also a decrease in $\delta^{18}O$. The high concentrations of TOC may also influence the water isotopic system, or any microbial activity, as well as any precipitation of hydrous minerals that may be induced by advective displacement.

There are no fundamental adaptations to the methods prompted by this study. The mechanical, hydraulic and electronic or sensor aspects of the experimental setup reliably performed for the duration of the experiments and even longer. Likewise, the analytical procedures were already optimised and adequate, naturally limited by very small sample volumes for some cases.

The large gas volumes exfiltrating mainly at the beginning of the experiments (Tab. 4.7-2), but in some cases continuing throughout the entire percolation period, cannot be explained by initial dead volumes and initially undersaturated porosity in the core, or He dissolved in the APW at

infiltration pressure (45 – 49 bar) and outgassing due to pressure decrease to 1 bar. During MAR1-1 and BOZ1-1 experiments, selective gas analysis revealed considerable volumes of Ar and Kr (where substituted for Ar) in the exfiltrating gas, which originates from the core confinement water, where Ar (or Kr) was used in the pressurised headspace. Therefore, an essentially gas-free confining pressure system was installed starting with samples from TBO STA2-1. However, both Ar and He in the exfiltrating system do not significantly influence the solution composition.

In future experiments, a piston pump generates the confining pressure, where no gas phase is in contact with the confining fluid (water). Also, hydraulic diaphragm accumulators were introduced for future experiments that intrinsically separate the pressurised medium (water in our case) from the pressurised nitrogen reservoir by a thick rubber diaphragm.

4.8 Water-isotope data from diffusive-exchange experiments

Lukas Aschwanden & Thomas Gimmi

The porewater isotope composition ($\delta^{18}O$, $\delta^{2}H$) was derived by isotope diffusive-exchange experiments conducted on core material of 111 samples collected across an interval of 260.6 – 1'029.3 m depth. The obtained highly resolved profiles for $\delta^{18}O$ and $\delta^{2}H$ cover the lithologies from the Wildegg Formation of the Malm to the Permian Weitenau Formation. All experiments were conducted at the University of Bern. The relevant data are summarised in Appendix A.

4.8.1 Data evaluation

4.8.1.1 Experimental and analytical data

All the isotope diffusive-exchange experiments followed the experimental and analytical protocol given in Waber (ed.) (2020). The evaluation of the experimental and analytical data underlying the derivation of the water stable isotope composition of the in situ porewater followed a standardised procedure as detailed below.

In order to qualify for a successful isotope diffusive-exchange experiment the following criteria had to be met (within the propagated analytical uncertainties) by the two experiments (so-called LAB[9] and NGW[10] experiments) conducted for one core sample:

- No severe leakage (evaporation). In most cases, the mass of the experiment container including rock and test water before and after experiment remained constant (± 0.04 g). If the difference in mass was > 0.04 g, corrections were applied to the measured isotope value of the equilibrated test water by Rayleigh-distillation calculations before calculating the porewater isotope ratio, assigning the mass loss to evaporation of the initial test water. If the correction of the $\delta^{18}O$ value for evaporation was > 0.5 ‰ VSMOW (typically meaning that the mass loss of test water was > 5% of the initial mass of test water), the porewater isotope value was marked as less reliable.

[9] LAB: Isotope diffusive-exchange experiments with laboratory tap water used as test water.

[10] NGW: Isotope diffusive-exchange experiments using test water depleted in ^{18}O and ^{2}H (melt water of Antarctic ice cores).

- Reasonable mass ratio of porewater to test water yielding a change in the isotope signal of the test water after equilibration outside the propagated analytical uncertainty. Porewater to test water ratios as low as 0.1 – 0.2 render the calculated isotope composition of the porewater less reliable, whereas at porewater to test water ratios of < 0.1 it becomes unreliable. The mass of porewater in an experiment is defined by the mass of rock and its gravimetric water content. The latter is not known when starting an experiment.
- Limited mass transfer between rock and test water, i.e. i) limited transfer of test water to rock (< 0.5 $m_{\text{test water}}$) caused either by high salinity of porewater compared to test water or hydrating mineral phases (e.g. anhydrite, halite) or ii) limited transfer of porewater to test water (< 0.02 g) caused by high salinity of test water compared to porewater. Such mass transfer between rock and test water may lead to isotope fractionation processes whose impacts on the experiments are poorly understood. Porewater isotope data not fulfilling these criteria are kept but classified as less reliable provided that the experiments do not show any further unconformities and that the calculated porewater isotope data and water contents derived from isotope mass balance agree well with those of neighbouring samples (i.e. within the propagated analytical uncertainty). If this is not the case (i.e. the data constitute outliers), the experiments are considered as failed.
- Stable isotope analyses of test water solutions within the required accuracy.

Of the 111 investigated samples (222 individual experiments) 6 experiment couples did not pass these criteria, mainly owing to 1) transfer of porewater to the test water, 2) porewater to test water ratios smaller than 0.1 (concerning anhydrite-rich samples) and 3) a large transfer of test water to rock (Tab. 4.8-1). Porewater isotope compositions calculated from these experiments are unreliable and will not be shown in the following graphs.

For 10 samples the experimental data resulted in an elevated uncertainty of the calculated isotope composition of the in situ porewater. Four samples show minor evaporation of the test water (5 – 10%; corrected by Rayleigh-distillation calculations) during the experiments, two samples show low porewater to test water ratios of 0.1 – 0.2, another two samples show minor transfer of porewater to test water and for the remaining two samples tiny pieces of rock material fell into the test water. Porewater isotope compositions calculated from these experiments are afflicted by somewhat larger uncertainties. These data are shown but marked with open symbols in the following graphs.

4.8.1.2 Calculation of porewater composition and water contents

Porewater $\delta^{18}O$ and $\delta^{2}H$-values were calculated using equation 76 in Appendix A in Waber (ed.) (2020) considering the ratio q of the gravimetric water contents of the individual subsamples used in the experiments (for details see Appendix A in Waber (ed.) 2020). Water contents could then also be calculated by mass balance from the porewater isotope values. The robustness of the calculated porewater $\delta^{18}O$ and $\delta^{2}H$-values was further tested according to the following criteria:

1. A relative difference of less than 20% between the water contents calculated from $\delta^{18}O$ and $\delta^{2}H$ data derived from the experiments with test water depleted in ^{18}O and ^{2}H (NGW subsamples).
2. A relative difference of less than 20% between the average water content calculated by isotope mass balance from $\delta^{18}O$ and $\delta^{2}H$ data and the average of the gravimetric water content of the two subsamples used in the experiments.

If the relative difference in the different water contents is larger than 20% the calculated porewater $\delta^{18}O$ and $\delta^{2}H$-values are considered less reliable. Such data may still be used for further interpretation by accepting the larger propagated uncertainty; they are marked with open symbols in the following graphs.

All of the 105 samples that passed the experimental quality criteria (*cf.* Section 4.8.1.1; including samples with elevated experimental uncertainties) pass criterion 1 above (Fig. 4.8-1), however, 6 samples do not pass criterion 2 (Fig. 4.8-2). Three of these samples that fail the comparison of the water contents are afflicted by larger uncertainties from the experiments themselves (*cf.* Section 4.8.1.1). In these cases, the failure of criterion 2 is due to experimental artefacts. The other 3 samples that fail the comparison of the water contents do not show any experimental irregularities. In these cases, the differences between the average of the water contents derived by isotope mass balance and the average of the gravimetric water content of the two subsamples likely reflect lithological heterogeneity of the different subsamples used in the two experiments. Note that in anhydrite-bearing lithologies hydration of anhydrite during the isotope diffusive-exchange experiments also plays a role, although its effect is unknown at this stage.

All samples that pass the above criterion 2 display a consistent, previously observed relationship between the average water content derived by isotope mass balance and the average of the gravimetric water content of the subsamples used in the experiments, the former being around 10% larger than the latter (Fig. 4.8-2). As the water content is generally well correlated with the clay-mineral content of the rocks (*cf.* Section 4.3), it was postulated that this difference might be associated with minor exchange with water of different isotope composition adsorbed on clay minerals (e.g. Pearson et al. 2003).

Tab. 4.8-1: Summary of samples which do not fulfil the quality criteria of the isotope diffusive-exchange experiments of BOZ1-1

Porewater isotope compositions calculated from these experiments are unreliable and are not shown in graphs (m_{pw}: mass porewater, m_{tw}: mass test water).

Sample ID	Formation	Transfer of porewater to test water	Transfer of test water to rock	Ratio m_{pw}/m_{tw}	Contamination by drilling fluid
BOZ1-1-413.63-PW	Hauptrogenstein	×			
BOZ1-1-787.44-PW	Bänkerjoch Fm.			< 0.1	
BOZ1-1-811.83-PW	Bänkerjoch Fm.			< 0.1	
BOZ1-1-846.00-PW	Schinznach Fm.				×
BOZ1-1B-879.74-PW	Zeglingen Fm.		×		×
BOZ1-1B-881.21-PW	Zeglingen Fm.				×
BOZ1-1B-907.62-PW	Zeglingen Fm.			< 0.1	
BOZ1-1B-987.48-PW	Dinkelberg Fm.		×		×

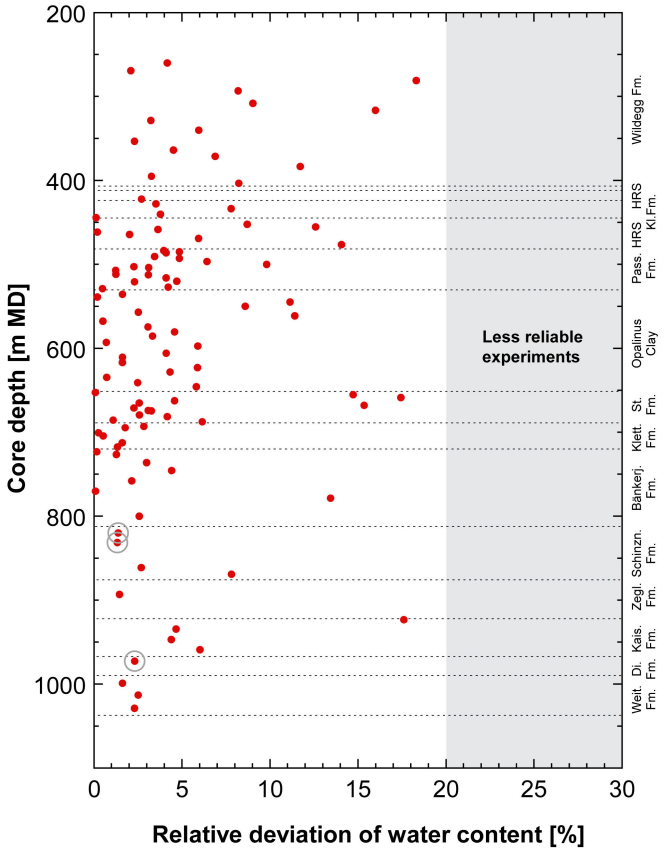

Fig. 4.8-1: Relative deviation of water contents obtained from $\delta^{18}O$ and $\delta^{2}H$ mass balance

The relative deviation is defined as the difference between the water contents calculated from the equilibrated $\delta^{18}O$ and $\delta^{2}H$ values, respectively, of the experiments with test water depleted in ^{18}O and ^{2}H (NGW) divided by the water content based on $\delta^{2}H$. Samples with a grey circle show some signs of contamination by drilling fluid (*cf.* Section 4.4).

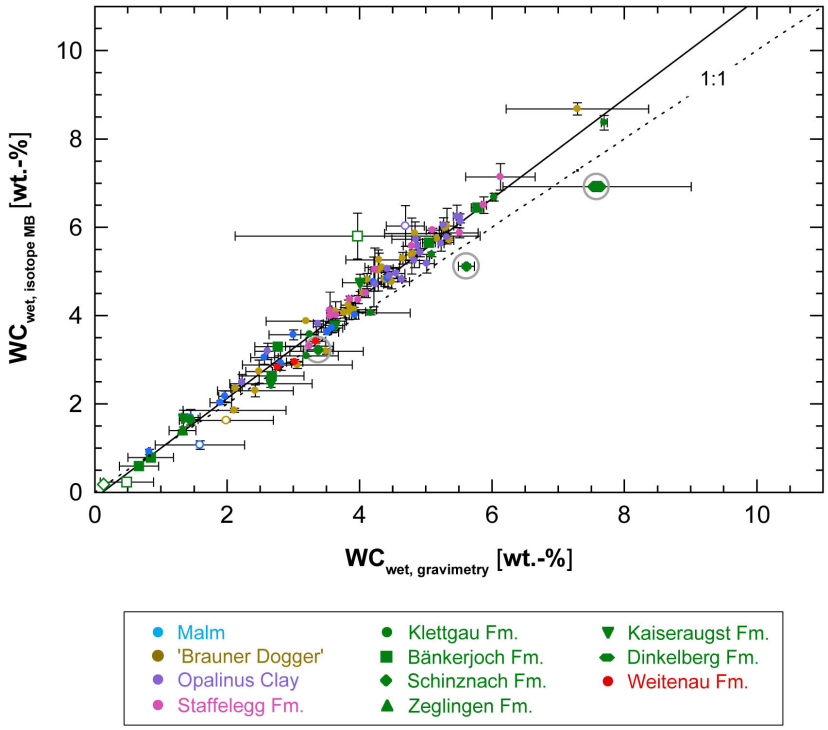

Fig. 4.8-2: Average water content obtained by water-loss at 105 °C ($WC_{wet,\ gravimetry}$) of subsamples LAB and NGW vs. average water content calculated from $\delta^{18}O$ and $\delta^{2}H$ mass balance from NGW diffusive-exchange experiments ($WC_{wet,\ isotope\ MB}$)

Open symbols refer to samples showing differences larger than 20% between the average water content derived by isotope mass balance and the average gravimetric water content of the two subsamples used in the experiment. Samples with a grey circle show signs of contamination by drilling fluid (*cf.* Section 4.4).

4.8.1.3 Contamination by drilling fluid

Contamination of some samples by drilling fluid – even in the central parts of the core material – was identified on the basis of aqueous extract solutions (*cf.* Section 4.4.2). This concerns 5 dolomite-rich samples, 3 from the Schinznach Formation and 2 samples from the Zeglingen Formation, as well as 2 sandstone samples from the Dinkelberg Formation (Tab. 4.4-2). Three of the dolomite samples (BOZ1-1-846.00-PW, BOZ1-1B-879.74-PW and BOZ1-1B-881.21-PW) show rather high porosities (Tab. 4.4-2) and likely elevated permeability allowing percolation of the drilling fluid to central parts of the drill core sample, which significantly affected the porewater isotope composition derived from the isotope diffusive-exchange experiments. Thus, the porewater isotope data of these three samples is not reliable and will not be shown in the following graphs (Tab. 4.8-1; for details see Section 5.7).

Three other samples for which drilling fluid contamination has been identified on the basis of aqueous extracts (BOZ1-1-820.53-PW, BOZ1-1-831.86-PW and BOZ1-1B-973.17-PW) show a distinctly lower porosity (and likely permeability; Tab. 4.4-2) and thus, the effect of contamination on the porewater isotope signature is much less pronounced (for details see Section 5.7). Accordingly, these samples are not excluded from the following graphs but marked with a grey circle being a less reliable datum.

For the seventh sample for which drilling fluid contamination has been identified (BOZ1-1B-987.48-PW) the isotope diffusive-exchange experiments failed (Tab. 4.8-1). Thus, only 3 samples are marked as being contaminated by drilling fluid in the following graphs.

4.8.2 $\delta^{18}O$ and $\delta^{2}H$-values of porewater

4.8.2.1 Depth profiles of porewater isotope composition

All the porewater isotope data that pass the various quality criteria are illustrated in Fig. 4.8-3 as a function of depth. Both $\delta^{18}O$ and $\delta^{2}H$-values of the porewater show well defined, curved profiles across the interval Wildegg Formation – Klettgau Formation. Although both tracers indicate the same general trends, some differences exist. $\delta^{18}O$-values of the porewater remain constant (at around -4.2 ‰ VSMOW) across the Wildegg Formation down to the base of the Passwang Formation. A minor positive excursion is indicated in the Hauptrogenstein at 466 m depth. From the base of the Passwang Formation the $\delta^{18}O$-values of the porewater increasingly become more negative across the Opalinus Clay and the Staffelegg Formation approaching a local minimum of -7.1 ‰ VSMOW at around 712 m depth in the Klettgau Formation. In contrast, $\delta^{2}H$ values of the porewater slightly increase across the Wildegg Formation down to the base of the Opalinus Clay (from around -44 ‰ VSMOW to -38‰ VSMOW) where they start to decrease towards the same local minimum as indicated by $\delta^{18}O$ values in the Klettgau Formation ($\delta^{2}H$ at ~ -46 ‰ VSMOW). The different shapes of the $\delta^{18}O$ and $\delta^{2}H$ profiles are also illustrated in Fig. 4.8-4, which shows the depth profile of deuterium excess (defined as $\delta^{2}H - 8 \times \delta^{18}O$; deuterium excess is +10 ‰ for a sample that lies on the GMWL, lower values of deuterium excess reflect sample positions to the right of the GMWL in a plot of $\delta^{18}O$ vs. $\delta^{2}H$; note that the deuterium excess as used at this stage carries no direct implications about the palaeoclimate at the time of infiltration; it is the result of several interactions – some acting in the deep underground). Across the Wildegg Formation down to the middle of the 'Brauner Dogger' deuterium excess shows a constant trend with values scattering between -13 ‰ and -6 ‰. In the middle of the 'Brauner Dogger' deuterium excess starts to steadily increase across the Opalinus Clay, the Staffelegg Formation and the Klettgau Formation approaching a general maximum of +14.0 ‰ at around 746 m depth in the top of the Bänkerjoch Formation where a trend reversal is indicated.

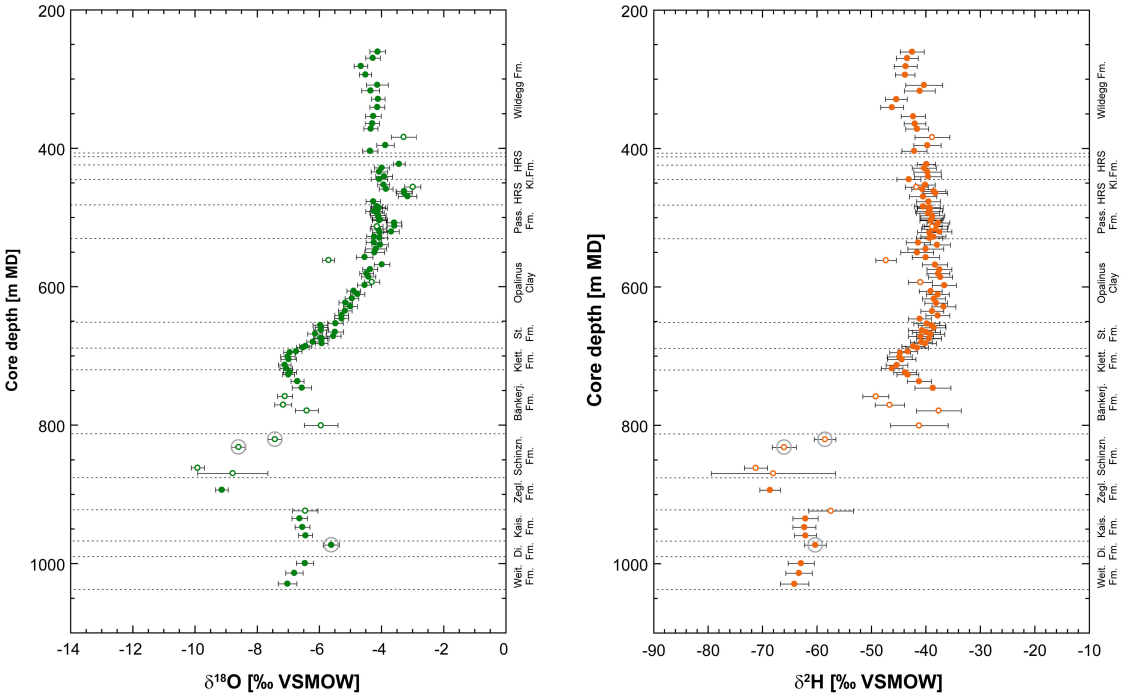

Fig. 4.8-3: Depth distribution of porewater $\delta^{18}O$ and $\delta^{2}H$-values obtained from isotope diffusive-exchange experiments

Open symbols refer to porewater isotope values which are less reliable owing to experimental artefacts (see text). Samples with a grey circle show signs of contamination by drilling fluid (*cf.* Section 4.4.2).

From the local minimum in the Klettgau Formation across the top of the Bänkerjoch Formation both $\delta^{18}O$ and $\delta^{2}H$-values of the porewater increase to values of -6.5 and -38.6 ‰ VSMOW, respectively, at around 746 m depth. Isotope profiles in the deeper Bänkerjoch Formation, the Schinznach Formation and the Zeglingen Formation are less well defined. This is mainly owing to i) the comparatively larger sample spacing, ii) experimental difficulties associated with these lithologies, e.g. low water contents, hydration of anhydrite (samples from the Bänkerjoch Formation marked with open symbols in Fig. 4.8-3 contain > 71 wt.-% anhydrite) and contamination with drilling fluid, which render the calculated porewater isotope signatures less reliable. Nevertheless, both $\delta^{18}O$ and $\delta^{2}H$ profiles indicate a strong gradient at the base of the Bänkerjoch Formation towards distinctly more negative values in the Schinznach Formation where a general minimum is reached at 862.2 m depth ($\delta^{18}O$ = -9.9 ‰ VSMOW; $\delta^{2}H$ = -71.1 ‰ VSMOW). In the underlying Zeglingen Formation only one sample provided reliable porewater isotope data indicating similarly negative values.

Isotope profiles in the Kaiseraugst Formation, Dinkelberg Formation and Weitenau Formation are again better defined at distinctly heavier isotope signatures compared to the overlying Muschelkalk units. Both profiles of $\delta^{18}O$ and $\delta^{2}H$ indicate a slight increase of $\delta^{18}O$ and $\delta^{2}H$ across the Kaiseraugst Formation, a local maximum (trend reversal) in the Dinkelberg Formation and slightly decreasing values across the underlying Weitenau Formation. However, note that most of the porewater isotope data overlap within the propagated analytical uncertainty.

Deuterium excess decreases from its maximum at the top of the Bänkerjoch Formation (+14 ‰) down to the Dinkelberg Formation (-15 ‰; Fig. 4.8-4) where the same trend reversal is indicated as for $\delta^{18}O$ and $\delta^{2}H$. Across the Weitenau Formation deuterium-excess again slightly increases towards heavier values.

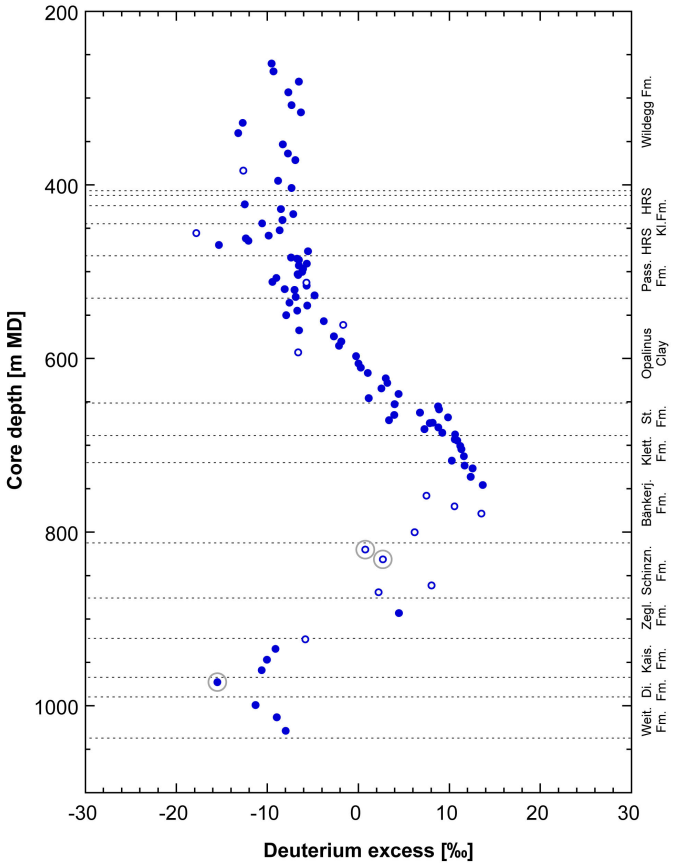

Fig. 4.8-4: Depth trend of deuterium excess in porewater based on the isotope diffusive exchange technique

Deuterium excess is +10 ‰ for a sample that lies on the GMWL. Lower values of deuterium excess reflect sample positions to the right of the GMWL in a plot of $\delta^{2}H$ vs. $\delta^{18}O$. Note that the deuterium excess as used at this stage carries no genetic implications about the origin of H_2O, e.g. on palaeoclimate at the time of infiltration. Open symbols refer to samples which are less reliable owing to experimental artefacts (see text). Samples with a grey circle show signs of contamination by drilling fluid (*cf.* Section 4.4.2).

4.8.2.2 $\delta^{18}O$ versus $\delta^{2}H$ and comparison with Global Meteoric Water Line

Porewater isotope signatures in the Malm fall to the right of the Global Meteoric Water Line (GMWL) and partly overlap with those in the underlying 'Brauner Dogger'. Some of the latter porewaters are slightly enriched in ^{18}O and ^{2}H compared to those in the Malm. From the 'Brauner Dogger' across the Opalinus Clay down to the base of the Staffelegg Formation the porewater isotope composition continuously evolves towards $\delta^{18}O$ and $\delta^{2}H$-values that plot on the GMWL, indicating a dominant meteoric component in the latter porewaters. Similarly, the isotope compositions of the porewater in the Klettgau Formation and the Bänkerjoch Formation have a

meteoric signature, however, partly at somewhat more negative values. At the base of the Bänkerjoch Formation, porewater $\delta^{18}O$ and $\delta^{2}H$ signatures sharply evolve to distinctly more negative values in the water-conducting zone of the Muschelkalk (see Section 5.8 for further discussion) falling slightly to the right of the GMWL. Porewaters in the underlying Kaiseraugst, Dinkelberg and Weitenau Formation are enriched in ^{18}O and ^{2}H and plot further to the right of the GMWL.

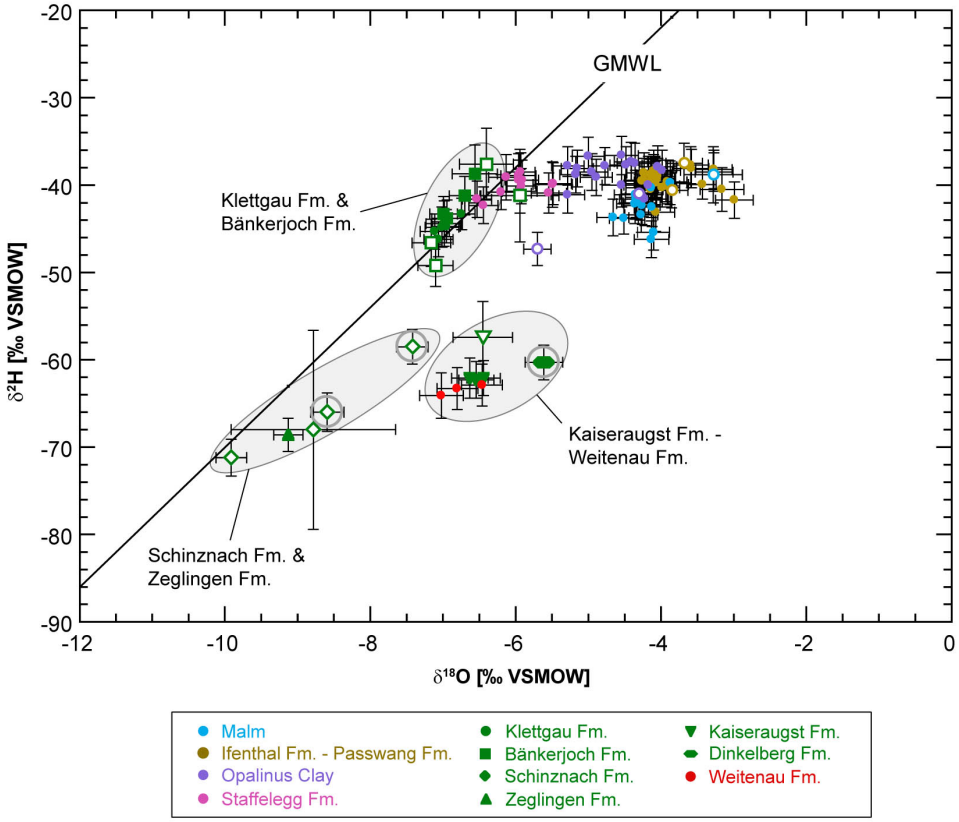

Fig. 4.8-5: $\delta^{2}H$ vs. $\delta^{18}O$-values of porewater obtained from isotope diffusive-exchange experiments

GMWL = Global Meteoric Water Line ($\delta^{2}H = 8 \times \delta^{18}O + 10$ ‰ VSMOW; Craig 1961), open symbols refer to porewater isotope values which are less reliable owing to experimental artefacts (see text). Samples with a grey circle show signs of contamination by drilling fluid (*cf.* Section 4.4.2).

4.9 Out-diffusion experiments

Carmen Zwahlen, Thomas Gimmi & H. Niklaus Waber

Out-diffusion (OD) experiments are another methodology to get insight into the porewater – rock system. Originally designed for crystalline rocks (e.g. Waber et al. 2012), OD experiments for sedimentary rocks are still in a developing stage. OD experiments are non-destructive with respect to the rock and run at higher S:L ratios compared to aqueous extraction tests (*cf.* Section 4.4). A disadvantage of OD experiments is the long duration over several months. Details about the methodology are given in the method report by Waber (ed.) (2020). Here, only the results derived from the final solutions in the experiment are presented, which allow comparisons with aqueous extract data. The full time series will be presented elsewhere.

4.9.1 Sample material and overview of analytical work

The nature of OD experiments restricts such experiments to non-swelling rocks that do not disintegrate when immersed into water over several months. Three drill core samples with different clay mineral contents (14 wt.-%, 42 wt.-% and 39 wt.-%) were chosen from the Klingnau Formation, the Hauptrogenstein and the Passwang Formation ('Humphriesi-Schichten', Fig. 4.9-1). The 3 cylindrical core samples had a mass of about 600 – 620 g and the mass of porewater in the core samples ranged from about 11 to 30 g. About 100 ml of water were added in the experiment, resulting in a solid to liquid ratio of 4.3 to 5.1. After an out-diffusion time of 256 days at 45 °C the closed cylinders were cooled to room temperature (20 °C) followed by removal of the test water and analysis of the solution. Additionally, aqueous extracts were conducted on material adjacent to the out-diffusion cores (see Section 4.4), sampled before running the OD experiments.

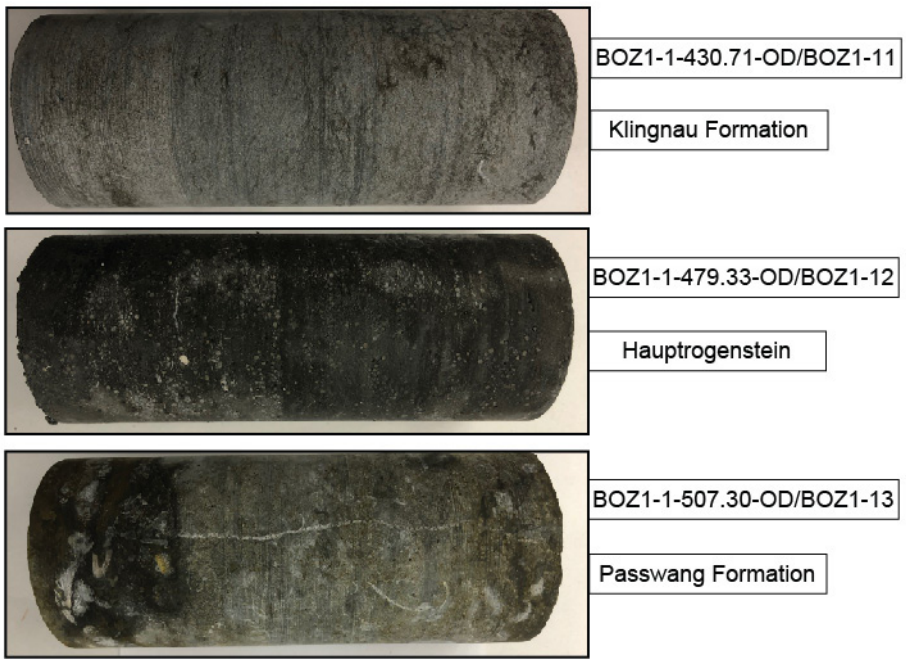

Fig. 4.9-7: Pictures of the three drill cores used for OD experiments from the Klingnau Formation, Hauptrogenstein and Passwang Formation ('Humphriesi-Schichten')

4.9.2 Final OD experiment solutions

The final concentrations of Cl and Br in bulk porewater were calculated for two hypothetical anion accessibility fractions (0.5 and 1) taking the removal of small aliquots during the experiment into account according to

$$C_{bulkOD} = \frac{C_{end}\,(V_{H2Oexp}+V_{pw}\,f_a)+\sum_{i=1}^{15} C_{int(i)}\,V_{int(i)}}{V_{pw}} \qquad \text{(Eq. 1)}$$

with C_{end} the concentration at the end of the OD experiment, V_{H2Oexp} the added water, V_{pw} the pore volume, C_{int} the concentration of sampled aliquots, V_{int} the volume of sampled aliquots, and f_a the anion accessible porosity fraction. The derived bulk porewater concentrations are presented in Tab. 4.9-1 along with data from aqueous extracts of the adjacent subsamples for comparison.

Tab. 4.9-1: Data from the OD experiments, including bulk porewater concentrations of conservative ions recalculated from the final OD solutions with hypothetical anion accessible porosity fractions of 0.5 and 1, and from aqueous extracts

The parameters to calculate the bulk PW OD conentration include for the three experiments (BOZ1-11, BOZ2-12 and BOZ2-13) C_{end} (192, 444 and 356 mg/L), V_{H2Oexp} (0.108, 0.107 and 0.113 L), V_{pw} (0.01, 0.03 and 0.02 L), $\sum C_{int}$ (1941.3, 4434 and 4256 mg/L), V_{int} (0.5, 0.5 and 0.5 ml), f_a, (1, 0.5).

Sample ID	**Clay mineral content**	**OD bulk PW**	**OD bulk PW**	**AqEx bulk PW**	**OD bulk PW**	**OD bulk PW**	**AqEx bulk PW**
		$f_a = 1$ Cl	$f_a = 0.5$ Cl	Cl	$f_a = 1$ Br	$f_a = 0.5$ Br	Br
	[wt.-%]	[mg/L]	[mg/L]	[mg/L]	[mg/L]	[mg/L]	[mg/L]
BOZ1-11	14	2124	2028	1738	6.8	6.5	
BOZ1-12	42	2095	1873	1156	5.3	4.7	5.2
BOZ1-13	39	2600	2422	3708	9.9	9.2	13.2

The bulk porewater Cl and Br concentrations of the three OD experiments differ by 5, 12 and 7%, respectively, between the two hypothetical anion accessible porosity fractions. This is a small difference, which arises from the three to ten times larger volume of added water compared to the amount of bulk porewater, where the anion accessible porosity fraction is factored in (see Eq. 1). We note in passing that for aqueous extracts, the amount of added water is even larger, and the samples are desintegrated, which fully justifies the use of $f_a = 1$ in the evaluation of those data.

The Cl bulk porewater concentrations from two of the three OD experiments are higher than the aqueous extract concentration, while those for the sample from the Passwang Formation (BOZ1-13) are lower. For Br, OD bulk porewater concentrations are similar as the AqEx concentration for the Hauptrogenstein sample, but lower for the Passwang Formation sample.

Several processes can be responsible for the observed concentration differences between the OD and the aqueous extracts. Higher concentrations in the aqueous extracts compared to the OD can result from the contribution of fluid inclusions that get destroyed during the sample preparation.

Concentrations calculated from OD data are affected by the assumed value of fa, with calculated concentrations becoming higher for higher fa (Tab. 4.9-2). Based on the idea that concentrations derived from OD and from aqueous extracts should in principle be identical, it would even be possible to derive fa from a direct comparison. However, the sensitivity to this parameter is relatively small, as seen above, and the differences are clearly beyond the limits set by the possible range of f_a. Local heterogeneities in water contents are another possible source of differences, as they may affect concentrations calculated from aqueous extracts, but its effect is also limited. Overall, it is currently unclear what may have caused differences beyond the analytical uncertainty, which is 5 – 10%.

Finally, the 'free' porewater concentration can be calculated from the bulk porewater concentrations in the usual, simplified way based on the anion accessible porosity fraction. Neglecting the difference in ionic strength between the final OD solution and the 'free' porewater, a consistent evaluation requires using the same value of f_a for this calculation as that used for the evalution of the experiment. Accordingly, for f_a of 0.5 the Cl and Br bulk porewater concentrations would double and for f_a of 1 they would stay the same. This results in a 'free' porewater concentration range presented in Tab. 4.9-2.

Tab. 4.9-2: Data of the OD experiments recalculated to 'free' porewater concentrations with a range given by hypothetical anion accessible porosity fractions of 0.5 and 1

Sample ID	**OD 'free' PW Cl** [g/L]	**OD 'free' PW Br** [mg/L]
BOZ1-11	2.1 – 4.1	6.8 – 13.0
BOZ1-12	2.1 – 3.7	5.3 – 9.4
BOZ1-13	2.6 – 4.8	9.9 – 18.4

5 Discussion of porewater data

5.1 Chloride data and estimation of Cl^- and Br^--accessible porosity

Paul Wersin, Martin Mazurek, Thomas Gimmi, Carmen Zwahlen

Chloride, a major compound in the porewater, has been determined by squeezing (Section 4.6), advective displacement (Section 4.7) and aqueous extraction (Section 4.4). This anion is considered to behave as a conservative species with no or very limited interaction with the minerals. The same can be said for bromide, which occurs at much lower concentrations in the porewater. In argillaceous rocks, anions are repelled from the negative structural charge of the clay-mineral surfaces and are thus affected by ion exclusion. In other words, they only 'see' part of the total water-filled porosity, the fraction of which is often termed anion-accessible porosity (Pearson 1999, Pearson et al. 2003). Ion exclusion is not complete according to theory and depends on distance from charged surfaces, but here this simplifying assumption is made for adopting a simplest possible model.

Knowing the concentration of Cl and/or Br in a sample from aqueous extraction ($C_{Cl\ in\ bulk\ porewater}$), the Cl-accessible porosity fraction, f_{Cl}, can be estimated from Cl and/or Br measurements in squeezing ($C_{Cl\ in\ squeezed\ water}$) or advective displacement ($C_{Cl\ in\ adv.\ displaced\ water}$) experiments, assuming that the latter represent the composition of the free porewater:

$$f_{Cl} = \frac{n_{anion-accessible}}{n_{total}} = \frac{C_{Cl\ in\ bulk\ pore\ water}}{C_{Cl\ in\ squeezed\ or\ adv.displaced\ water}}$$

$C_{Cl\ in\ bulk\ porewater}$ is calculated from

$$C_{Cl\ in\ bulk\ pore\ water} = \frac{C_{Cl\ in\ aq.extract}}{WC_{dry}\ {}^{S}/_{L}}$$

with C = concentration [mg/L], n = porosity [–], WC_{dry} = water content relative to dry rock mass [g/g], S/L = (dry) solid/liquid ratio of aqueous extraction experiment [g/g]. The Br-accessible porosities are derived in an analogous fashion.

The anion-accessible porosities have been derived according to the above equation for squeezed and advectively displaced porewaters (Tabs. 4.6-7 and 4.7-16). Both methods enable to mobilise porewater that is thought to represent the mobile porewater and a proxy of the so-called "free" porewater (not affected by the negatively charged clay surface). It should be noted, however, that the two methods operate by entirely different mechanisms. Whereas porewater is mobilised by mechanical compaction implying a deformation of the porespace in the squeezing method, this is achieved by a strong hydraulic and pressure gradient and an artificial porewater in the advective displacement method. Thus, method-specific artefacts may be expected and likely not the same volume of the porespace is sampled by the two methods. In the case of Cl, experimental artefacts appear to be minor as suggested from previous studies (e.g. Mazurek et al. 2021). Referring to squeezed waters, it is generally assumed that the waters squeezed at the lowest pressure best reflect the in-situ porewater (Mazurek et al. 2015, Wersin et al. 2016). For the advectively displaced waters, the first two aliquots are assumed to be the most representative of the in-situ porewater (Section 4.7).

The derived values of the Cl-accessible porosity fraction (f_{Cl}) for the two datasets are shown as a function of the clay-mineral content in Fig. 5.1-1 (left). Broadly consistent porosity fractions are obtained from the two methods, showing no trend with clay-mineral content above 25 wt.-%, which corresponds to the sample with lowest clay-mineral content. The corresponding mean value from both methods is 0.42 ± 0.08[11]. The AD data, however, tend to have lower f_{Cl} values relative to SQ data, even though they their clay-mineral contents tend to be lower. Overall, the derived values are somewhat lower than in the deep borehole BUL1-1, but in the same range as in TRU-1-1 and MAR1-1 The latter two boreholes, however, suggested an increasing trend of f_{Cl} with decreasing clay-mineral content already from values below 40 wt.-%, which is not reflected in the SQ and AD datasets of BOZ1-1 (for BUL1-1, such a trend appeared only at values < 20 wt.-%). The chloride concentrations and thus the ionic strengths are the lowest in the BOZ1-1 borehole, followed by MAR1-1, TRU1-1 and BUL1-1. A lower ionic strength tends to decrease the anion accessibility according to theory (but quantification for specific samples is difficult).

A further possibility to estimate anion-accessible porosities in argillaceous rocks is via through-diffusion tests with anionic tracers (Cl, Br) in combination with a water tracer (e.g. HTO). From the ratio of the derived diffusion-acessible porosity of the anion and the water tracer the anion-acessible (diffusion) porosity fraction can be obtained. Note that the volume of the anionic porespace deduced from diffusion tests does not necessarily correspond to the mobilised water fractions of AD or SQ. Through-diffusion experiments of HTO and ^{36}Cl were carried out on 33 samples of the BOZ1-1 borehole at PSI (Van Loon & Glaus *in prep*.). The corresponding Cl-accessible porosity fractions are illustrated in Fig. 5.1-1 (right). These reveal a considerable scatter at clay-mineral contents < 40 wt.-%, but nevertheless a generally weakly increasing trend of f_{Cl} with decreasing clay-mineral content is observed. Some outliers are evident:

- The sample from the upper Hauptrogenstein ('Spatkalk') shows a high value for f_{Cl}. The same is true for two samples from the Klingau Formation (all are labelled in Fig. 5.1-1, right). These samples have in common that they contain 1 – 6 wt.-% goethite and thus relate to mineralogically distinct lithologies and therefore pore architectures. This is also evident from the pore characteristics derived from N_2 adsorption: The samples from the upper Hauptrogenstein and from the Klingnau formation show rather large average pore radii compared to other limestones or calcareous marls.
- The sample from the Klettgau Formation also shows a high f_{Cl}. It is a heterogeneous sandstone (quartz + feldspars = 60 wt.-%), consisting of cm-thick, alternating beds of sandy and clay-rich material.
- Two samples, one from the Wildegg Formation and one from the Passwang Formation, fall off the general trend and have low f_{Cl}. At this stage, these aberrant values cannot be explained by mineralogical arguments.

Disregarding these outliers, the agreement between SQ/AD and diffusion data is fair to poor. In particular, the latter data display lower Cl-accessible porosities in the Opalinus Clay, as discussed below. Moreover, the relationship with clay-mineral content is not matched between the datasets. It is also worth noting that the diffusion data of BOZ1-1 generally suggests lower f_{Cl} values compared to analogous data from the BUL1-1 and TRU1-1 boreholes.

[11] Note that the average is pulled down by one AD sample (dolomitic marl) from the Klettgau Formation.

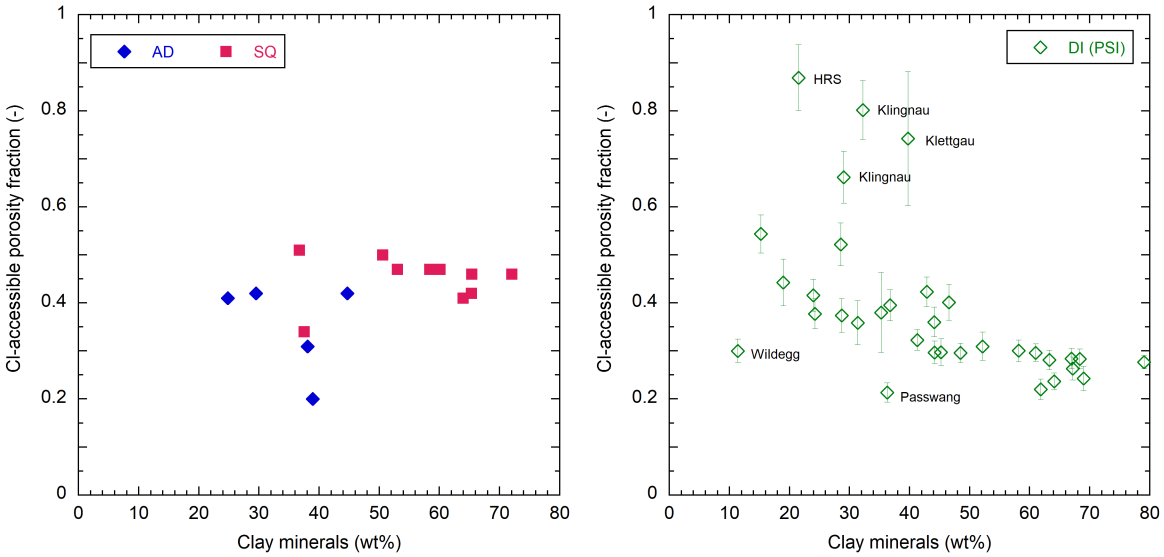

Fig. 5.1-1: Cl-accessible porosity fraction as a function of the clay-mineral content, left: AD and SQ data; right: diffusion data (PSI)

Diffusion data indicate propagated analytical errors.

Within the sampled interval, the lithologies in the BOZ1-1 profile vary substantially. In order to derive a porewater profile for Cl, the anion accessibility in these lithologies must be known or assumed. On the basis of the f_{Cl} -clay-mineral content trend displayed by SQ and AD data, a f_{Cl} value of 0.42 is used for clay-mineral contents ≥ 25 wt.-%. Below this clay-mineral content, a linear increase of f_{Cl} to a value of 1 at a clay-mineral content of zero is assumed. Diffusion data (disregarding the samples that fall off the general trend) and data of previous boreholes (Mazurek et al. 2021, Aschwanden et al. 2021, Mäder et al. 2021) qualitatively support this trend for lower clay-mineral contents. However, this represents very likely an oversimplification.

The fact that f_{Cl} shows such a wide range when plotted against the clay-mineral content suggests that the latter is not the only parameter that determines anion accessibility. Mean pore size, grain-size distribution, fabric and other factors are expected to affect anion accessibility as well. Note that the negative structural charge of the clays is predominately carried by the smectite and illite components. Furthermore, according to theory, anion accessibility also varies with the salinity and composition of the porewater, i.e., it is not just a material property. All these partly inter-dependent effects cannot be properly quantified at this stage, which severely limits the application of theoretical models.

An uncertainty range of ± 20% is considered for f_{Cl}, as has been used for previous boreholes. For BOZ-1-1, an even larger uncertainty range cannot be excluded, based on the discrepancy beween AD/SQ data and diffusion data. This uncertainty propagates into the calculated Cl concentrations in the anion-accessible porewater, i.e., an error of ± 20% must be considered in addition to the propagated analytical error.

For Br, only advective displacement data are available. The derived f_{Br} values as a function of the clay-mineral content are illustrated in Fig. 5.1-2. The mean f_{Br} value for the four samples where these values could be derived is 0.53 ± 0.12. This is higher than the corresponding mean f_{cl} value for the same four AD samples (0.39 ± 0.05). The reason for this difference is not clear at this stage.

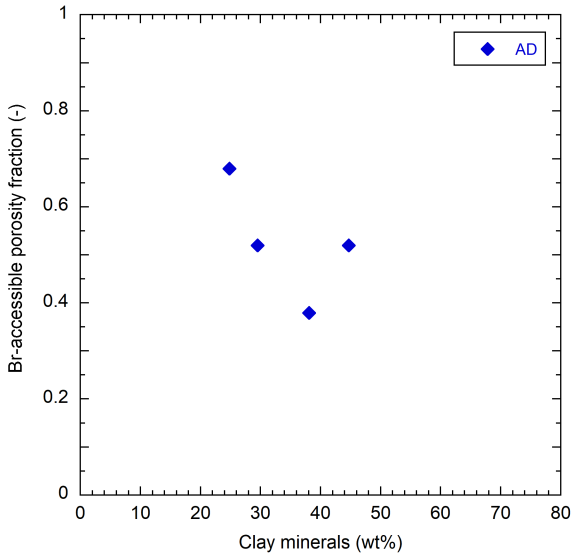

Fig. 5.1-2: Br-accessible porosity fraction as a function of the clay-mineral content derived from AD data

Fig. 5.1-3 illustrates the Cl-accessible porosity fraction as a function of depth. Comparison of the broadly consistent SQ and AD data with the diffusion data indicate both similarities and differences depending on the stratigraphic unit. Thus, a rather good match of data is revealed in the units confining the Opalinus Clay, i.e. the Passwang Formation and the Staffelegg Formation. In the Opalinus Clay itself, however, a systematic shift between AD/SQ and diffusion data is evident. The former data display constant f_{Cl} values, with an average of 0.44 ± 0.03, whereas the latter data show distinctly lower values with generally decreasing trend with depth. This is explained by the clay-mineral content that tends to increase with depth in the Opalinus Clay and the diffusion data that suggest a decrease of f_{Cl} with increasing clay-mineral content (Fig. 5.1-1 right).

A striking feature are the high Cl-accessibilities obtained for the Klingnau Formation and the upper Hauptrogenstein from the diffusion data. As stated above, these samples contain goethite, which reflects distinct depositional environments and therefore pore architectures. Low external surface areas (Section 4.3.5) in these units indicate relatively large mean pore sizes, as shown in Fig. 4.3-17.

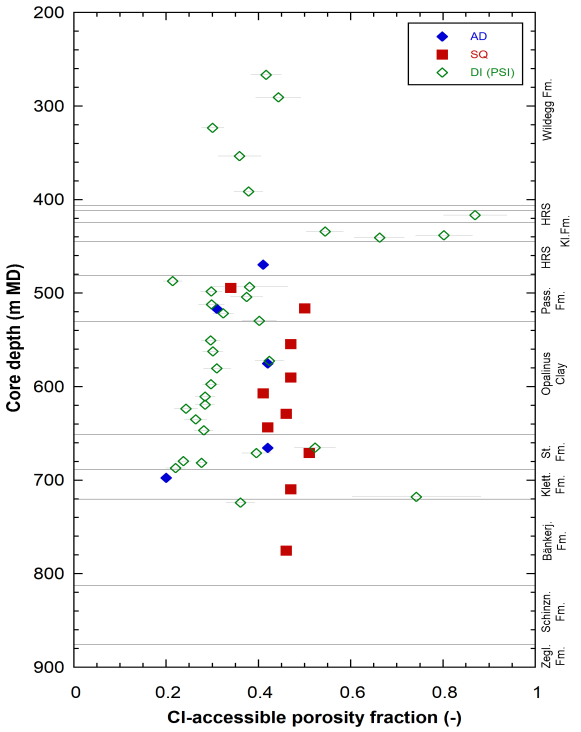

Fig. 5.1-3: Cl-accessible porosity fraction as a function of depth

5.2 Chloride, bromide and Br/Cl profiles

Paul Wersin, Martin Mazurek, Thomas Gimmi, Carmen Zwahlen

The chloride profile depicted in Fig. 5.2-1 includes aqueous extraction data[12] re-calculated to porewater concentrations assuming the relationship between clay-mineral content and f_{Cl} as discussed in Section 5.1. The Cl data based on squeezing and advective displacement, as well as those for the groundwater in the Muschelkalk, are also shown. The error bars include the propagated analytical uncertainty and, for aqueous extraction data, an additional 20% that reflect the uncertainty related to f_{Cl} (see Section 5.1, Fig. 5.1-1).

Data from all three methods are consistent within the extended error bars for the aqueous extraction data. However, the squeezing concentrations systematically deviate to slightly lower values as discussed below. Note that contamination for selected components (e.g. Si, K) by drilling fluid was identified for seven samples from the Schinznach, Zeglingen and Dinkelberg Formations used for aqueous extraction (Section 4.4.2). The corresponding Cl and Br contents are nevertheless shown. Regarding samples affected by K silicate drilling mud, the maximum estimated proportion of contamination for Cl and Br lies within the analytical uncertainty except for the sample from the Zeglingen Formation at 881.21 m depth, where the contamination could

[12] For AqEx Cl-data shown in Chapter 5 "dry" extracts were selected when available due to the generally lower error in water content compared to "wet" extracts. The former were performed on the same material that was subsequently used for extraction, while the latter refer to adjacent but not identical material, so local heterogeneity may play a role here.

exceed 20%. Moreover, three samples from the Zeglingen and Dinkelberg Formations are affected by the NaCl drilling mud, but in these cases the impact on Cl and Br cannot be quantified (Section 4.4.2).

The Cl profile shows a steady decrease from the Muschelkalk aquifer (~10 g/L) towards the Klettgau Formation where Cl concentrations reach ~ 0.5 g/L. In the overlying units, the profile is well constrained and supported by the dense sampling in the Opalinus Clay and confining units. Thus, Cl concentrations display a marked increase in the Staffelegg Formation, above which they remain roughly between 2 – 5 g/L up to the top of the cored sequence in the Wildegg Formation The generally rather constant profile shows an excursion towards lower values in the upper layers of the Passwang Formation at ~ 490 m depth. From the base of the Hauptrogenstein, the Cl profile exhibits a weak steady decrease from ~ 5 g/L to ~ 2 g/L at the top of the sequence at 260 m depth.

There are two outliers in the Passwang Formation at 507 m depth, which originate from an iron oolitic horizon, and one outlier at 414 m depth from a sample in the Hauptrogenstein with 11 wt.-% goethite. In the latter zone very high f_{Cl} values were obtained from diffusion data (Fig. 5.1-1). A high f_{Cl} value for the sample at 414 m depth would result in a lower Cl concentration, more consistent with the neighbouring data, than the value of 6'974 mg/L assuming the "standard" relationship with clay mineral content. Likewise, the outliers from the iron-oolitic horizon at 507 m likely also have higher f_{Cl} values than those used for deriving the Cl profile, given the experience from analogous data from the Hauptrogenstein and the Klingnau Formation (see also Fig.5.1-1).

The Cl profile is clearly influenced by an active aquifer located close to the Keuper/Staffelegg Formation boundary, where no groundwater sample could be extracted but where a major fault zone was identified (Section 2.4). Note that the $\delta^{18}O$ and $\delta^{2}H$ profiles indicate a similar profile shape in this area (Section 5.7). The bounding aquifer above the Opalinus Clay is less clearly defined. The excursion close to the top of Passwang Formation hints at an active aquifer system. The same excursion is evident from the Br profile (see below), but $\delta^{18}O$ and $\delta^{2}H$ profiles do not show any indications in this regard (Section 5.7). An excursion of the $\delta^{37}Cl$ profile is observed at 470 m (lower Hauptrogenstein) (Fig. 5.2-3), about 20 m above the excursions seen for Cl and Br. It should be noted, however, that the $\delta^{37}Cl$ is profile less well constrained in view of fewer samples compared to the other two profiles, and that the interpretation of ^{37}Cl data is not straightforward, as local maxima or minima do not necessarily coincide with the aquifer locations. Furthermore, it should also be pointed out that there are no evident structural features that would suggest higher permeabilities or a water-conducting zone in this section of the Passwang Formation.

The SQ data are slightly shifted compared to the re-calculated AqEx and AD data. This might be due to slight filtration occurring during squeezing already at the lowest squeezing pressure. On the other hand, it should be noted that the selected anion-acessible porosity fraction (f_{Cl} 0.42 for a clay-mineral content 25 wt.-%) and the associated extrapolation procedure is prone to considerable uncertainty. If a f_{Cl} value of 0.45 (representing the mean value of SQ data alone) is chosen, then the SQ data better matches AqEx data, whilst AD data points also still well lie within the overall profile (Fig. 5.2-2 left).

Considering f_{Cl} values from diffusion data leads to a much larger shift in the Cl profile. These data suggest very low f_{Cl} values, notably for Opalinus Clay samples (mean f_{Cl} = 0.30). Fig. 5.2-2 (right) illustrates the Cl profile based on f_{Cl} values from diffusion data alone in which an analogous relationship with clay-mineral content was applied (but with a limiting clay-mineral content of 40% instead of 25%). The profile defined by AqEx data is rather similar in the confining units with the ones based on AD/SQ data, but in Opalinus Clay there is considerable mismatch with SQ data (note that in this region there is only a single AD data point). The maximum Cl

concentration in Opalinus Clay is increased to ~ 4.5 g/L and the profile in this formation appears noisier compared to the smoother profile defined from f_{Cl} values based on AD/SQ data. While we cannot completely rule out AqEx data re-calculated from anion-acessible porosities derived from diffusion data, we lend more support to AqEx data re-calculated from SQ/AD f_{Cl} data.

In summary, a broadly consistent Cl profile above the (probable) Keuper aquifer is obtained from squeezing, advective displacement and aqueous extraction data. A well-defined profile is identified, with some scatter which is larger in the upper, more heterogeneous part of the sequence. This scatter is related predominantly to the uncertainty in anion-accessible porosity and to a lesser extent to the uncertainty in the water content. In this analysis, a simple relationship of the anion-accessible porosity with the clay-mineral content (as proxy of surface charge) based on squeezing and advective displacement data was used. It is worth noting that other relationships with the clay-mineral content (e.g. linear extrapolation from clay-mineral content (e.g. linear extrapolation from clay-mineral content < 40 wt.-%, or < 50 wt.-%) resulted in a slightly larger scatter in the data. Considering (lower) f_{Cl} values based entirely on diffusion data leads to a higher Cl concentration in the Opalinus Clay and to more scatter in the re-calculated AqEx data.

The groundwater sample in the Muschelkalk has a Cl concentration of ~ 10 g/L (9.7 – 10.0 g/L; Lorenz et al. *in prep.*). Below the Muschelkalk groundwater sample, the Cl profile shows large variations which are difficult to interpret at this stage (*cf.* Fig. 5.2-1 left). In general, it should be noted that NaCl polymer was used as drilling fluid in the section below 825 m depth which may have partially affected the core samples. The data suggest a strong variation in the Zeglingen Formation reaching the lowest values of ~ 1.5 g/L at about 880 m depth where a large fault zone was detected (Section 2.4). Further down, Cl levels appear to sharply rise again towards the zone where a halite layer was detected (~ 914 m depth), from where a general drop with depth towards the Permian strata is noted. The very high Cl concentration at 987.48 m is likely the result of drilling fluid contamination. Note that traces of halite were detected in the vicinity by XRD analysis (Section 4.2).

The $\delta^{37}Cl$ profile (Fig. 5.2-3) reveals rather constant δ values from the Staffelegg Formation up to the Malm. A slight negative excursion is indicated in the Hautprogenstein. Below the Staffelegg Formation there appears to be a generally increasing trend (with considerable scatter) towards the footwall of the Muschelkalk. The lowest porewater samples display a similar $\delta^{37}Cl$ values as expected for the halite layer[13] at about 914 m depth.

[13] The $\delta^{37}Cl$ value of rock salt, which was not measured in BOZ1-1 but in the BUL1-1 borehole, is shown in Fig. 5.2-3.

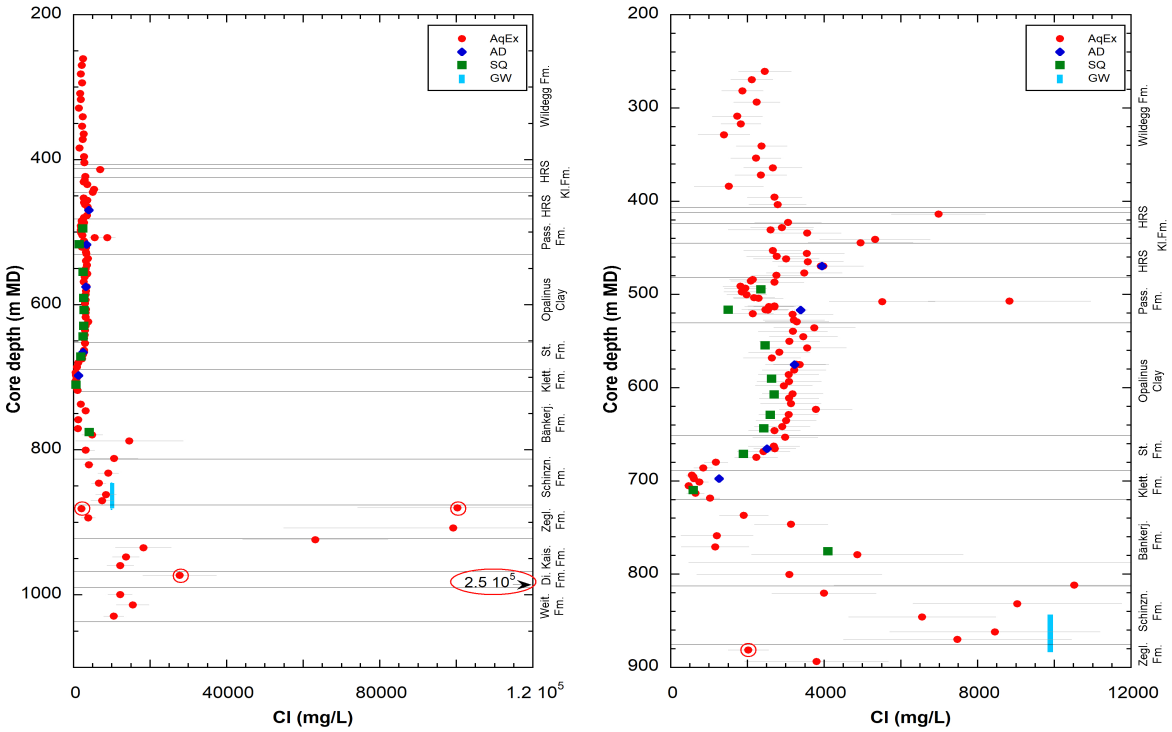

Fig. 5.2-1: Cl profiles at different scales (depth and concentration) with data from squeezing, advective displacement, aqueous extraction, and groundwater samples

Aqueous extraction data re-calculated to Cl-accessible porosity assuming the relationship between accessibility and clay-mineral content as discussed in Section 5.1. Encircled points: samples potentially affected by drilling fluid. Error bars on the data from aqueous extraction include propagated analytical uncertainty plus another 20% that reflect the uncertainty related to f_{Cl}. Note that SQ sample 516.27 might also be affected by the drilling fluid (Section 4.6.3).

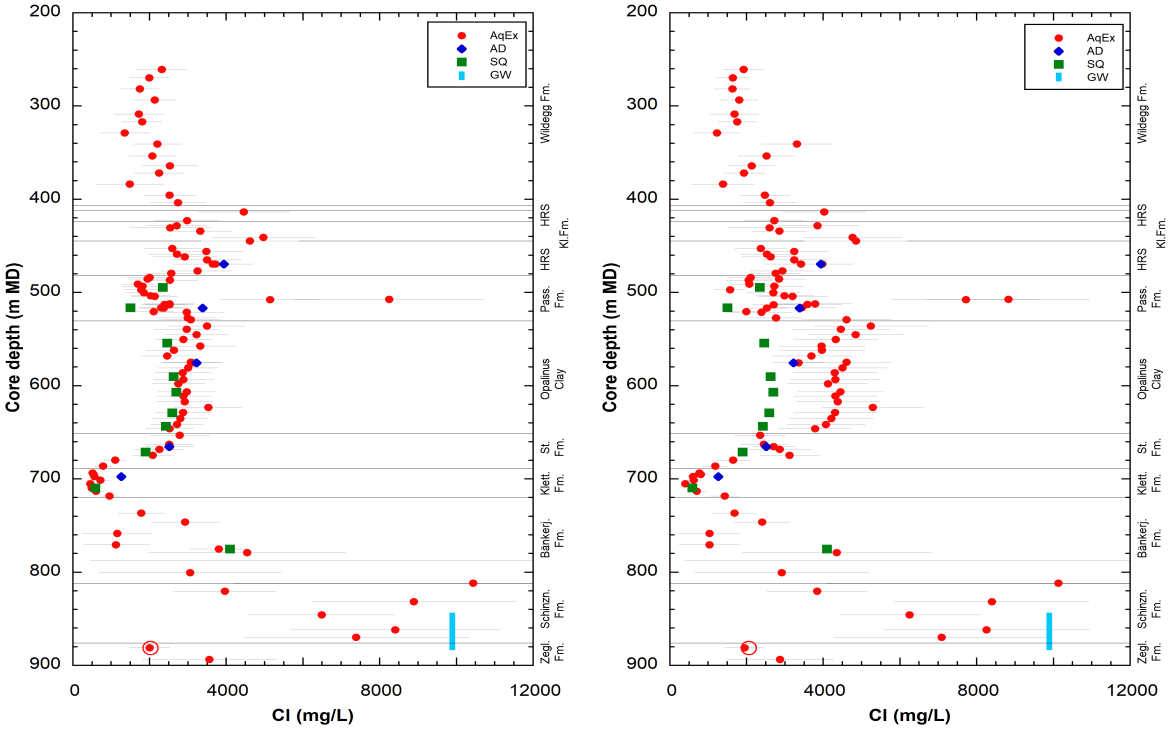

Fig. 5.2-2: Alternative Cl profiles based on f_{Cl} from squeezing data (left) and from diffusion data (right) (see text)

Aqueous extraction data re-calculated to Cl-accessible porosity assuming f_{Cl} = 0.45 for clay-mineral content > 25 wt.-% (left) and f_{Cl} = 0.30 for clay-mineral content > 40 wt.-% (right). Error bars on the data from aqueous extraction include propagated analytical uncertainty plus another 20% that reflect the uncertainty related to f_{Cl}. Encircled points: samples potentially affected by drilling fluid. Note that SQ sample 516.27 might also be affected by the drilling fluid (Section 4.6.3).

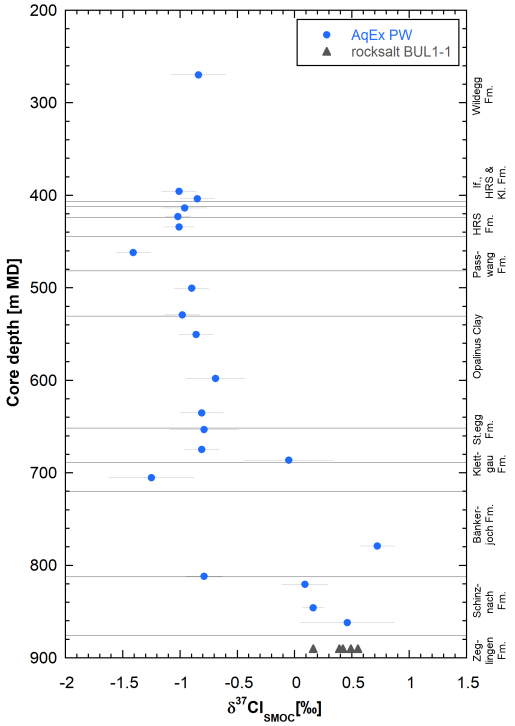

Fig. 5.2-3: Profile of $\delta^{37}Cl$ with data from aqueous extraction

The Br profile shows an increasing trend from the Klettgau Formation up to the top of the Opalinus Clay (Fig. 5.2-4). An excursion towards lower values is observed in the Passwang Fm, similar to Cl. From the bottom of the Hauptrogenstein a decreasing trend towards the top of the cored sequence is noted. Outliers occur in various iron oolitic layers, as also observed in the Cl concentration. The Br profile is thus similar to the Cl profile. This is also the case for the profile in the Triassic formations, where the scatter is considerable, which may be at least partially related to analytical issues (low porosity, Br contents close to the limit of detection, potential sample contamination). Note the shift of "dry" extracts compared to "wet" extracts depicted in the Passwang Formation and Hauptrogenstein (see also next paragraph).

The similarity between Br and Cl in the section Klettgau Formation-Wildegg Formation is also illustrated in the Br/Cl ratios (Fig. 5.2-5). The (1000*Br/Cl) (molar units) increases from ~ 1.0 in the Klettgau Formation to ~ 1.5 at the top of the Opalinus Clay. From there the increasing trend is continued, albeit with more scatter, up to the top of the cored sequence. The "dry" extracts exhibit a deviation from the trend, shifting to lower values in the Passwang Formation and Hauptrogenstein. These samples display somewhat lower Br concentrations than the corresponding "wet" extracts (Section 4.4). Possible reasons for this difference could be sorption of Br to the organic matter possibly modified during heating to 105 °C or due to a change in microstructure during the heating process preventing release of Br during subsequent aqueous extraction. On the other hand, the two AD samples from the same unit (Passwang Formation and Hauptrogenstein) exhibit a similar shift of Br/Cl ratios as the "dry" extracts. Moreover, such a shift is depicted by two of the three samples from out-diffusion (OD) experiments. The reason for this shift of AD and OD samples relative to the general trend in not clear at this stage. It was not observed in the previous boreholes of BUL1-1, TRU1-1 or MAR1-1.

Br/Cl ratios strongly increase from the top to the bottom of the Bänkerjoch Formation from where they drop towards the Muschelkalk aquifer. The scatter in the Schinznach and Zeglingen Formations is considerable, which may be partly related to contamination with NaCl-based drilling fluid. From there an increasing signal is noted down to the lowest sample in the Weitenau Formation.

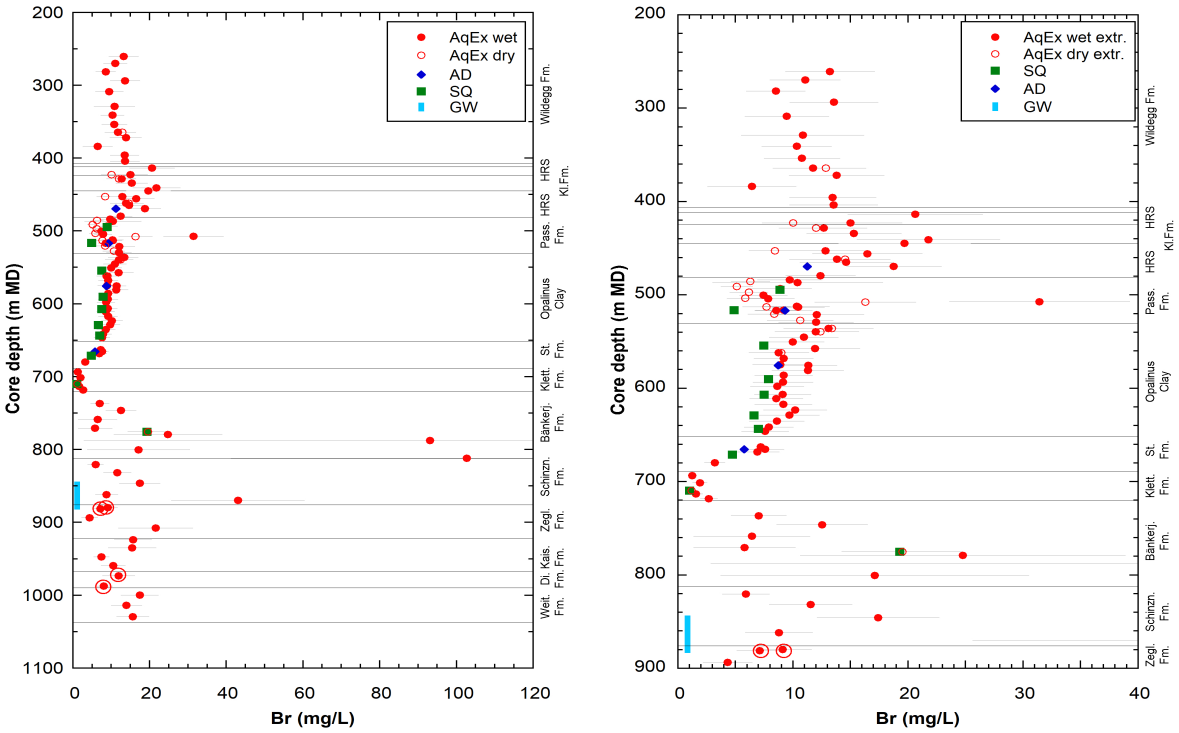

Fig. 5.2-4: Br with data at two different depth scales from squeezing, advective displacement, aqueous extraction and groundwater samples

Aqueous extraction data in the Br profile re-calculated to Br-accessible porosity assuming the relationship between accessibility and clay-mineral content as discussed in Section 5.1. Encircled points: samples potentially affected by drilling fluid. Error bars on the data from aqueous extraction include propagated analytical uncertainty plus another 20% that reflect the uncertainty related to f_{Br}. Note that SQ sample 516.27 might also be affected by the drilling fluid (Section 4.6.3).

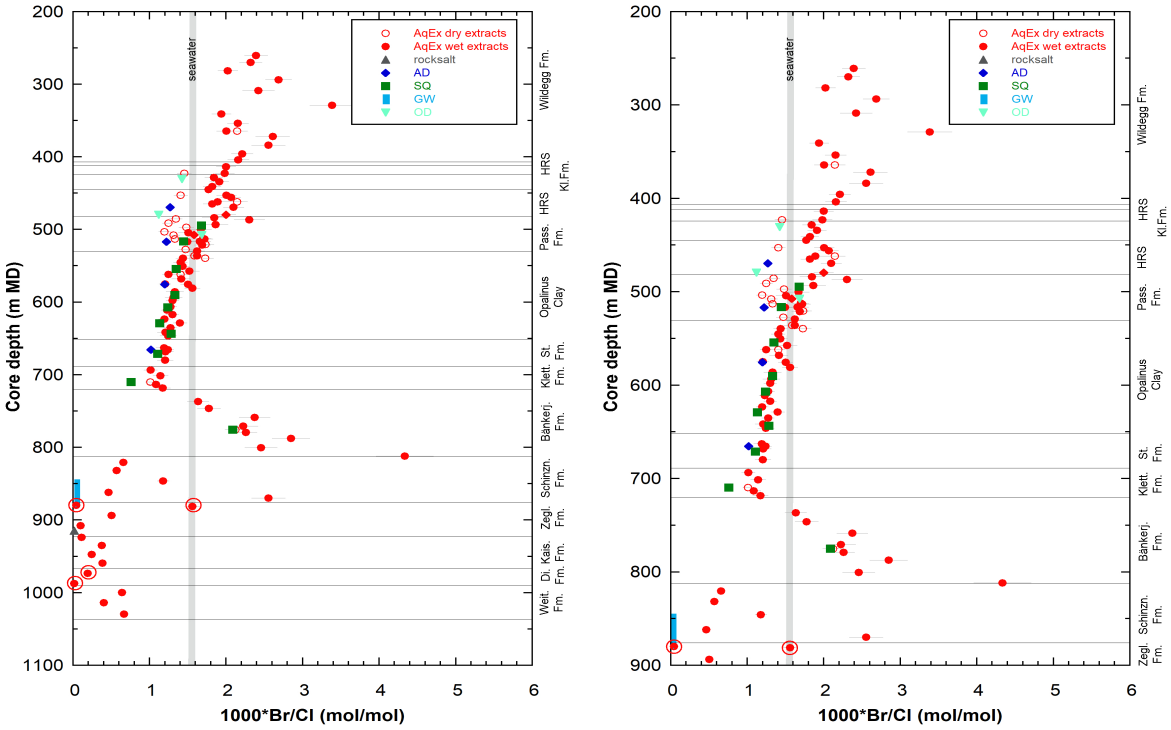

Fig. 5.2-5: Br*1000/Cl ratios (mol/mol) at two different depth scales with data from squeezing, advective displacement, aqueous extraction, out-diffusion and rock salt (from BUL1-1) samples

Grey bar: range of modern seawater. Encircled points: samples potentially affected by drilling fluid. Note that SQ sample 516.27 might also be affected by the drilling fluid (Section 4.6.3).

5.3 Sulphate and SO_4/Cl profiles

Paul Wersin, Martin Mazurek, Thomas Gimmi

Sulphate data from squeezing, advective displacement and aqueous extraction are illustrated in logarithmic and linear scales in Fig. 5.3-1. Data from aqueous extraction were re-calculated to concentrations in anion-accessible porewater (see below) assuming conservative behaviour of sulphate. This assumption is not true at least in anhydrite-bearing lithologies in the Bänkerjoch and Zeglingen Formations where mineral dissolution contributed to SO_4 concentrations in the extracts.

The very high SO_4 concentrations obtained for the re-calculated aqueous extracts in the Bänkerjoch and Zeglingen Formations are not meaningful because of anhydrite dissolution during extraction (Fig. 5.3-1 left). High concentrations are also exhibited in some samples in the Schinznach and Kaiseraugst Formations, although no anhydrite or gypsum could be detected by XRD in these samples. Such phases might, however, be present below the detection limit of XRD.

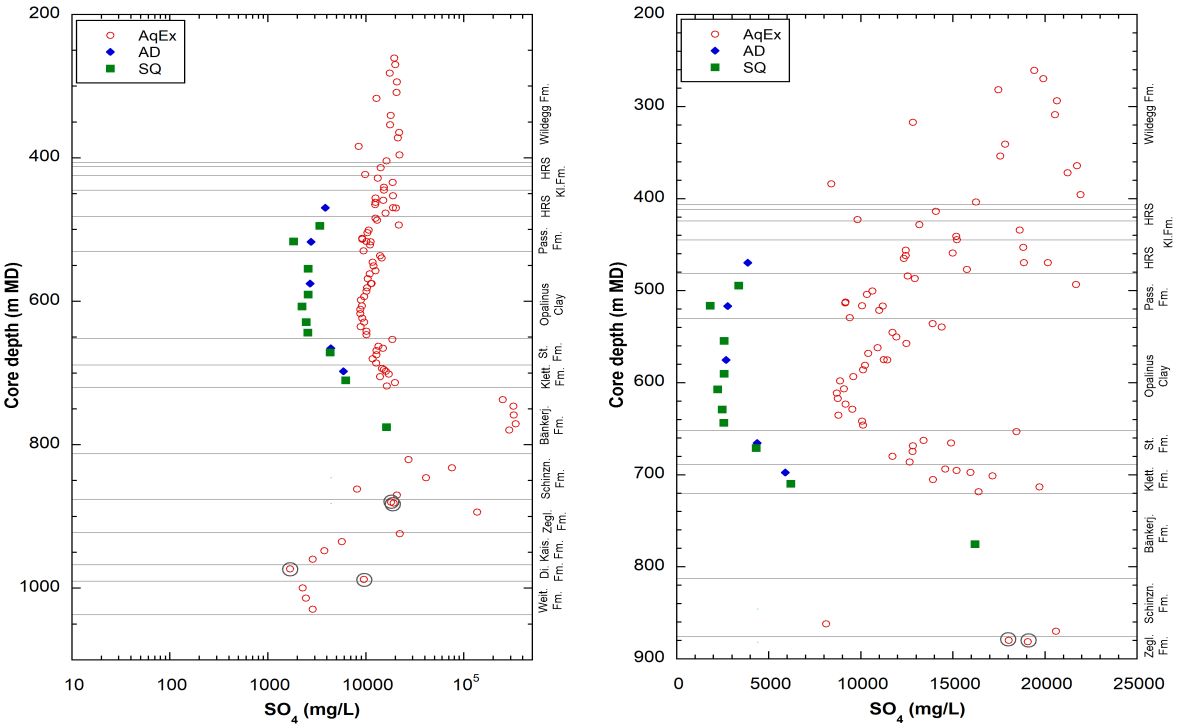

Fig. 5.3-1: SO_4 profiles (logarithmic and linear scales) with data from squeezing, advective displacement and aqueous extractions; left: entire data (logarithmic scale); right: data down to 900 m depth with SO_4 concentrations < 25 g/L (linear scale)

Aqueous data re-calculated to SO_4-accessible porosity assuming the same relationship between accessibility and clay-mineral content as applied above for Cl. Encircled points: samples potentially affected by drilling fluid. Note that SQ sample 516.27 might be also affected by the drilling fluid (Section 4.6.3).

SO_4 concentrations based on squeezing and advective displacement yield distinctly lower and less scattered values in comparison to the re-calculated data from aqueous extraction. A closer look at the sequence Passwang Formation – Klettgau Formation reveals consistent concentrations between squeezing and advective displacement data. The profile is flat within the Passwang Formation and Opalinus Clay with concentrations of 2 – 3 g/L (Fig. 5.3-1 right). Below, the concentrations increase with depth in the Staffelegg and Klettgau Formations, reaching 6 g/L at the bottom of the latter formation. The trend appears to continue in the Bänkerjoch Formation, where the lowest (anhydrite-bearing) squeezing sample displays a concentration of 16 g/L. The increase in SO_4 in the Staffelegg and Klettgau Formations is paralleled by a decrease of Cl (Fig. 5.3-2). In this sequence, the porewater thus shifts from a more Na-Cl dominated to a more Na-SO_4 dominated chemistry.

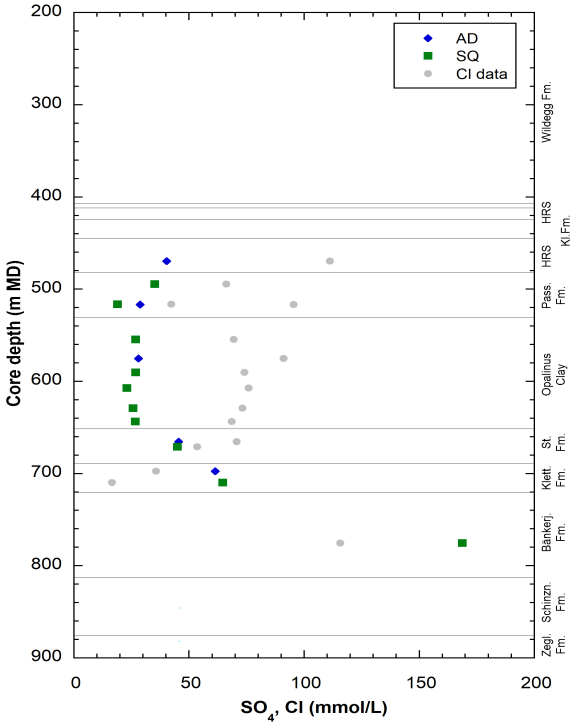

Fig. 5.3-2: SO_4 profile with data from squeezing and advective displacement

Corresponding Cl concentrations (from AD and SQ) are also shown.

Note that SQ sample 516.27 might be affected by the drilling fluid (Section 4.6.3).

The aqueous extraction data re-calculated to anion-accessible porosity exhibit systematically higher and more variable concentrations than the SQ/AD data. A similar discrepancy between squeezing/advective displacement data on the one hand and aqueous extraction data on the other hand has been observed for other boreholes, such as Schlattingen-1 (Wersin et al. 2013), the BUL1-1 borehole (Mazurek et al. 2021), the TRU1-1 borehole (Aschwanden et al. 2021), the MAR1-1 borehole (Mäder et al. 2021) as well as in in the Mont Terri Rock Laboratory (Wersin et al. 2020). In the latter case, waters sampled from packed-off boreholes exhibited similar sulphate concentrations and SO_4/Cl ratios as waters squeezed from nearby drillcores. All pore-waters from squeezed and advectively displaced samples here are close to equilibrium with regard to celestite. Celestite could be identified in some samples of the matrix of the Opalinus Clay and Passwang Formation samples at Mont Terri and Schlattingen-1 by a combined SEM/ microprobe study (Jenni et al. 2019). Samples from advective displacement and squeezing are generally undersaturated with regard to gypsum, and gypsum is not thought to play a role in this issue. The reason for the higher sulphate levels derived from aqueous extraction compared to squeezing/ advective displacement data is not understood at this stage, in spite of a recent systematic aqueous extraction study on Opalinus Clay including Mont Terri and BUL1-1 samples (Debure & Gailhanou 2019, Aschwanden & Wersin 2020).

The depth profile of SO_4/Cl ratios (Fig. 5.3-3) shows similar trends as the SO_4 profile. The high molar SO_4/Cl ratios up to more than 100 in aqueous extracts from anhydrite-bearing units in the lower sequence of the profile point to the dissolution of sulphate-bearing mineral phases during extraction. The general discrepancy between AD/SQ data on the one hand and AqEx data on the other are clearly evident and not discussed further. In the Dogger and Malm part, SO_4/Cl ratios in AD/SQ remain distinctly below 1. A strong drop with decreasing depth in the Klettgau and

Staffelegg Formations, followed by constant ratios of ~0.4 in the Opalinus Clay up to the lower Hauptrogenstein are evident. Below the Bänkerjoch Formation, where no data from AD/SQ are available, SO_4/Cl ratios from aqueous extracts suggest a decreasing trend down to the Muschelkalk aquifer. Note that molar SO_4/Cl ratios are generally higher than that of modern seawater (0.052).

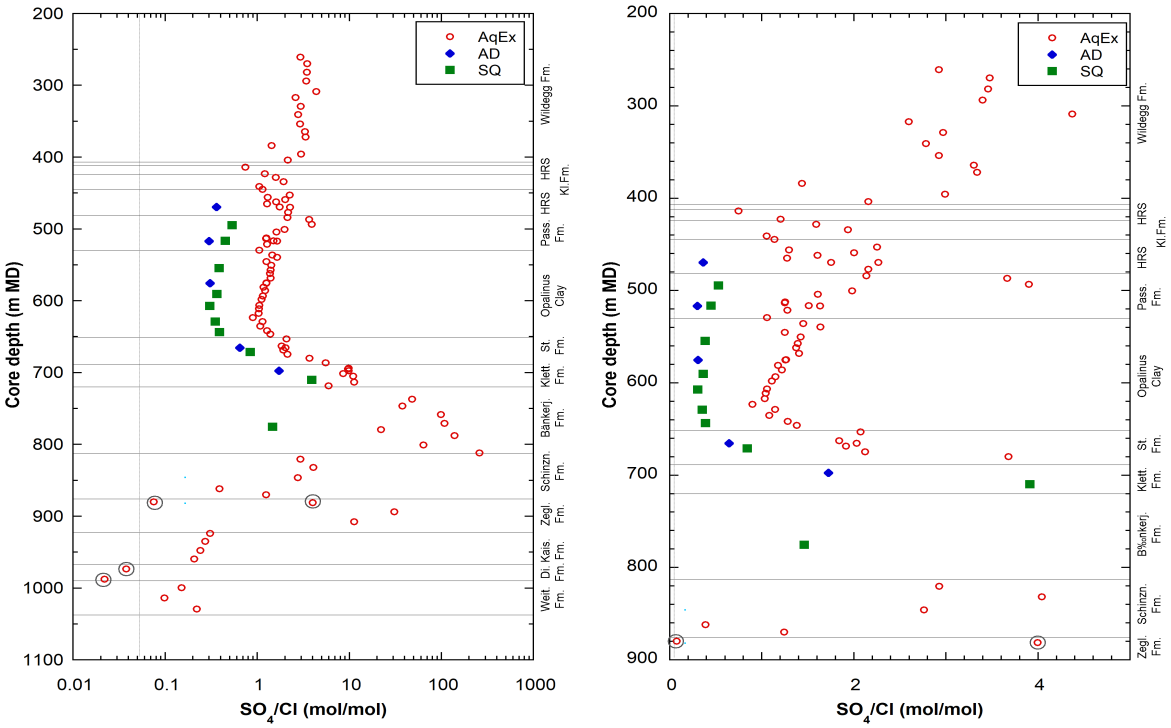

Fig. 5.3-3: Profiles showing molar SO_4/Cl ratios obtained from different methods in logarithmic and linear concentration scales

Data from aqueous extracts of some samples from sequence below the Staffelegg Formation are not seen in the right graphic (values > 5 mol/mol). Vertical line: ratio of modern seawater, Encircled points: samples potentially affected by drilling fluid. Note that SQ sample 516.27 might also be affected by the drilling fluid (Section 4.6.3).

5.4 Cation concentrations in porewaters

Paul Wersin, Eric C. Gaucher, Thomas Gimmi

Squeezing and advective displacement are the two methods that yield direct information on the cation concentrations in the porewater. Moreover, these can be estimated by simple modelling from the cation exchange data, notably from the cation occupancies on the exchanger. Aqueous extraction data, on the other hand do not enable straightforward determination of porewater cations because of their modification via cation exchange and mineral reactions during the extraction process.

Both the squeezing and advective displacement method may potentially induce changes in porewater composition, thus also affecting cation composition and distribution. Data from previous boreholes and the Mont Terri rock laboratory, however, suggest, that using not too high squeezing pressures and very early samples in the case of squeezing and advective displacement,

respectively, experimental artefacts are relatively minor (e.g. Wersin et al. 2016, Wersin et al. 2020), or at least some level of consistency between AD and SQ data is obtained (Mazurek et al. 2021, Aschwanden et al. 2021, Mäder et al. 2021). It should be pointed out that microbial processes probably occured during the AD experiments of BOZ1-1, as indicated for example by anomalous nitrate levels (Section 4.7). This obviously also affects the cationic charge.

Depth profiles for Na, Ca, Mg, K and Sr in porewater are illustrated in Fig. 5.4-1. Overall, cation data from squeezing and advective displacement are broadly consistent, although in the case of Na, squeezing data appear to be slightly lower than those of advective displacement, while the opposite is observed for K. Note that for Cl, the main anion, a similar difference between AD and SQ is noted as for Na, the main cation. There is a general tendendency of the major cations to decrease from the Passwang Formation towards the bottom of the Opalinus Clay, in line with the decrease in salinity and chloride (Fig. 5.2-1). In the uppermost Staffelegg Formation there appears a marked increase to higher cation concentrations relative to those in the Opalinus Clay, especially in the Na and Ca concentrations, which is paralleled by the increase of SO_4.

Below the Klettgau Formation, there is only one squeezing sample located in the central part of the Bänkerjoch Formation It suggests an increasing trend in Na, K, Mg and to a lesser extent in Ca concentrations, the latter likely related to anhydrite dissolution. Mg exhibits an unusually high concentration (~ 2'000 mg/L), thus contributing significantly to the cationic charge in this sample.

Na carries the main cationic charge in the entire profile. It correlates very well with Cl (the main anionic charge carrier) in the upper part of the rock sequence (Malm–OPA) (Fig. 5.4-2 left). In the lower sequence, however, the correlation between these two ions is much less pronounced. In fact, Cl concentrations strongly decrease with depth in the Staffelegg Formation and Klettgau Formation, whereas Na levels remain rather constant. The apparent deficit in anionic charge in sequence is compensated by sulphate, which contributes significantly to the anionic charge in these lithologies (Fig. 5.4-2 left).

The porewater composition thus gradually changes from a Na-Cl dominated type to a Na-SO_4 dominated type in the Keuper units. More specifically, the AD and SQ samples point to a Na-(Ca)-Cl-SO_4 type in the Hauptrogenstein-Opalinus Clay sequence and to a Na-(Ca)-SO_4-Cl type in the Staffelegg Formation-Klettgau Formation sequence. The SQ sample in the Bänkerjoch Formation is of Na-Mg-SO_4-Cl-type. This water type classification is based on Jäckli (1970), where ions with > 50 eq.-% are underlined, ions with 20 – 50 eq.-% are not underlined and ions with 10 – 20 eq.-% are put into brackets. Note that the groundwater from the Keuper aquifer from the Riniken borehole was found to be of Na(-Ca)-SO_4-Cl type (Pearson et al. 1991).

The Ca/Na ratio reveals a bell-shaped profile (Fig. 5.4-2 right), increasing from the top and the bottom of the Opalinus Clay towards the overlying and underlying units, respectively. Within the Opalinus Clay, a weakly decreasing trend with depth is noted. Below the Klettgau, there appears to be a decreasing trend (but note that only one sample is available) towards the Muschelkalk aquifer.

The relationships of cations and their consistency with exchangeable cation populations are further discussed in Section 5.6.

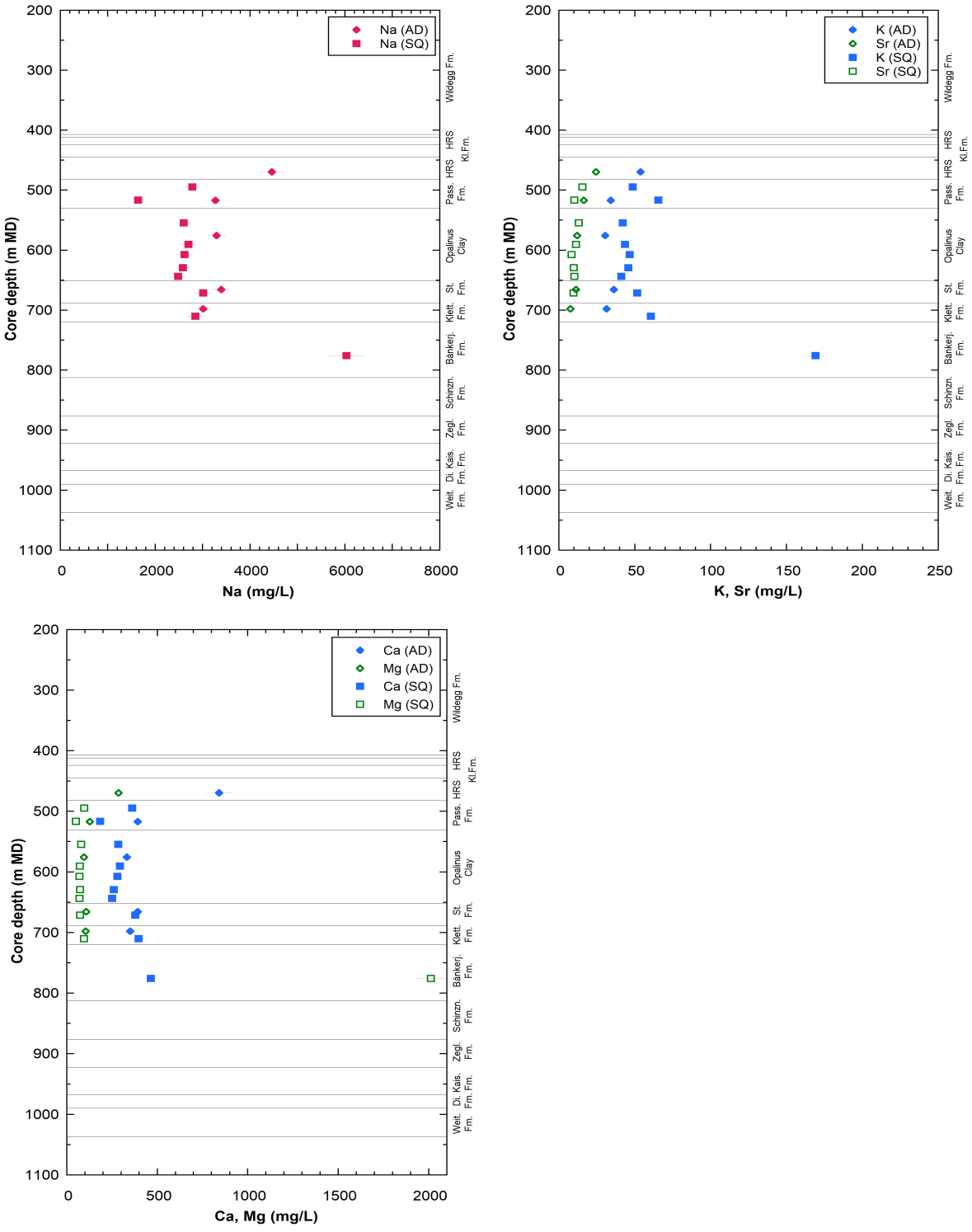

Fig. 5.4-1: Profiles for Na, Ca, Mg, K and Sr in porewater with data from squeezing, advective displacement

Note that SQ sample 516.27 might be affected by the drilling fluid (Section 4.6.3).

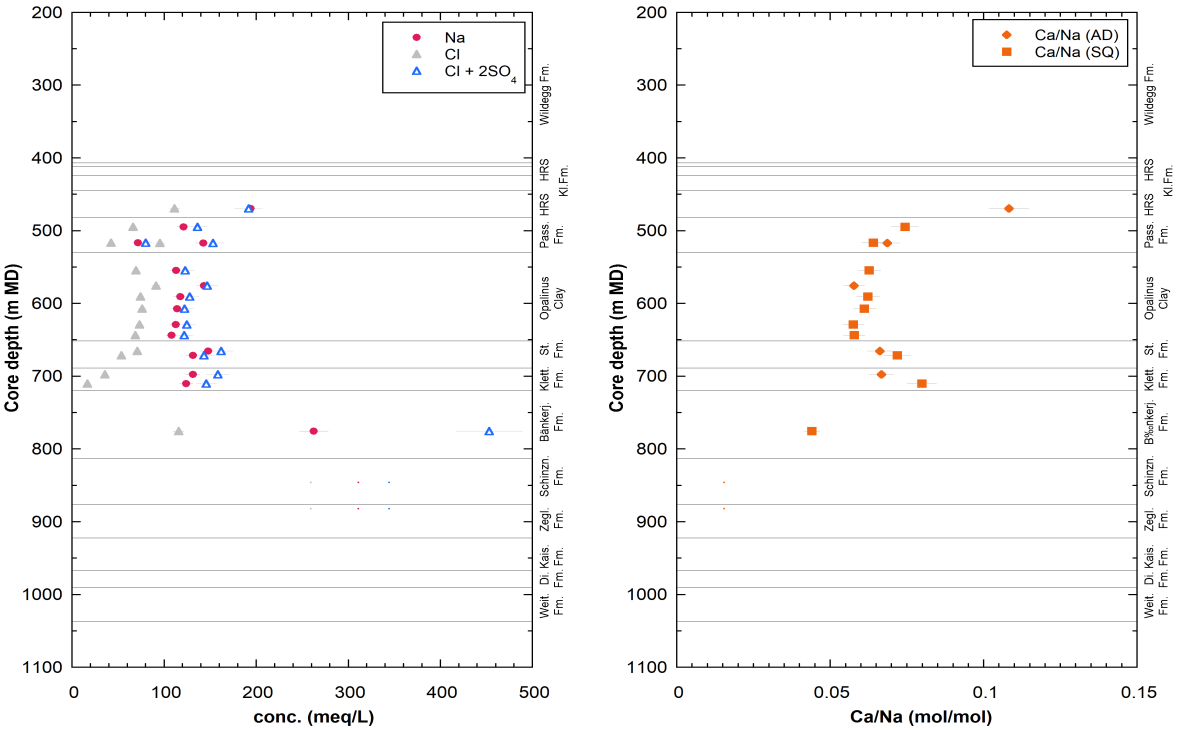

Fig. 5.4-2: Profiles for Na, Cl and ΣCl+SO_4 in porewater (SQ and AD samples) in meq/L (left), Ca/Na ratio (molar units) for SQ and AD samples (right)

Note that SQ sample 516.27 might be affected by the drilling fluid (Section 4.6.3).

5.5 Dissolved carbon species (inorganic, organic), alkalinity, pH and P_{CO2}

Paul Wersin, Eric C. Gaucher, Thomas Gimmi

5.5.1 Dissolved inorganic carbon, alkalinity, pH and P_{CO2}

The two methods yielding information on the carbonate system of the porewater are squeezing and advective displacement. Notably, with the two methods TIC, alkalinity (determined by titration) and pH can be measured. Alkalinity may include other compounds (e.g. low-molecular organic acids) than carbonate species (HCO_3^-, CO_3^{2-}) and thus TIC is considered to be a more reliable parameter for constraining the carbonate system of the porewaters (Wersin et al. 2020).

Knowing pH and TIC, the (dissolved) carbonate system is entirely constrained (at constant temperature and pressure) according to Gibb's phase rule and the CO_2 partial pressure can be calculated. It should be noted that it is not straightforward to obtain reliable measurements on these parameters which are prone to perturbations. For example, degassing of CO_2 during the squeezing process may alter pH and TIC parameters[14] (Tournassat et al. 2015, Wersin et al. 2020). In the case of advective displacement, degassing or ingassing of CO_2 during the experiment and/or after sample collection (Waber (ed.) 2020) may occur. A further perturbation that may arise from the latter method is related to microbial activity inducing high nitrate levels (Section 4.7.5). Equilibrium with calcite, omnipresent in the sedimentary sequence, imposes a further constraint

[14] But alkalinity is not affected by changes in CO_2 partial pressures as long as no dissolution/precipitation reaction occurs.

on pH/P_{CO2}. Thus, from the measured Ca, TIC and pH, the saturation state with regard to calcite can be calculated, providing a plausibility test regarding the carbonate system. It is worth noting, however, that calculated saturation indices for calcite close to zero do not a priori confirm that measured parameters, such as pH and TIC reflect in-situ conditions. In fact, perturbations during the experimental procedure might lead to a new equilibrium with calcite at different pH/P_{CO2} conditions.

Tab. 5.5-1 shows the measured pH, TIC data together with the derived P_{CO2} and saturation index for calcite from speciation calculations from PHREEQC. Note that the AD data only in-line pH data, but not the pH measured later in the lab are considered. The reason is that speciation calculations indicate that waters using in-line pH are generally closer to calcite saturation. For SQ, alkalinity and pH were measured in the lab in Bern after squeezing in Japan. In general, measured pH values for AD range from 6.8-7.7, whereas those for SQ are higher, in the range of 8.5 – 9, as also illustrated in Fig. 5.5-1 (left). Conversely, TIC values for AD are higher compared to SQ. Calcite SI values for AD vary from close to zero to 0.8. In the case of SQ, clearly supersaturated conditions with respect to calcite are noted with all SI values larger than 1. Regarding P_{CO2}, measured AD data indicate values of -1.4 to -2.4 bar in log units, whereas for SQ values are considerably lower (-3.2 to -4.8), as also illustrated in Fig. 5.5-1 (right).

Tab. 5.5-1: Measured pH and TIC as well as calculated P_{CO2}, $SI_{calcite}$ and pH from AD and SQ experiments (see text)

a) pH measures in-line (AD) and in the lab (SQ).

From measured parameters						**Calculated assuming calcite eq.**		
Method	Depth	pH [a)]	TIC	log$P(CO_2)$	$SI_{calcite}$	log$P(CO_2)$	pH	NO_3
	[m]		[mmol/L]	[bar]	[-]	[bar]		[mmol/L]
AD	469.40	7.38	3.69	-2.23	0.50	-1.71	6.87	50.04
AD	516.72	6.84	7.26	-1.41	-0.06	-1.47	6.90	7.47
AD	575.26	7.75	6.45	-2.30	0.80	-1.47	6.94	9.82
AD	665.40	7.53	7.99	-1.99	0.67	-1.31	6.86	1.89
AD	697.51	7.43	2.71	-2.36	-0.01	-2.37	7.44	0.15
SQ	494.48	8.92	1.51	-4.17	1.28	-2.54	7.47	0.10
SQ	516.27	9.24	0.84	-4.77	1.12	-3.15	7.87	0.05
SQ	554.36	8.99	1.88	-4.15	1.37	-2.40	7.43	0.09
SQ	590.32	9.02	1.93	-4.17	1.41	-2.35	7.40	0.11
SQ	607.13	9.00	1.47	-4.27	1.28	-2.59	7.52	0.10
SQ	629.09	8.79	2.06	-3.87	1.22	-2.40	7.45	0.14
SQ	643.35	8.97	1.49	-4.22	1.21	-2.67	7.59	0.10
SQ	671.15	8.90	1.29	-4.21	1.17	-2.72	7.57	0.18
SQ	709.84	9.05	3.09	-4.01	1.61	-1.97	7.22	0.28
SQ	775.39	8.49	5.63	-3.20	1.26	-1.70	7.11	0.19

In a second step, compositions are corrected with aid of PHREEQC until calcite saturation is achieved, assuming that CO_2 exchange occurred during the experimental procedure. This process is known to occur during the squeezing process. The processes shifting the carbonate equilibrium in the AD experiments may also be related to CO_2 exchange, but in addition also to other reactions if microbial processes are active (which cannot be corrected with the chosen approach). This calculation leads to pH and P_{CO2} values shown in Tab. 5.5-1 and Fig. 5.5-1. Corrected SQ data

show P_{CO2} values of roughly -2 to -3 bar in log units (except for the lowest sample in Klettgau Formation with a value -1.7), whereas calculated AD data display P_{CO2} values from -1.3 to -2.4. Most of the calculated P_{CO2} values from SQ data appear to be in a reasonable range, based on data from previous work on Mont Terri or Schlattingen (Wersin et al. 2020). Regarding AD data, the P_{CO2} values remain in a similar range as before the correction, demonstrating that – as excpected – CO_2 exchange has probably not been a very relevant process in the AD experiments. In any case, the high TIC values of AD are conspicuous. This may be (at least partially) related to microbial processes and resulting elevated nitrate levels observed in four of the five experiments. In fact, the sample with lowest NO_3 level at 697.51 m depth shows values of pH (7.4) and P_{CO2} (-2.37 log(bar)) which are in line with the expected range based on previous studies (Wersin et al. 2020).

In summary, re-calculating P_{CO2} and pH conditions assuming calcite equilibrium seems to lead to reasonable values for SQ samples based on current understanding. This suggests that perturbations resulting from CO_2 exchange during the squeezing experiment could be accounted for by simple modelling. It further suggests that pressure solution of carbonates which may occur at higher pressures did not occur to a large extent. In the case of the AD samples, the correction procedure does not seem to significantly alter or improve the pH/P_{CO2} data. The generally high TIC in the AD data may be related to microbial activity affecting the carbonate system to a variable degree.

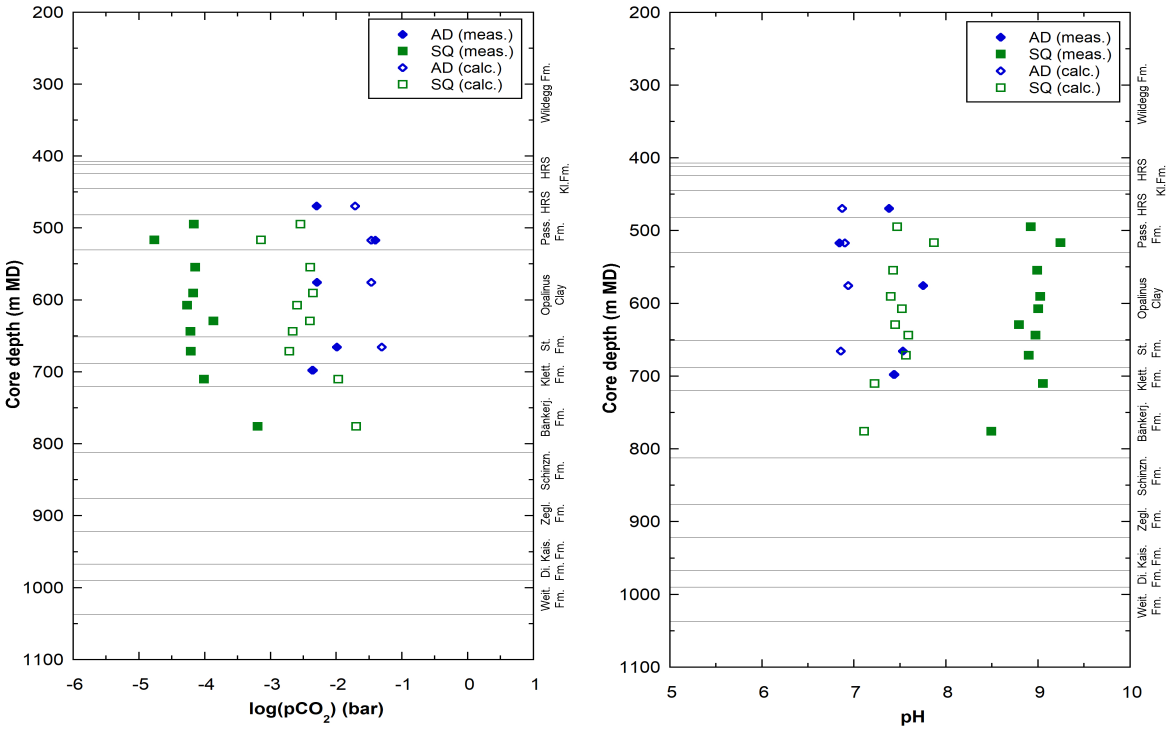

Fig. 5.5-1: pH (left) and calculated P_{CO2} values from AD and SQ (see text)

Full symbols: based on measured data; open symbols: calculated calcite equilibrium via CO_2(g) exchange. Note that SQ sample 516.27 might be affected by the drilling fluid (Section 4.6.3).

5.5.2 Dissolved organic carbon

Information on dissolved organic carbon is available from advective displacement (AD) and squeezing (SQ) data as well as from aqueous extracts of AD cores (AqEx-AD):

1. SQ: TOC
2. AD: TOC, low molecular-weight organic acids (LMWOA)
3. AqEx-AD: low molecular-weight organic acids (LMWOA)

Moreover, the (solid) organic carbon content (C_{org}) from the corresponding SQ and AD samples is available besides those from PW, RP, DI, and OD samples.

Before discussing the dissolved organic carbon data, it is worth mentioning some general points: The organic carbon in the sedimentary rock consists of refractory kerogen and only a small fraction is extractable by solvents (< 1%). The water soluble-organic carbon is even smaller, thus for example reaching a few mg C/L in the porewater of Opalinus Clay at Mont Terri or in the Callovo-Oxfordian Formation sampled from seepage boreholes (Courdouan Merz 2008; Courdouan et al. 2007a & b). Higher concentrations (several tens to hundreds of mg C/L) are generally measured in porewaters extracted from core samples, such as from squeezing or advective displacement (Wersin et al. 2013, Wersin et al. 2020). In the case of aqueous extracts, significant amounts of organic carbon are released to the solution. This indicates that a fraction of the "solid" carbon fraction is mobilised during the extraction process. It also suggests that the preferential release of loosly bound small organic molecules from the solid organic matter.

The TOC concentrations from AD and SQ data are shown in Fig. 5.5-2. Generally speaking, these are roughly consistent between the two methods, in the range of 100 – 150 mg C/L, except for one AD sample in the Hauptrogenstein with ~ 700 mg C/L. The shape of the TOC profile appears similar to that of solid organic C (C_{org}) (Fig. 5.5-2 below), displaying slightly higher organic C levels in the Opalinus Clay compared to the adjacent formations.

A further point to note is that microbial activity in the AD cores, as suggested from the high nitrate concentrations, did not affect TOC levels to a large extent, except perhaps in the Hauptrogenstein sample where the TOC level is particularly high. That sample also displays by far the highest nitrate concentration (~ 3'000 mg/L). Acetate concentrations determined from five AD samples (Appendix B) are variable, ranging from < 20 – 200 mg acetate /L (or < 8 – 77 mg C/L). The fraction of acetate thus varies between < 6 – 70% of the TOC. The concentrations of the other LMWOA (lactate, proprionate, formate) are below detection (< 20 mg/L). The LMWOA measured from the aqueous extracts of AD cores after the experiment (not shown) indicate a similar pattern as the advectively displaced waters. They have similar shares of acetate relative to TOC and no measureable other LMWOA.

In conclusion, results from AD and SQ indicate consistent TOC data of 100 – 150 mg/L. Based on previous studies (Courdouan Merz 2008 and others) these TOC concentrations are higher than those expected in-situ. It appears that boths methods lead to a release of loosely-bound or "sorbed" organic matter (e.g. Durce et al. 2015).

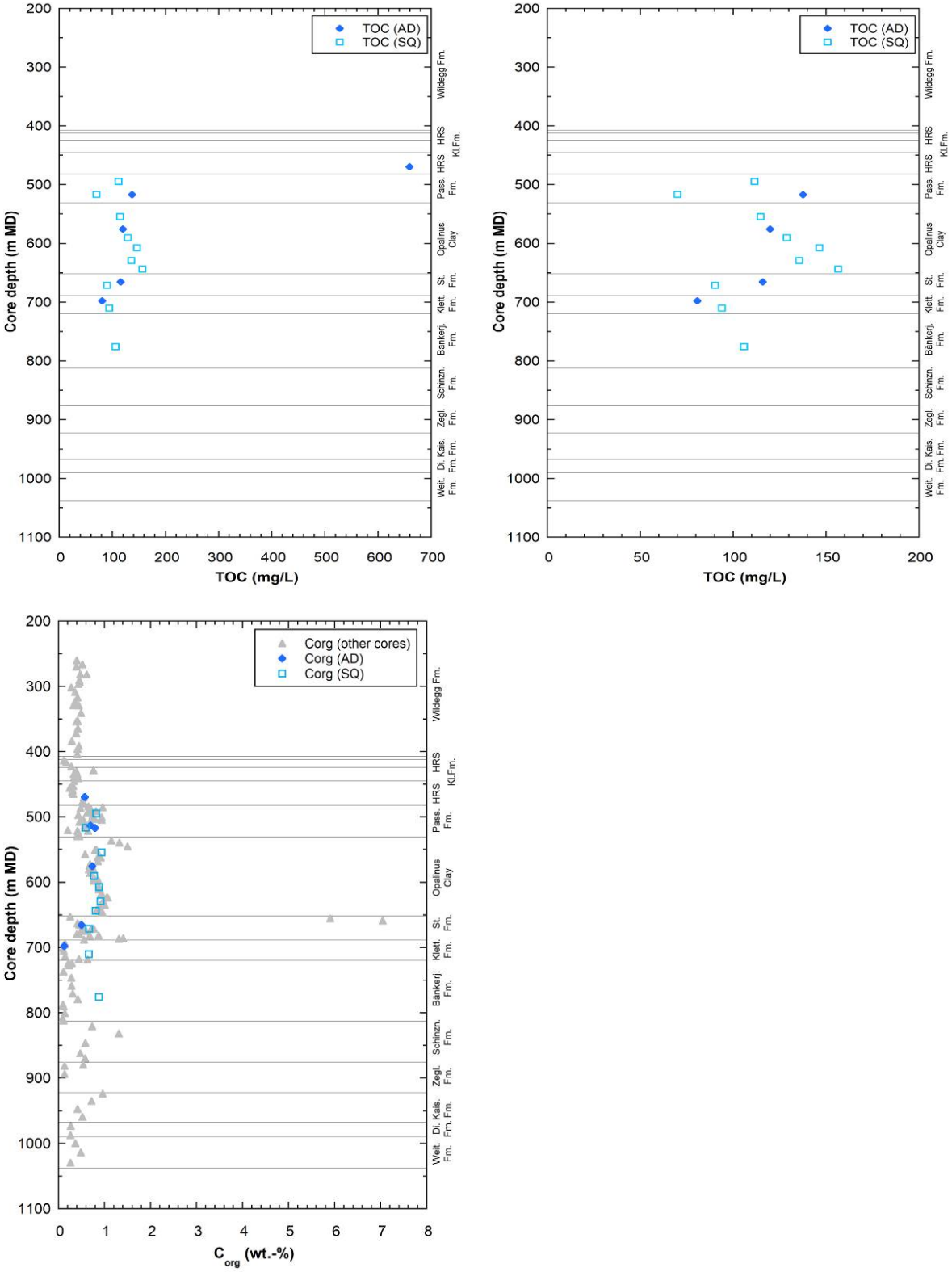

Fig. 5.5-2: TOC concentrations in porewater samples at different scales (pannels above) from AD and SQ and organic carbon content in rock (below)

Note that SQ sample 516.27 might be affected by the drilling fluid (Section 4.6.3).

5.6 Cation exchange capacity and exchangeable cation population

Paul Wersin & Martin Mazurek

5.6.1 Corrected exchangeable cation data

As mentioned in Section 4.5, in order to obtain the exchangeable cation concentrations, the total extracted cation data need to be corrected for cations arising from the dissolution of salts porewater and the cations released from (potential) mineral dissolution. As shown from previous work (e.g. Hadi et al. 2019) and also indicated from speciation calculations presented in Section 4.5 (Tab. 4.5-4), carbonate mineral dissolution is minimised with the appropriate S/L ratio, extraction time and pH conditions. Such conditions were applied to the Uni Bern dataset.

Two correction methods were applied based on the extracted concentrations of the main anions chloride and sulphate (Bradbury & Baeyens 1998, Hadi et al. 2019). The first correction method attributes dissolved Cl and SO_4 from the Ni-extracts to Na ($NaCl/Na_2SO_4$) and leaves the other cations unchanged. The second method attributes Cl to Na and SO_4 to Ca ($NaCl/CaSO_4$), leaving the other cations unchanged. In both methods, the CEC is calculated from the sum of cations (ΣCAT) minus the concentrations (normalised to meq/kg_{dry_rock}) of Cl and SO_4. The corresponding data are shown in Tab. 5.6-1.

The relative difference between the uncorrected and corrected ΣCAT is within 4 – 9%.

The graphical representation of Ni consumption vs. ΣCAT (Fig. 5.6-1) illustrates the good correlation between these two parameters. The values for the corrected ΣCAT are close to those of Ni consumption, albeit generally slightly lower by -14 to 0%. The good match between the two datasets supports the validity of the correction procedure for deriving the CEC based on the sum of cations.

Furthermore, Fig. 5.6-2 indicates a fair correlation between clay-mineral content and CEC parameters. Disregarding the sample at 516.72 m from the Passwang Formation which contains the highest CEC, the correlation is improved. Further correlations are discussed in the following section.

The exchangeable cations are expressed as cation fractional occupancies (in equivalent fractions) in Tab. 5.6-1. Na and Ca are the main exchangeable cations, followed by Mg and K. The Sr occupancies are considerably lower (0.4 – 0.7 eq.-% of the CEC).

Tab. 5.6-1: Sum of cations and cation occupancies obtained from Ni-en extraction after correction (Uni Bern data)

First line for each sample indicates fractional cation occupancies obtained by the $NaCl/Na_2SO_4$ correction method, the second line those obtained by the $NaCl/CaSO_4$ method.

Sample Type	**Depth** [m]	**Formation**	**Clay-mineral content** [wt.-%]	**Ni cons.** [meq/kg$_{rock}$]	**ΣCAT total** [meq/kg$_{rock}$]	**ΣCAT corr.** [meq/kg$_{rock}$]	**Na**	**K**	**Ca**	**Mg**	**Sr**
							Fractional occupancy (equivalent units) [-]				
AD	469.40	Hauptrogen-stein	25	56.2	60.7	55.1	0.34 0.41	0.07	0.41 0.33	0.18	0.006
AD	513.25	Passwang Fm.	51	137.4	135.8	130.7	0.42 0.45	0.05	0.38 0.35	0.15	0.007
AD	516.72	Passwang Fm.	38	160.7	153.7	148.2	0.39 0.42	0.06	0.39 0.37	0.15	0.007
AD	575.26	Opalinus Clay	45	107.3	111.7	107.1	0.46 0.49	0.05	0.35 0.33	0.13	0.006
AD	665.40	Staffelegg Fm.	30	84.2	77.0	72.6	0.43 0.48	0.06	0.34 0.30	0.16	0.006
AD	697.51	Klettgau Fm.	39	141.0	133.2	126.6	0.40 0.45	0.06	0.35 0.30	0.18	0.004

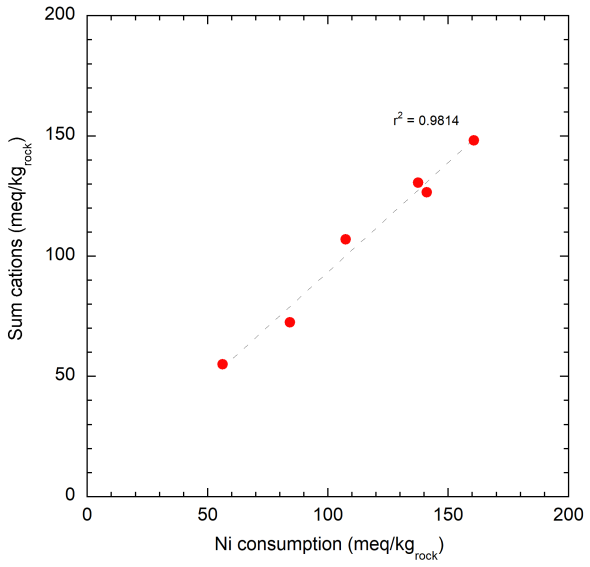

Fig. 5.6-1: Ni consumption vs. corrected sum of cations (data of Uni Bern)

Dashed line: linear trendline.

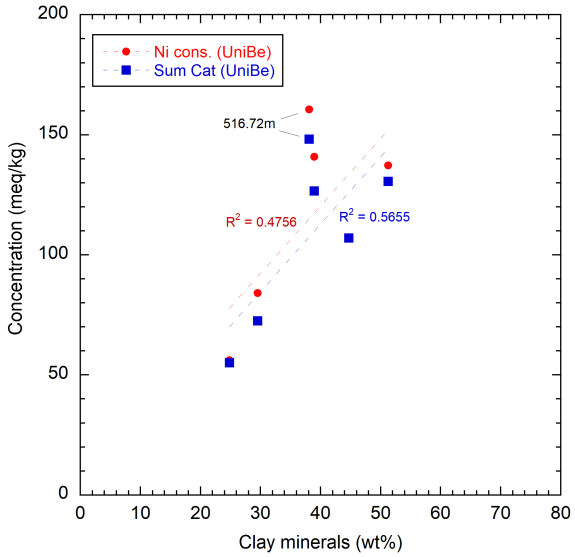

Fig. 5.6-2: Cation exchange capacity (Ni consumption and corrected sum of cations) as a function of the clay-mineral content (data of Uni Bern)

Note that for two samples Ni consumption and (corrected) sum of cations values are almost identical, therefore red points do not appear on figure.

5.6.2 Comparison with data from PSI

A dataset including 32 samples from the BOZ1-1 borehole was elaborated by PSI (Marques Fernandes & Baeyens *in prep.*). Samples originated from the Wildegg Formation down to the Bänkerjoch Formation

In a first step, the CEC at PSI was estimated for all samples from Ni consumption with the Ni-en extraction method. Subsequently, the main dataset was generated via CsCl extraction, from which the CEC and the exchanger population were obtained. The CEC was derived by subtracting the anions (Cl, SO_4, HCO_3/CO_3) from the cations (Na, Ca, Mg, K, NH_4, Sr). The exchanger population was derived by two correction methods: (1) attributing Cl and SO_4 to Na and TIC to Ca, and (2) attributing Cl to Na and SO_4 and TIC to Ca. Note that these two methods are analogous to the ones used for the Uni Bern samples presented above, except for the additional consideration of TIC. The contribution of the latter is less relevant in the case of the Uni Bern data (see Tab. 4.5-4) because of the much higher solid/liquid ratios and thus a lower contribution of mineral dissolution (carbonates) to measured cation concentrations.

The conditions applied in the different extraction methods of PSI and Uni Bern are compared in Tab. 5.6-2. Important differences of the PSI methods relative to that of the Uni Bern are (i) the lower solid/liquid ratios, (ii) the smaller amount of solid mass and (iii) the more variable concentration of the index cation depending on the expected CEC.

Tab. 5.6-2: Comparison of extraction conditions applied by Uni Bern and PSI

	University of Bern	**PSI**	**PSI**
Extraction method	Ni-ethylenediamine	Ni-ethylenediamine	CsCl
Initial extract solution concentration	98 – 107 mmol/L [a)]	3.3 mmol/L	11 – 34 mmol/L
Solid/liquid ratio	~ 0.9 kg/L	~ 0.033 kg/L	0.05 – 0.16 kg/L
Amount of solid used	~ 30 g	~ 1 g	~ 1.5 – 5 g [a)]
Extraction time	24 h	24 h	24 h
Final pH	8.3 – 8.5	8.6 – 8.8	8.6 – 9.5
Sample disaggregation	Disintegration by hand to a few mm^3 pieces	Milled and passed through 1 mm sieve	Milled and passed through 1 mm sieve
Sample storage time prior to preparation	1 – 14 days	Several months [b)]	Several months [b)]
Extraction in glovebox	Yes	No	Yes

[a)] S/L ratio adjusted to obtain the expected index cation consumption-to-CEC ratio.

[b)] inside glovebox

Cation exchange capacity and corrected sum of extracted cations

The Ni-en consumption and the corrected ΣCAT data (the latter from Ni-en extraction in the case of Uni Bern and CsCl extraction in the case of PSI) are shown in Fig. 5.6-3. From the comparison of these two datasets, the following findings can be derived:

- The CEC values obtained from Ni consumption exhibit consistent values for both datasets (Fig. 5.6-3 left). In this context, it should be noted that the two datasets were not performed on the same samples, thus CEC variations at similar depths due to mineralogical variation can be expected.
- The CEC values obtained from the corrected sum of cations also indicates consistency between Uni Bern and PSI (Fig. 5.6-3 right). Comparison of neighbouring samples suggests an even better match between the two datasets compared to Ni consumption data. This is evident for example for the samples at about 513 m, 517 m and 575 m depth.
- Both datasets indicate approximate consistency between Ni consumption and corrected ΣCAT data. In the case of Uni Bern data, the corrected ΣCAT data is generally slightly lower (by –14 to 0%), whereas the PSI data shows variations in both directions (-24 to +17%). There is one outlier in the PSI data, a limestone sample with a clay content < 1 wt.-% at 808 m depth from the Keuper, where the difference is almost 400%. This underpins the limitation of the CEC methods (Ni consumption, CsCl extraction) for very clay-poor samples.
- In general, both datasets show the expected positive trend between clay-mineral content and CEC, both for Ni consumption and (corrected) sum of cations (Fig. 5.6-4). A group of data at ~ 40 wt.-% clay-mineral content, most of which belong to the Passwang Fm., fall off the general trend, showing rather high CEC values. The data below 20 wt.-% clay-mineral content do not show a real trend.

- The trend improves when illite content or smectite content is considered instead of clay-mineral content. In fact, the CEC is primarily induced by the structural negative charge of these minerals, whereby the negative charge carried by smectite is about four times larger than that of illite. The correlation between the sum of illite and 4x smectite content and the CEC is clearly superior to that exhibited by the clay-mineral content, as illustrated in Fig. 5.6-5.
- Both Ni consumption and corrected ΣCAT data from the two laboratories are thought to be representative measures of the CEC in view of the overall data consistency. The difference between these data is largely within the analytical error.

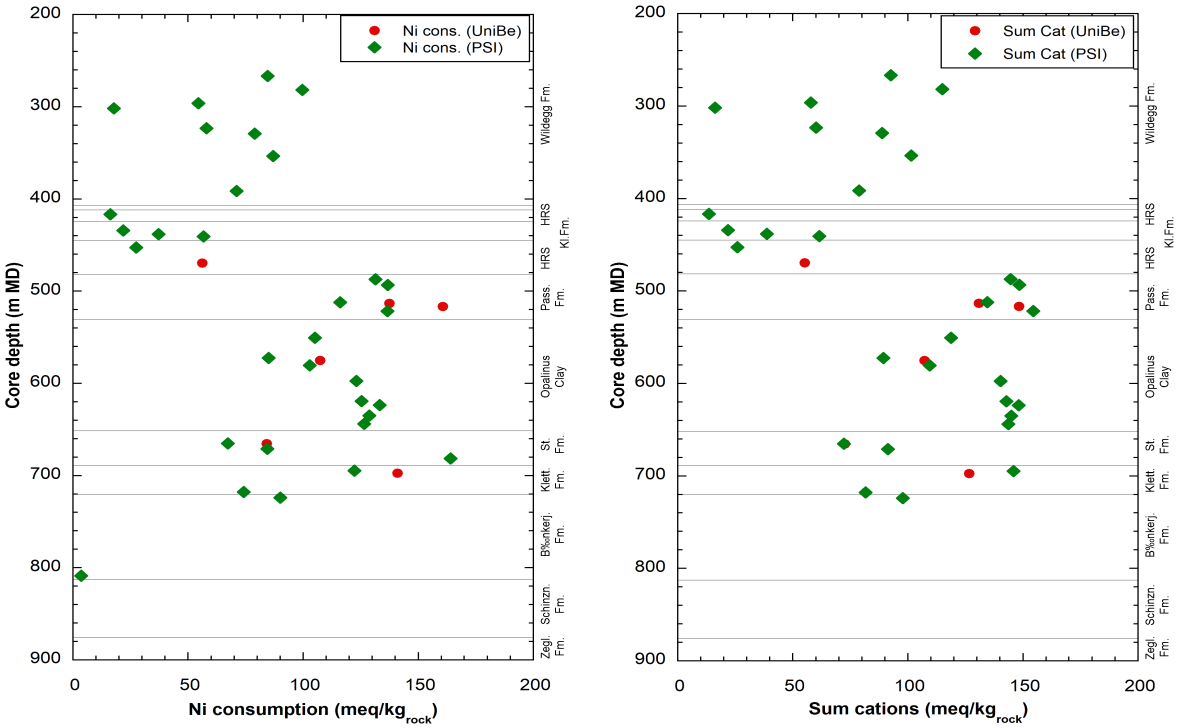

Fig. 5.6-3: Comparison of CEC data from Uni Bern and from PSI; Ni consumption data (left) and (corrected) sum of cations data (right)

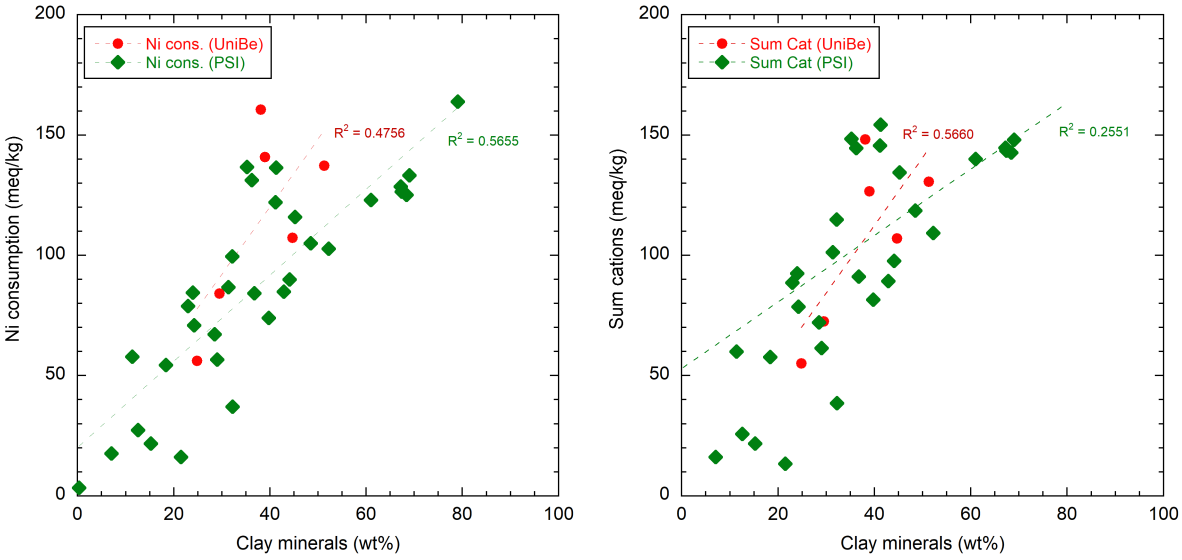

Fig. 5.6-4: CEC data as function of the clay-mineral content; left: Ni consumption data; right: Corrected sum of cations

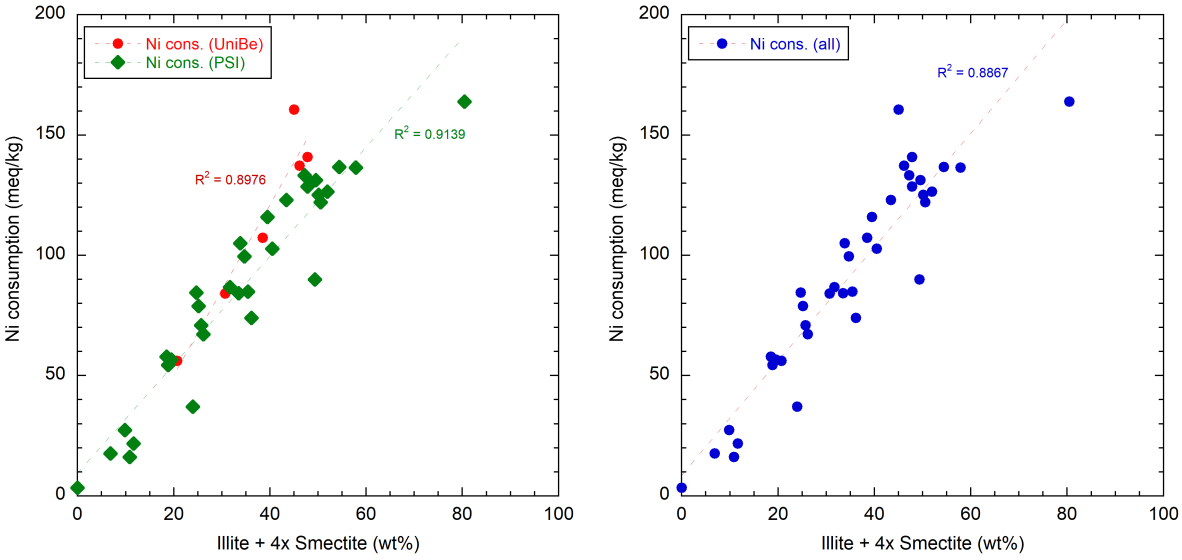

Fig. 5.6-5: Ni consumption as function of the sum of illite content and 4× smectite content

Exchangeable cation occupancies

The advantage of comparing fractional cation occupancies rather than the extracted cation concentrations is that they are normalised to the sum of cations (as proxy for the CEC) and do not directly depend on the clay-mineral content of the sample.

Fig. 5.6-6 shows the Na and Ca occupancies derived from the two correction methods. Note that in method 1 Cl and SO_4 are attributed to Na, whereas in method 2, SO_4 and, in the case of PSI data, also TIC is attributed to Ca. Thus, the Na fraction is minimised in method 1 and maximised in method 2, while the opposite is true for Ca. With regard to the PSI dataset, there are four calcareous samples (301.54 m, 416.35 m, 434.29 m, 808.61 m) for which the correction procedure

leads to negative Na and/or Ca occupancies, thus to an over-correction. These samples are not considered in the analysis. Besides the two datasets, the calculated occupancies from the SQ and AD porewater data are shown. The calculations were done using the PHREEQC simulator and the well-established single-site cation exchange model for Opalinus Clay (Pearson et al. 2011, Wersin et al. 2016).

Comparison of "measured" Uni Bern and PSI exchangeable cation data illustrates broadly consistent trends for all measured exchangeable cations, as illustrated in Figs. 5.6-6 to 5.6-8, except for K (Fig. 5.6-7 right). The "calculated" exchangeable cation populations based on SQ and AD data support the overall trends. Note that PSI also included NH_4 in their analysis. Their fractional occupancies are, however, very low (< 0.02).

For K, PSI data display systematically higher occupancies, which is related to the extraction by CsCl mobilising a larger pool of K present in the illite fraction compared to the Ni-method. The same discrepancy was already observed in previous boreholes (Mazurek et al. 2021, Aschwanden et al. 2021, Mäder et al. 2021). There is one outlier, a calcareous sample at 452.61 m depth from the Hauptrogenstein, notable in all the occupancy profiles.

In the case of Na, Uni Bern data display consistently slightly higher Na occupancies than the PSI data. The "calculated" values based on AD/SQ data are similar to the Uni Bern data derived from method 2. The Ca/Na ratio generally shows better agreement between the two datasets (Fig. 5.6-9). The difference between the datasets corrected by method 1 and 2, respectively, increases towards the top of the sequence. In fact, the PSI dataset obtained from method 1 exhibits a strong shift to higher Ca/Na ratios within the Hauptrogenstein-Wildegg Formation[15]. From these trends it appears that method 2 (NaCl, $CaSO_4$/$Ca(HCO_3)_2$ correction) yields more reliable data within these carbonate-rich units. In general, the Ca/Na ratio shows an increase from the Klettgau Formation to the Staffelegg. Formation, approximately constant values in the Opalinus Clay and Passwang Fm, above which a steady increase is noted again (Fig. 5.6-9 left). The trend is better defined in the (Ca+Mg)/Na as illustrated in Fig. 5.6-9 right, where only data corrected with method 2 are shown. The calculated AD/SQ data are broadly consistent with the "measured" data corrected with method 2, showing a slight shift to lower values in the Ca/Na and (Ca+Mg)/Na ratios, especially in the upper part (Passwang Fm-Hauptrogenstein).

The Mg/Ca ratio is constant over most of the profile (Fig. 5.6-10 left), but strongly increases in the Bänkerjoch Formation Note that in this formation magnesite was detected (Section 4.2). A high Mg concentration was also found in the squeezed water sample at 775.39 m depth which is manifested by a very high calculated Mg/Ca occupancy ratio.

The Sr/Ca ratio is also constant over most of the profile, (Fig. 5.6-10 right), but showing scattered values below the Opalinus Clay.

[15] Note that in this sequence no Uni Bern data are available.

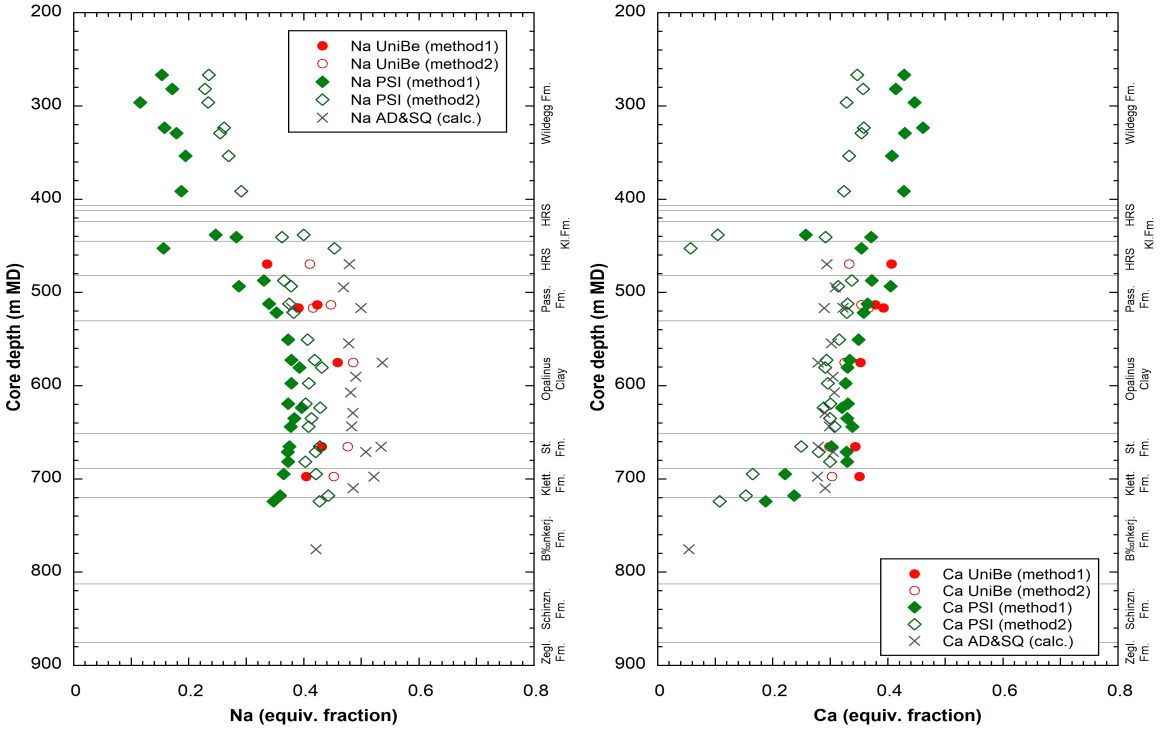

Fig. 5.6-6: Na (left) and Ca (right) occupancies according to Uni Bern and PSI data and calculated from AD/SQ data

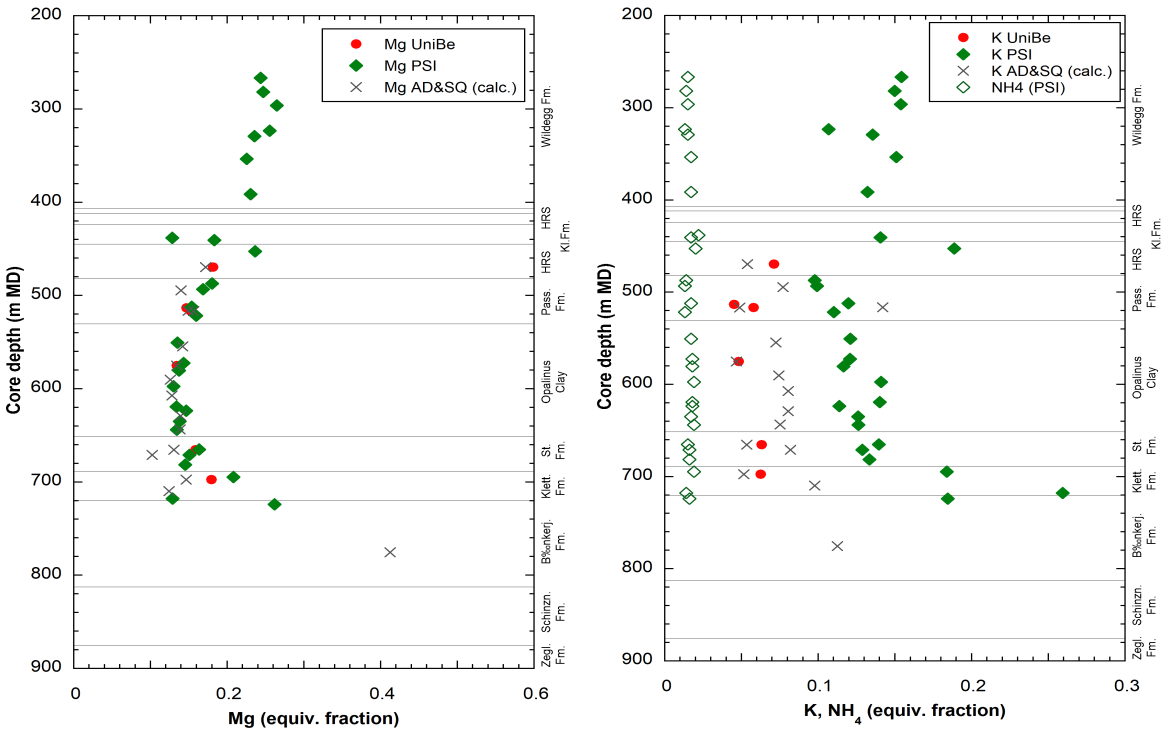

Fig. 5.6-7: Mg (left) and K, NH_4 (right) occupancies according to Uni Bern and PSI data and values calculated from AD/SQ data

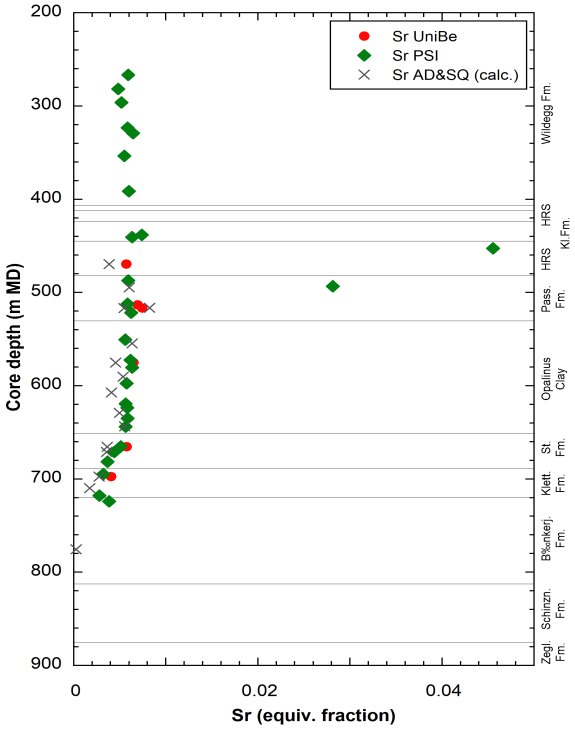

Fig. 5.6-8: Sr occupancies according to Uni Bern and PSI data and calculated from AD/SQ data

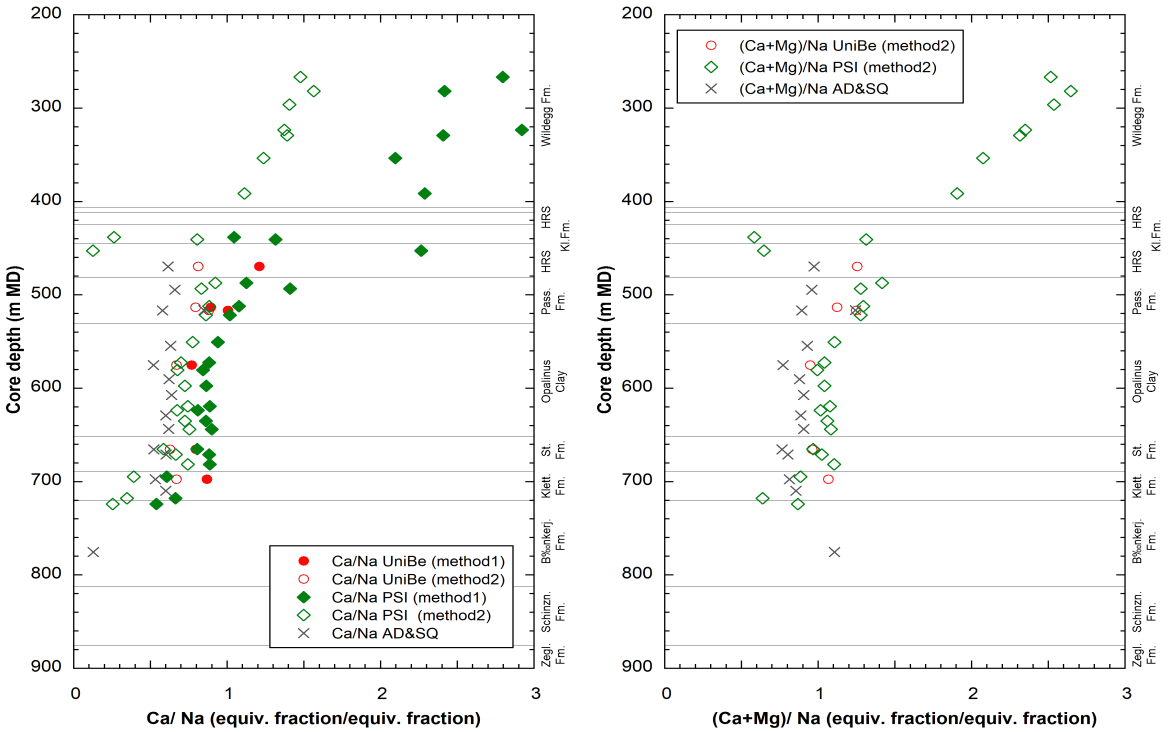

Fig. 5.6-9: Ca/Na ratios (left) and (Ca+Mg/Na) (right) according to Uni Bern and PSI data and calculated from AD/SQ data

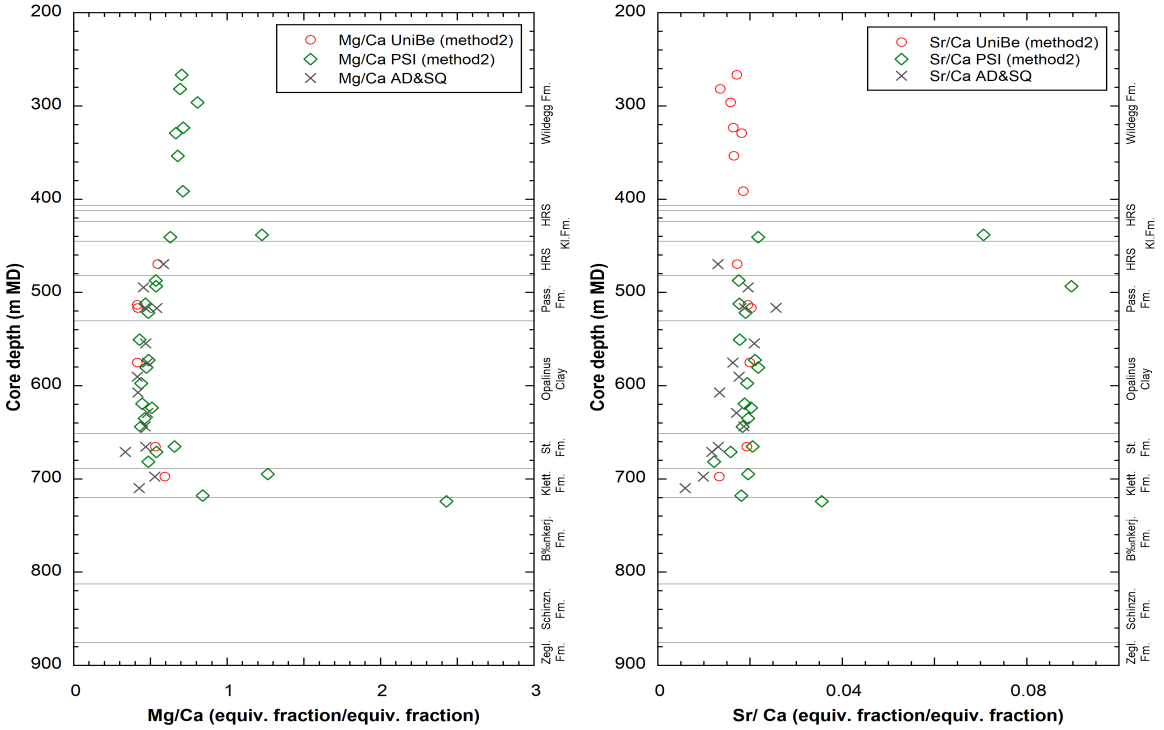

Fig. 5.6-10: Mg/Ca ratios (left) and Sr/Ca ratios (right) according to Uni Bern and PSI data and calculated from AD/SQ data

Extracted anions

The amounts of Cl and SO_4 extracted (Fig. 5.6-11) are consistent between the two datasets of PSI and Uni Bern. Note that for PSI data, Cl data from aqueous extraction are shown, because CsCl was used for extraction of exchangeable cations. These Cl data compare well with those analysed in the Ni-en extracts of Uni Bern. Both these datasets agree with the (larger) AqEx dataset of Uni Bern which is also illustrated in Fig. 5.6-11 (left). Regarding SO_4, the amounts extracted by aqueous extraction also indicate a general agreement between the two laboratories. On the other hand, somewhat less SO_4 was extracted by the Ni-en extraction procedure compared to aqueous extraction. The same trend has also been observed in previous boreholes BUL1-1, TRU1-1 and MAR1-1, but the reason thereof is not known at this point.

The Cl data reveal rather constant values from the Wildegg Formation down to the lower part of the Opalinus Clay. From there a decreasing trend towards the upper Klettgau Fm is noted. Higher Cl concentrations were extracted from three calcareous samples from the Klingnau Formation and Hauptrogenstein. This might reflect release of Cl from fluid inclusions during the extraction procedure.

The extracted SO_4 levels are generally somewhat higher (on an equivalent basis) relative to Cl. An increasing trend above and below the Opalinus Clay is observed. There are two outliers from the general trend, one at 434.29 m and the other at 493.15 m. The lowermost sample, located at the bottom of the Bänkerjoch Formation, shows an exceptionally high amount of extracted SO_4, induced by the dissolution of anhydrite present in this sample.

Total inorganic carbon (TIC) measured in the PSI extracts is 1 – 10 mmol/kg_{rock}. This is higher than expected for Uni Bern extracts. TIC was not measured in the latter but calculated to be below 1 mmol/kg_{rock} based on the assumption of calcite equilibrium (data not shown). The higher TIC in the PSI extracts is explained by the lower S/L ratio which induces a higher proportion of dissolved carbonate from carbonate minerals.

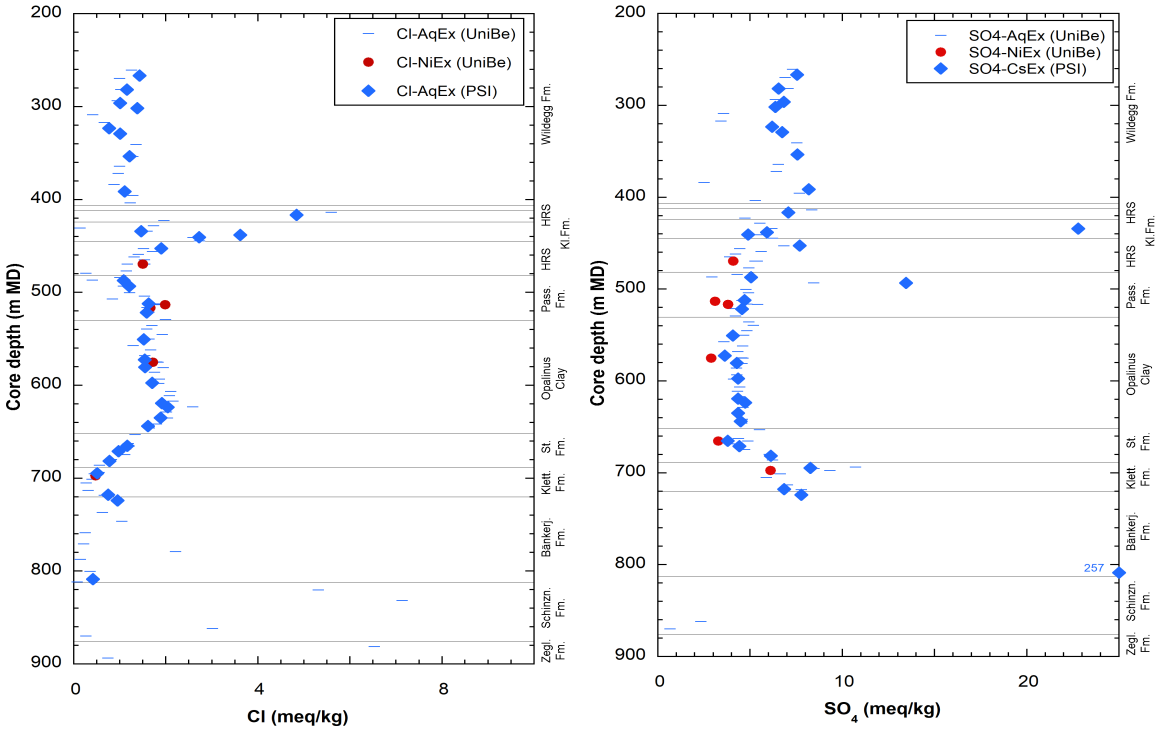

Fig. 5.6-11: Extracted Cl (left) and SO_4 (right) in mg/kg_{rock} according to Uni Bern and PSI data

5.7 Stable water isotopes

Lukas Aschwanden & Thomas Gimmi

5.7.1 Comparison between different methods for the determination of stable porewater isotope compositions

The porewater oxygen and hydrogen isotope compositions were determined using three different methods including the isotope diffusive-exchange (Section 4.8), advective displacement (Section 4.7) and high-pressure squeezing (Section 4.6) methods. Data of the three techniques are available for the section 470 – 780 m where clay-rich rocks dominate, and all methods can be applied. For the clay-poor rocks of the Malm and the Muschelkalk only data from isotope diffusive-exchange experiments are available. For the advective displacement technique, the average of the first two displaced solution aliquots is considered as being most representative for the in situ porewater. For the squeezed water, the one obtained at the lowest squeezing pressure (200 MPa or 300 MPa) is considered as being most representative for the in situ porewater.

All the porewater isotope data, together with those for the groundwater sample from the Muschelkalk aquifer (*cf.* Section 2.3), are shown in Fig. 5.7-1 as a function of depth. For isotope data from isotope-diffusive exchange experiments the error bars reflect the propagated experimental and analytical uncertainty. For isotope data from advective displacement and high-pressure squeezing experiments only the analytical error is illustrated. In general, for δ^2H, the three methods agree well (within the uncertainty). However, for $\delta^{18}O$ both isotope data from high-pressure squeezing and even more those from advective displacement show lower values compared to the data from isotope diffusive-exchange experiments. The reason for this is currently unknown.

5.7.2 Comparison with groundwater data and depth profiles

Owing to low hydraulic conductivities neither in the Malm nor in the Keuper of BOZ1-1 groundwater samples could be collected (8×10^{-11} m/s and 3×10^{-12} m/s, respectively). The porewater isotope composition shows a continuous evolution in $\delta^{18}O$ and δ^2H across the interval Wildegg Formation – Staffelegg Formation down to the Gansingen Member in the Klettgau Formation where a local minimum is indicated. Although no groundwater sample could be collected in the Keuper of BOZ1-1 the shapes of the isotope profiles indicate that exchange with water bodies located in the Klettgau Formation plays a role for the evolution of porewater $\delta^{18}O$ and δ^2H signatures in the over- and underlying rock units.

The $\delta^{18}O$ and δ^2H-values of groundwater from the Muschelkalk aquifer agree well with those of the porewater obtained from samples in the packed-off interval (i.e. within the propagated uncertainty; one sample shows slightly higher isotope values than the groundwater and a comparatively large propagated uncertainty; porewater isotope compositions of both samples are less reliable owing to experimental difficulties). The Muschelkalk groundwater appears to represent minima of $\delta^{18}O$ and δ^2H and the adjacent porewaters indicate remarkably steep gradients towards heavier values up- and downwards. Such steep gradients indicate either that the isotope signal in the groundwater is geologically young, and/or the diffusion coefficients in the clay-poor Schinznach Formation are very low.

As indicated by aqueous extracts, three core samples from the Schinznach Formation, two core samples from the Zeglingen Formation and two core samples from the Dinkelberg Formation show variable degrees of contamination by drilling fluid (*cf.* Section 4.4.2). Three of the contaminated samples (BOZ1-1-846.00-PW, BOZ1-1B-879.74-PW and BOZ1-1B-881.21-PW) were collected within the packed-off interval where the Muschelkalk groundwater was sampled. The latter shows $\delta^{18}O$ and δ^2H values of -10.1‰ VSMOW and -73.5‰ VSMOW, respectively (Lorenz et al. *in prep.*), whereas the drilling fluid is distinctly enriched in ^{18}O and ^2H (-5.9 and -40.5‰ VSMOW, respectively; Lorenz et al. *in prep*). The three contaminated samples have distinctly heavier isotope signatures ($\delta^{18}O$ = -6.9 to -6.4‰ VSMOW; δ^2H = -52.9 to -47.6‰ VSMOW) than the groundwater and the uncontaminated porewater of neighbouring samples in the packed-off interval. Mixing calculations using the uncontaminated porewater of neighbouring samples and the drilling fluid as the two endmembers indicate an admixture of 67–82% of drilling fluid to the porewater of the three contaminated samples. This renders their isotope composition derived from the diffusive-exchange experiments unreliable and thus, they are excluded from all graphs. Such high degrees of contamination seem not unrealistic considering the rather high porosities of these samples (Tab. 4.4-2) and likely elevated permeability allowing percolation of large amounts of drilling fluid to central parts of the drill core samples.

For the remaining three contaminated samples from the top of the Schinznach Formation and from the Dinkelberg Formation (BOZ1-1-820.53-PW, BOZ1-1-831.86-PW and BOZ1-1B-973.17-PW; *cf.* Section 4.4.2) the degree of contamination cannot be estimated owing to i) the lack of information on the uncontaminated porewater isotope composition at the top of the Schinznach Formation and ii) the lack of the NaCl drilling mud analysis from the Dinkelberg Formation. However, these samples show distinctly lower porosities (and likely permeability; Tab. 4.4-2) compared to the three highly contaminated samples described above and thus, the effect of contamination on the porewater isotope signature is much less pronounced.

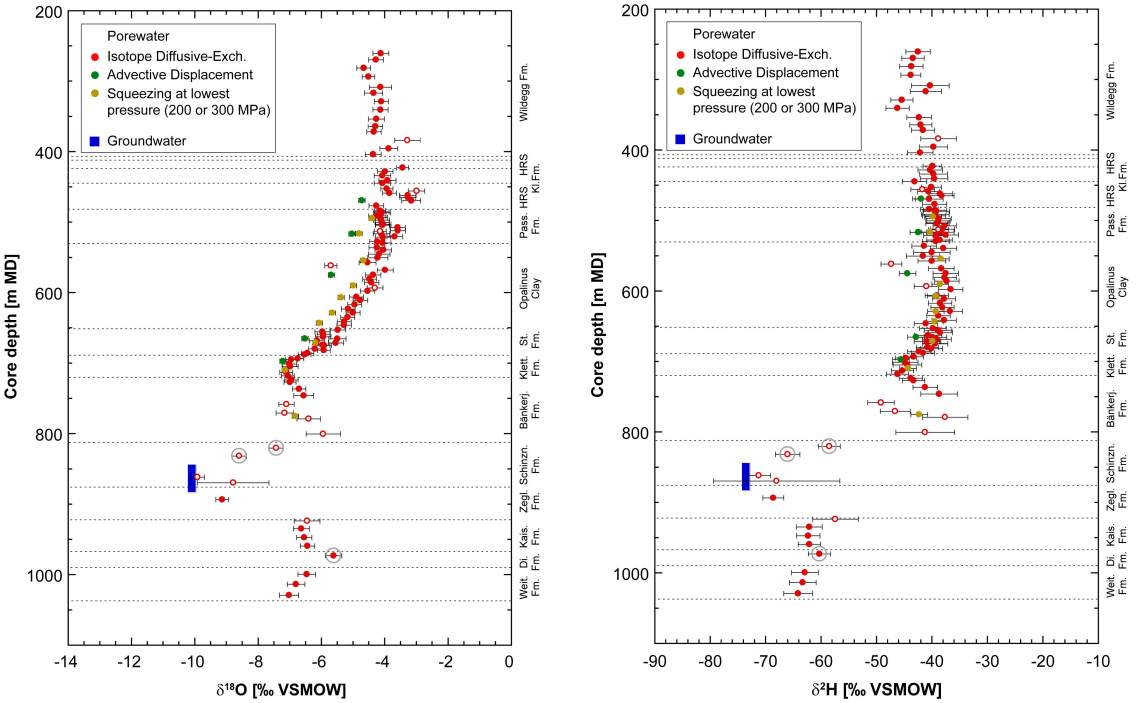

Fig. 5.7-1: Depth trends of $\delta^{18}O$ and $\delta^{2}H$ in groundwater and porewater derived by all techniques

Bars indicate propagated analytical errors (diffusive exchange) or simple analytical errors (squeezing, advective displacement). Groundwater data are from Lorenz et al. (*in prep.*). Open symbols refer to porewater isotope values which are less reliable owing to experimental artefacts (*cf.* Section 4.8). Samples with a grey circle show signs of contamination by drilling fluid (*cf.* Section 4.4.2).

5.7.3 $\delta^{2}H$ versus $\delta^{18}O$ and comparison with Global Meteoric Water Line

Fig. 5.7-2 illustrates all data in a $\delta^{18}O$ vs. $\delta^{2}H$ diagram. Such diagrams provide information on e.g. climatic conditions during recharge and indications on water-rock interactions or mixing of different water components. Porewater in rocks of the Wildegg Formation and the underlying interval Ifenthal Formation – Passwang Formation are enriched in ^{18}O and ^{2}H and plot far to the right of the Global Meteoric Water Line (GMWL). Shown by the solid red arrow 1 in Fig. 5.7-2, the porewater isotope composition shows a continuous evolution in $\delta^{18}O$ and $\delta^{2}H$ from the Passwang Formation to the base of the Staffelegg Formation where porewater isotope values fall on the GMWL. This suggests a dominant meteoric component in the latter porewaters. The pronounced deviation of the porewater $\delta^{18}O$ – $\delta^{2}H$ signatures with respect to the Global Meteoric

Water Line at the top of the section in the Wildegg Formation and the Dogger units overlying the Opalinus Clay indicates long residence times of these porewaters, with values affected by exchange with groundwater in over- and underlying water-conducting zones, and possibly by water – rock interactions. The evolution of the isotope signatures from the Passwang Formation down to the base of the Staffelegg Formation appears to be dominated by exchange with groundwater in the underlying water-conducting zones. The $\delta^{18}O$ and $\delta^{2}H$ profiles with their negative excursions in the Klettgau Formation suggest the presence of mobile groundwater at these depths (see Section 5.7.2).

Similar to the porewater at the base of the Staffelegg Formation, isotope signatures of porewater in the Klettgau Formation and in the Bänkerjoch Formation also plot along the GMWL – partly at somewhat more depleted isotope signatures (solid red arrow 2 in Fig. 5.7-2) – indicating the presence of a dominant meteoric component. Moreover, this component is enriched in ^{18}O and ^{2}H compared to modern recharge. At the base of the Bänkerjoch Formation porewater $\delta^{18}O$ and $\delta^{2}H$ signatures sharply evolve towards most negative values in the water-conducting zone of the Muschelkalk (solid red arrow 3 in Fig. 5.7-2). This evolution does not follow the GMWL but a trajectory somewhat below the GMWL (even when considering that many of these values are considered as less reliable according to quality criteria). Following the above hypothesis of exchange between porewater and groundwater in the Klettgau Formation, exchange in the system Keuper-Muschelkalk seems not well advanced. This is in line with the observation that $\delta^{18}O$ and $\delta^{2}H$ signatures of the Muschelkalk groundwater fall within the range of modern recharge, however, slightly shifted to the right of the GMWL. The deviation from the GMWL is likely due to mixing with isotopically different water components and/or water – rock interactions.

Porewater in the underlying interval Kaiseraugst Formation – Weitenau Formation again show isotope signatures enriched in ^{18}O and ^{2}H compared the Muschelkalk porewater and groundwater (solid red arrow 4 in Fig. 5.7-2). Their position far to the right of the GMWL indicates long residence times of these porewaters.

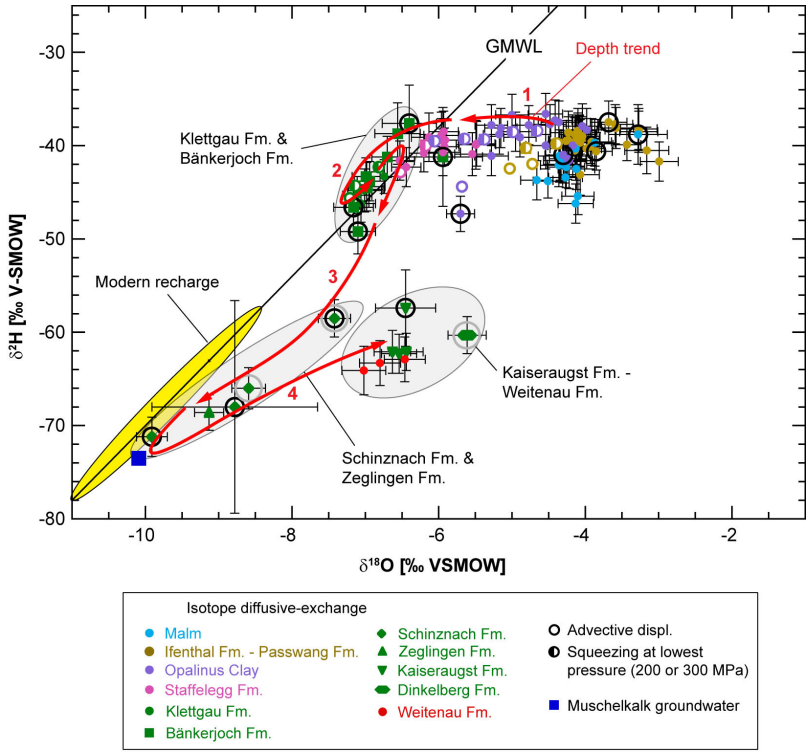

Fig. 5.7-2: δ^2H vs. $\delta^{18}O$ for groundwater and porewater derived by all techniques

Bars indicate propagated analytical errors (diffusive exchange) or simple analytical errors (squeezing, advective displacement). Groundwater data are from Lorenz et al. (*in prep.*). GMWL = Global Meteoric Water Line (defined as $\delta^2H = 8\ \delta^{18}O + 10$; Craig 1961). Range of modern recharge from Kullin & Schmassmann (1991). Samples in circles are less reliable owing to experimental artefacts (black circles; *cf.* Section 4.8) and/or possible contamination by drilling fluid (grey circles; *cf.* Section 4.4.2). See text for details on the numbering of red arrows (depth trend).

6 Final remarks and main conclusions

RWI team

High quality cores could be extracted from the BOZ-1-1 borehole, which enabled to acquire high quality mineralogical, petrophysical and porewater data using a well-established procedure. Drilling operations proceeded without major problems down to the Muschelkalk where, however, a considerable loss of drilling mud and also of a packer system occurred. After cementing the lowest section, a side track (BOZ-1-1B) was drilled which delivered cores from the Zeglingen Formation (where further mud losses occurred) down to the end of the cored section at the footwall of the Weitenau Formation A few cores from the Muschelkalk and the underlying Buntsandstein were found to be affected by drilling fluid contamination (see below).

Because of low transmissivities encountered, groundwater could be only sampled from the Muschelkalk aquifer.

As in previous boreholes, a number of systematic depth trends are observed for the contents of clay minerals, quartz and calcite. The ratio of the illite-to-smectite end-member clays also shows a systematic variation. The lower part of the Klingnau Formation and the upper part of the 'Spatkalk' are macroscopically brownish, which is due to considerable contents of goethite. Samples from these sections have distinct characteristics, such as high grain density, high anion accessibility and low external surface area.

The depth trends of mineral contents correlate well with those of petrophysical parameters. Water content and porosity correlate positively with clay-mineral content. A strong negative correlation of these parameters is seen with anhydrite content, and values trend towards zero in pure anhydrite samples. This may also mean that diffusion coefficients become very low, and so anhydrite-rich beds may represent zones with a particularly high transport resistance.

The external specific surface area (BET, N_2 adsorption) correlates broadly with water contents and with clay-mineral contents, but with some outliers. The samples from the upper Hauptrogenstein and from the Klingnau Formation fall below the general trend between external surface area and water content, meaning that they have a different pore architecture compared to most of the other samples. Average radii of external pores derived from N_2 adsorption (neglecting interlayer water) are ~ 1 – 5 nm (diameter ~ 2 – 10 nm) in clay-rich lithologies and ~ 2 – 16 nm (diameter ~ 3 – 31 nm) in calcareous marls, sand-, silt- or limestones. The latter tend to have bimodal pore size distributions, with peaks at diameters near or slightly above 10 nm and near 100 nm, while the former tend to have a dominant peak below a diameter of ~ 10 nm.

Drilling fluid contamination was identified in seven aqueous extraction samples, from which four are affected by potassium silicate drilling mud and the remaining three samples by the sodium chloride drilling mud. However, estimates of the extent of contamination by the potassium silicate drilling mud showed that the contamination exceeds the analytical uncertainty of Br and Cl solely in a few samples. The contamination by the Na-Cl drilling mud resulted in secondary halite precipitation detected in XRD, but it remains difficult to quantify the contamination and hence to judge the reliability of those aqueous extraction data.

Porewaters in the interval Wildegg Formation – Passwang Formation are enriched in ^{18}O and ^{2}H and plot far to the right of the Global Meteoric Water Line (GMWL) indicating long residence times. With increasing depth $\delta^{18}O$ and $\delta^{2}H$ evolve towards values falling on the GMWL at the base of the Staffelegg Formation, suggesting a dominant meteoric component. Similarly, $\delta^{18}O$

and δ^2H in the Klettgau Formation and in the Bänkerjoch Formation also plot along the GMWL – partly at somewhat lower values (but higher than modern recharge) with a local minimum in the Klettgau Formation. Although no groundwater sample could be collected in the Keuper of BOZ1-1 the $\delta^{18}O$ and δ^2H profiles with their negative excursions in the Klettgau Formation suggest the presence of mobile groundwater at this depth. Accordingly, exchange with this groundwater plays an important role for the evolution of the porewater isotope composition in over- and underlying units. At the base of the Bänkerjoch Formation $\delta^{18}O$ and δ^2H signatures sharply evolve towards most the negative values observed in the BOZ1 profile in the water-conducting zone of the Muschelkalk. This evolution does not follow the GMWL but a trajectory somewhat below the GMWL. Following the above hypothesis of exchange between porewater and groundwater in the Klettgau Formation, exchange in the system Keuper-Muschelkalk seems not well advanced. This is in line with the observation that $\delta^{18}O$ and δ^2H of the Muschelkalk groundwater fall within the range of modern recharge, however, slightly shifted to the right of the GMWL. Moreover, the adjacent porewaters indicate remarkably steep gradients towards heavier values up- and downwards. Such steep gradients indicate that the isotope signal in the Muschelkalk groundwater is geologically young, and/or the diffusion coefficients in the matrix of clay-poor Schinznach Formation are very low.

Anion-accessible porosities could be derived from squeezed (SQ) and advectively displaced (AD) porewaters as well as from through-diffusion tests carried out at PSI. Squeezing and advective displacement data yield broadly consistent Cl-accessible porosity fractions (f_{Cl}) with average values of ~ 0.42 ± 0.08 for clay-mineral contents ≥ 25 wt.-%. The diffusion data show a somewhat different behaviour compared to the former two methods, contrary to previous boreholes such as BUL1-1 and TRU1-1. Thus, from the latter method a weakly decreasing trend at clay-mineral contents beyond 25 wt.-% and generally lower f_{Cl} values can be discerned. Notably, low f_{Cl} values in the Opalinus Clay were derived from diffusion data, which are not in line with the other datasets (SQ, AD) and which currently cannot be explained. At lower clay-mineral contents (< 25 wt.-%), diffusion data suggest the expected increasing trend of f_{Cl} with decreasing fraction of clay minerals, but a number of samples fall off this trend, in particular from the upper units (Wildegg Formation – Hauptrogenstein). Note that no SQ and AD data are available at these low clay-mineral contents.

The Cl and Br profiles show a curved shape between the Klettgau Formation and the Passwang Formation, with constant Cl concentrations of ~3 g/L in the Opalinus Clay. The profile shape indicates the presence of an active aquifer in the Keuper, which is supported by the shapes of the $\delta^{18}O$ and δ^2H profiles. The Cl and Br profiles further hint at the presence of an aquifer system in the Passwang Formation but this is neither supported by the other tracers ($\delta^{18}O$, δ^2H ^{37}Cl) nor by structural observations and thus remains hypothetical. The profiles of $\delta^{18}O$ and ^{37}Cl rather suggest a positive excursion in the Hauptrogenstein. In that formation as well in the Passwang Fm, there are several outliers to the general profiles, which are, at least partially, related to iron oxide-rich oolitic samples. Below the Keuper aquifer, Cl and Br concentrations show an increasing trend towards the Muschelkalk aquifer. Futher down in the sequence, the scatter in the data is considerable and some very high chloride contents are observed. These may be related to the dissolution of the salt layer in the Zeglingen Formation, but contamination by the NaCl brine drilling fluid cannot be ruled out.

The depth profile of the Br/Cl ratio reveals remarkable consistency between the three datasets AqEx, SQ and AD. It is better defined than that of Cl or Br, due to the fact that no assumptions on anion accessibility need to be made and the uncertainty regarding recalculation to the rock porosity cancels out. From the Klettgau Formation, a slight but steady increase in Br/Cl ratio up to the uppermost samples in the Wildegg Formation (ranging from ~ 1 to ~ 2 for 1000 Br/Cl molar units) is noted. Below the Klettgau Formation, this ratio increases strongly in the Bänkerjoch

Formation, but then decreases abruptly within the Schinznach Formation towards the Muschelkalk aquifer (0.04), indicating the influence from dissolution halite from the underlying salt layers. Below, an increasing tendency with considerable scatter down to the Permian is noted.

The sulphate data obtained from SQ and AD, which covers the Hauptrogenstein to the Bänkerjoch Formation are consistent. The corresponding SO_4 profile indicates a curved shape, with slightly decreasing concentrations from the Hautptrogenstein to the Passwang Formation, constant values in the Opalinus Clay and a strong increase in the Staffelegg Formation and continuing in the Keuper units. Conversely, AqEx data yield systematically higher and more variable concentrations, as has been observed in the previous boreholes and the Mont Terri Rock Laboratory. SO_4/Cl ratios deduced from SQ and AD are constant (~ 0.4 in molar units) within the Passwang-Opalinus Clay sequence, but increase strongly in the Staffelegg and Klettgau Formation (up to ~ 4), from where they seem to decrease towards the Muschekalk aquifer (~ 0.1).

The cation data obtained from SQ and AD are broadly consistent. The profiles of all measured cations (Na, Ca, Mg, K, Sr) indicate approximately constant values across the Passwang-Klettgau Formation sequence and an increasing trend in the Bänkerjoch Formation Na follows the same trend as Cl in the upper part of the profile, but diverges from Cl further down, where SO_4 contributes significantly to the anionic charge. The Mg concentration is particularly high in the Bänkerjoch Formation where it reaches 2 g/L, likely related to the sporadic presence of magnesite.

The cation exchange capacity (CEC) correlates with the clay-mineral content. An even better correlation can be deduced with the sum of illite and smectite endmember mineral contents, the main carriers of the CEC. The main exchangeable cations are Na and Ca, followed by Mg and K. The exchanger composition (cation occupancies) is approximately constant in the Staffelegg Formation and across the Opalinus Clay. Above a steady decrease of Na at the expense of Ca and Mg into the Malm units is observed. Below the Staffelegg Formation, some scatter in the exchanger composition is indicated, but a clear increase in the Mg component can be discerned. The exchanger composition determined from extraction methods is in broad agreement with that obtained from modelling of the SQ and AD porewater data.

The porewaters in the Opalinus Clay and bounding formations are rather dilute compared to previous boreholes from ZNO and NL. Thus, the maximum Cl concentrations in the sequence are about 4 g/L. Moreover, these porewaters have a larger share of SO_4 and a higher SO_4/Cl ratio. The porewaters are of Na-(Ca)-Cl-SO_4 type (according to the nomenclature of Jäckli 1970) in the upper units, shifting to Na-(Ca)-SO_4-Cl in the Klettgau Formation, and to Na-Mg-SO_4-Cl in the Bänkerjoch Formation

The pH/P_{CO2} conditions deduced for the SQ and AD data appear somewhat perturbed due to CO_2 exchange during the squeezing experiments, and in case of AD, mainly due to microbial processes resulting in elevated nitrate concentrations. Nevertheless, reasonable pH/P_{CO2} conditions could be estimated in case of SQ data from simple modelling considering CO_2 exchange during the experiments. Both methods yield consistent TOC concentrations of 50 – 150 mg/L. These concentrations, however, are not thought to fully reflect in-situ porewater conditions, but rather the easily mobilisable fraction from the solid organic matter.

Even though an in-depth interpretation and comparison with the boreholes from other siting areas is beyond the scope of this report, a few points can nevertheless be made:

- Tracer profiles as well as structural observations yield strong indications of an active aquifer in the upper Keuper, although no groundwater samples could be extracted from that area. On the other hand, the existence of a bounding aquifer above the Opalinus Clay is not clear. Some indications for an aquifer in the upper Passwang Formation are seen in the Cl and and Br profiles, but this is supported neither by stable water isotope data nor by structural evidence.
- The mean f_{Cl} value of 0.42 from AD and SQ for clay-mineral contents > 25 wt.-% is similar to that found for TRU-1-1 (0.45) and MAR1-1 (0.46), but lower than derived for BUL1-1 (0.52). In view of the remaining uncertainty related to the anion-accessible porosity fraction and its relationship to the clay-mineral content and other parameters, these differences should not be overemphasised. It is worth noting that the f_{Cl} values derived from diffusion experiments of PSI are distinctly lower for Opalinus Clay, a feature that was not observed in previous boreholes.
- The porewaters in the Opalinus Clay and its confining units from BOZ1-1 are more dilute than those analysed in other siting regions, with chlorinities in the range of 3 – 4 g/L. The share of sulphate and the SO_4/Cl ratio, however, are larger than in the previous TBO boreholes.
- Waters obtained from squeezing and advective displacement indicate broadly consistent data regarding major ion composition in spite of some perturbation noted from pH/P_{CO2} data. The overall consistency of cation data is supported by cation exchange data.

7 References

Allison, J.D., Brown, D.S. & Novo-Gradac, K.J. (1991): MINTEQA2/PRODEFA2, a geochemical assessment model for environmental systems: Version 3.0 user's manual. Environmental Research Laboratory, Office of Research and Development, U.S. Environmental Protection Agency, 106 p.

Aschwanden, L. & Wersin, P. (2020): Experimental study of sulphate in the Opalinus Clay: Results from extraction tests. Nagra Arbeitsbericht NAB 20-17.

Aschwanden, L., Camesi, L., Gimmi, T., Jenni, A., Kiczka, M., Mäder, U., Mazurek, M., Rufer, D., Waber, H.N., Wersin, P., Zwahlen, C. & Traber, D. (2021): TBO Trüllikon-1-1: Data report – Dossier VIII: Rock properties, porewater characterisation and natural tracer profiles. Nagra Arbeitsbericht NAB 20-08.

Bradbury, M.H. & Baeyens, B. (1998): A physicochemical characterisation and geochemical modelling approach for determining porewater chemistries in argillaceous rocks. Geochim. Cosmochim. Acta 62, 783-795.

Cappa, C.D., Hendricks, M.B., DePaolo, D.J. & Cohen, R.C. (2003): Isotopic fractionation of water during evaporation. Journal of Geophysical Research 108/D16.

Courdouan Merz, A. (2008): Nature and reacivity of dissolved organic matter in clay formations evaluated for the storage of radioactive waste. PhD thesis. ETH Zurich.

Courdouan, A., Christl, I., Meylan, S., Wersin, P. & Kretzschmar, R. (2007a): Characterization of dissolved organic matter in anoxic rock extracts and in situ pore water of the Opalinus Clay. Applied Geochemistry 22, 2926-2939.

Courdouan, A., Christl, I., Meylan, S., Wersin, P. & Kretzschmar, R. (2007b): Isolation and characterization of dissolved organic matter from the Callovo-Oxfordian formation. Applied Geochemistry 22, 1537-1548.

Craig, H. (1961): Isotopic variations in meteoric waters. Science 133, 1702-1703.

Debure, M. & Gailhanou, H. (2019): GD experiment: Experimental study of sulphate in Opalinus Clay. Unpubl. Mont Terri Technical Note. Mont Terri Project, Switzerland.

Durce, D., Bruggeman, C., Maes, N., Van Ravestyn, L. & Brabants, G. (2015): Partitioning of organic matter in Boom Clay: Leachable vs mobile organic matter. Applied Geochemistry 63, 169-181.

Gimmi, T. & Waber, H.N. (2004): Modelling of tracer profiles in porewater of argillaceous rock in the Benken borehole: Stable water isotopes, chloride and chlorine isotopes. Nagra Technical Report NTB 04-05.

Hadi, J., Wersin, P., Mazurek, M., Waber, H.N., Marques Fernandes, M., Baeyens, B., Honty, M., De Craen, M., Frederickx, L., Dohrmann, R. & Fernandez, A.M. (2019): Intercomparison of CEC method within the GD project. Mont Terri Technical Report TR 2017-06. Mont Terri Project, Switzerland.

Horita, J., Cole, D.R. & Wesolowski, D.J. (1995): The activity-composition relationship of oxygen and hydrogen isotopes in aqueous salt solutions: III. Vapor-liquid water equilibration of NaCl solutions to 350 C. Geochim. Cosmochim. Acta 59, 1139-1151.

Jäckli, H. (1970): Kriterien zur Klassifikation von Grundwasservorkommen. Eclogae geol. Helv. 63/2, 389-434.

Jenni, A., Aschwanden, L., Lanari, P., de Haller, A. & Wersin, P. (2019): Spectroscopic investigation of sulphur-containing minerals in Opalinus Clay. Nagra Arbeitsbericht NAB 19-23.

Kullin, M. & Schmassmann, H. (1991): Isotopic composition of modern recharge. *In:* Pearson F.J., Balderer, W., Loosli, H.H., Lehmann, B.E., Matter, A., Peters, Tj., Schmassmann, H.-J. & Gautschi, A. (1991): Applied Isotope Hydrogeology – A Case Study in Northern Switzerland. Studies in Environmental Science 43, Elsevier, Amsterdam, 65-89.

Lorenz, G.D. et al. (*in prep.*): Borehole BOZ1-1 (Bözberg): Fluid sampling and analytical hydrochemical data report. Unpublished Nagra Interner Bericht.

Madritsch, H. & Hammer, P. (2012): Characterisation of Cenozoic brittle deformation of potential geological siting regions for radioactive waste repositories in northern Switzerland based on structural geological analysis of field outcrops. Nagra Arbeitsbericht NAB 12-41.

Mäder, U. (2018): Advective displacement method for the characterisation of porewater chemistry and transport properties in claystone. Geofluids 2018, Article ID 8198762, doi.org/10.1155/2018/8198762.

Mäder, U. & Waber, H.N. (2017): Results of advective displacement / multi-component transport experiments from claystone samples of the Schlattingen borehole. Nagra Arbeitsbericht NAB 17-16.

Mäder, U., Aschwanden, L., Camesi, L., Gimmi, T., Jenni, A., Kiczka, M., Mazurek, M., Rufer, D., Waber, H.N., Wersin, P., Zwahlen, C. & Traber, D. (2021): TBO Marthalen-1-1: Data report – Dossier VIII: Rock properties, porewater characterisation and natural tracer profiles. Nagra Arbeitsbericht NAB 21-20.

Marques Fernandes, M. & Baeyens. B. (*in prep.*): Sorption measurements of Cs, Ni, Eu, Th and U on rock samples of Opalinus Clay and confining geological units from deep boreholes at the potential siting regions for a deep geological repository for radioactive waste in Switzerland: Jura Ost, Nördlich Lägern and Zürich Nordost. Nagra Technical Report NTB 22-02.

Mazurek, M. (2017): Gesteinsparameter-Datenbank Nordschweiz – Version 2. Nagra Arbeitsbericht NAB 17-56.

Mazurek, M. & Aschwanden, L. (2020): Multi-scale petrographic and structural characterisation of the Opalinus Clay. Nagra Arbeitsbericht NAB 19-44.

Mazurek, M., Oyama, T., Wersin, P. & Alt-Epping, P. (2015): Pore-water squeezing from indurated shales. Chemical Geology 400, 106-121.

Mazurek, M., Aschwanden, L., Camesi, L., Gimmi, T., Jenni, A., Kiczka, M., Mäder, U., Rufer, D., Waber, H.N., Wanner, P., Wersin, P. & Traber, D. (2021): TBO Bülach-1-1: Data Report – Dossier VIII: Rock properties, porewater characterisation and natural tracer profiles. Nagra Arbeitsbericht NAB 20-08.

Naef, H., Büchi, M., Bläsi, H.R., Deplazes, G. & Gysi, M. (2019): Lithology Manual – Lithological description of drill cores and cuttings in Northern Switzerland. Nagra Arbeitsbericht NAB 19-11.

Parkhurst, D.L. & Appelo, C.A.J. (2013): Description of input and examples for PHREEQC Version 3: A computer program for speciation, batch-reaction, one-dimensional transport, and inverse geochemical calculations. No. 6-A43. US Geological Survey.

Pearson, F.J. (1999): What is the porosity of a mudrock? *In:* Aplin, A.C., Fleet, A.J. & Macquaker, J.H.S. (eds.): Muds and Mudstones: Physical and fluid flow properties. Geological Society, London, Special Publications 158, 9-21.

Pearson, F.J., Balderer, W., Loosli, H.H., Lehmann, B.E., Matter, T., Peters, T., Schmassmann, H. & Gautschi, A. (1991): Applied isotope hydrogeology-a case study in northern Switzerland. Stud. Environ. Sci. 43, Elsevier, New York.

Pearson, F.J., Arcos, D., Bath, A., Boisson, J.Y., Fernandez, A.M., Gäbler, H.E., Gaucher, E., Gautschi, A., Griffault, L., Hernan, P. & Waber, H.N. (2003): Mont Terri project – geochemistry of water in the Opalinus Clay formation at the Mont Terri rock laboratory. Federal Office for Water and Geology Rep. 5, Bern, Switzerland.

Pearson, F.J., Tournassat, C. & Gaucher, E.C. (2011): Biogeochemical processes in a clay formation in situ experiment: Part E – Equilibrium controls on chemistry of pore water from the Opalinus Clay, Mont Terri underground research laboratory, Switzerland. Applied Geochemistry 26, 990-1008.

Rufer, D. (2019): Field Manual: Drillcore sampling for analytical purposes. Nagra Arbeitsbericht NAB 19-13.

Rufer, D. & Mazurek, M. (2018): Pore-water extraction and characterization: Benchmarking of the squeezing and adapted isotope diffusive exchange methods. NWMO Technical Report NWMO-TR-2018-14. Nuclear Waste Management Organization, Toronto, Canada.

Sheppard, S. & Gilg, H. (1996): Stable isotope geochemistry of clay minerals: "The story of sloppy, sticky, lumpy and tough" Cairns-Smith (1971). Clay Minerals 31, 1-24.

Thoenen, T., Hummel, W., Berner, U. & Curti, E. (2014): The PSI/Nagra Chemical Thermodynamic Database 12/07. PSI Bericht Nr. 14-04, Paul Scherrer Institut, Villigen, Switzerland.

Thommes, M., Kaneko, K., Neimark, A.V., Olivier, J.P., Rodriguez-Reinoso, F., Rouquerol, J. & Sing, K.S. (2015): Physisorption of gases, with special reference to the evaluation of surface area and pore size distribution (IUPAC Technical Report). Pure and Applied Chemistry 87, 1051-1069.

Tournassat, C., Vinsot, A., Gaucher, E.C. & Altmann, S. (2015): Chemical conditions in clayrocks. *In:* Tournassat, C., Steefel, C.I., Bourg, I.C. & Berrgaya, F. (eds.): Natural and engineered clay barriers. Developments in Clay Science 6, Chapter 3, 71-100. Elsevier.

Van Loon, L.R. & Glaus, M. A. (*in prep.*): Diffusion measurements of HTO, $^{36}Cl^-$ and $^{22}Na^+$ on rock samples of Opalinus Clay and confining geological units from deep boreholes at the potential siting regions for a deep geological repository for radioactive waste in Switzerland: Jura Ost, Nördlich Lägern and Zürich Nordost. Nagra Technical Report NTB 22-01.

Waber, H.N. (ed.) (2020): SGT-E3 deep drilling campaign (TBO): Experiment procedures and analytical methods at RWI, University of Bern (Version 1.0, April 2020). Nagra Arbeitsbericht NAB 20-13.

Waber, N., Gimmi, T. & Smellie, J.A.T. (2012): Reconstruction of paleoinfiltration during Holocene using porewater data. Geochim. Cosmochim. Acta 94, 109-127.

Wersin, P., Mazurek, M., Waber, H.N., Mäder, U.K., Gimmi, T., Rufer, D. & de Haller, A. (2013): Rock and porewater characterisation on drillcores from the Schlattingen borehole. Nagra Arbeitsbericht NAB 12-54.

Wersin, P., Mazurek, M., Mäder, U.K., Gimmi, T., Rufer, D., Lerouge, C. & Traber, D. (2016): Constraining porewater chemistry in a 250 m thick argillaceous rock sequence. Chemical Geology 434, 43-61.

Wersin, P., Pekala, M., Mazurek, M., Gimmi, T., Mäder, U.K., Jenni, A., Rufer, D. & Aschwanden, L. (2020): Porewater chemistry of Opalinus Clay: Methods, modelling & buffering capacity. Nagra Technical Report NTB 18-01.